

Multi-diagnostic Investigations of the Equatorial and Low-latitude Ionospheric Electrodynamics and Their Impacts on Space-based Technologies

Author: Sovit M. Khadka

Persistent link: <http://hdl.handle.net/2345/bc-ir:108001>

This work is posted on [eScholarship@BC](#),
Boston College University Libraries.

Boston College Electronic Thesis or Dissertation, 2018

Copyright is held by the author, with all rights reserved, unless otherwise noted.

Boston College
The Graduate School of Arts and Sciences
Department of Physics

**MULTI-DIAGNOSTIC INVESTIGATIONS OF
THE EQUATORIAL AND LOW-LATITUDE
IONOSPHERIC ELECTRODYNAMICS AND
THEIR IMPACTS ON SPACE-BASED
TECHNOLOGIES**

A dissertation by

SOVIT M. KHADKA

Submitted in Partial Fulfillment of the Requirements

for the Degree of

Doctor of Philosophy

April 2018

© Copyright by **Sovit M. Khadka** 2018

Recommended Citation

Khadka, Sovit M. (2018), *Multi-Diagnostic Investigations of the Equatorial and Low-Latitude Ionospheric Electrodynamics and their Impacts on Space-Based Technologies*, Ph.D. Dissertation, Boston College, United States.

MULTI-DIAGNOSTIC INVESTIGATIONS OF THE EQUATORIAL AND LOW-LATITUDE IONOSPHERIC ELECTRODYNAMICS AND THEIR IMPACTS ON SPACE-BASED TECHNOLOGIES

Author: Sovit M. Khadka

Advisors: Prof. Michael J. Naughton and Dr. Cesar E. Valladares

Committee Members: Prof. Pradip Bakshi

Prof. Krzysztof Kempa

Dr. Keith M. Groves

Abstract

The equatorial and low-latitude ionosphere of the Earth exhibits unique features on its structuring, coupling, and electrodynamics that offer the possibility to forecast the dynamics and fluctuations of ionospheric plasma densities at later times. The scientific understanding and forecasting of ionospheric plasma are necessary for several practical applications, such as for mitigating the adverse effects of space weather on communication, navigation, power grids, space mission, and for various scientific experiments and applications. The daytime equatorial electrojet (EEJ), equatorial ionization anomaly (EIA), as well as nighttime equatorial plasma bubble (EPB) and plasma blobs are the most prominent low-latitude ionospheric phenomena. This dissertation focuses on the multi-diagnostic study of the mechanism, properties, abnormalities, and interrelationships of these phenomena to provide significant

contributions to space weather communities from the ground- and space-based measurements.

A strong longitudinal, seasonal, day-to-day variability and dependency between EEJ, ExB vertical plasma drift, and total electron content (TEC) in the EIA distribution are seen in the equatorial and low-latitude region. In general, the EEJ strength is stronger in the west coast of South America than in its east coast. The variability of the EEJ in the dayside ionosphere significantly affects the ionospheric electron density variation, dynamics of the peak height of F2-layer, and TEC distributions as the EEJ influences the vertical transport mechanism of the ionospheric plasma.

The eastward electric field (EEF) and the neutral wind play a decisive role in controlling the actual configuration of the EIA. The trans-equatorial neutral wind profile calculated using data from the Second-generation, Optimized, Fabry-Perot Doppler Imager (SOFDI) located near the geomagnetic equator and a physics-based numerical model, LLIONS (Low-Latitude IONospheric Sector) give new perspectives on the effects of daytime meridional neutral winds on the consequent evolution of the asymmetry of the equatorial TEC anomalies during the afternoon onwards. The spatial configurations including the strength, shape, amplitude and latitudinal extension of the EIA crests are affected by the EEF associated with the EEJ under undisturbed conditions, whereas the meridional neutral winds play a significant role in the development of their asymmetric structure in the low-latitude ionosphere.

Additionally, the SWARM satellite constellation and the ground-based LISN (Low-Latitude Ionospheric Sensor Network) data allow us to resolve the space-time ambiguity of past single-satellite studies and detect the drastic changes that EPBs and plasma blobs undergo on a short time scale. The coordinated quantitative analysis of a plasma density observation shows evidence of the association of plasma blobs with EPBs via an appropriate geomagnetic flux tube. Plasma blobs were initially associated with the EPBs and remained at the equatorial latitude right above the EPBs height, but later were pushed away from geomagnetic equator towards EIA latitudes by the EPB/ depleted flux tubes that grew in volume.

Further, there exists a strong correlation between the noontime equatorial electrojet and the GPS-derived TEC distributions during the afternoon time period, caused by vertical $E \times B$ drift via the fountain effect. Nevertheless, only a minor correlation likely exists between the peak EEJ and the net postsunset ionospheric scintillation index (S4) greater than 0.2. This study not only searches for a mutual relationship between the midday, afternoon and nighttime ionospheric phenomena but also aims at providing a possible route to improve our space weather forecasting capability by predicting nighttime ionospheric irregularities based on midday measurements at the equatorial and low latitudes.

Table of Contents

	Page
Dedication	(vi)
Acknowledgements	(vii)
List of Figures	(ix)
List of Tables	(xiii)
Quotation	(xiv)
Chapter 1: INTRODUCTION	1
1.1 Motivation.....	1
1.2 Research Objectives.....	2
1.3 Overview of Present Study.....	3
1.3.1 Description.....	3
1.4 Organization of the Dissertation.....	6
Chapter 2: ELECTRODYNAMICS OF THE LOW-LATITUDE	
IONOSPHERE	9
2.1 Near-Earth Space Environment.....	9
2.1.1 Structures of Earth's Atmosphere.....	10
2.1.2 Ionosphere and its Layers.....	14
2.1.3 Chemistry of Layers.....	18
2.2 Features of the Low-Latitude Ionosphere.....	21
2.2.1 Equatorial Ionosphere.....	21

2.2.2 Structures in the Low Latitude Ionosphere.....	22
2.2.3 Equatorial Electrojet (EEJ).....	25
2.2.4 Equatorial Ionization Anomaly (EIA).....	27
2.2.5 Equatorial Spread-F, Plasma Bubbles and Plasma Blobs.....	29
2.3 Physics of the Equatorial and Low-Latitude Ionosphere	31
2.3.1 Wind Dynamo and Plasma Dynamics.....	35
2.3.2 Ionospheric Currents and Electric Fields	37
2.3.3 Equatorial Plasma Fountains.....	39
2.3.4 Pre-Reversal Enhancement (PRE).....	42
2.3.5 Rayleigh-Taylor Instability (RTI).....	44
Chapter 3: INSTRUMENTATION AND METHODOLOGY	48
3.1 Remote Radio Wave Techniques.....	49
3.1.1 Radar.....	50
3.1.2 GPS: Basic Concepts.....	55
3.1.2.1 Total Electron Content (TEC) Measurement.....	60
3.1.2.2 Ionospheric Scintillations Measurement.....	62
3.1.3 Vertical Sounders (Ionosondes).....	65
3.2 Magnetic Sensors and Optical Techniques.....	71
3.2.1 Magnetometer.....	71
3.2.2 Fabry Perot Interferometer.....	75
3.2.2.1 SOFDI.....	78
3.3 In-situ Techniques.....	79

3.3.1 SWARM Satellite Constellation.....	79
3.3.1.2 Objectives of SWARM Satellite Mission.....	80
Chapter 4: VARIABILITY OF THE EQUATORIAL ELECTROJET	
AND RELATED IONOSPHERIC FEATURES	82
4.1 Introduction.....	84
4.2 Instrumentation, Datasets, and Techniques.....	88
4.3 Analysis and Results.....	93
4.3.1 Narrow Longitudinal Variability of Equatorial Electrojet (EEJ).....	93
4.3.2 Day-to-Day Variability of the Counter Equatorial Electrojet (CEJ).....	95
4.3.3 Seasonal Variability of the Morning EEJ Depression (MED).....	97
4.3.4 F-Layer Height Variability in Association with MED.....	99
4.3.5 Effects of the MED and AED on Peak Height of F2-Layer and TEC.....	102
4.3.6. Impacts of the MED on GPS-TEC.....	104
4.4 Discussion.....	106
4.5 Summary and Conclusions.....	108
Chapter 5: EFFECTS OF EEJ AND NEUTRAL WIND ON	
EQUATORIAL ANOMALY DYNAMICS	111
5.1 Introduction.....	112
5.2 Instrumentation, Datasets, and Methodology.....	117
5.3 Analysis and Results.....	119
5.3.1 Annual, Seasonal and Day-to-Day Variability of EIA.....	120

5.3.2 Day-to-Day Variability of EEJ, Drifts, and EIA Strengths.....	125
5.3.3 Comparison of Neutral Wind from LLIONS Model and SOFDI Data.....	131
5.4 Interpretation and Discussions.....	141
5.5 Summary and Conclusions.....	145

Chapter 6: SATELLITE AND GROUND-BASED OBSERVATIONS

OF IONOSPHERIC PLASMA IRREGULARITIES 148

6.1 Introduction.....	149
6.2 Instrumentation and Data Processing.....	153
6.3 Analysis and Results.....	156
6.3.1 Identification of EPBs and Blobs Signature from SWARM.....	156
6.3.2 Ionospheric Plasma Depletions: EPB Events	159
6.3.3 Ionospheric Plasma Enhancements: Blob Events	164
6.4 Interpretation and Discussion.....	168
6.5 Summary and Conclusions.....	171

Chapter 7: INTERRELATIONSHIP BETWEEN SEVERAL

IONOSPHERIC PARAMETERS 174

7.1 Introduction.....	175
7.2 Data Selection and Analysis.....	179
7.2.1 EEJ and Estimation of Vertical Drifts.....	180
7.2.2 Determination of Latitudinal TEC Profiles.....	183
7.2.3 Determination of Net S4.....	186

7.3 Concurrent Observations of EEJ, TEC, and S4 Index.....	188
7.4 Discussion.....	192
7.5 Summary and Conclusions.....	195
Chapter 8: SUMMARY AND FUTURE RESEARCH	197
8.1 Overview of Dissertation Results.....	197
8.1.1 Variability of EEJ and its Consequences.....	198
8.1.2 Asymmetry of EIAs.....	199
8.1.3 Evolution to Decay of EPB/ Blobs	199
8.1.4 Mutual Relationship between Ionospheric Parameters.....	200
8.2 Space Weather and Impacts on Space-based Technologies.....	200
8.3 Directions for Future Research.....	204
Chapter 9: REFERENCES	208
APPENDIX	244
I. Abbreviations.....	244
II. Publications and Manuscripts.....	247
III. VITA.....	248

DEDICATION

This dissertation is dedicated to my parents
for their love, encouragement,
and tireless support.

Acknowledgements

I would like to express my sincere gratitude to my dissertation supervisor, Dr. Cesar E. Valladares. His constant supervision, encouragement, guidance, and support empowered me to develop a deep and comprehensive understanding of the subject matter and to succeed in the great achievement of completing the research part of my Ph.D. degree. This dissertation work has also been carried out under the supervision of Prof. Michael J. Naughton. I am very grateful to him for his insight, guidance, and generous support and also enabling me to conduct off-department research of my interest. I would like to thank my committee members, Prof. Pradip Bakshi, Prof. Krzysztof Kempa, and Dr. Keith M. Groves for their time, interest, valuable comments, and support to improve this dissertation. I would also like to thank my academic advisor Prof. Ziqiang Wang for his guidance.

I am especially indebted to Patricia H. Doherty, Director of the Institute for Scientific Research (ISR), Boston College, who has provided me an opportunity to do research without any lack of support. She has also provided me extensive personal and professional guidance and communicated me a great deal about scientific research. I would also like to extend my sincere thanks to the professors, scientists, and staff of the Physics Department and the Institute for Scientific Research. I am particularly grateful to Dr. Rezy Pradipta, Dr. Kathleen Kraemer, and Dr. Robert Sheehan for their immense help and assistance in concluding this dissertation. Mr. Dev Raj Joshi and Mr. Nawa Raj Dahal have been fantastic friends and colleagues for years and are also a source of inspiration for my work.

I am also hugely appreciative to research scientist Dr. Edgardo Pacheco and Director Dr. Marco Milla of Jicamarca Radio Observatory (JRO), Peru for mentoring me during my stay in the observatory in 2014 summer, and sharing their Upper Atmospheric expertise so willingly. I cannot continue without thanking Percy Condor, Oscar Veliz, and Cesar de la Jara and many others for their support in training and performing experiments in JRO. In the same vein, I would like to especially thank Professor Andrew J. Gerrard of New Jersey Institute of Technology (NJIT) who has provided me the SOFDI data and also explained about instrumentation techniques for neutral wind measurement.

Nobody has been more precious to me in the pursuit of this project than the members of my family. Most importantly, I would like to thank my first teachers, my parents Bhim Bahadur and Bishnu Maya, who raised me with love and supported me in all my pursuits. They are the ultimate role models of my achievement. I want to express my warm indebtedness to my wife, Prativha, for her patience and support throughout my Ph.D. study. I also thank my daughters Simran and Shristi whose angelic smiles and innocent activities always refreshed me as well as provided me unending inspiration.

Finally I like to thank the former and current Nepali community in Boston for their support and inspiration during my graduate years.

Thank you.

Sovit M. Khadka
Physics Department/
Institute for Scientific Research
Boston College
April 2018

List of Figures

Chapter 2

Figure	Page
2.1: Different layers of upper atmosphere of the Earth.....	13
2.2: Development of the ionospheric layers during day and night.....	15
2.3: a) Electron production rate with height, photon flux, and neutral density.....	17
b) Electron density profile at noon, midnight, solar cycle.....	17
2.4: a) Vertical profiles of the mixing of constituents in ionosphere.....	20
b) Temperature profile against altitude in the Earth's atmosphere.....	20
2.5: Electrojet current densities inferred from the CHAMP satellite.....	26
2.6: EIA-TEC in the American low latitude from the LISN GPS network.....	28
2.7: Signature of EPB recorded by Jicamarca Incoherent Scatter Radar.....	30
2.8: Collisional and collisionless regime of the ionosphere.....	32
2.9: Comparison of daytime ionospheric conductivities with altitude.....	34
2.10: Ionospheric dynamo driven by the average Sq current system.....	36
2.11: Amplification mechanism of EEF to form EEJ current during noon.....	38
2.12: Mechanism of the plasma fountain effect for the generation of EIA.....	41
2.13: PRE signatures as strong vertical plasma drift at dusk near low latitude.....	43
2.14: Mechanism of the Rayleigh Tylor instability for EPB formation.....	45

Chapter 3

3.1: Main radar antenna in Jicamarca Radio Observatory (JRO), Peru.....	52
3.2: Echo from JRO radar showing different layers of the ionosphere.....	54
3.3: Design of the orbital planes of GPS satellite that fly around the Earth.....	56

3.4: Experimental set up for the measurement of ionospheric phenomena.....	59
3.5: Geometry of TEC measurement strategies using GPS receivers.....	61
3.6: GPS sites under LISN and other network in Central and South America.....	64
3.7: An idealized ionogram made near local noon of the day.....	68
3.8: Normal ionogram from undisturbed and disturbed ionospheric layers.....	70
3.9: a) Magnetic field generated due to EEJ and its influence on magnetometer.....	74
b) Noontime enhancement of H-component as a signature of EEJ at equator.....	74
3.10: Schematic of a Fabry-Perot Interferometer (FPI).....	76
3.11: Orbit configuration of the constellation of SWARM trio satellites.....	81

Chapter 4

4.1: Instrument sites and the shifting of geomagnetic equator in South America.....	89
4.2: Narrow longitudinal variability of the EEJ in South America.....	94
4.3: Day-to-day variability of the counter EEJ during at Jicamarca and Piura stations during (a) solar minima 2008 and, (b) solar maxima 2013.....	96
4.4: Seasonal variability of the MED during quiet days in 3 years.....	98
4.5: a) EEJ variation with MED event.....	100
b) Virtual heights corresponding to three sounding frequencies.....	100
c) Virtual height at (and also ± 1 hour) MED events the 2008.....	100
d) Same as (c) for the solar maximum year 2013.....	100
e) Responses of virtual heights of F-layer ionosphere to MED.....	101
4.6: a) <u>Top Panel</u> - Three day variability of the EEJ and associated morning and afternoon depressions in 2008. <u>Middle Panel</u> - Variability of the peak height of F2-layer (hmF2) ionosphere corresponding to EEJ. <u>Bottom Panel</u> - TEC	

patterns derived from ionogram in association with EEJ.....	103
b) Same as (a) but for the solar maximum year 2013.....	103
4.7: Three days' MED and GPS-TEC in December 2013.....	105

Chapter 5

5.1: Geomagnetic latitudinal profiles of the annual and day-to-day variability of EIA crest of TEC for 3 years.....	121
5.2: Fifteen days scatter plots of latitudinal variations of maximum TEC data and their average in the equinox and solstice.....	123
5.3: H-component and their difference from magnetometer stations.....	126
5.4: Average vertical drift from Jicamarca ISR at geomagnetic equator.	128
5.5: Contour of TEC along 70°W on August 7, 8, 9, 10 for 2011.....	130
5.6: Meridional wind, measured (modeled) by SOFDI (LLIONS).....	132
5.7: LLIONS-modeled meridional neutral wind against geographic latitude.....	135
5.8: A comparison of LISN-measured and LLIONS-modeled TEC variations.....	138
5.9: Latitudinal profiles of TEC in 4 hours interval against geographic latitude.....	140
5.10: A possible evolution and mechanism of wind created asymmetry in EIA.....	144

Chapter 6

6.1: a) SWARM constellation b) Location of LISN-GPS receivers.....	155
6.2: a) EPBs, and b) Blobs against UT and magnetic latitude.....	158
6.3: a) Plasma density depletions b) SWARM constellation passes	161
6.4: One-hour variations (total 7 hrs) of TEC against latitude along the 55°W.....	163
6.5: a) Plasma density enhancement, (b) SWARM path along enhancement.....	165
6.6: a) Hourly variations (7 hrs.) of TEC against latitude, (b) TEC by 8 GPS.....	167

6.7: Illustrations of (a) Bubble Growing Phase, and b) Bubble Developed Phase.....170

Chapter 7

7.1: (a) Normalized H component at Jicamarca and Piura.....181
(b) Inferred vertical drift using artificial neural network technique.....181

7.2: Vertical TEC profiles during 19 – 22 UT within $\pm 30^\circ$ magnetic latitude.....184

7.3: (a) Relative S4 index observed at Antofagasta, (b) Net S4 index against UT.....187

7.4: Day-to-day variability of EEJ observed at Jicamarca and Piura in 2008.....189

7.5: Latitudinal distributions of TEC profiles in the Peruvian sector.....190

7.6: Day-to-day variability of S4 index up to either sides of EIA in 2008.....191

7.7: Correlation of peak EEJ with (a) max TEC, (b) separation of EIA,
(c) $S4 > 0.2$, and (d) $S4 < 0.2$ 193

Chapter 8

8.1: Highlights of space weather effects arise from solar transients.....202

List of Tables

Chapter 4

Table	Page
4.1: Coordinates of ground-based magnetometer stations used to estimate EEJ in South American low latitudes	91

QUOTATION

To conquer oneself is a greater task than conquering others.

- Buddha

This page is intentionally left blank.

Chapter 1

INTRODUCTION

Contents	Page
1.1 Motivation	1
1.2 Research Objectives	2
1.3 Overview of Present Study	3
1.3.1 Description	3
1.4 Organization of the Dissertation	6

1.1 Motivation

The geospace environment has become a prominent scientific paradigm in many modern technological communities including communication, navigation and power grids systems that directly influence daily human life activities. The near-Earth space environment encompasses a large number of complex physical processes and effects which are mainly influenced by activities of the Sun. Out of many atmospheric layers of the Earth, the ionosphere has remained a focus of space research and continues to hold interest because of its unique electrodynamics and central role on radio wave propagation. Although the ionosphere is a very thin layer with strong abundancies of plasma particles, its density perturbation poses challenging threats that cause severe radio signal disruptions and hence failures of the communication and navigation systems. A

forecasting capability of occurrence of plasma irregularities with precise time and location is not straightforward, and varying degrees of scientific efforts have been committed to investigating their electrodynamics and seeding conditions till today. The unique electrodynamics of the low-latitude ionosphere provides practical opportunities for space weather prediction. The fundamental principle of this dissertation is to provide a possible route to predict and mitigate space weather effects on man-made technological devices of communication and navigation with a general understanding of the structure and electrodynamics of the equatorial and low latitude ionosphere from ground and space-based observations.

1.2 Research Objectives

This dissertation intends to study the nature of ionospheric plasma structuring in the geomagnetic low-latitude regions especially for the drivers of ionospheric scintillation and plasma bubbles through models and the observational analysis of ground as well as space-based data. We outline here a number of scientific questions that the research is trying to address, which are not only essential but also critical to space weather communities.

- What are the characteristic features and spatial/ temporal variability of the low-latitude ionospheric phenomena [including Equatorial electrojet (EEJ), Equatorial ionization Anomaly (EIA), and Equatorial Plasma Bubble (EPB)] over the South American sector?

- How can we effectively utilize multi-diagnostic observation techniques together with computer models to diagnose and understand the low-latitude ionospheric phenomena mentioned above (EEJ, EIA, and EPB)?
- Can we identify physical mechanism(s) that might have played role in causing those features and variability?
- Can we find correlations between various features of these low-latitude ionospheric phenomena, which could be used for forecasting near-future behavior of the regional ionosphere based on real-time measurements (or data) obtained a few hours earlier?

1.3 Overview of Present Study

The equatorial and low-latitude ionosphere of the Earth is a powerful podium for space weather study. This is because it presents unique features on structuring, coupling and electrodynamic, and exhibits rapid as well as slow responses to the changes of its various fundamental inputs. In this dissertation, we present a general overview of detailed investigations of the generation, structures, and development of equatorial plasma irregularities and their interconnectedness with other ionospheric phenomena. The fundamental structure and electrodynamic concepts pertaining to the upper atmosphere, mainly the ionosphere with emphasis on the equatorial and low-latitude ionosphere are presented here.

1.3.1 Description

The ionosphere is a shell of charged particles surrounding the Earth that is produced primarily by extreme ultraviolet (EUV) radiation from the Sun. Therefore, the

ionospheric plasma content is expected to follow the Sun's behavior. At the magnetic equator, the Earth's magnetic field lines are horizontal forcing the ionospheric plasma to flow along the field lines, favoring the initiation of different types of plasma structures. Solar heating and tidal oscillations propagating from below set the thermosphere in motion due to the interaction between the neutral atmosphere and the plasma component near 100 km altitude. This interaction generates large-scale electric fields through a dynamo action, known as the E-region dynamo. This electric field controls the F-region dynamics during the day, but diminishes to almost no effect after sunset due to the decay of E-region densities. During the night, the F-region dynamo sets the F region in motion driven by the zonal neutral wind.

An important feature of the low-latitude ionospheric variability is an enhancement of the plasma density that is observed at both sides of the magnetic equator. These enhancements have been called the Appleton (also named equatorial) ionization anomaly (EIA) [Appleton, 1946]. The anomaly is also observable using latitudinal profiles of total electron content (TEC) gathered using a network of GPS receivers [Valladares et al., 2001]. The anomaly is the result of the upward motion of the plasma at the magnetic equator and its consequent diffusion poleward along the magnetic field line [Hanson and Moffett, 1966] driven by pressure gradient and gravity forces. Figure 1 shows a schematic representation of the fountain effect and the formation of the equatorial anomaly across Brazil. The broken lines indicate the direction of the plasma flow. During the day and early evening, the F-region plasma moves upward creating a density gradient along the field lines. This produces a pressure gradient force parallel to gravity and both

together drive the plasma as indicated in Figure 1. The TEC anomaly starts to develop as early as 1100 LT. It moves away from the equator with increasing local time, as the equatorial F-region moves to higher altitudes, reaching a maximum development around 2000 LT. After 2100 LT the crests of the anomaly sometimes move rapidly towards the equator as the equatorial ionosphere moves downward. This latter process has been called “the reverse fountain effect” [Sridharan *et al.*, 1993; Balan and Bailey, 1995]; it is propelled by a reversal of sign of the pressure gradient force allowing the plasma to move upward and equatorward along the field lines. The presence of a meridional wind blowing outwards from the summer hemisphere will create an asymmetry in the amplitude of the crests with smaller densities on the wind lee side [Walker *et al.*, 1994]. Several experimental and modeling studies have reported the coupling between the ionosphere and the troposphere. The FUV images introduced by *Sagawa et al.* [2005] revealed the existence of a 4-node longitudinal structure in the latitudinal displacement of the equatorial ionization anomaly (EIA) around the Earth. This effect was explained in terms of an eastward propagating (non-migrating) diurnal tide with zonal wave number 3 (DE3) excited by tropical tropospheric latent heat release able to modulate the lower thermospheric winds [Hagan *et al.*, 2007], resulting in modulation of the electric field in the lower ionosphere [Immel *et al.*, 2006]. The modulated electric field produces a wave number 4 longitudinal structure in the EIA region across the Earth when observed in a Sun-synchronous frame. These studies asserted the role of energy inputs from the lower atmosphere in producing a day-to-day variability, and indicated the importance of non-migrating tides.

Other thermospheric sources of energy are planetary waves (PW) able to penetrate up to 100 km altitude and introduce multi-day periodicities by modulating tidal amplitudes [Fuller-Rowell et al., 2008]. In summary, all these studies concur that to fully understand the day-to-day variability of the low-latitude ionosphere, it is essential to estimate the energy and momentum inputs originated from the lower parts of the atmosphere [Hagan et al., 2001; Rishbeth, 2006; Fuller-Rowell et al., 2008].

The low-latitude ionosphere of the Earth presents unique features on structuring, coupling, electrodynamics and exhibits rapid as well as slow responses to the changes of its various fundamental inputs. The equatorial electrodynamic (ExB) plasma drift originated from electric field and Earth's magnetic field play a fundamental role on the distribution and composition of low latitude ionospheric plasma and on the generation of plasma waves and density structures. Low latitude quiet-time ionospheric electric fields, plasma drifts and currents result mostly from the dynamo action of E and F region neutral winds driven by solar and lunar tides, but can also be significantly affected by atmospheric gravity and planetary waves with time scales from tens of minutes to about a month [Fejer, 2015].

1.4 Organization of the Dissertation

Starting with a general introduction of the low-latitude ionosphere, the content of this dissertation systematically deals with a description of the specific research analysis of ionospheric phenomena that occur in the low latitudes. To fulfill the demand of the objectives of the dissertation presented in the above section, the following is the study

design. Chapter 2 gives an overview of the geospace environment emphasizing the electrodynamics of the equatorial and low-latitude ionosphere. The electrodynamics and mechanism associated with the main equatorial phenomena EEJ, EIA, PRE, EPB, and Blobs are reviewed in detail. The mechanism associated with above phenomena, e.g., ionospheric current associated with hemispherical neutral dynamo, plasma fountain effects based on ExB drifts, and Rayleigh-Taylor instability for the explanation of plasma bubbles and blobs have been introduced.

In Chapter 3, experimental techniques and methodologies have been reviewed from which data have been used to address the conclusion in this research work. The physics behind the measurement techniques adopted in different instruments have also been explained. Instruments are categorized under radio, sensor, optical and in-situ techniques. The principles and measurement techniques used by the Jicamarca radar antenna, LISN GPS, magnetometers, ionosondes, SOFDI interferometer, C/NOFS and SWARM satellites are briefly discussed. In Chapter 4, the equatorial electrojet current is described at length on its structure, features, variability, uniqueness and its associations. Besides its origin, evidence of its dependence on latitude, longitude, season, solar flux and geomagnetic activity are introduced. The narrow longitudinal and seasonal variability of EEJ is also discussed for the American low latitudes. The equatorial E and F region ionosphere are reviewed using data collected via ground-based instruments. The morning as well as afternoon depression of EEJ and its association on the motion of F layer ionosphere is also explained for the quiet days. In Chapter 5, the origin of the equatorial ionization anomaly, the characteristics of the plasma fountain, and detailed investigation

of its asymmetry structure created by meridional neutral wind are presented. The results from GPS TEC and interferometer obtained from SOFDI ionospheric campaigns near equatorial regions are analyzed to give the sense of meridional neutral wind for the formation of EIA asymmetry. Chapter 6 reports motion of the ionospheric irregularities in the form of plasma bubbles and blobs from simultaneous measurement of space-based SWARM constellation and ground-based LISN data. Chapter 7 pertains to the mutual relationship of the ionospheric event discussed in chapter 4, 5 and 6. The night time ionospheric irregularities signified by S4 index and its association with daytime EEJ and GPS-TEC are explained in solar minimum as well as solar maximum conditions. Finally, in Chapter 8, we review the results presented in this dissertation. We conclude with suggestions for future research work on equatorial and low-latitude ionospheric science.

Chapter 2

ELECTRODYNAMICS OF THE LOW-LATITUDE IONOSPHERE

Contents	Page
2.1 Near-Earth Space Environment	9
2.1.1 Structures of Earth's Atmosphere	10
2.1.2 Ionosphere and its Layers	14
2.1.3 Chemistry of Layers	18
2.2 Features of the Low-Latitude Ionosphere	21
2.2.1 Equatorial Ionosphere	21
2.2.2 Structures in the Low-Latitude Ionosphere.....	22
2.2.3 Equatorial Electrojet (EEJ)	25
2.2.4 Equatorial Ionization Anomaly (EIA)	27
2.2.5 Equatorial Spread-F, Plasma Bubbles and Plasma Blobs	29
2.3 Physics of the Equatorial and Low-Latitude Ionosphere	31
2.3.1 Wind Dynamo and plasma Dynamics	35
2.3.2 Ionospheric Currents and Electric Fields	37
2.3.3 Equatorial Plasma Fountains	39
2.3.4 Pre-Reversal Enhancement (PRE)	42
2.3.5 Rayleigh-Taylor Instability (RTI)	44

2.1 Near-Earth Space Environment

The dynamic Sun is the main source of energy transfer in the solar system that produces a large variability in the geospace environment and planetary space weather phenomena. The Sun influences space environment directly and indirectly via radiative, thermal, dynamical, and electrodynamical processes. The planetary atmosphere is stably stratified

and consists of different regions of varying chemical and physical properties because of the variability, transfer, and distribution of the different forms of solar energy. Indeed, the terrestrial ionosphere would not exist in the absence of the Sun. This chapter presents the physics, chemistry and physiological aspects in the domain of the Sun-Earth interaction region in the low-latitude where ionization, photo-dissociation and variability processes are controlled by solar and magnetospheric processes from above and by internal waves from below. The electrodynamics associated with various low latitude ionospheric phenomena and its interconnectedness will also be discussed. This chapter deals with the physical processes controlling the structure, composition, and dynamics of planetary atmospheres emphasizing the Earth. In addition, it discusses the formation and maintenance of ionospheric layers, both photochemical and diffusion-controlled ones (E, F1, and F2), and the applicability of these models to magnetic and nonmagnetic planets [Bauer, 1973].

2.1.1 Structures of Earth's Upper Atmosphere

The Earth's atmosphere, the gaseous envelope, is divided into distinct layers each with its own specific trait demarcated by temperature, chemical composition, dynamics, and density. The solar radiation absorption capability of atmospheric particles increases the temperature as well as plasma density variation with altitude. Moving skyward from the Earth's surface, taking into account the temperature variation with altitude, these layers are named the troposphere (ground to 10km), stratosphere (10km to 50km), mesosphere (50km to 85km), thermosphere (85km to 700km), and exosphere (700km to ~10,000km). The exosphere gradually vanishes into the domain of interplanetary space. Similarly, if

the ionization rate is considered, the atmosphere of the Earth can be divided into two main layers: the neutral atmosphere and the ionosphere.

- The troposphere: Most of the terrestrial atmospheric weather phenomena occur in this layer. It ranges from the surface to the tropopause at around 10-12km. It is defined by a well-mixed composition of primarily molecular nitrogen and oxygen, with decreasing temperatures with altitude.

- The stratosphere: The blanket of the Earth that protects us from hazardous radiation is in this region. It is called the ozone layer. It extends from the tropopause to a height of around 45-50 km. Its temperature increases with height due to the absorption of solar ultraviolet radiation, and this region is thermodynamically stable.

- The mesosphere: This is the coolest region of the atmosphere where most of the meteorites that enter into the atmosphere burn up. It extends from the stratopause (45-50 km) altitude up to the mesopause around 90-95 km. This region experiences very little solar absorption and consists of primarily molecular nitrogen and oxygen, but, in addition, there are many minor species. Some metals, such as iron and sodium, are suspended in the mesosphere from meteoritic debris.

- The thermosphere: This is the hottest part of the atmosphere, where the temperature becomes almost constant with altitude even though it initially increases with altitude. It extends from about 90 km to 500 km. The thermosphere is the region where most of the radiation from the atmospheric atoms and molecules in the visible spectrum

originate, i.e., the night glow, day glow, and aurora. The transition to the thermosphere is due to the dissociation of diatomic oxygen and ionization through solar radiation absorption.

- The exosphere: This is the uppermost layer of the atmosphere where the atmosphere gets very tenuous. Particles of light species, like hydrogen, if moving fast enough, are able to escape the Earth's gravity. Gas molecules in this region are unlikely to collide with other molecules due to the low-density atmosphere. The outermost region where the geomagnetic field controls particle motion is termed the magnetosphere. The thermosphere is coupled energetically, dynamically, and chemically to the mesosphere at its lower bound, and to the exosphere and magnetosphere at its upper bound.

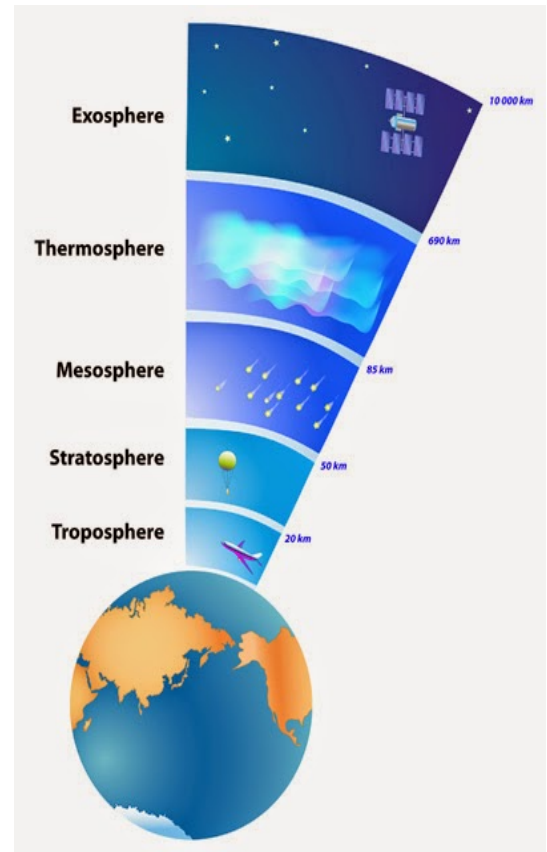
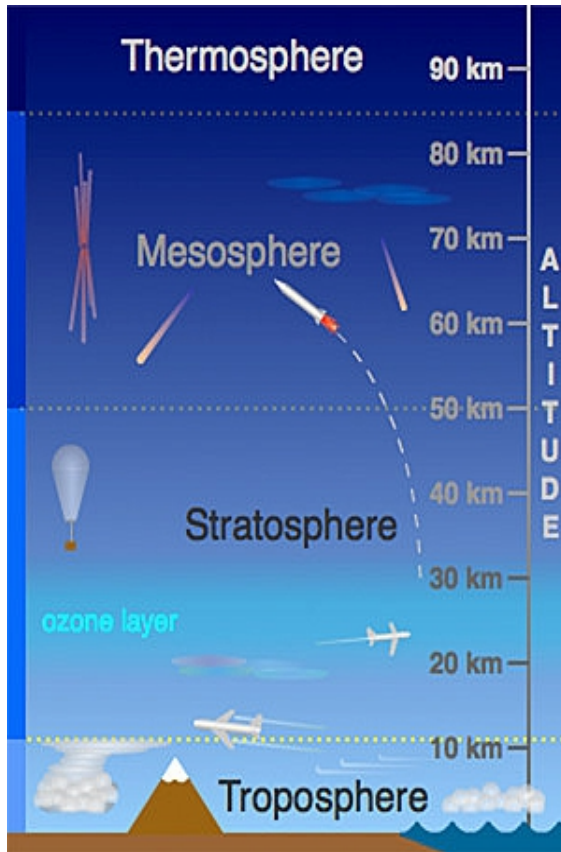
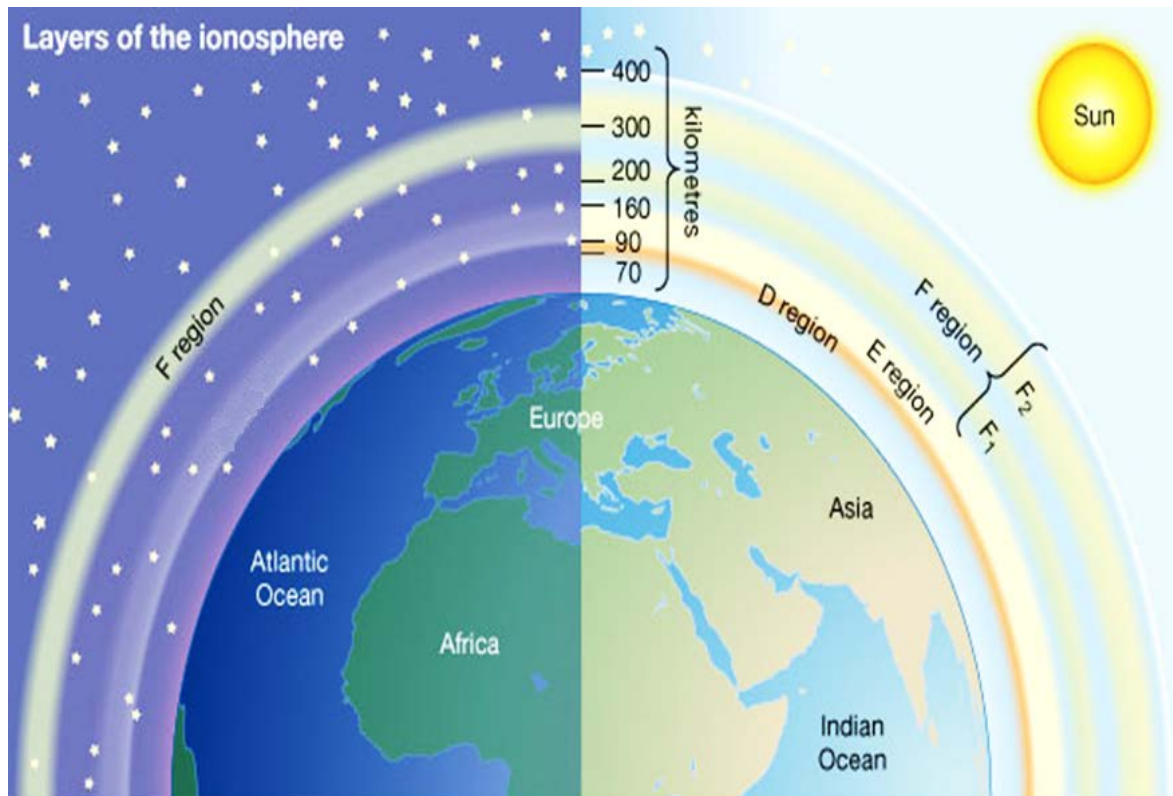


Figure 2.1: Diagrams showing the different layers of the upper atmosphere of the Earth from bottom to top: troposphere–stratosphere–mesosphere–thermosphere [Image: www.ucar.edu].

2.1.2 Ionosphere and its Layers

Strictly speaking, the ionosphere is not a distinct layer like the others mentioned above. Instead, the ionosphere is a series of regions that share some of the volume of the mesosphere and thermosphere. Here, high-energy radiation from the Sun has knocked electrons loose from their parent atoms and molecules. Solar extreme ultraviolet radiation and electron precipitation are the two major sources of energy input for dissociation and ionization into the thermosphere and ionosphere. Photoionization by solar radiation is the main source of plasma in the low-latitude ionosphere whereas ionization by energetic particle impacts the neutral ionosphere at high latitudes. The electrically charged atoms and molecules that are formed in this way are called ions, giving the ionosphere its name and endowing this region with some special properties. The ionosphere extends from about 60 to 1000 km, and its vertical structure is divided into several layers depending upon the local time of day. Specifically, the electron density profile variation exhibits three main layers, the D, E and F-regions as shown in the figure below (Figure 2.2). During the daytime, the F layer further splits into the F1 and F2-layers whereas, during the nighttime, the D and E layers disappear. The different layers are characterized by a density maximum at a certain altitude and a density decrease with altitude on both sides of the maximum [*Schunk and Nagy, 2000*].



© 2012 Encyclopædia Britannica, Inc.

Figure 2.2: Diagram describing the development of the ionospheric layers during day and night [Image: *Encyclopedia Britannica, Inc.*].

- The D-Layer: This is the lowest part of the ionosphere which ranges from about 60 to 90km. It appears only during day-time and is controlled by the ionization of neutrals by solar X-Rays and cosmic rays. The D layer is normally not dense enough to reflect radio waves. The dynamics of the D-region are mostly dominated by the neutral atmosphere. N_2 , O_2 and O created by chemical processes are the most abundant neutral species in this region. The electron concentration in the D-layer ranges from 10^7 to 10^{10} e^-/m^3 .

- The E-Layer: This layer was recognized first because of its reflective properties on radio waves used in telecommunications. This region is chemically dominated molecular ions such as N_2^+ , O_2^+ , NO^+ as its primary constituents and extends from ~90 km to 150 km altitude. The E region plasma is weakly ionized, and collisions between charged particles are not important. The electron concentration in the E-layer varies between 10^{10} and 10^{11} e^-/m^3 but drops to about 10^9 during the nighttime due to recombination processes.

- The F-layer: This is the permanent region of the Earth's ionosphere, with an altitude ranging from 130 to 1000 km. Major neutrals are N_2 and atomic oxygen O , the latter being the main constituent above 200 km. Therefore, ion production in the F-region is due to the ionization of atomic oxygen O by Far Ultra Violet (FUV) or extreme Ultra Violet (EUV) radiations.

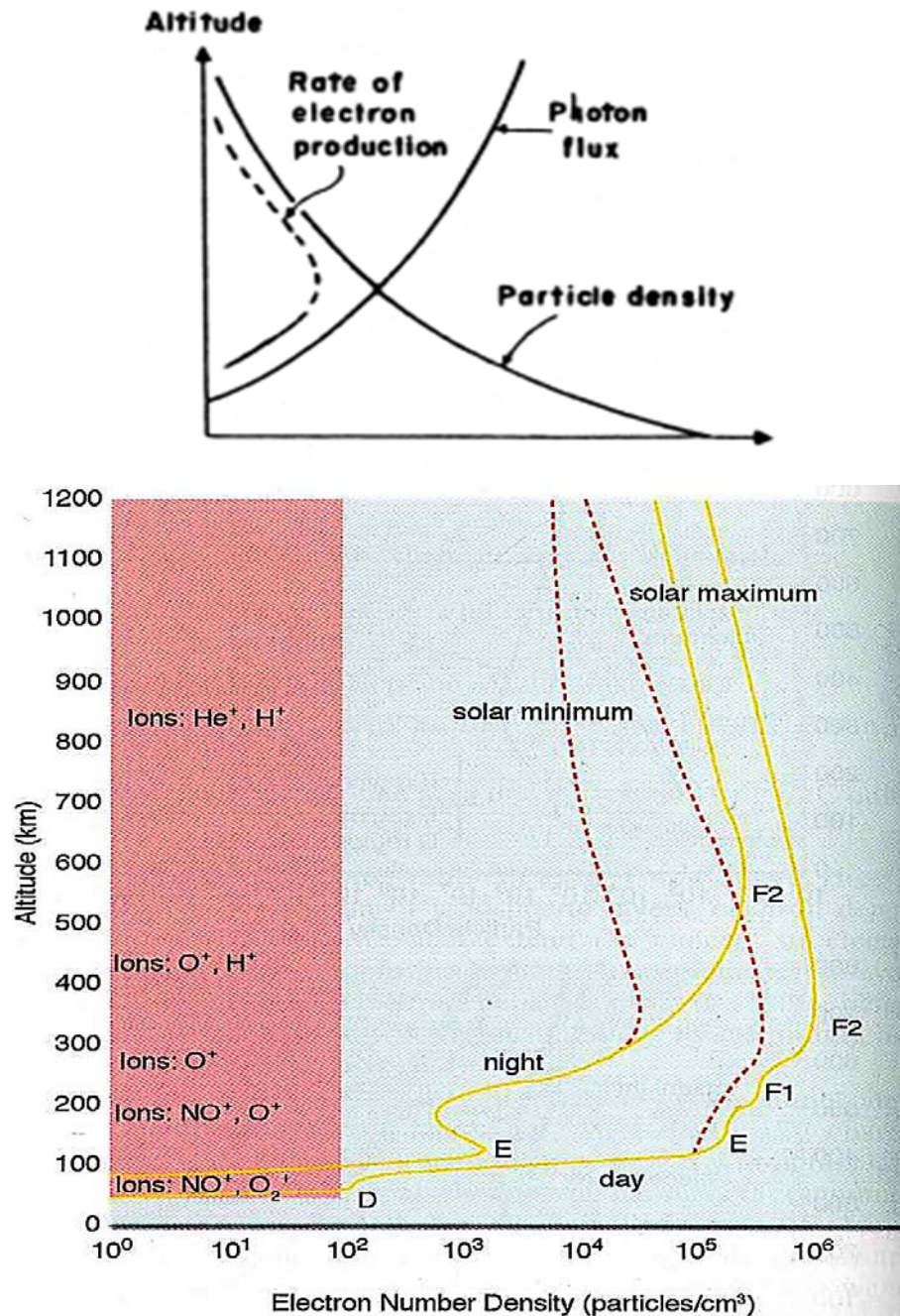


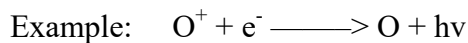
Figure 2.3: (a) The electron production rate with height as a function of the intensity/ photon flux of ionizing radiation as well as the density of the neutral gas particle. (b) Electron density profile of the equatorial ionosphere at noon and midnight for solar minimum and solar maximum conditions. Electron density of the F2-peak (250-300 km) is the largest value along the ionospheric profile and strongly depends on solar activity [Image: Knipp, 2011].

The F-region sometimes exhibits a double peak in the electron concentration N_e , corresponding to two sub-layers F1 and F2 showing specific photochemical reactions. In the F region (150-250km), ion-atom interchange and transport processes start to become important, and in the F2 region, the ionization maximum occurs as a result of a balance between plasma transport and chemical loss processes [Schunk and Nagy, 2000]. The plasma in this region is partially ionized, and collisions between the different charged particles and between charged particles and neutrals must be taken in to account [Schunk and Nagy, 2000].

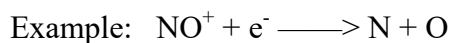
2.1.2 Chemistry of Layers

The Ionosphere is an excellent example of a natural laboratory for the study of atomic and molecular plasma processes. Absorption of Extreme Ultra Violet (EUV) radiation by thermospheric neutral species leads to photo-ionization in higher altitudes and Lyman- α and cosmic radiation in lower altitudes, which creates the bulk of the plasma that, makes up the ionosphere, a conducting layer at and above about 60km altitude. Types of ionospheric chemical reactions are [Solomon, 2017]:

Radiative Recombination

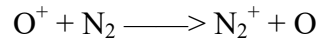
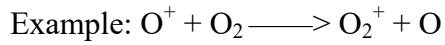


Dissociative Recombination



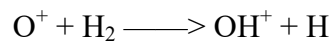
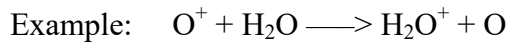
Charge Exchange

$WX^+ + YZ \rightarrow WX + YZ^+$; moderately fast, rate coefficients of the order of 10^{-10}
 $cm^3 s^{-1}$



Atom-Ion Interchange

$X^+ + YZ \rightarrow XY + Z^+$; rate depends on the strength of the YZ bond



N_2^+ , O_2^+ , and O^+ are the most abundantly produced ions in the Earth's ionosphere because N_2 , O_2 and O are the most abundant neutral species in the lower part of the thermosphere. However, the most abundant ions below 300 km are O^+ , NO^+ , and O_2^+ . Atom-ion interchange of O^+ with N_2 is very slow, due to the strength of the N_2 bond. This creates the high, dense, persistent "F₂ region" and much interesting ionospheric variability.

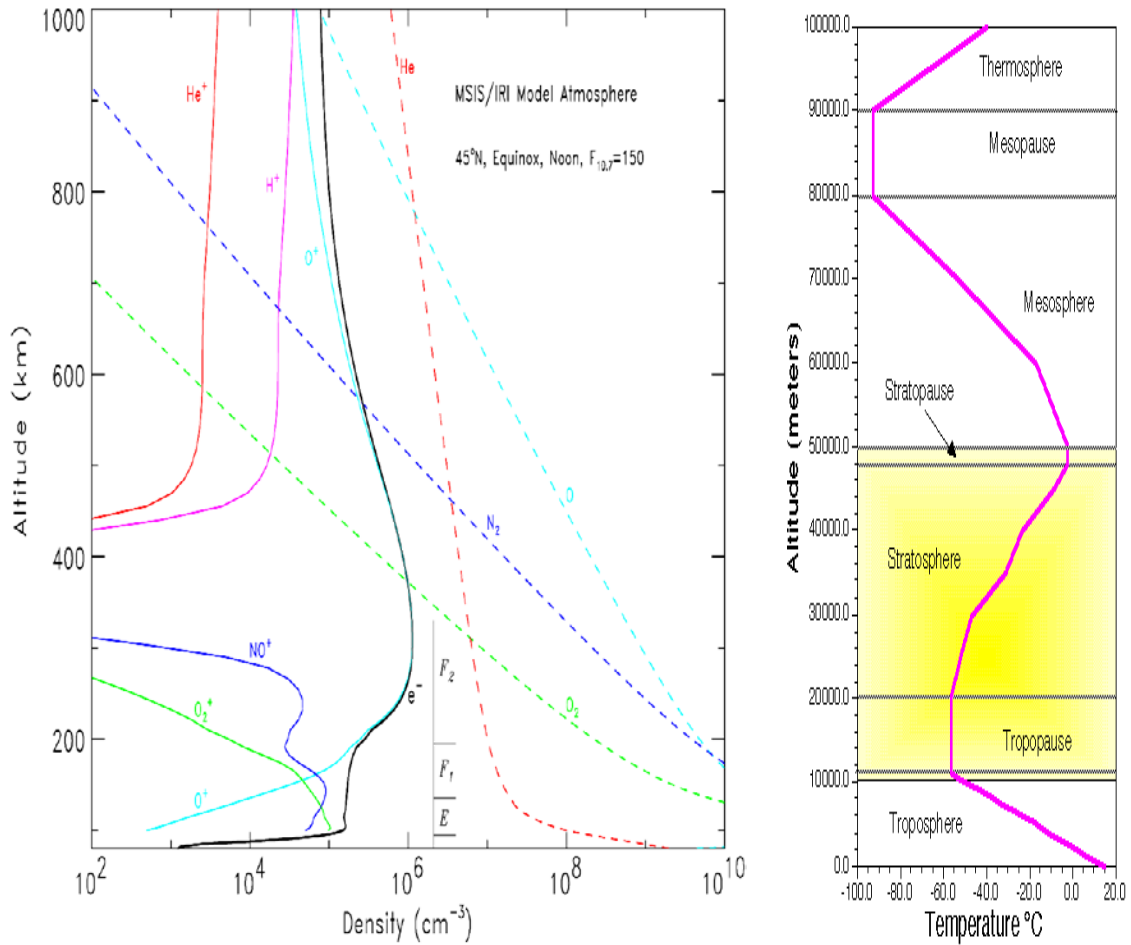


Figure 2.4: (a) Vertical profiles of the mixing ratio of selected species of constituents showing ionospheric chemistry. (b) Temperature profile against altitude in the Earth's atmosphere [Image: Solomon, 2017].

2.2 Features of the Low-latitude Ionosphere

The absorption of solar radiation in the ultra-violet and shorter wavelength bands by the Earth's upper atmosphere creates a layer of free electrons and ions between about 60 km to 1000 km altitude. The layer, called the ionosphere, is capable of influencing the propagation of radio waves [Rishbeth, 1988; Kelley, 1989; Schunk and Nagy, 2000]. The differential solar heating of the upper atmosphere, mainly the thermosphere on the day and night side hemispheres, creates horizontal pressure gradients. The resultant global neutral wind system effectively distributes momentum and energy within conducting layers and beyond [Rama Rao, 2006; Sridharan, 1998]. The electrodynamic process of the low-latitude ionosphere is governed by the movement of the electrically conducting upper atmosphere across the geomagnetic field by the thermospheric wind which in turn provides the mechanical energy for global scale dynamo action within $\pm 60^\circ$ latitudes [Sridharan, 1998]. The ionospheric electrodynamic process is highly variable in the low latitudes. This day to day variability of its processes has attracted the attention of scientists since more than a half century.

2.2.1 Equatorial Ionosphere

The equatorial and low latitude ionosphere is the region where the Earth's magnetic field lines are nearly horizontal. This uniqueness provides a constraint on the motion of the plasma particles that comprise the ionosphere and produces distinctive behavior in the equatorial ionosphere. Due to the unique configuration of the mutually perpendicular electric field (east-west), geomagnetic field (north-south) and electron density gradient (upward), the equatorial ionosphere is susceptible to very dramatic electrodynamic

effects [Rama Rao, 2006]. Some of the most important low latitude phenomena are: the equatorial electrojet, equatorial ionization anomaly, plasma depletions and enhancements (blobs). These phenomena are strongly latitude, longitude, temporal, season, solar cycle and, geomagnetic activity dependent [Fejer, 2015].

2.2.2 Structures in the Low-Latitude Ionosphere

The plasma instability in the low latitude is mainly driven by the combined effects of the geomagnetic field, ionospheric electric field, and vertically downward neutral wind in the presence of a vertically upward density gradient. This dissertation reviews the current state of understanding of equatorial plasma instabilities at low latitudes and the general properties of the irregularities to study their relationship to possible seeding mechanism.

A few widely recognized categories of ionospheric irregularities are listed below:

- Sporadic E-Layers:

This is an enhancement of the E region ionization for a short period that can be observed at all latitudes and is highly variable in space and time. The origins and causes of sporadic-E occurrence change with the geomagnetic region considered. For example, E_s occurrence in the equatorial region seems to be correlated with the equatorial electrojet, in mid-latitude with the wind shear and polar E_s are associated with auroral corpuscular bombardment (energetic electron precipitation from the magnetosphere). At equatorial latitudes, gradient instabilities also play an important role in creating sporadic E layers, while at high latitudes they can be created by convection electric fields [Schunk and Nagy, 2000]. They have been well studied with backscatter radars and ionosondes, which

allowed deriving not only occurrence statistics but also physical properties such as their plasma frequency f_0E_s , virtual height $h'E_s$, or thickness of the layer [Wautelet, 2013].

- Spread-F Layers:

Equatorial spread F is a spectacular phenomenon of a plasma instability in which the equatorial region ionosphere is restructured after sunset with rising plumes of low ionization. These plasma instabilities occur over a broad range of time and length scales, spanning several orders of magnitude that make the ionospheric F region an excellent place to test new plasma and fluid turbulence theories. These plasma irregularities have become important to us because of their tendency to interfere with the operation of space borne and ground based technological systems. Specifically, a signal emitted from a source above the Earth's atmosphere interacts with the ionosphere as it travels through space to the receiving point, usually a receiving station on the ground [McDaniel, 1998; Wautelet, 2013].

- Traveling Ionospheric Disturbances (TIDs):

Wave-like fluctuations of the ionospheric electron density are induced by internal atmospheric gravity waves (AGWs) in the neutral atmosphere are called TIDs [Yeh and Liu, 1974]. They are understood to be the signature of AGWs in the ionospheric plasma. Here, the ionosphere plays the role of a passive tracer. In the F-layer, neutral density is very weak, and charged particle motion is mapped along the magnetic field lines. The passage of an AGW modifies the charged particle height with up/down motions, which implies different recombination rates, and translates into changes in f_0F_2 , hF_2 and N_e

[*Wautelet, 2013*]. There are two classes of TID's: large-scale TID's characterized by higher speeds (400-1000 m/ s) and longer periods (0.5-3 hours) with wavelengths greater than 1000 km, and medium-scale TID's characterized by lower speeds (100-250 m/ s) and shorter periods (15 min-1 hour) with wavelengths of several hundred km [*Ogawa et al, 1987*]. TID's have been observed by various methods including vertical soundings, incoherent scatter radars, HF Doppler measurements, total electron content measurements by Faraday rotation, and in situ measurements of electron density [*Francis, 1975; Ogawa et al, 1987*].

- Space Weather, Storms, & Geomagnetic Disturbances:

Space weather refers to the variable conditions on the Sun and in the space environment that can influence the performance and reliability of space-borne and ground-based technological systems, as well as endanger life or health. Equatorial ionospheric storms result from modifications in the zonal electric field, meridional neutral winds, neutral gas temperature, and chemical composition [*Sastri et al., 2003*]. However, the most important contributor to the storm time behavior of the equatorial F region is the electric field disturbance. During quiet time, the equatorial ionosphere is largely controlled by the dynamo generated electric fields and the plasma fountain process associated with it, with the meridional winds acting as a modulator of field-aligned plasma transport associated with the fountain process [*Bailey et al., 1997*]. Storm time modifications in equatorial zonal electric fields fall into two broad categories, (1) the solar wind-magnetosphere dynamo, associated with prompt or direct penetration of the magnetospheric convective electric field [*Senior and Blanc, 1984; Spiro et al., 1988*] and (2) the ionospheric

disturbance dynamo field due to the global thermospheric wind circulation associated with Joule heating at high latitudes [*Blanc and Richmond, 1980; Sreeja et al, 2009*].

2.2.3 Equatorial Electrojet (EEJ)

The EEJ is an intense band of current flowing in the east-west direction with around a roughly $\pm 3^\circ$ latitudinal extent centered at the magnetic equator in the ionospheric E-region. It looks like a very simple ionospheric phenomenon but can be used to address several outstanding question in low latitude aeronomy. This phenomenon is mainly due to the electrodynamical process of a horizontally stratified ionosphere with anisotropic conductivities. This current is driven primarily by Sq current (as shown in Figure 2.5) due to the global scale hemispheric dynamo action of the neutral wind that meets at the equator and manifests as a primarily east-west electric field over the dip equator.

It is also responsible for the strong enhancement in the horizontal component (H) of Earth's magnetic field observed by magnetometers over the equator. This height is a strongly collisional regime that results in the generation of a vertical hall polarization field that, crossing with the east-west field is responsible for the generation of the EEJ. Figure 2.5 shows a longitudinal variability for enhancement of the eastward current jet.

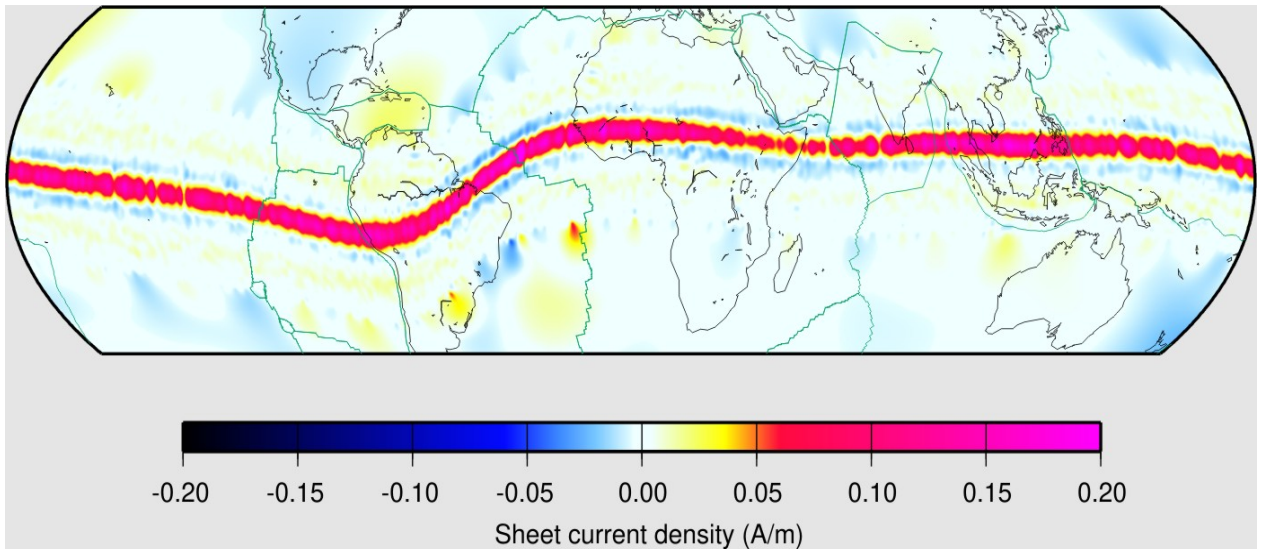


Figure 2.5: Electrojet current densities inferred from 2600 passes of the CHAMP satellite over the magnetic equator between 11:00 and 13:00 local time [Image: geomag.org].

2.2.4 Equatorial Ionization Anomaly (EIA)

The EIA is one of the prominent equatorial ionospheric/thermospheric processes. This process consists of the development of a double humped structure in the latitudinal profile of the F region plasma densities during daytime with the crest located at $\pm 15^\circ$ - 20° dip latitude and the trough situated over the dip equator [Sridharan, 1998]. The eastward electric field acts perpendicularly to the north-south geomagnetic field lines and gives rise to a vertically upward directed plasma motion. As the plasma rises, it encounters the horizontal lines of force of the Earth's magnetic field. The electrons diffuse along these field lines and reenter the main body of the ionosphere where the field lines cut through the F region, giving rise to large clumps of ionization at magnetic latitudes of ± 15 - 20° on either side of the magnetic equator as illustrated in Figure 2.6. These clumps are called the peaks or crests, and the low ionization region over the equator is called the trough of the equatorial or Appleton anomaly [Rama Rao, 2006].

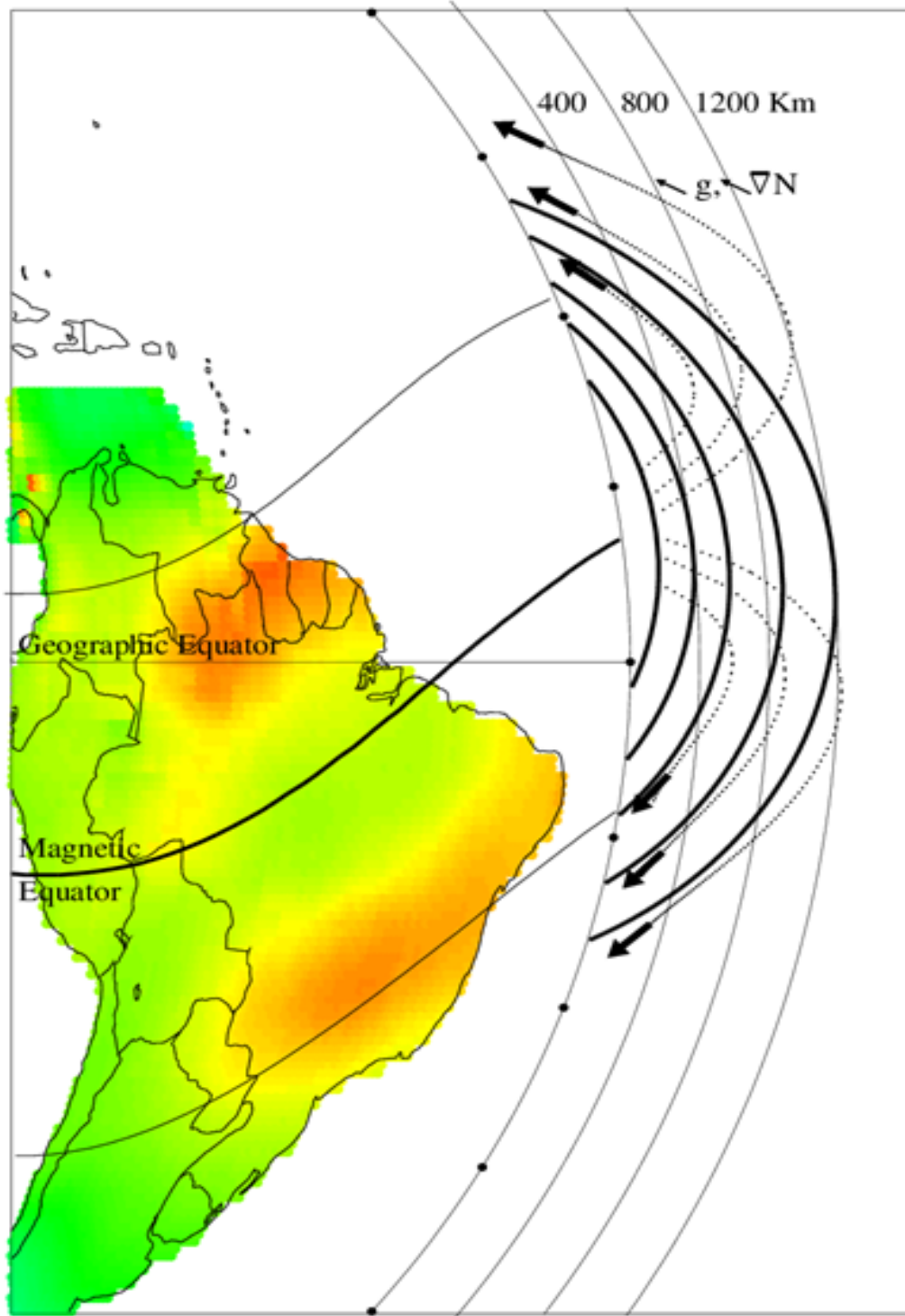


Figure 2.6: A typical example of an equatorial ionization anomaly in the American low latitude revealed by TEC data from the LISN GPS network.

2.2.5 Equatorial Spread-F, Plasma Bubbles and Plasma Blobs

In general, the postsunset plasma instabilities capable of generating diffuse echoes on ionograms that occur in the equatorial ionosphere are called equatorial spread F (ESF). The irregularities associated with ESFs occur over a broad range of time and length scales, spanning several orders of magnitude [Ossakow, 1981]. At night, a fully developed spread F is characterized by equatorial plasma bubbles (EPBs), which are vertically elongated wedges of depleted plasma that drift upward from beneath the bottomside F layer reaching altitudes as high as 1500km [Schunk and Nagy, 2000]. The development of large scale ESF irregularities is mainly driven by the Rayleigh-Taylor (RT) instability mechanism operating in the post sunset bottomside F-region. Plasma bubbles cause severe ionospheric turbulence at night in the equatorial F region. Bubbles are commonly produced in the bottomside of the F region and move into higher altitudes where they are detected with in situ satellite instrumentation [Kil et al., 2015].

Plasma blobs are another type of irregularity which are characterized by plasma density enhancements relative to ambient plasmas. Although bubbles and blobs have opposite characteristics, one phenomenon (bubble) has been understood as a cause and the other phenomenon (blob) as an effect [Kil et al., 2015]. The eastward electric field inside an EPB would push up high-density plasma at the EIA crest plasma density peak when the EPB flux tube reaches EIA latitudes. This would result in the occurrence of a blob just above the EPB flux tube [Le et al, 2003; Kim and Hegai, 2016].

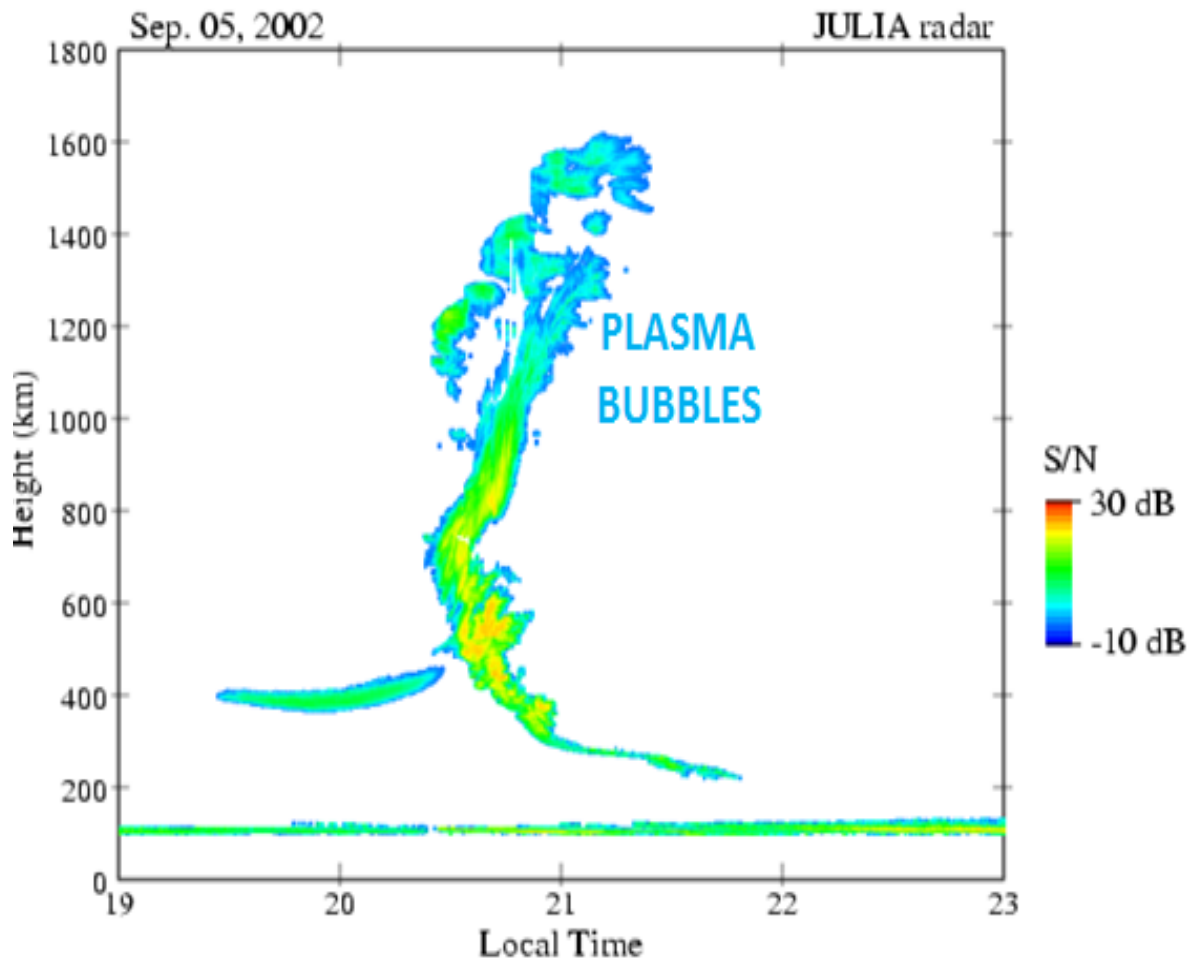


Figure 2.7: A signature of an equatorial plasma bubble recorded by the Jicamarca Incoherent Scatter Radar in the low latitude ionosphere.

2.3 Physics of the Equatorial and Low-Latitude Ionosphere

The unique geomagnetic field and electric field in the low latitude ionosphere have been drawing the attention of aeronomers and space scientists. Electric fields in the low and middle latitude ionosphere result from currents driven internally by neutral winds and gravity, and externally by applied potentials. The resulting internal electric polarization fields arise from the need to make the total current divergence free. By considering the current drivers many of the attributes of the observed ion and electron drifts can be understood including the E- and F-region dynamos, the initial growth of ionospheric depletions, and the effects at high latitudes [*Heelis, 2004*].

Solar radiation, an EM wave, is mainly responsible for the production of the ionospheric plasma. The interaction of EM waves with the ionosphere ranges from the collisionless regime to a highly collisional regime depending on the altitude. Above 150km the interaction is essentially collisionless, which means that the electron-neutral collision frequency is much lower than the ion gyrofrequency; the ion-neutral collision frequency is lower than the ion-cyclotron frequency. Below 150 km the process is collisional. The physical processes for wave absorption are very different in these two cases. A transition regime can be seen between the collisionless and collisional regimes [*Manheimer et al., 1997*]. Figure 2.8 illustrates the various regimes based on electron-neutral and ion-neutral collisions.

Ionospheric current diversion

Collisionless regime
Field-aligned current only

Weakly collisional regime
Field-aligned current starts diverting

Strongly collisional regime
Pedersen current carried by ions
Hall current carried by electrons

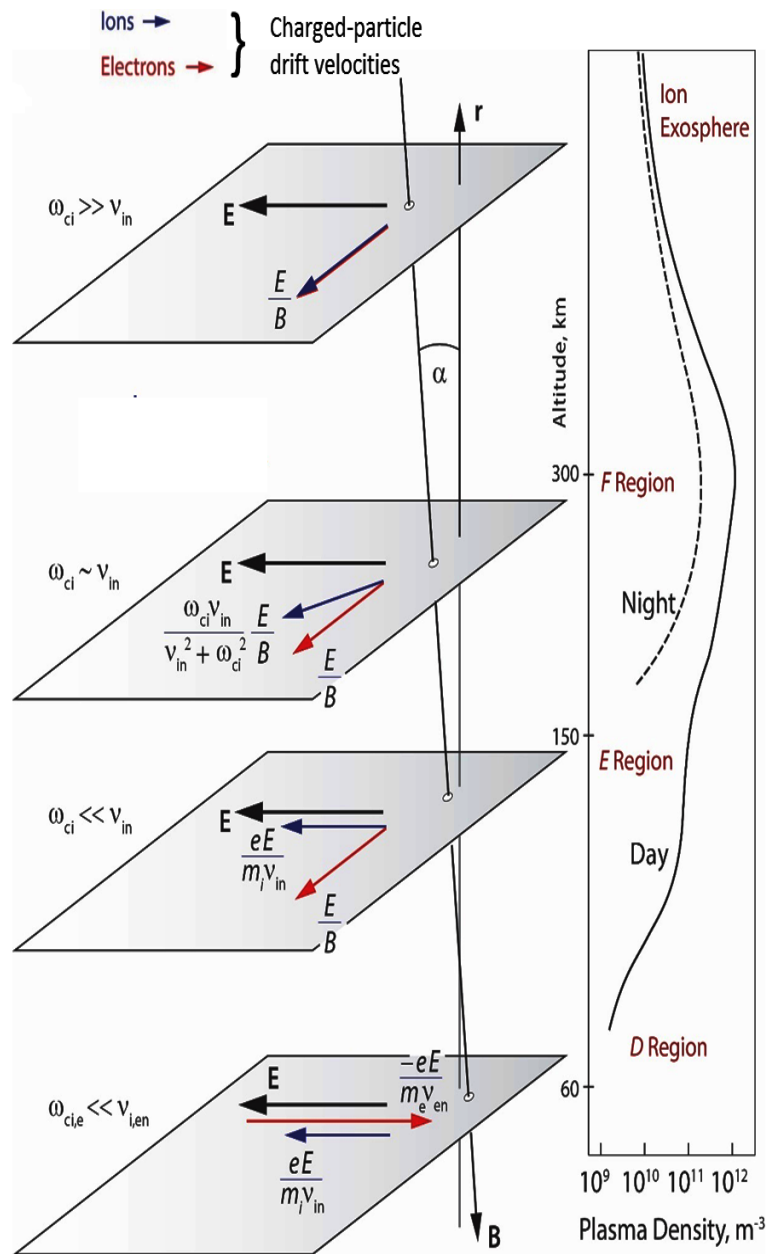


Figure 2.8: Different regions of the ionosphere showing the collisional and collisionless regime, and their coupling processes at high latitude. At equatorial latitudes, the geomagnetic field acts perpendicular to the zenith [Image adapted from Lotko, 2017].

Solar radiation sets up a global system of neutral winds that push the ionospheric plasma across magnetic field lines. Electric fields and currents are generated and these play an important role in the distribution of ionization. On the other hand, collisions between the neutral atmosphere and the ions, the ions and electrons, and the neutrals and electrons are the cause of the conductivity in the ionosphere. The ionospheric conductivity plays a major role in the electrodynamics of the F-region. These conductivities are Pedersen, Hall, and parallel conductivity. The conductivity parallel to the electric field, and perpendicular to the magnetic field, is called the Pederson conductivity. The conductivity perpendicular to both the electric and magnetic fields is called Hall conductivity, while the conductivity parallel to the magnetic field alone is defined as the parallel conductivity. The magnitudes of these conductivities as a function of altitudes are shown in Figure 2.9. The Pedersen and Hall conductivity decrease with increasing altitude, whereas the parallel conductivity increases continuously with altitude. The parallel conductivity is several orders of magnitude larger than both the Pedersen and Hall conductivities everywhere above 100 km. Therefore, ionospheric electric fields can be transferred along these lines virtually uninhibited [*Chapagain, 2011*].

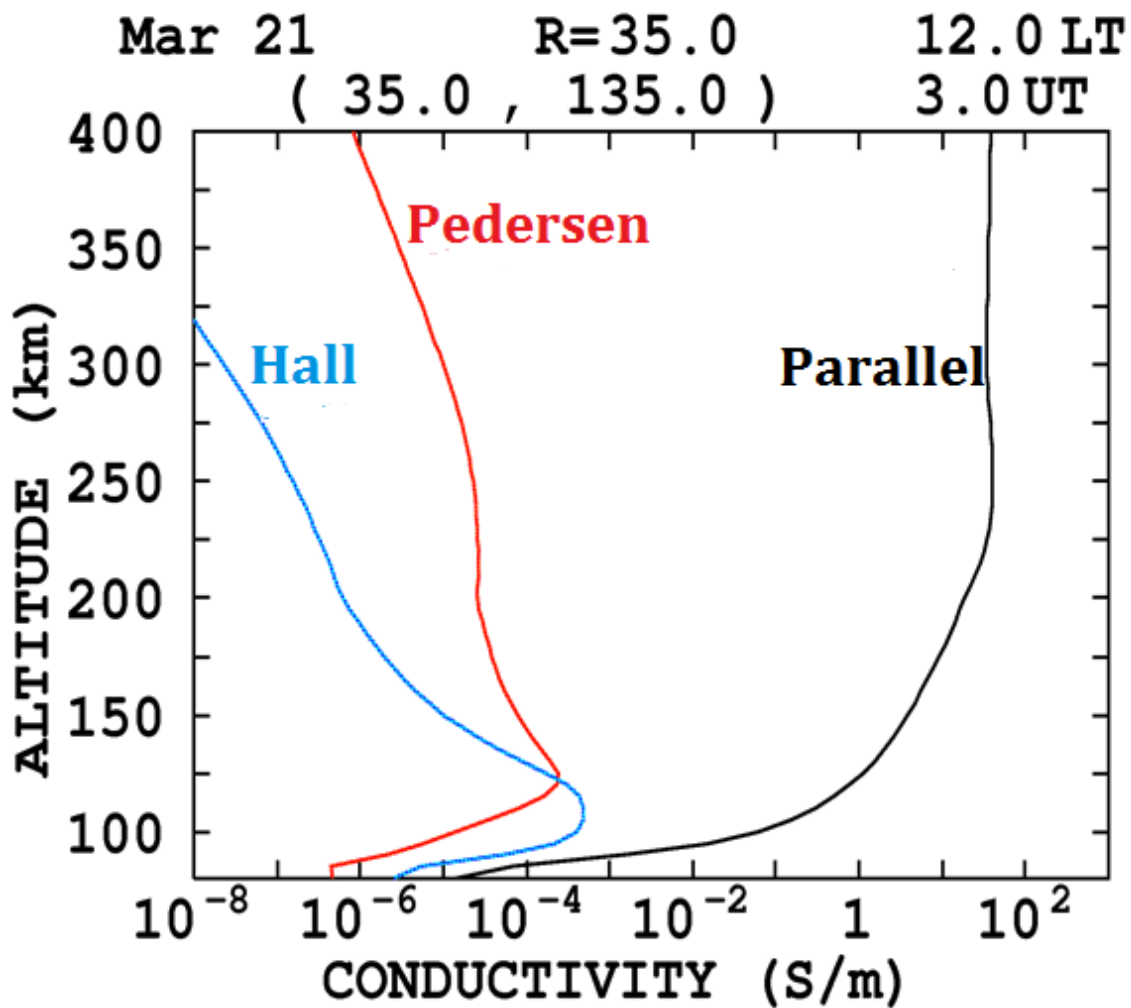


Figure 2.9: A comparison of daytime ionospheric conductivities (Parallel, Pedersen, and Hall) as a function of altitude in the location (35° N, 135° E) under the noon-time March equinox condition for low solar activity [Image: Yamazaki and Maute, 2017].

2.3.1 Wind Dynamo and Plasma Dynamics

The thermosphere is where the differential heating of the upper atmosphere results in the neutral winds, which in turn provide the mechanical energy for the global scale dynamo action and the generation of electric fields. These electric fields are responsible for a variety of electrodynamical processes including several plasma instabilities peculiar to the specific geographical location [Sridharan, 1998]. The ions and electrons in the E region are coupled to the neutral components of the atmosphere and follow their dynamics. Atmospheric winds and tidal oscillations of the atmosphere force the E region ion component to move across the magnetic field lines, while the electrons move more slowly, perpendicular to both field and the neutral wind. The relative movement creates an electric current, and the separation of charges produces an electric field, which in turn affects the current. Because of this, the E region bears the name dynamo layer, the generator of which is the atmospheric wind motion. The current system created by this tidal motion of the atmosphere is called the solar quiet or Sq current. The Sq system forms two vortices, one in the northern and the other in the southern hemisphere, which touch each other at geomagnetic equator [Baumjohann & Treumann, 2012].

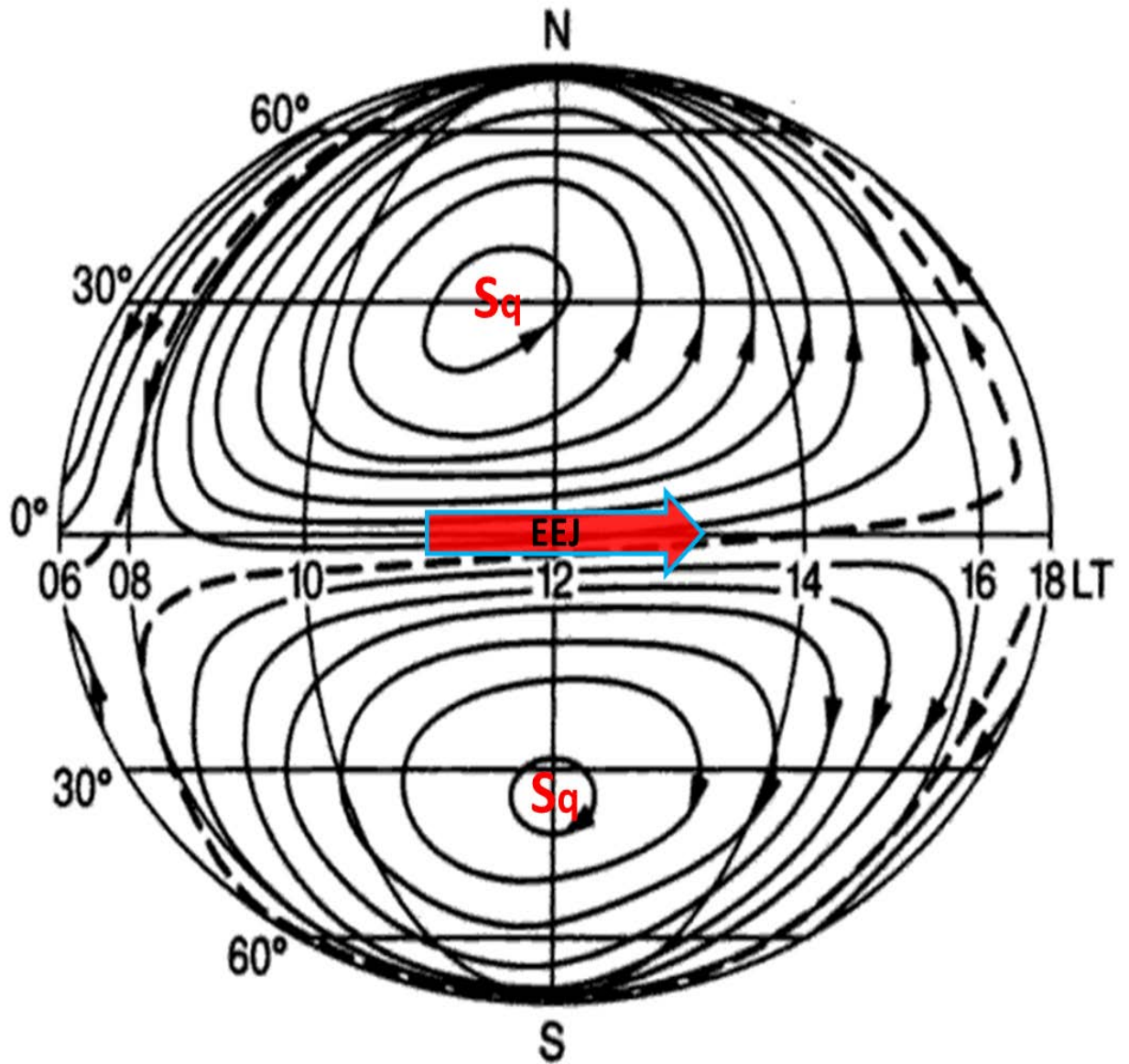


Figure 2.10: Ionospheric dynamo driven by the average Sq current system in which the tidal neutral wind system in the ionospheric dynamo layer acts as the driving force [Image adapted from *Baumjohann & Treumann, 2012*].

2.3.2 Ionospheric Currents and Electric Fields

The ionospheric currents cause a large part of the variation of the geomagnetic field, although most of the geomagnetic field itself is generated by the dynamo action in the Earth's core. The currents flow according to the Ohm's law, but the electric conductivity is anisotropic because of the effect of the geomagnetic field. The atmospheric solar tides represent a major contribution to the climatology of the electrojet region [Forbes, 1981]. At the geomagnetic equator, the Sq current system of the southern and northern hemispheres touch each other and form a jet like current in the ionosphere called the electrojet. The special geometry of the magnetic field at the equator, together with a nearly perpendicular incidence of solar radiation, cause an equatorial enhancement in the effective conductivity, which leads to an amplification of the jet current [Baumjohann & Treumann, 2012].

The mechanism of current amplification can be explained as follows. The primary Sq Pedersen current ($\sigma_p E_y$) flows eastward (e.g. in Figure 2.10), parallel to the primary ionospheric current. This primary electric field drives a Hall current ($\sigma_h E_y$) which flows vertically downward causing charge separation in the equatorial ionosphere and creates polarization electric fields (E_z). The polarization electric field drives a vertical Pedersen current ($\sigma_p E_z$) opposing the Hall current until it compensates for it. The secondary polarization electric field generates a secondary Hall current ($\sigma_h E_z$). The total current in the eastward direction consists of the sum of the primary Pedersen current ($\sigma_p E_y$) and the secondary Hall current ($\sigma_h E_z$). The conductivity associated with this total current is called Cowling conductivity (σ_c) and equal to $(\sigma_p) + (\sigma_h)^2 / (\sigma_p)$.

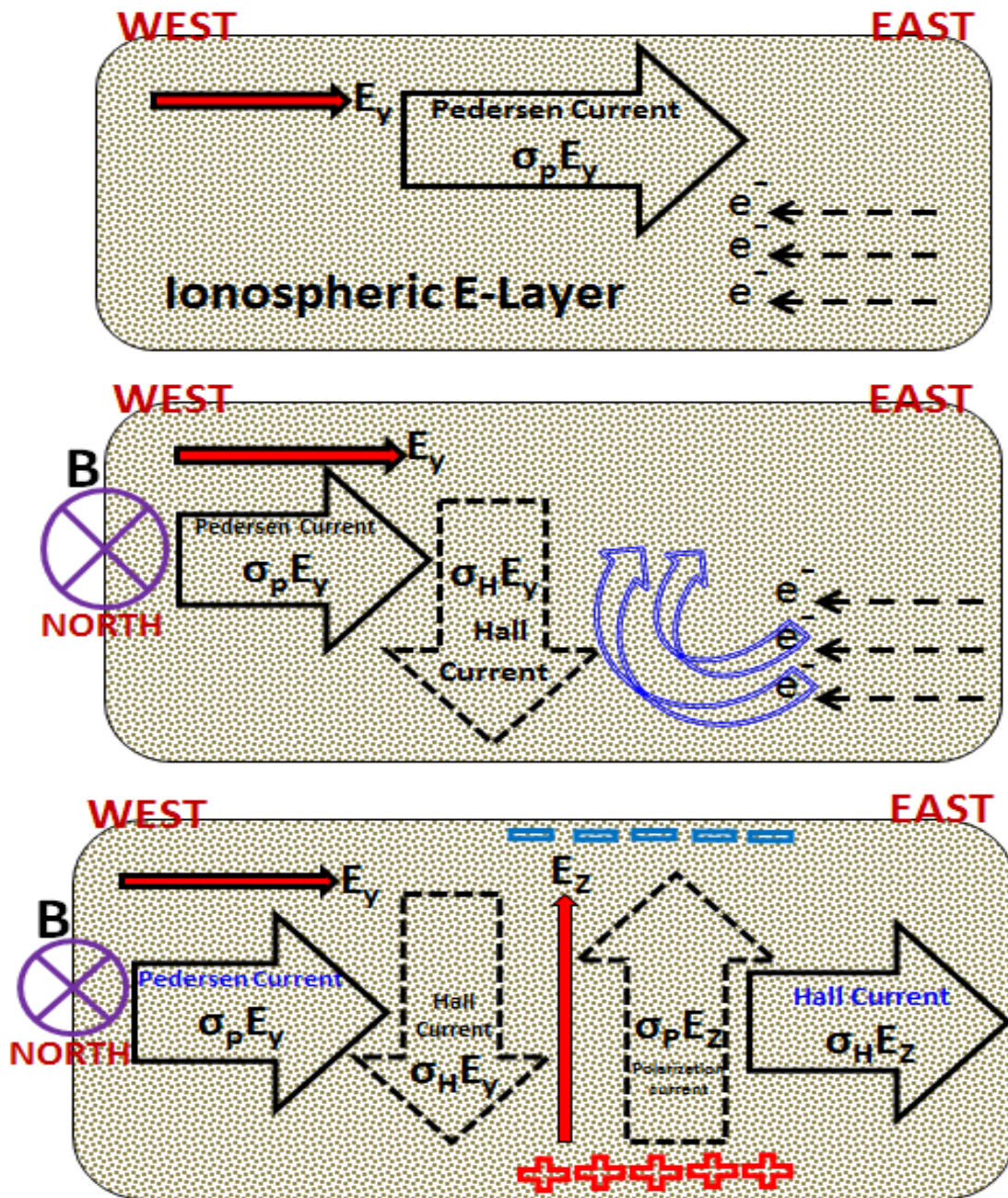


Figure 2.11: Mechanism of the amplification of eastward electric field to form equatorial electrojet current during noon.

Cowling conductivity is higher than Pedersen conductivity, which explains the amplification and concentration of the equatorial electrojet current [Baumjohann & Treumann, 2012] above the equator as shown in figure 2.11.

2.3.3 Equatorial Plasma Fountains

The ExB vertical plasma drift in the daytime raises ionized plasma near the geomagnetic equator to great heights, where recombination take place at a slower pace. As it reaches a certain height, the plasma diffuses down along the magnetic field lines and moves away from the equator under the action of the pressure gradient and gravity. This process will ultimately dump additional plasma either side of the geomagnetic equator forming two crests about $\pm 15^\circ$ to $\pm 20^\circ$ latitude regions. These combined phenomena of electromagnetic drift and diffusion produce a fountain-like pattern of plasma motions. This phenomenon is referred to as the fountain effect or the equatorial fountain [Pfaff, 2012]. This abnormal ionization distribution is termed the equatorial ionization anomaly or Appleton anomaly. The equatorial anomaly usually starts to build up at 11:00 am, with a maximum about 14:00 local time (LT), and a second often larger peak, occurring in the late evening. The latitude of the peak electron density formations is often not symmetric about the magnetic equator because of plasma transport along the magnetic field lines produced by an interaction with the neutral winds [Chapagain, 2011]. Basically, there are two competing mechanisms for the asymmetric formation of the equatorial anomaly a) Intra-hemisphere Transport, and b) Trans-equatorial Transport [Khadka et al., 2018]. As the meridional neutral wind crosses the equator, it will drive plasma to higher ionospheric heights along field lines where recombination proceeds at a slower pace. This leads to

higher plasma density in the windward direction than that of leeward direction. Also, the trans-equatorial neutral winds usually cause the plasma to be pushed from the one hemisphere to the other hemisphere as there is a weak fountain. These two processes are the reason behind the asymmetrical form of equatorial anomaly peaks between the two hemispheres.

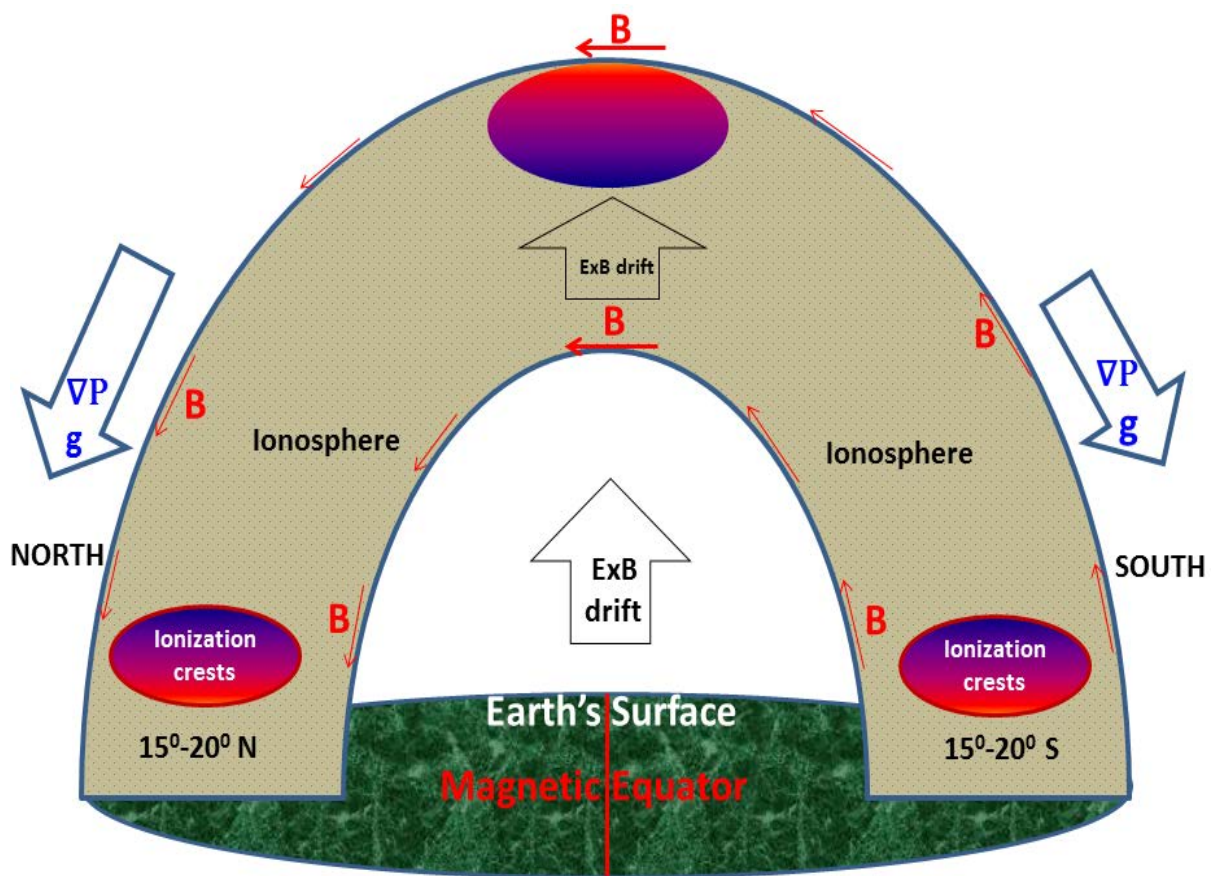


Figure 2.12: Mechanism of the plasma fountain effect for the generation of the equatorial ionization anomaly in the low latitude ionosphere.

2.3.4 Pre-Reversal Enhancement (PRE)

Gradients in the neutral wind-driven currents and E region conductivities generate polarization electric fields, causing the ionospheric plasma to drift primarily in the direction of the E region tidal neutral winds. These polarization electric fields in the low-latitude ionosphere cause plasma near the magnetic dip equator to rise during the day under an eastward zonal component of the electric field and descend during the night [Eccles *et al*, 2015]. The eastward daytime electric field in the E and F regions of the equatorial ionosphere often shows a significant and fairly sharp increase just before it reverses to its nighttime westward direction [e.g., Balsley, 1973; Fejer *et al.*, 1979; Fejer, 1981, Farley *et al*, 1986]. Near sunset, a brief and intense uplift of the electric field, which results in a height increase in the equatorial ionosphere and an increase in the growth rate of the generalized Rayleigh-Taylor instability (RTI), is called the pre-reversal enhancement (PRE) [Kelley *et al*, 2009a]. The PRE can help to initiate the RTI, which may generate small scale structure such as equatorial spread F. The magnitude of this prereversal enhancement depends upon various factors such as season, level of magnetic activity, and phase of the solar Cycle [Farley *et al*, 1986].

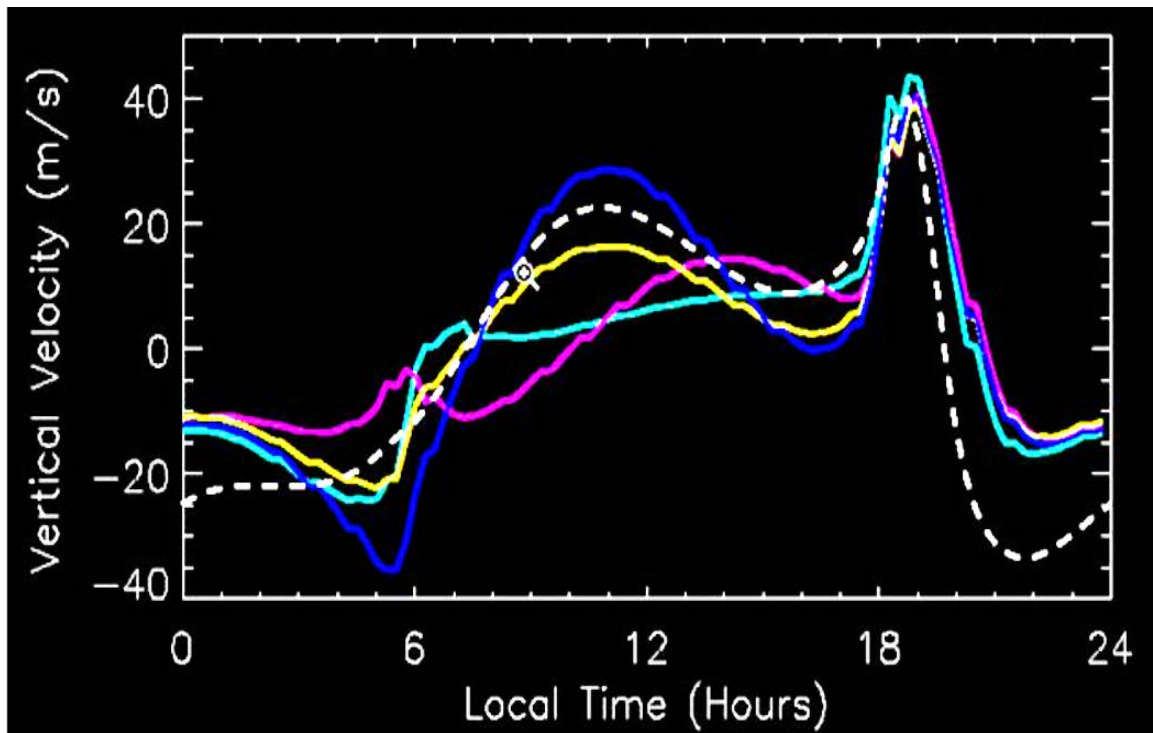


Figure 2.13: The PRE signatures are seen as strong vertical plasma drift at dusk near low latitude ionosphere [Image: <http://slideplayer.com>].

2.3.5 Rayleigh-Taylor Instability (RTI)

The RT instability is the instability of an interface between two fluids of different densities in which a heavier fluid is resting on top of a lighter fluid within a gravitational field [Rayleigh 1880; Taylor 1950; Dungey, 1956; Ott, 1978]. Any fluctuation at the fluid interface allows gravity to pull the high-density fluid downwards so that the low-density fluid ends up on top and an interchange of the two fluids takes place. More generally, Figure 2.14 shows a schematic diagram the classical and simple configuration for the Rayleigh- Taylor instability.

The primary source by which this instability is triggered is a gravitational force acting on an inverted density gradient (a heavy fluid supported by a light fluid) [Chakrabarti and, Lekhina, 2003]. The gravitational force is downward, antiparallel to the density gradient, and the magnetic field is horizontal, into the paper (Figure 2.14). As small perturbation (δE) is triggered in a current system $\mathbf{g} \times \mathbf{B}$. These fields, in turn, cause an upward $\delta E \times \mathbf{B}$ drift of plasma in the region of plasma depletion and a downward drift in the region where density is high. Lower (higher) density plasma is therefore advected upward (downward), creating a large perturbation, and the system becomes unstable. In the ionospheric case, the light fluid is the low density plasma which carries a gravity driven current that provides the $\mathbf{J} \times \mathbf{B}$ force, preventing the plasma from freely falling [Kelley, 2009a]. Additionally, the onset of ESF may also be affected by the breaking of gravity waves propagating upward from the lower altitude and by electric field perturbations of high latitude origin during magnetically disturbed conditions.

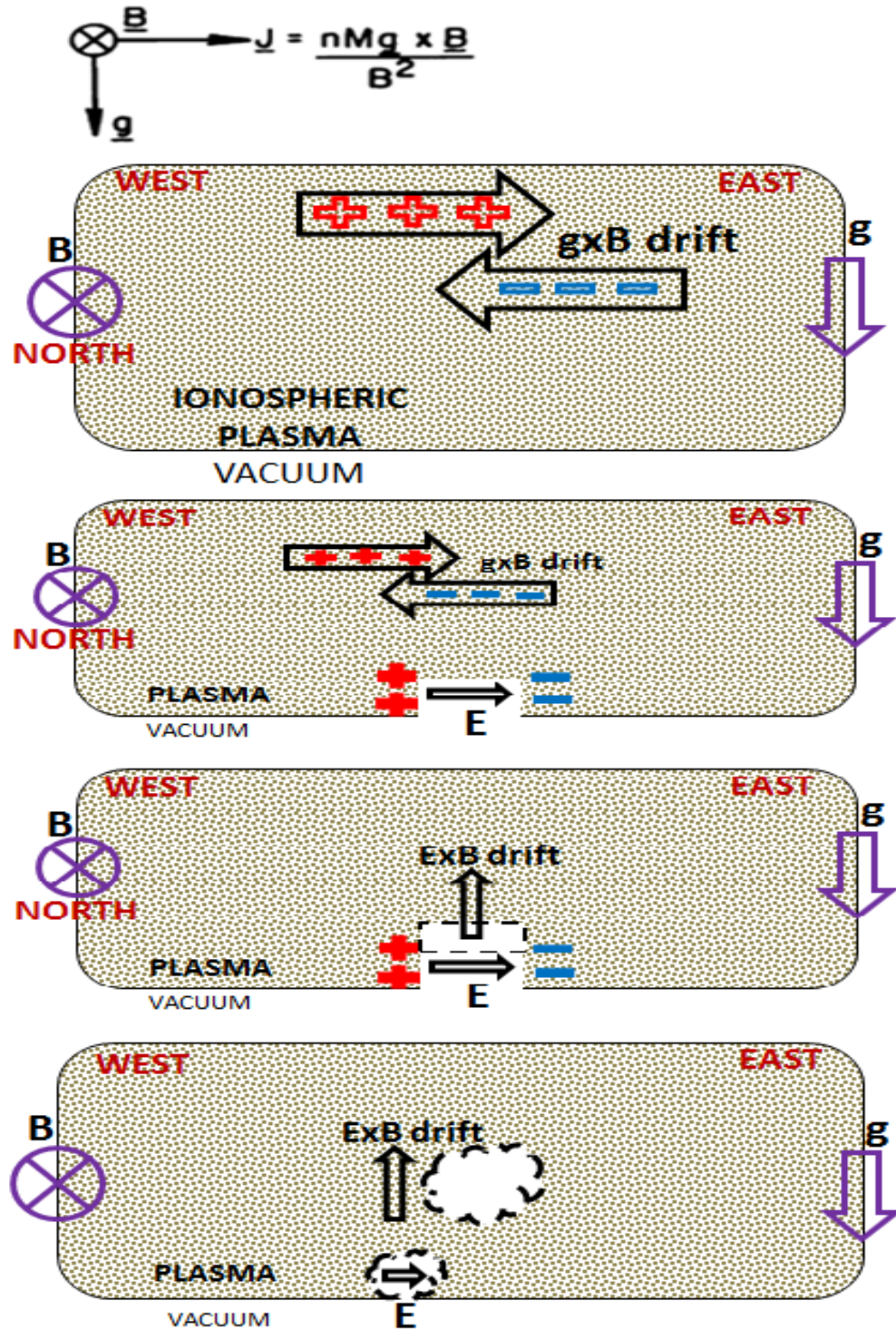


Figure 2.14: Diagram illustrates the mechanism of the Rayleigh Tylor instability that shows how the plasma bubble form in the low latitude ionosphere.

On the other hand, there are several processes, such as meridional neutral winds, electric field shear effects, diffusion, and E-region conductivity, which inhibit the growth of the irregularities [Chapagain, 2011]. A further explanation of the RTI instabilities is given in Chapter 6 as well.

Further, a strong vertical plasma density gradient at the bottomside of the F layer and a strong upward plasma drift during the night combine to destabilize the plasma [Carter, et al., 2016]. Rayleigh-Taylor instability can be triggered whenever a certain geometric relationship holds between the electron density gradient in the equatorial ionosphere and the forces acting on the plasma [Zalesak and Ossakow, 1982]. The linear growth rate γ of the generalized R-T instability was derived by Zalesak and Ossakow [1982] for an infinitesimal perturbation on the system. Later, the R-T linear growth rate is adapted by Sultan [1996], and further reconstructed by Gentile et al. [2006] and Carter, et al. [2016] as

$$\gamma_{\text{RT}} = \frac{\Sigma_p^F}{\Sigma_p^E + \Sigma_p^F} \left(V_p - U_L^p - \frac{g_e}{v_{\text{eff}}} \right) K^F - R_T,$$

where the first term V_p is the upward plasma drift speed, the second term U_L^p is the Pedersen conductivity-weighted neutral wind perpendicular to the magnetic field in the magnetic meridian plane, and the third term g_e/v_{eff} is the altitude-corrected gravity divided by the flux tube integrated effective ion-neutral collision frequency, weighted by the electron density. These terms are multiplied by the flux tube integrated F (Σ_p^F) and E region (Σ_p^E) Pedersen conductivity ratio and K^F , which is the F region flux tube electron

content height gradient (i.e., $1/N_e(\partial N_e/\partial h)$, where N_e is the flux tube electron content).

Finally, R_T is the flux tube integrated recombination rate.

Chapter 3

INSTRUMENTATION AND METHODOLOGY

Contents	Page
3.1 Remote Radio Wave Techniques.....	49
3.1.1 Radar.....	50
3.1.2 GPS: Basic Concepts.....	55
3.1.2.1 Total Electron Content (TEC) Measurement.....	60
3.1.2.2 Ionospheric Scintillations Measurement.....	62
3.1.3 Vertical Sounders (Ionosondes).....	65
3.2 Magnetic Sensors and Optical Techniques.....	71
3.2.1 Magnetometer.....	71
3.2.2 Fabry Perot Interferometer.....	75
3.2.2.1 SOFDI.....	78
3.3 In-situ Techniques.....	79
3.3.1 SWARM Satellite Constellation.....	79
3.3.1.2 Objectives of SWARM Satellite Mission.....	80

This chapter reviews the basic techniques for studying the terrestrial ionosphere, with particular emphasis on the principles, capabilities, and limitations of the techniques when they are used to probe the low-latitude ionosphere. The low-latitude ionospheric electrodynamics can be probed by using several techniques from the ground as well as from space. For Shuttle/ Spacelab mission communication and navigational applications, the ionosphere is a natural laboratory for studying complex processes that occur near Earth and throughout the universe. Although the existence of conducting layers of the upper atmosphere had been suggested by *Balfour Steward in 1882*, the first remote radio

sensing of the Earth's ionosphere started in late 19th to the beginning of 20th century [Appleton's Nobel Prize Lecture, 1947]. Radio probing experiments of the ionosphere by Guglielmo Marconi in 1901 and frequency change experiment by *Appleton and Barnett in 1925* laid stepping stones in probing the ionosphere. Understanding the ionosphere is very important in this modern era to investigate space weather related phenomena and their impact on machinery as modern civilization is highly dependent on technological systems. In this dissertation work, we use various instruments for active sensing of the upper atmosphere using both ground-based and satellite-borne radars that are categorized under radar techniques, magnetic sensor techniques, optical technique, and in-situ techniques in following sub-sections. The essential physical parameters of the ionosphere which have been studied extensively over the half century are 1) the density and temperature of both ionized and neutral particles; 2) the chemical composition of the ionized and neutral particles; and 3) the electric and the magnetic field [Bauer and Nagy, 1975]. We present the principles and a description of the instruments in this dissertation, whose data are shown and used to study ionospheric electrodynamics. Additionally, space weather impacts on space-based technologies in the equatorial and low latitude sectors are also explained.

3.1 Remote Radio Wave Techniques

The remote sensing of the ionospheric plasma density and temperature profiles with observations of the solar irradiance at altitudes above ionosphere enables studies of the physics and chemistry that govern the formation of the ionosphere and its characteristics. Coupling the observation with magnetospheric satellite observation enables studies of

magnetospheric dynamics. The two main active remote sensing instruments used for observing the ionospheric plasma density are ionosondes and scatter radars.

Active remote sensing of the ionosphere is essential not only for understanding the basic physics of this near-space region but also for predicting the impacts of space weather events on our technology-dependent society. Active remote sensing through planetary radar astronomy continues to make important contributions to our understanding of the solar system, planning for space missions to extraterrestrial objects, and in particular for the tracking and characterization of near-Earth asteroids that may pose a threat to society. Radio waves reflect and scatter from discontinuities in the index of refraction of the medium in which they propagate. In the upper atmosphere, the primary source of such discontinuities is gradients of the plasma density. Hence, upper atmospheric active remote sensing is primarily sensing of the ionospheric plasma. It is, however, possible to study both the magnetosphere and the neutral atmosphere using those ionospheric observations. Ion-neutral collisions produce measurable effects in radar returns. At altitudes where those effects are significant, it is possible to estimate thermospheric properties from the plasma observations [*National Academies of Sciences, Engineering, and Medicine, 2015*].

3.1.1 Radar

The incoherent scatter radar (ISR) technique, since its introduction in the early 1960's, has proved to be the most used and powerful ground-based remote sensing technique which can provide the most information about the terrestrial ionosphere than any other technique [*Hunsucker, 1991, Gordon, 1958*]. Using incoherent scatter technique, vertical

electron density profiles, electron and ion temperatures, ion composition and photoelectron flux, the ionospheric electric field and a variety of other parameters can be measured [Venkatesh, 2013]. It is a ground based radio techniques which can provide the most information of the terrestrial ionosphere during calm as well as extremely perturbed case.

Here, we used data from the Jicamarca incoherent and coherent scatter radar observations located near the geomagnetic equator. ISRs are single-frequency radars that observe backscatter from thermal fluctuations of the plasma at altitudes between 90 to 3000 km with significant density up to the point where returns become too weak to detect. These observations, when coupled with the well-developed theory of incoherent-scattering from plasmas, provide altitude profiles of a number of parameters, including plasma density, plasma temperature, plasma velocity, ionic composition, and ion-neutral collision frequency. ISRs provide detailed high-fidelity information at a few strategic locations [National Academies of Sciences, Engineering, and Medicine, 2015]. Moving upward from the ground, strong collisions between the ionized and neutral constituents in the lowest altitude region become weaker and weaker in the topside of the ionosphere. Especially, the region between collisional to collisionless is a natural laboratory for the study of plasma behavior.

The ISR theory that needs to be understood is the concept of ‘coherent’ vs. ‘incoherent’ scattering. Incoherent scattering applies to the specific case where the dynamics of individual electrons can be considered completely independent of the rest of the particles.



Figure 3.1: The main radar antenna in Jicamarca Radio Observatory (JRO), Peru, one of the largest of all the incoherent scatter radars (ISRs) in the world where the magnetic dip angle is about 1° . The main antenna consists of a 300m x 300m square array composed of 18,432 cross-polarized dipoles.

In this case, no collective feature in the spatial distribution of electrons may be produced and maintained by the random motions of electrons [Akabari et al. 2017].

In general, the spectrum of the scattered signal consists of two parts, one due to the ions and other due to electrons. If the radar wavelength is much smaller than the Debye length, the scattered energy is entirely due to the electronic component. On the other hand, for radar wavelengths much larger than the Debye length, the largest part of the scattered energy resides in the ionic component. The electron and ion temperatures and other parameters can be measured [Dougherty and Farley, 1960; Evans, 1969], by using various properties of the received spectrum.

In the ionosphere, a purely incoherent scattering only occurs when the ISR probing wavelength is smaller than the Debye length [Dougherty and Farley, 1960, Bhatt, 2010]. At spatial scales greater than the Debye length, however, the motions of individual electrons are affected by the electrostatic fields of other charged particles, such that the collective behavior of particles acquires ‘self spatio-temporal coherence’ in the form of plasma waves. Such coherent behavior, in turn, introduces constructive interference in the scattered fields from individual electrons and leads to the concentration of the spectral power into narrow resonant peaks whose characteristics are determined by the corresponding plasma waves.

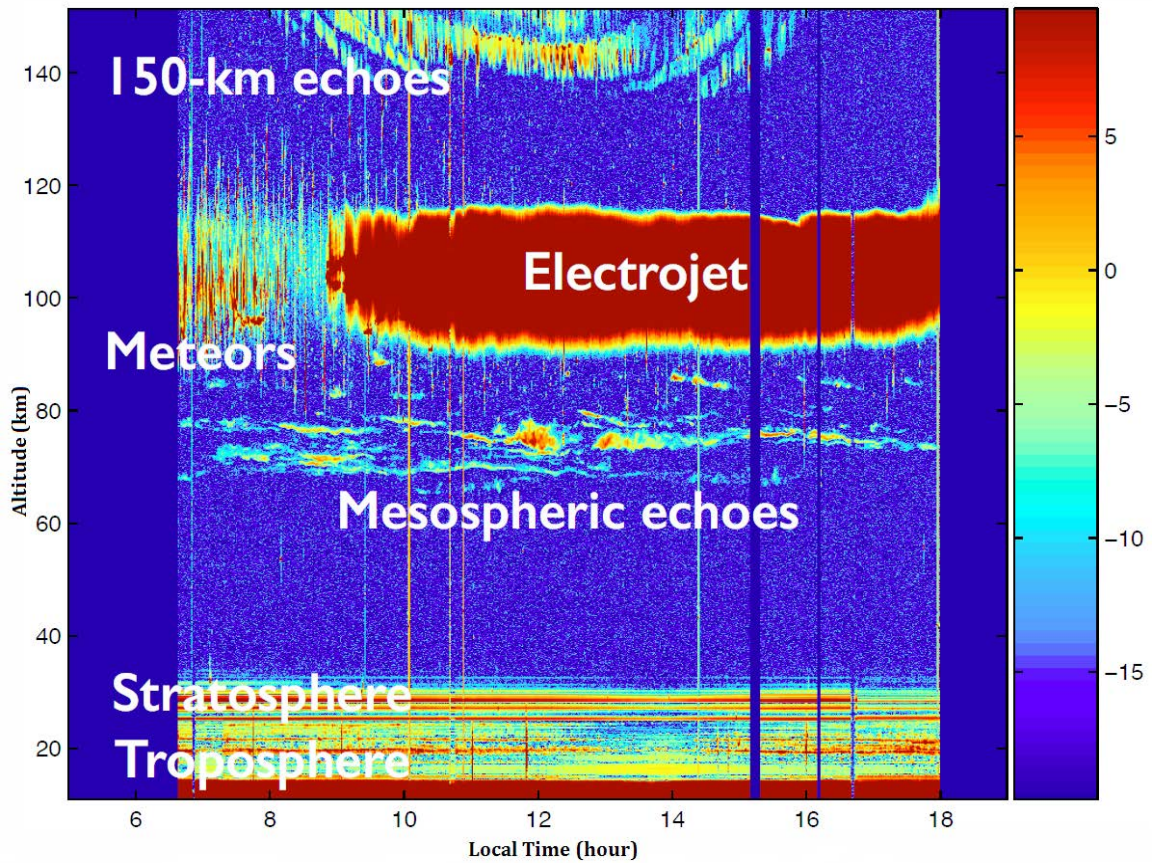


Figure 3.2: Experimental echoes from JRO radar showing turbulence from different layers of the equatorial ionosphere [Courtesy of *Marco Milla*].

Consequently, ISR measurements from the ionosphere are almost never purely incoherent except some echoes obtained with the 50-MHz Jicamarca radar. On the other hand, ISR measurements are often not purely coherent either (except echoes from plasma instabilities) as the total scattered field is composed of contributions from a continuous distribution of self-coherent plasma waves within the illuminated volume whose phases are random with respect to each other [Akabari, 2015]. However, such cases are also termed as ‘incoherent scattering’ in radar communities.

3.1.2 GPS: Basic Concepts

Global Positioning System (GPS) is a satellite based system that consists of 32 or more artificial satellites, which orbit the Earth in 6 distinct but uniformly distributed orbital planes at an altitude of 20,200km. GPS satellites circle the Earth twice per day with an orbital speed of about 14000 km/hour in a precise orbit and continuously transmit signals providing positioning, navigation and timing (PNT) information to military and civilian users worldwide using a mathematically applied ‘triangulated’ position. GPS satellites are not in geosynchronous or geostationary orbits, but the satellite orbits are distributed so that at least 4 satellites are always visible from any point on the Earth at any given instant (with up to 12 visible at one time). Each satellite carries with it an atomic clock that "ticks" with a nominal accuracy of 1 nanosecond (1 billionth of a second). The ionosphere is as assumed to be a thin layer in GNSS processing, so that signals from global navigation satellites must transit the ionosphere on their way to the receivers.

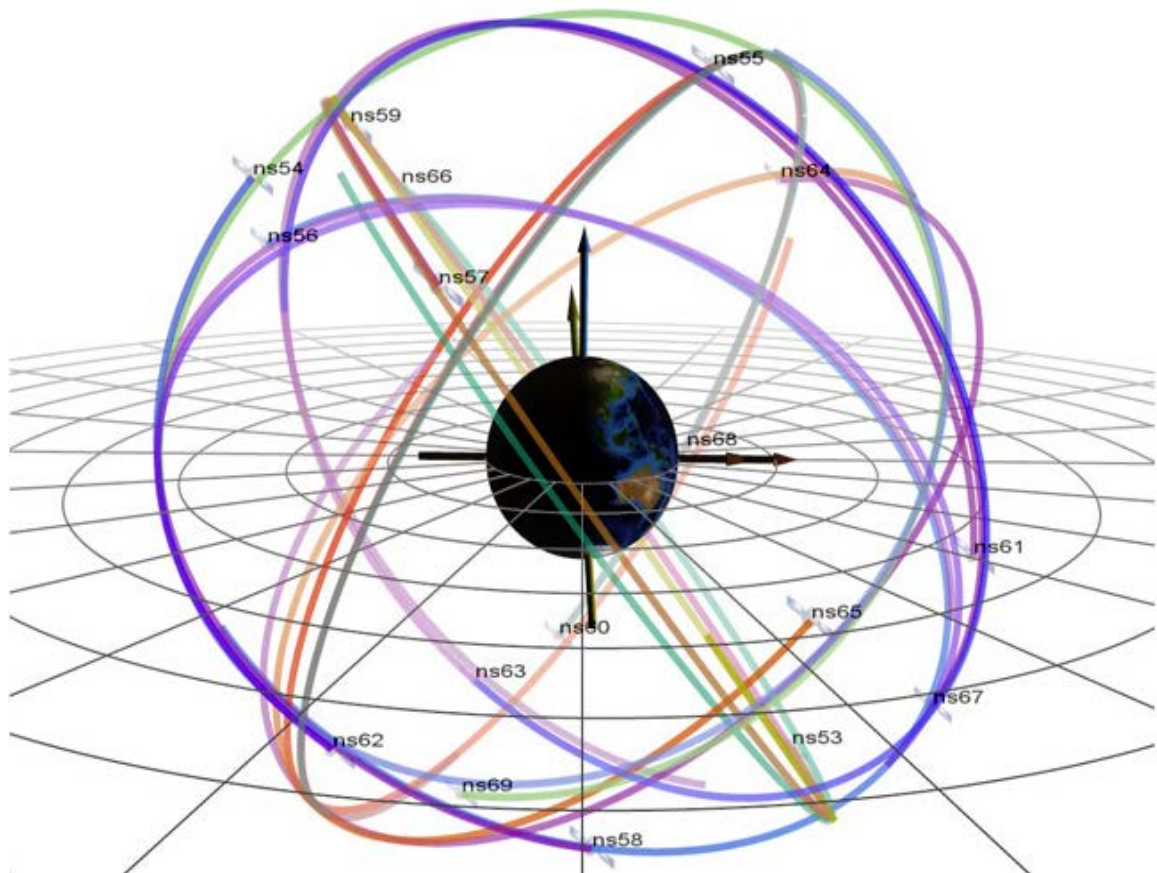


Figure 3.3: Basic design of the GPS satellite constellation ('navigational satellites', or ns) that fly around the Earth in 6 different orbital planes [Image: www.lanl.gov].

The passage exacts a toll in the form of an added delay of the pseudorandom-noise-code signals and an advance of the phase of the signals' carriers, due to the presence of the ionosphere's free electrons.

These perturbations must be taken in to account in some way to achieve high accuracy in GNSS positioning, navigation, and timing applications [*Langley, 2000; Coster et al., 2003*]. GPS was developed by the United States Department of Defense (DoD) to provide a satellite-based navigation system for the U.S. military. It was later put under joint DoD and Department of Transportation control to provide for both military and civilian navigation uses, and has become a part of daily life.

The GPS receivers can be used to monitor ionospheric instabilities. The satellite broadcasts two carrier frequencies, the L1 carrier wave at 1575.42 MHz, and L2 at 1227.60 MHz. These dual frequencies are chosen to eliminate ionospheric dispersion, one of the major sources of systematic range error. The pseudo ranges, which are derived from signal travel time to the receiver, use two pseudorandom noise (PRN) codes. These codes are modulated onto the carrier frequencies. The first code, which is available for civilians, is the C/A- code (Course/Acquisition-code), which has a wavelength of approximately 300 meters and is modulated only upon L1. The second code, the P-code (Precision-code) is available only to the military and a few designated users. P-code, with a wavelength of approximately 30 meters and is modulated on both L1 and L2. The technique used to transmit the signals from the satellites involves transmitting a carefully formulated code known as pseudo-random sequences. The received signals and the

transmitted sequences are compared to one another, and the travel time for the signal is found by measuring when the two signals are most closely correlated. The Navigation Message can be found on the L1 channel, being transmitted at a very slow rate of 50 bps. The Navigation Message includes information on the Broadcast Ephemeris, satellite clock corrections, almanac data, ionosphere information, and satellite health status [Spilker et al., 1996].

The accuracy and reliability of GPS is a function of both system and environmental factors. System factors are associated with the three GPS segments: space, control, and user which include errors in the satellite clock and ephemeris information, hardware channel biases, satellite geometry effects and thermal noise errors. Environmental factors are associated with propagation phenomena and include electromagnetic interference from external sources, ionospheric effects (including those associated with both the quiescent and the disturbed ionosphere), tropospheric delays, obscuration, and multipath [Klobuchar, 1991; Knight, 2000].

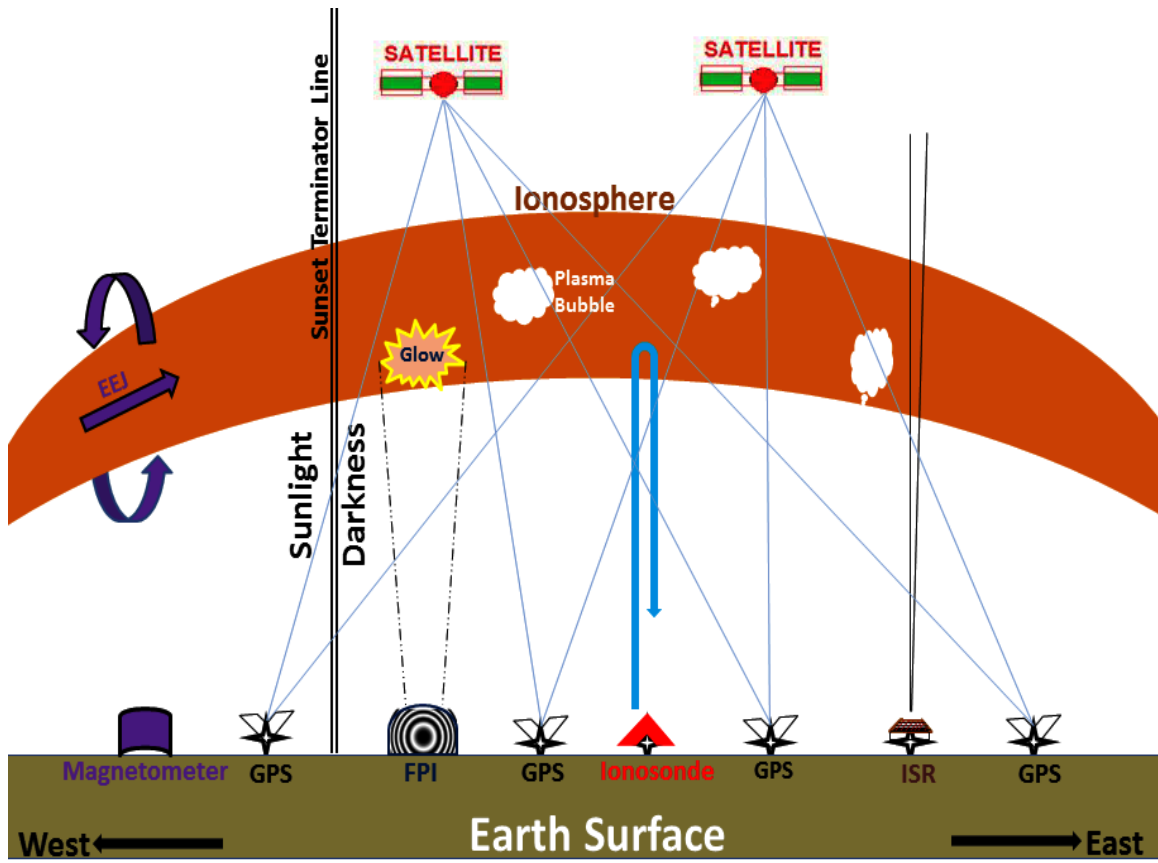


Figure 3.4: Experimental set up for the measurement/ study of ionospheric phenomena using ground- and space-based instruments.

3.1.2.1 Total Electron Content (TEC) Measurement

The Total Electron Content (TEC) is the total number of electrons present along a path between a radio transmitter and receiver. Radio waves are affected by the presence of electrons. The more electrons in the path of the radio wave, the more the radio signal will be affected. For ground to satellite communication and satellite navigation, TEC is a good parameter to monitor for possible space weather impacts. The plasma density in the ionosphere is modified by changing solar Extreme Ultra-Violet radiation, geomagnetic storms, atmospheric waves, and tides that propagate up from the lower atmosphere. The TEC will, therefore, depend on local time, latitude, longitude, season, geomagnetic conditions, solar cycle and activity, and troposphere conditions.

The signals travelling through the ionosphere experience group delay on the modulation, RF carrier phase advance, Doppler shift of the carrier frequency, distortion of pulse waveform, Faraday rotation of waves, and angular refraction of wave path. All of the above effects are proportional to the total electron content (TEC) encountered by the wave when traveling through the ionosphere. It is defined as,

$$TEC = \int_{Receiver}^{Satellite} n(h)dh$$

Where $n(h)$ is the electron content per unit volume as a function of height along with the propagation path between satellite and receiver. The unit of TEC is TECU, where $1TECU = 10^{16}$ electrons/m².

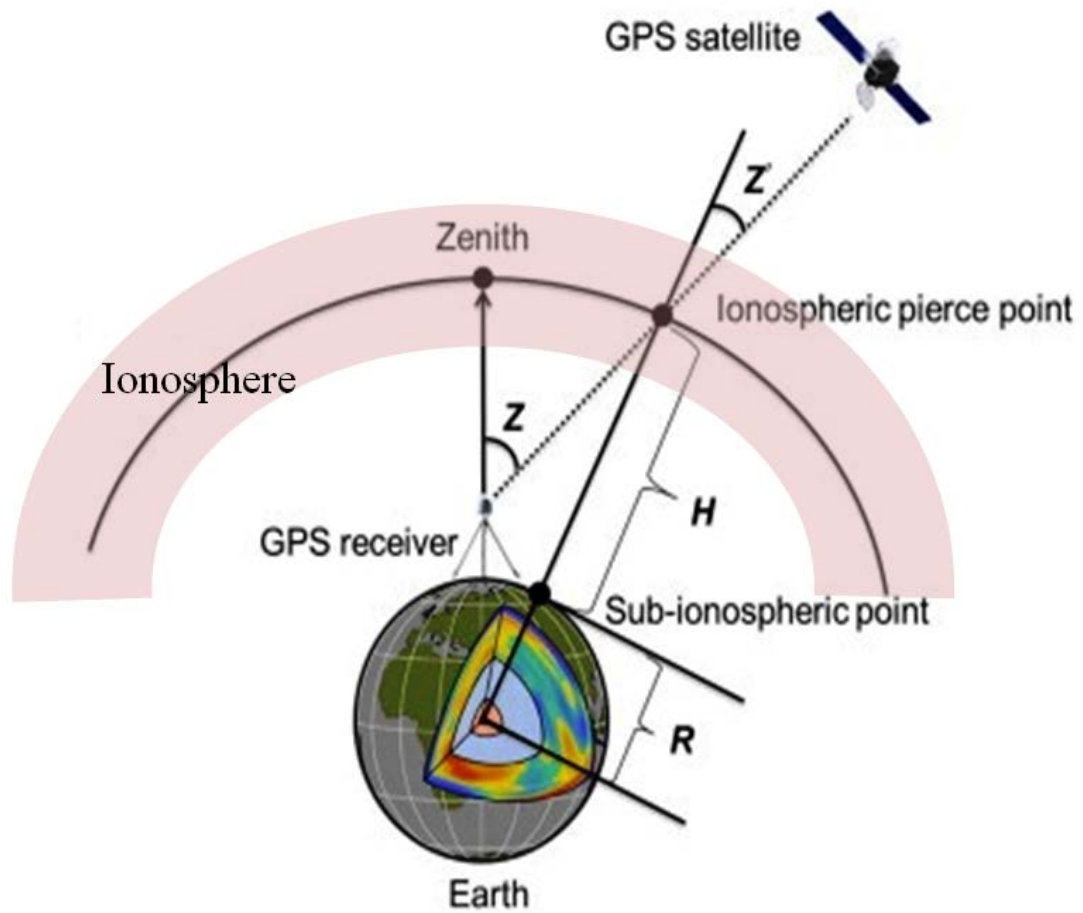


Figure 3.5: Sketch showing the geometry of vertical and slant TEC measurement strategies using GPS receivers [Image adapted from *Kao et al., 2014*].

A GPS receiver measures TEC values along a slanted path that is almost never along the true vertical. Assuming that there are no spatial variations the following formula is used to convert the slant TEC to “vertical” TEC:

$$\text{TEC} \times \text{Cos}(\text{arcSin}(0.94092 * \text{Cos}(\text{elevation angle}))).$$

Due to this approximation, it is called the “equivalent” vertical TEC. Hence, the equivalent vertical TEC is defined as the calculated vertical TEC based on measured slant TEC. This conversion is done with a mapping function which is associated with a trigonometric factor. This terminology is well used in the GPS/GNSS community.

3.1.2.2 Ionospheric Scintillations Measurement

Scintillations are fluctuations of the parameters of trans-ionospheric waves, i.e., their phase, amplitude, direction of propagation and polarization. It is a stochastic (random) phenomenon. It is considered that when a radio wave propagates inside the irregular or turbulent medium the phase varies. During the propagation in free space down to the receiver, radio waves cancel and produce fading [Priyadarshi, 2015]. It is caused by a varying refractive index created by charged particles in the ionosphere; periods of scintillation often accompany and are the result of solar storms. Scintillation results in simultaneous deep fades and rapid phase shifts in the GPS signal [Olivarez, 2013]. Scintillation activity is represented by the S4 index, which is the normalized standard deviation of signal intensity. The intensity of the ionospheric scintillation is characterized by the variance in receiver power S_4 , which is a dimensionless number called amplitude scintillation index,

$$S_4 = \frac{\sqrt{(\langle I^2 \rangle - \langle I \rangle^2)}}{\langle I \rangle}$$

Where I is the signal intensity, and S_4 is a dimensionless number with a theoretical upper limit of 1.0. There are two defined regimes of amplitude scintillation: weak and strong, which roughly correspond to the type of scattering associated with each. Strong scintillation is generally considered to occur when S_4 is greater than ~ 0.6 and is associated with strong scattering of the signal in the ionosphere. Below this is weak scintillation. An S_4 level below 0.3 is unlikely to have a significant impact on GPS. The effects of scintillation are very prominent during the evening hours. Here in this dissertation, the S_4 index derived from the amplitude scintillation of the GPS signals are used more widely than the phase scintillation.

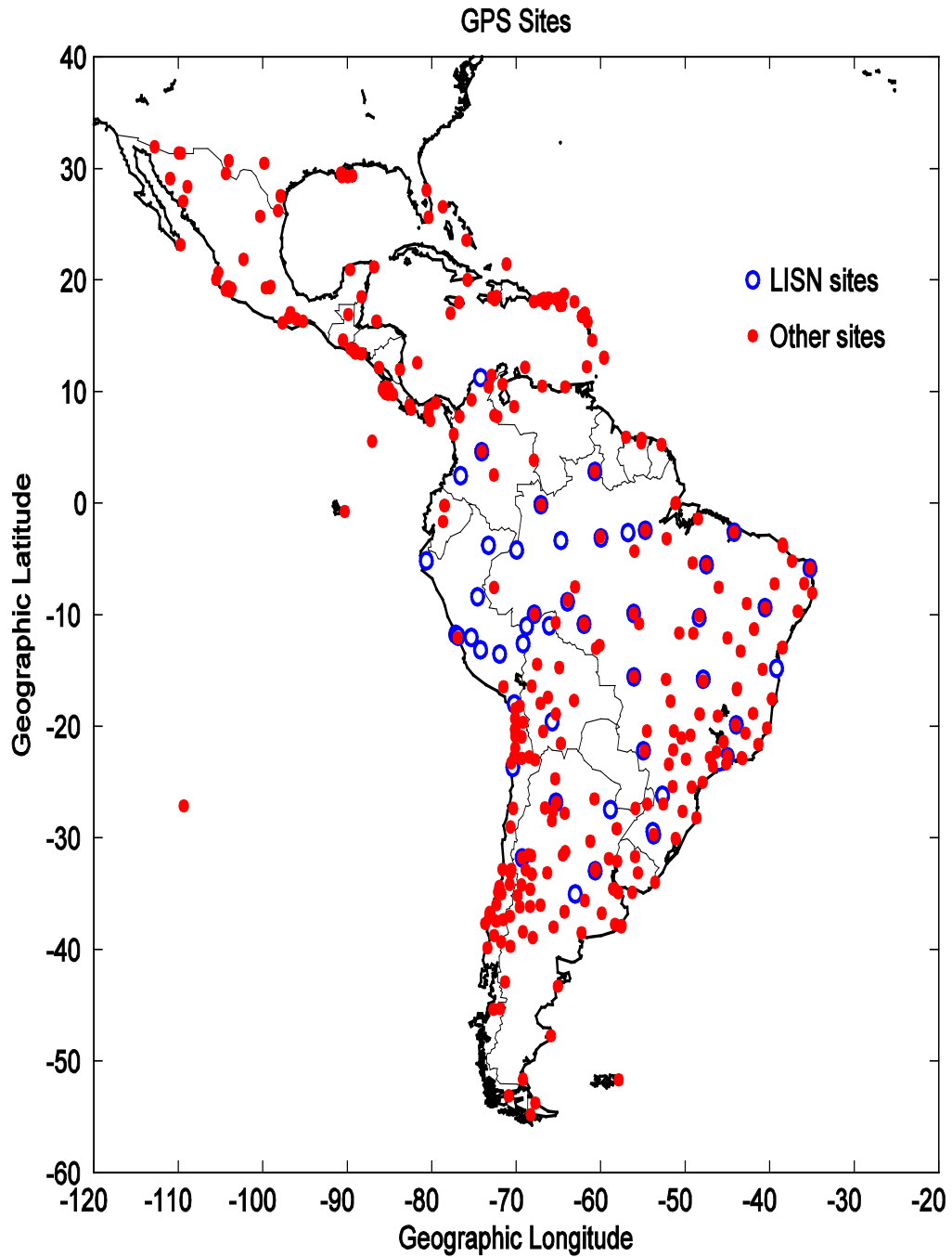


Figure 3.6: GPS sites in LISN and other network distributed in Central and South America. LISN contemplates the setup of 50 GPS stations, 5 Magnetometers and 5 Ionosondes for advancement in Equatorial Aeronomy.

3.1.3 Vertical Sounders (Ionosondes)

A sounding technique using Ionosonde is an important tool for investigation of the global structure of the upper atmosphere. The atmosphere itself is not physically uniform but has significant variations in temperature, pressure, and chemical constituents with altitude. Under these circumstances, the ionization in the atmosphere forms several horizontal layers, and so the electron concentration and therefore the refractive index of the ionosphere varies with height. By broadcasting a range of frequencies, and measuring the time it takes for each frequency to be reflected, it is possible to estimate the concentration and height of each layer of ionization. Ionosondes are swept frequency devices that measure plasma density as a function of altitude up to the altitude where the density peaks. They transmit short pulses at a series of frequencies below the peak plasma frequency of the ionosphere and observe the time between transmission and reception of each pulse to determine the altitude from which it was reflected. They cannot provide information on the plasma above the altitude of the peak [*National Academies of Sciences, Engineering, and Medicine, 2015*].

The path of the radio wave is affected by free charges in the medium through which it is traveling. The refractive index is governed by the electron concentration, magnetic field of the medium, the frequency of the radio wave and polarization of the transmitted wave. The refractive index is inversely proportional to the frequency of the transmitted wave. The presence of the earth's magnetic field causes the ionosphere to be bi-fringent leading to two possible ray paths (ordinary and extraordinary components) depending on the polarization of the transmitted wave [*Venkatesh, 2013*].

An Ionosonde broadcasts a sweep of frequencies, usually in the range of 0.1 to 30 MHz. As the frequency increases, each wave is refracted less by the ionization in the layer, and so each penetrates further before it is reflected. As a wave approaches the reflection point, its group velocity approaches zero, and this increases the time-of-flight of the signal. Eventually, a frequency is reached that enables the wave to penetrate the layer without being reflected. For ordinary mode waves, this occurs when the transmitted frequency just exceeds the peak plasma frequency of the layer. In the case of the extraordinary wave, the magnetic field has an additional effect, and reflection occurs at a frequency that is higher than the ordinary wave by half the electron gyrofrequency.

In its simplest form, an ionosonde works, following *Hunsucker [1991]*, basically as follows: an oscilloscope sweep is initiated, and a short time later the transmitter sends a short pulse of radiofrequency energy at a given radio frequency upwards toward the ionosphere. After a time delay of a few milliseconds, the pulse reflected from an ionospheric layer returns to the receiver and is displayed on the same oscilloscope sweep. If the ground conductivity is high and ionospheric absorption is low, several echoes (or "multiples") may be observed. The "virtual height" of the layer may be directly deduced from the time delay between the transmitted and received pulses, assuming that the radio wave travels at the speed of light. If the transmitter and receiver frequency are then slowly varied together over a range of typically 1-20 MHz, an ionogram - a plot of virtual height versus frequency is obtained.

The refractive index n of a medium of electron density N for a radio frequency f is approximately given by,

$$n = (1 - e^2 N / 4\pi^2 \epsilon_0 m_e f^2)^{1/2}$$

Where e and m_e are the electron charge and the rest mass respectively, and ϵ_0 is the permittivity of free space. Substantial reflection of the signal may be expected as n approaches zero and the electron density required to reflect a signal of frequency f_c is then $N = 4 \pi^2 \epsilon_0 m_e f^2 / e^2$.

$$n^2 = 1 - \left(\frac{f_c}{f} \right)^2$$

$$\text{Where, } f_c^2 = N \cdot e^2 / 4 \pi^2 \epsilon_0 m_e$$

The frequency at which a wave just penetrates a layer of ionization is known as the critical frequency of that layer. The critical frequency (f_c) is related to the electron density by the simple relation;

$$f_c^2 = N \cdot e^2 / 4 \pi^2 \epsilon_0 m_e$$

The quantity f_c is the plasma frequency i.e. the natural frequency of oscillation for plasma density (N_e). Inserting the values of constants, we get,

$$f_c = 9.99 \times (\sqrt{N}), \text{ for ordinary mode}$$

$$f_c = 9.99 \times (\sqrt{N_e}) + 0.5 \cdot B e / m_e, \text{ for extraordinary mode}$$

In above relations, f_c is the critical frequency in Hz, N is the electron concentration per meter cubed, B is the magnetic field strength, e is the charge on an electron and m is the mass of an electron.

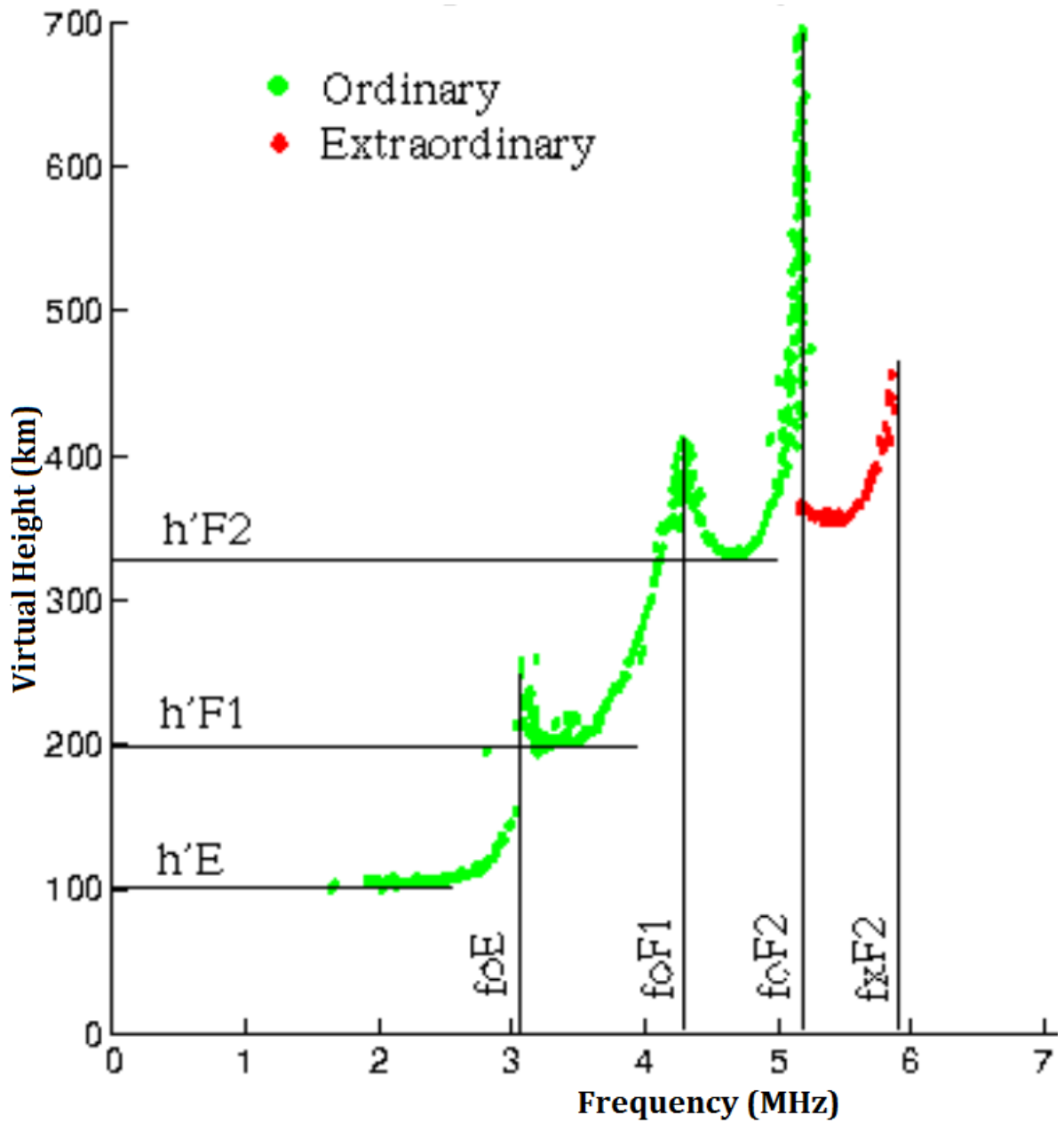


Figure 3.7: An idealized ionogram made near local noon of the day. The flattened base of each parabola is the location of the layer peak of the ionosphere [Image: www.ukssdc.ac.uk].

All transmitted frequencies above this critical frequency will penetrate the layer without being reflected. Their group velocity will, however, will be slowed by any ionization, and this will add to the time-of-flight. If such a wave encounters another layer, whose plasma frequency is higher than the frequency of the wave, it will be reflected, and the return signal will be further delayed as it travels back through the underlying ionization. The apparent or virtual height indicated by this time delay will, therefore, be greater than the true height. The difference between true-height and virtual height is governed by the amount of ionization that the wave has passed through. Recreating the true-height profile of electron concentration from ionogram data is an important use of Ionosonde data.

An ionogram is a graph of time-of-flight against the transmitted frequency and a measure of the ionospheric reflection height with frequency. The ionograms are used to determine the electron density distribution as a function of height $N_e(h)$, from the bottom of the E layer to the peak of the F2 layer except under spread-F conditions. Each ionospheric layer shows up as an approximately smooth curve, separated from each other by a cusp (where trace tends to become vertical) indicative of the critical frequencies f_0E , f_0F1 and f_0F2 . The critical frequencies are those frequencies at which the signals penetrate the respective layers, which are a measure of the maximum electron densities of the respective layers. The critical frequency of each layer is scaled from the asymptote, and the vertical height of each layer is scaled from the lowest point in each curve. Data from the Ionosonde located and operated at Jicamarca is used in the present study [Venkatesh, 2013]

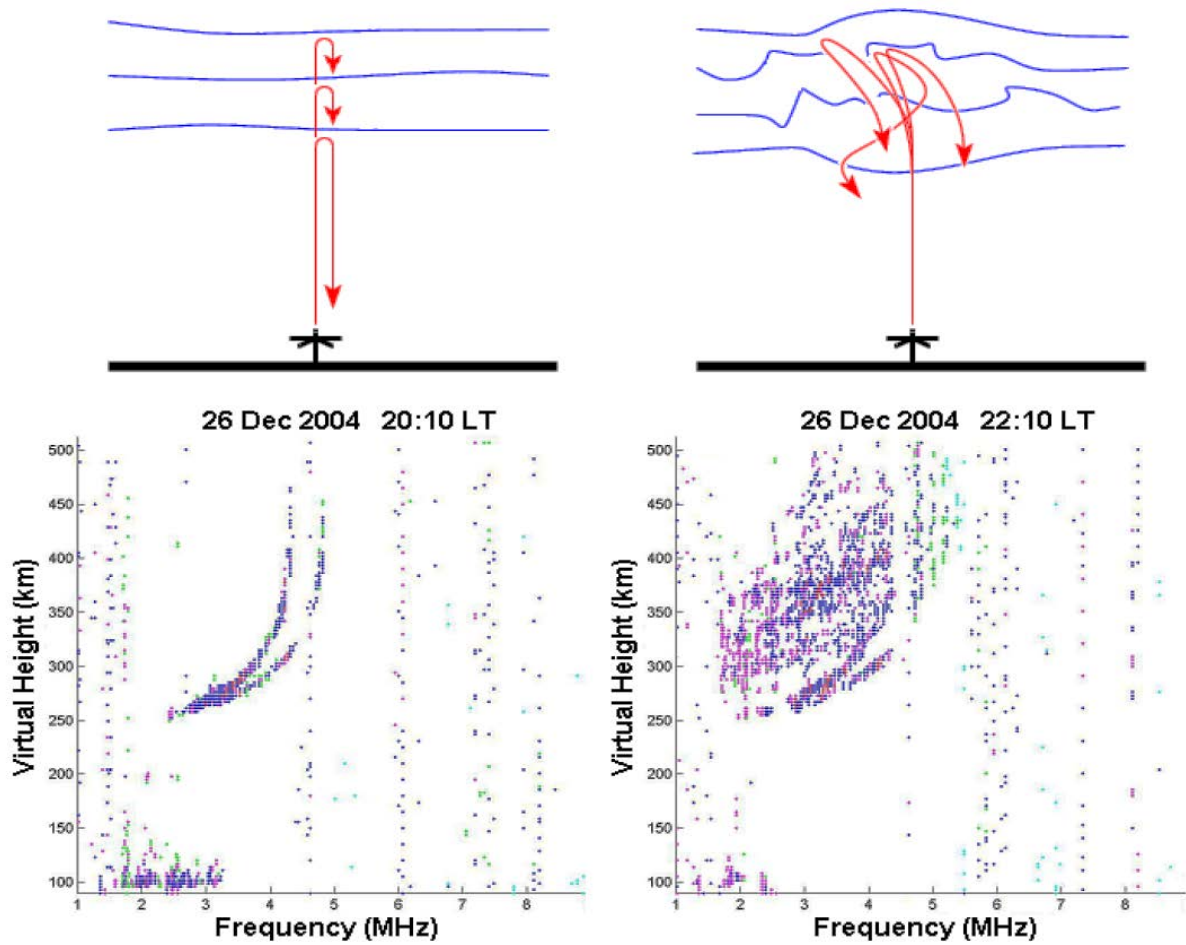


Figure 3.8: Characteristic signature of echoes from different ionospheric layers seen in the ionogram corresponding to non-turbulence (left) and turbulence (right) conditions with altitudes [Courtesy of *Rezy Pradipta*].

3.2 Magnetic Sensors and Optical Techniques

For aeronautical studies, a variety of passive and active sensors as well as optical methods, exist in the current space science community. Here, we present introductory principle of a fluxgate magnetometer as a sensor and Fabry Perot interferometer (FPI) as optical instruments. These instruments are used to probe the upper atmosphere for solar-terrestrial research and monitoring or forecasting space weather. Fluxgate magnetometers provide high precision measurements of the variability of the Earth's magnetic fields and can be used to infer the currents that transport energy and momentum through the magnetosphere and ionosphere [Miles, 2017]. Fabry-Perot interferometers (FPIs) are used to measure atmospheric wind and temperature in the mesosphere and thermosphere through nocturnal airglow emissions [Shiokawa, et al 2001]. Recently, SOFDI (Second-generation Optimized Fabry Perot Doppler Imager), a newly designed FPI has been employed for daytime measurements as well. FPI has made its appearance in a large number of disciplines; from basic spectroscopy, to laser cavity development, to optical computing, to the telecommunications industry [Gerrard, 2011a].

3.2.1 Magnetometer

Magnetometers are powerful sensors and very sensitive to the variation as well as the absolute magnitude of components associated with magnetism; including strengths of the earth's magnetic field. It is a tool for determining the distribution of ionospheric currents, field-aligned currents, electric potential, the Joule heat production rate, and the auroral particle injection rate over the entire polar region, with a suitable time resolution [Akasofu and Kamide, 1985].

Measurement of the magnetic fields is of interest for various scientific purposes, navigation, geophysical survey, and metal detectors. The measurement of geomagnetic phenomena provides essential tools for the understanding of magnetic field strength as well as the electromagnetic environment of the Earth. A magnetometer measures magnetic flux density at the point in space where the sensor is located but requires a nonmagnetic environment to function properly [Ripka, 2001]. The working principle of the magnetometer, referring Ripka, [2001], is as follows: each magnetometer has two primary coils and a pick up secondary coil surrounds the primary coils. An alternating current passes through the two primary coils; symmetrical voltage pulses are then generated in the secondary coil each time the AC current changes direction. However, if an external magnetic field exists, it can distort the voltage pulses in the secondary coil. The magnetometer reacts by supplying a buckling current through the second coil to drive the voltage pulses back to their symmetric state. The magnitude of the buckling current is proportional to the earth's magnetic field strength and aligned to the axis of the magnetometers [Ripka, 2001].

Fluxgate magnetometers and proton precession magnetometers are the two types most commonly used in magnetic observatories [Love, 2008]. Fluxgate magnetometers sense the local magnetic field as a consequence of Faraday's law. Basically inspired by Ripka [2001, 2003] and further interpreted by Miles [2017], in principle, for a coil of wire with a high magnetic permeability core, a changing magnetic flux Φ will induce a voltage V_i

related to the number of wire turns N the area of the turns A , the magnetic constant μ_0 , the relative permeability of the core μ_r and the magnetic field H .

$$V_i = \frac{d\phi}{dt} = \frac{d}{dt}(NA\mu_0\mu_r H)$$

Observing that A , μ_r and H can be time varying and considering each separately gives a generalized induction equation,

$$V_i = (NA\mu_0\mu_r) \frac{dH}{dt} + (N\mu_0\mu_r H) \frac{dA}{dt} + (NA\mu_0 H) \frac{d\mu_r}{dt}$$

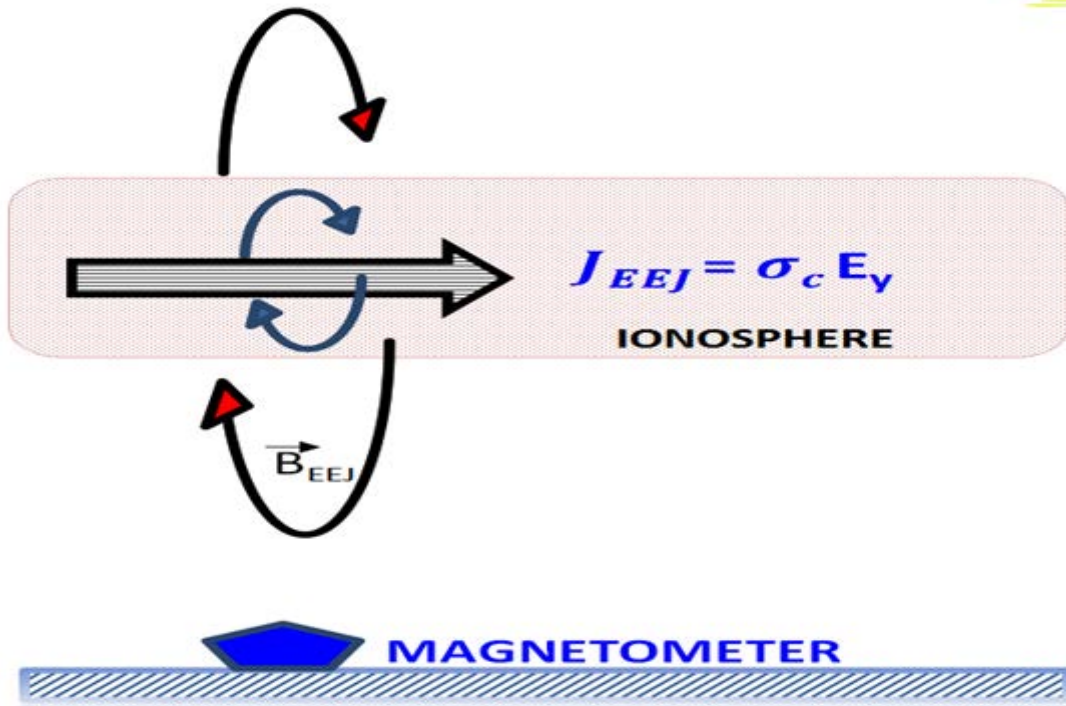
The dH/dt term is the basis of an induction coil magnetometer, the dA/dt is typically either negligible, or an error term and the $d\mu_r/dt$ term allows the sensing of H and is the basis of the fluxgate action. A high-permeability core will normally concentrate the local magnetic field, enhancing the flux through a sense coil. Modulating μ_r will modulate the flux carried in the core, and hence the flux surrounded by the sense coil.

For the equatorial electrojet, the ionospheric current associated with electrojet is related to horizontal component of earth's magnetic field as,

$$J_{EEJ} \sim \Delta H$$

The magnetic field at every location on earth has a specific strength and direction. The direction of the magnetic field line is defined by the dip angle, which is the angle between the magnetic field line and a line tangent to the earth's surface. Close to the earth's poles, the magnetic field line points down into or up out of the ground with a magnetic dip angle close to 90° .

(a)



(b)

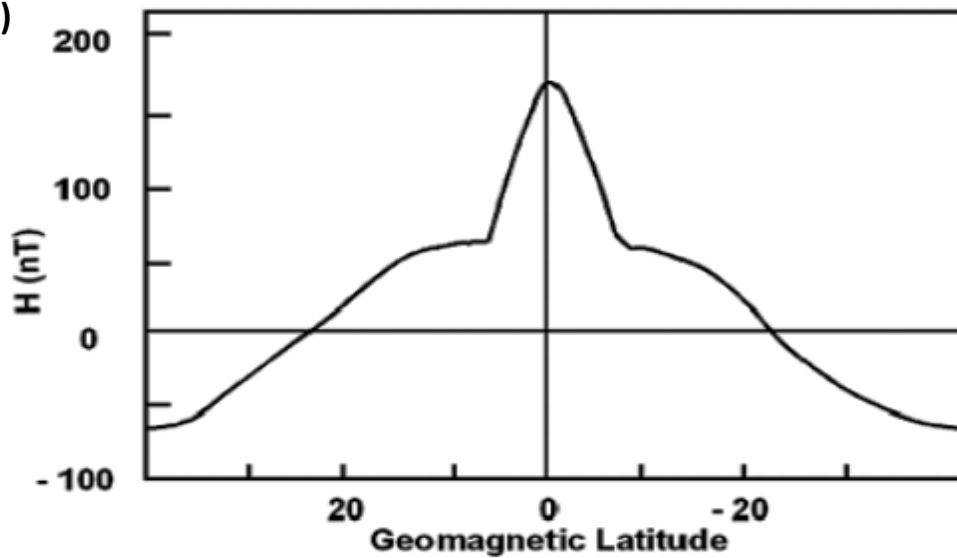


Figure 3.9: (a) Cartoon showing magnetic field generated due to EEF (and then EEJ) and its influence on magnetometer reading on the ground. (b) Equatorial noontime enhancement of horizontal component of Earth's magnetic field (H) as a signature of EEJ in the magnetometer reading at geomagnetic equator.

The magnetic field strength is significantly higher at the poles due to the fact that many magnetic field lines converge at the poles. At the earth's equator, the magnetic field lines are almost horizontal and point from magnetic north to magnetic south with a magnetic dip angle close to 0° . The magnetic field strength is weaker at the equator than at the poles as the magnetic field lines are more spread out.

3.2.2 Fabry Perot Interferometer

The Fabry-Perot interferometer (FPI) is a very powerful and versatile tool for spectroscopic measurement. It consists of two parallel flat semi-transparent reflecting surfaces separated by a fixed distance, called an etalon [*Fabry and Perot, 1897; Hernandez, 1986*]. A monochromatic light wave incident upon an etalon at an arbitrary angle to the normal of the mirror surfaces will undergo multiple reflections within the mirrors. The intensity distribution of the etalon-reflected and etalon-transmitted interfering beams is found to be, because of the circular symmetry of the device, a set of bright concentric rings, or fringes, on a dark background for the transmission case, and a complementary set of dark fringes on a light background for the reflection case. The angular diameter of these fringes is dependent on the spacing between the etalon mirrors and the inverse wavelength (i.e. wavenumber) of the radiation. Thus, the basic function of a Fabry-Perot device is to transform wavelength into an angular displacement; however, in this process, the etalon adds something of its own to the resultant fringes [*Hernandez, 1986*].

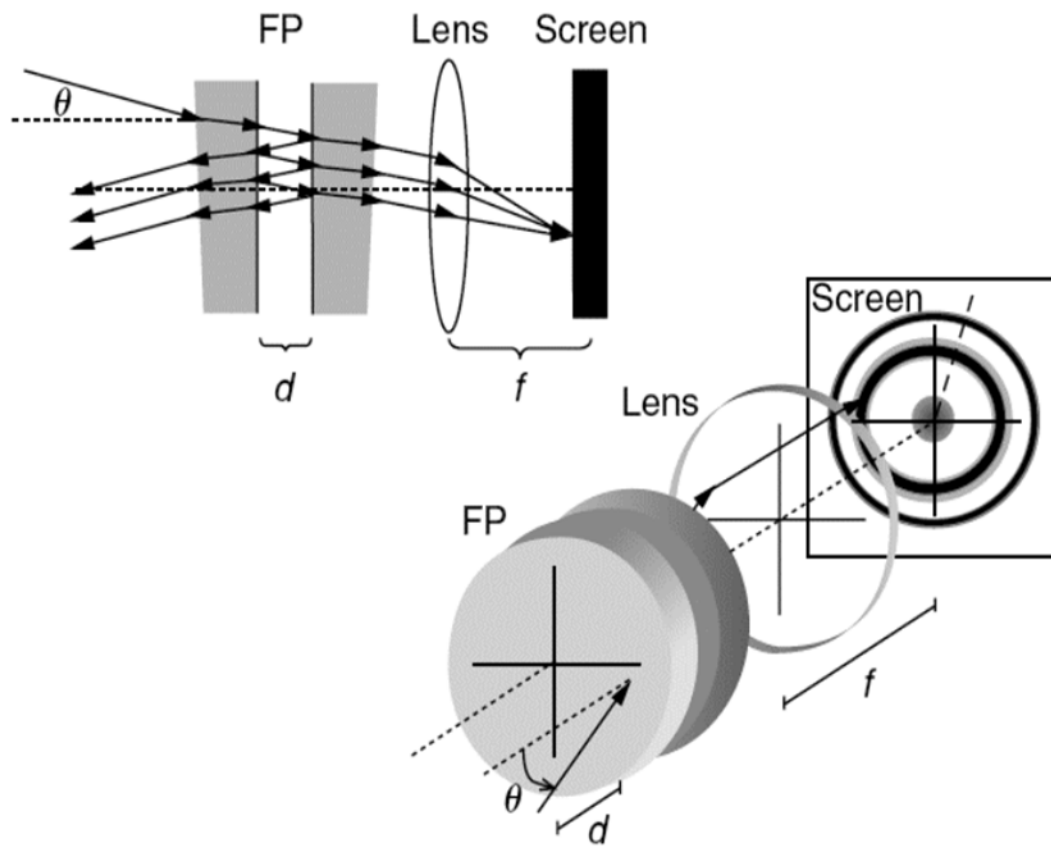


Figure 3.10: Schematic of a Fabry-Perot Interferometer [Image: Kelley, 2009b].

The etalon of FPI consists of two flat transparent plates of glass that are mounted parallel with a separation gap, d , and with internal faces coated with a mirror surface with reflectivity, R . peak transmission occurs over a series of n orders when

$$n \lambda = 2 \mu d \cos \theta$$

where θ is the angle through the FPI etalon relative to the normal to the etalon, μ is the refractive index of the medium between the plates (sensitive to density variations), and λ is the wavelength of the light ray at angle θ .

The lack of any angular dependence about the optical axis in this expression indicates azimuthal symmetry for the interferogram and indeed, what is observed is a series of circular interference circles appearing as equal area rings concentric with the optical axis. The pixel spacing between orders decreases in proportion to the square root of the radius from the optical axis. The higher frequency orders lie closer to the optical axis, i.e., the wavelength scale varies from blue to red as the angle θ increases [Meriwether, 2004].

The first application of the FPI to thermospheric/ionospheric measurements was by Babcock [1923] with measurements of the upper mesospheric green line at 557.7345 nm, now known to be the 1D2-1S0 transition of atomic oxygen (OI). This particular line is generated in a narrow altitude region centered around ~96 km altitude, and spectroscopic measurements of the emission line result in a measured Doppler shift and Doppler broadening when compared to a reference line. These Doppler shifts and Doppler widths can, therefore, be converted to absolute wind measurements via

$$v_r/c = (\lambda_m - \lambda_0) / \lambda_0$$

Where V_r is the radial component of the wind velocity (and thus requires multiple measurements to obtain the full wind vector), λ_m is the measured wavelength at the peak

of the emission line, λ_0 is the corresponding Doppler reference wavelength, and c is the speed of light. FPI observations of other atmospheric lines originating from different altitudes can, therefore, yield important base-state dynamical parameters necessary for understanding the upper atmosphere [Gerrard, 2011a].

3.2.2.1 SOFDI

Ion-neutral collisional coupling will occur in the F-region depending on the direction and magnitude of the thermospheric winds. These effects need to be characterized because this “ion drag” coupling will modify the F layer ionospheric structure by changing its vertical profile and its height [Meriwether, 2004].

The SOFDI (Second-generation Optimized Fabry Perot Doppler Imager) is a specially designed new approach of the interferometer for daytime measurements from OI 630-nm emission which is based upon the reduction of the overall instrumental spectral width through the combination of etalon transmission functions at three different resolutions. The daytime result represents a major advance in ground-based daytime FPI operations. The Fabry-Perot etalons, optics, housing, pressure/thermal and motion control systems of the SOFDI instrument were designed and integrated by Michigan Aerospace Corporation, Inc. The SOFDI FPI instrument is housed within a relocatable trailer. As explained in [Gerrard and Meriwether, 2011; Gerrard, 2011b], this night time technique/measurement into the daytime regime comes with a considerable increase in instrumental complexity. Specifically, additional etalons, serving to both decrease the transmission width of the overall instrument function/response and to block adjacent

transmission windows which are located at integer values of the free spectral range from the primary order of interest, need to be included into the optical system. The additional etalons in SOFDI ultimately reduce the solar “noise” continuum, thus increasing the signal-to-noise ratio of the measurement.

3.3 In-situ Techniques

In-situ measurements techniques consist instrumentation positioned directly within the ionosphere and in contact with the plasma environment. A wide range of measurements can be made from this technique because it has ability to fully capture the spatial variability of geophysical parameters. Monitoring and prediction of solar-terrestrial processes are increasingly important for our society which depends more and more on advanced technology that relies on continuous power availability, radio wave communication and navigation, and satellite operation [Stolle *et al.*, 2013].

3.3.1 SWARM Satellite Constellation

SWARM mission is dedicated to unraveling one of the most mysterious aspects of our planet: the magnetic field. Although invisible, the magnetic field and the electric currents in and around the Earth generate complex forces that have an immeasurable impact on everyday life. The results from SWARM give a unique “view” inside the Earth from space to study the composition and processes of its interior and also allows analyzing the Sun’s influence within the Earth system. In addition practical applications in many different areas, such as space weather, radiation hazards, navigation and resource management, will benefit from its concept [Friis-Christensen *et al.*, 2006]. SWARM

satellite mission launched in 2013 consists of a constellation of three circular, near-polar orbiting spacecraft. Two of them, Swarm A and B, start their orbit at an altitude of 460 km and descend down to 300 km over the mission period. Satellites A and B fly side-by-side in a formation with a longitudinal separation of about $\sim 1.4^\circ$ (corresponding to a distance of 160 km at the equator or difference of 6 min in local time) and the orbits cross each other near the poles. The orbit inclination is 87.4° . The third satellite, Swarm C, flies at a slightly higher altitude of 530 km with an orbital inclination of 88° and with an orbital period of about 90 seconds longer than satellites A and B. Swarm C will be in phase with A and B every 92 hours (~ 4 days) and being 180° out of phase about every 46 hours (~ 2 days) [Stolle *et al.*, 2013]. Due to the near-polar orbits of each SWARM satellite, the on-board magnetometers record a full profile in latitude of the ionospheric current signatures at satellite altitude and offer a unique opportunity to estimate the equatorial electric field from measurements of the geomagnetic field [Alken *et al.*, 2013].

3.3.1.1 Objectives of SWARM Satellite Mission

According to ESA website, SWARM mission aims to address following objectives:

- studies of core dynamics, geodynamo processes, and core-mantle interaction
- mapping of the lithospheric magnetization and its geological interpretation
- determination of the 3D electrical conductivity of the mantle
- investigation of electric currents flowing in the magnetosphere and ionosphere
- identifying the ocean circulation by its magnetic signature
- quantifying the magnetic forcing of the upper atmosphere

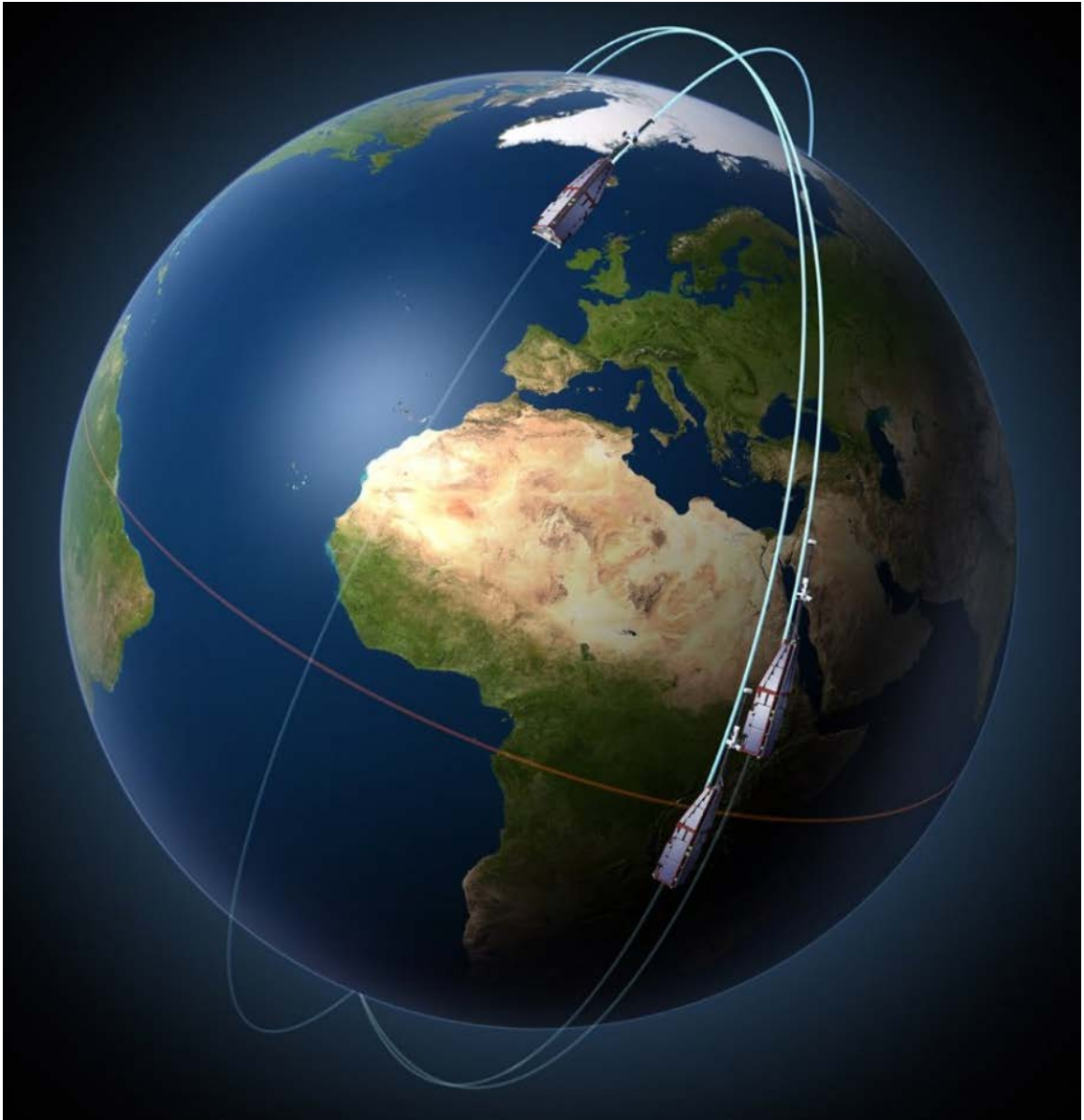


Figure 3.11: The orbit configuration of the constellation of SWARM trio satellites. SWARM is used to identify and measure magnetic signals stemming from Earth's inner core to the near-Earth electromagnetic environment and the impact of solar wind on Earth [Image: *ESA*].

Chapter 4

Variability of the Equatorial Electrojet and Related Ionospheric Features

Contents	Page
4.1 Introduction.....	84
4.2 Instrumentation, Datasets, and Techniques.....	88
4.3 Analysis and Results.....	93
4.3.1 Narrow Longitudinal Variability of Equatorial Electrojet (EEJ).....	93
4.3.2 Day-to-Day Variability of Counter Equatorial Electrojet (CEJ).....	95
4.3.3 Seasonal Variability of the Morning EEJ Depression (MED).....	97
4.3.4 F-Layer Height Variability in Association with MED.....	99
4.3.5 Effects of MED and AED on Peak Height of F2-Layer and TEC.....	102
4.3.6. Impacts of MED on GPS-TEC.....	104
4.4 Discussion.....	106
4.5 Summary and Conclusions.....	108

The dayside ionospheric current along the geomagnetic equator, driven by the eastward electric field (EEF), is assumed to control the development, dynamics, and structuring of F-region plasma in the low latitudes. Quantitative understanding on the role of the EEF (thus the electrojet) on the equatorial and low-latitude ionospheric electron density variability is very useful in estimating ionospheric total electron content (TEC) with improved accuracy and corresponding range delays in communication and navigation systems.

In the present report, the data in four different longitude sectors located along geomagnetic equator were examined, and the influence of the equatorial electrojet (EEJ) on the digisonde-inferred vertical ExB drift and Global Positioning System (GPS)-derived ionospheric TEC is investigated in the South American continent. Our findings from this comparative study demonstrate that the EEJ is weaker on the eastern side, gradually becomes stronger towards the western side of South America, and was accompanied by vertical drifts as well as TEC distributions. The TEC profiles associated with the EEJ reveal that EEJ strengths have a strong influence on the shape, size, amplitude, and separation of Equatorial Ionization Anomaly (EIA) crests as seen through the ionospheric TEC distribution.

Additionally, geomagnetically quiet-time characteristics of the normal EEJ and the morning/ afternoon counter electrojets (CEJs) are evaluated and illustrated using data from ground-based magnetometers in the American low-latitude sector. The role of the morning, noon, and afternoon CEJ on the dynamics of the height of the peak ionization in the F-layer, as well as GPS-TEC distributions at low latitudes, have been discussed using various ionospheric parameters obtained from ionosondes and GPS data. In particular, the annual, seasonal, and day-to-day variations of forenoon counter electrojets and their correlation on accompanying features of ionospheric F-Layer in the low latitudes have been studied in detail. Further, the time delay between the occurrences of the forenoon counter electrojet and the well-influenced height and density of the F-layer is studied, and the corresponding results are presented. It has been found that the forenoon CEJ has a

pronounced influence on equatorial plasma fountain, the height of the peak ionization in the F-layer and TEC at low latitudes.

4.1. Introduction

Interestingly, the geomagnetic field strength depends not only on the geodynamo of the inner core magma of the bulk Earth but also on the ionospheric current due to the E region dynamo at the upper atmosphere. An ionospheric current produced by the motion of plasma across the lines of force of the geomagnetic field generates an E region dynamo at the upper atmosphere, creating variability on the geomagnetic field strength [Steward, 1882; Vestine, 1954; Schuster 1908]. The amplitude of the daily variation of the horizontal geomagnetic field intensity (**H**) measured at the dip equator is called the equatorial electrojet (EEJ), after Chapman, [1951]. The EEJ is a narrow laterally limited ($\pm 3^\circ$ latitudes) band of intense eastward current flowing at the ionospheric E region over the dip equator, and produces strong geomagnetic field variations during the daytime. For the first time, Gouin, [1962] reported a case of the reversal of daily variation of H phenomena around midday near the geomagnetic equator and suspected that the change in this characteristic is either due to a shift in the latitude of the ionospheric current or extraordinarily amplified L-effect during a lunation. The phenomenon of negative depressions of the regular H-field, when the electrojet starts to flow westward direction is called the counter electrojet (CEJ) [Gouin and Mayaud, 1967]. Occasionally, during early morning and late afternoon, the horizontal component of the Earth's magnetic field (**H**) (and hence the EEJ) gets depressed rapidly with negative magnitude for a few hours. Both EEJ and CEJ events have an impact on the ionospheric layer dynamics. The unique

physical properties of the equatorial ionosphere (e.g. EEJs, CEJs) hold great promise for unraveling the governing mechanism of the dayside ionospheric dynamics and the onset of the enigmatic plasma structures in the geospace environment.

At equatorial latitudes, geomagnetic field lines are horizontal and acting perpendicular to the enhanced eastward electric field (EEF), creating vertical ExB drift which can lift plasma to the higher altitudes. Due to gravity and pressure gradient forces, elevated plasma diffuses downward via the fountain effect mechanism along the geomagnetic field lines creating two electron density crests at $< 20^\circ$ latitude in either hemisphere. This is called the Equatorial Ionization Anomaly (EIA) [Appleton, 1946], which is also known as Appleton anomaly. It is speculated that the EIA is shortly reduced during CEJ events. During quiet days, both EEJ and CEJ can influence ionospheric parameters, e.g. EIA, foF2 (maximum frequency of the F-layer), hmF2 (peak height of F-layer ionosonde echoes). Since these are important products of vertical ExB drift to uplift plasma, information on the CEJ can help to understand F-region dynamics. It has been suggested that a full understanding of the ionospheric dynamics cannot be obtained if the velocity and its driving force, at which ionospheric plasma moves, are not known [Woodman, 1970, Scherliess and Fejer, 1999, Stoneback et al., 2011]. The daytime vertical ExB drift velocity is the main transport mechanism that determines total electron content (TEC) distributions over low latitude ionospheric parameters, e.g. EIAs, ESFs, EPBs. The TEC distribution is an indicator of ionospheric variability and defined as the total number of electrons per square meter along the line of sight from the transmitter on the satellite to the receiver (GPS) on the ground. It is measured in units of TECU (1 TEC Unit = 10^{16}

electrons/m²). The radio signals traverses the ionosphere carrying signatures of the dynamic medium and thus offers opportunities for ionospheric research and scientific application [Bhuyan and Borah, 2007].

Even though features of EEJ strengths have been studied extensively [Rastogi, et al., 1962; MacDougall, 1969; Balsley, 1970, Deshpande, et al., 1977; Onwumechili and Agu, 1981, Patil et al., 1990; Anderson, et al., 2002, Hysell et al., 2007; Yizengaw et al., 2014, Venkatesh et al., 2015, Yamazaki et al., 2017], relatively little is known about how EEJ strengths affect the latitudinal distribution of the ionospheric total electron content (TEC) on at low latitudes, and whether there is significant longitudinal variation [Kane,1975; Huang, 1989; Scherliess et al., 2008; Jee et al., 2005, Seemala & Valladares, 2011]. If information on the generation, evolution, latitudinal extent and relapses of the TEC EIA is gathered before it occurs, that will increase the prediction capability of future development of ionospheric irregularities.

Multiple studies have suggested the existence of various ionospheric sources and variabilities of CEJ during geomagnetically quiet periods. It has been suggested that the tidal wind [Richmond 1973; Anandarao, 1976; Forbes and Lindzen, 1976], strong vertical wind [Raghavarao and Anandarao, 1980], solar flares [Rastogi et al, 1975; Rangarajan and Rastogi, 1981], geomagnetic lunar tides [Bartels and Johnston 1940; Onwumechili and Akasofu, 1972; Rastogi 1974; Marriott et al 1979], sudden stratospheric warming [Stening et al., 1977; Sridharan et al., 2009; Fejer et al., 2010], interaction of gravity waves and tides [Anandarao,1976; Vineeth et al. 2007; 2009], and

meteor-affected ionized particles [Muralikrishna and Kulkarni 2008; Vineeth et al., 2016] can have pronounced effects on the electrojet current and produce CEJ features. The most recent reports also concentrated on CEJ variability features at different places and different times of the day [Chandrasekhar et al., 2017; Bhardwaj and Rao, 2017, Rabiou et al., 2017; Pandey et al., 2018]. Even though abundant investigations have been made of the origin and variability of CEJ, long term variations of timeslot-based sectional depression of the EEJ (morning or afternoon) are equally promising for drawing new findings regarding its association with F-layer dynamics, but these have not been addressed using ground observations yet.

The F-layer is the region with the maximum plasma density in the ionosphere that acts as a reflector of signals in the HF radio spectrum, making possible worldwide radio communications. Predicting day-to-day characteristics of the depression of the EEJ, and its consequences on the F-layer dynamics in the equatorial and low-latitude ionosphere is of great interest to rocket launching experiments [Robert F. Pfaff, *personal communication, June 2017*], radio communication users ranging from broadcasters to radio amateurs, and two way radio communication systems users.

The scientific understanding and forecasting of the ionospheric plasma are necessary for several practical applications, and for mitigation of the adverse effects of space weather on communication, navigation, power grids, experimental optical emissions, and several other applications. The study of the daytime equatorial electrojet can provide a precise and reliable signature for forecasting ionospheric layer dynamics. Sometimes, the flow of

the EEJ current system reverses its direction temporarily during magnetically quiet as well as disturbed conditions producing CEJ in the morning, at noon, and in the afternoon. This analysis focused on the day-to-day characteristics of the EEJ and CEJ (morning/afternoon) and is conducted quantitatively to understand their role on the equatorial and low-latitude ionospheric F-layer dynamics, as well as plasma density variabilities during geomagnetically quiet days. The unique strength of the present analysis is the seasonal and long term variation of MED and accompanying F-Layer height variability derived from ionosonde in the Peruvian sector. This study categorically contributes to bringing minor but crucial ionospheric phenomena that have great influence on electrodynamics and may also be used as an ionospheric diagnostic tool for many scientific specifications.

4.2. Instrumentation, Datasets, and Techniques

The geomagnetic equator in South America swings about 12° below the geographic equator in the west coast but is located north of the geographic equator on the east coast. This property of the magnetic field in the continent is one of the natural sources for the longitudinal variability of several ionospheric parameters. The equatorial ionospheric F region is an important region to investigate and examine variations in the ionosphere's shape along with chemical constituents, layer dynamics, and physical processes within it. Also, the major part of the global TEC is distributed along the equatorial ionosphere and prone to display ionospheric disturbances/ scintillation because of its dynamic nature. We have used data from magnetometers, ionosondes, and GPS receivers in the low latitudes.

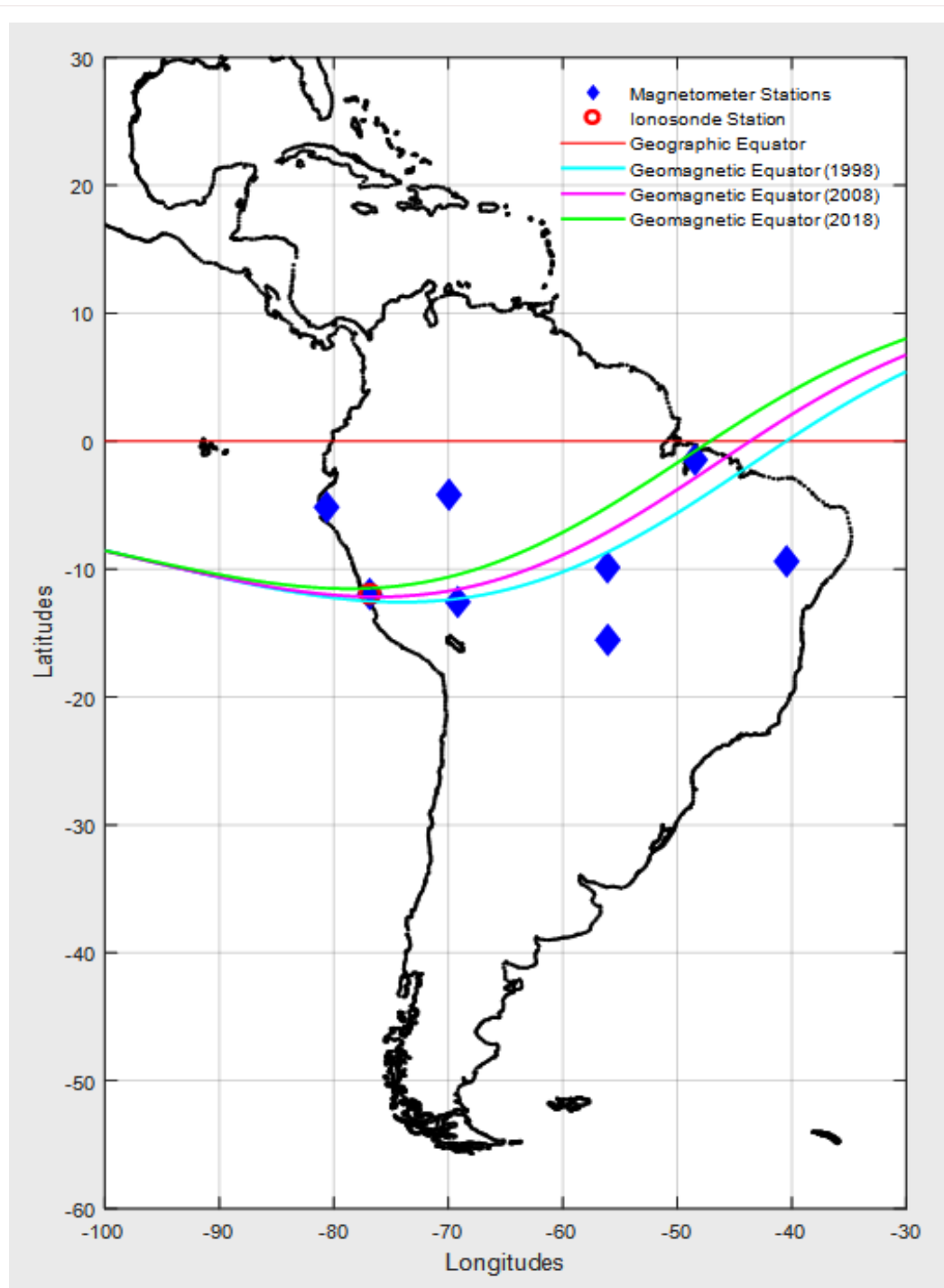


Figure 4.1: Map showing instrument locations in South America for the current analysis and the shifting of geomagnetic equator with time.

Here, we have chosen equatorial regions to process and analyze the data from a permanent array of geophysical instruments deployed in the low latitude region of South America which has had a great impact in the study of equatorial ionospheric phenomena. Figure 4.1 shows the locations of the analyzed instruments (magnetometers and ionosonde) on the continental map of South America. Data from magnetometers listed in Table 1, located in the low latitudes, are analyzed to estimate the longitudinal variability of EEJ. Data from Jicamarca ionosonde collected along the equatorial latitude are utilized to analyze the dynamics of the ionospheric layers.

The daytime EEJ and CEJ can be calculated with a pair of magnetometers by taking the difference between measurements at a dip equator station and an off-dip equator station [Rastogi and Klobuchar, 1990]. Data from the off-dip equator station are normally used directly to represent the global Sq contribution and to subtract from the dip equator station to derive the EEJ and CEJ. We used four pairs of ground magnetometer measurements from stations located as shown in Figure 4.1, and their coordinates charted in Table 1 along the South American sector. Each pair consists of one station close to the dip equator and another station at an off-dip equator location around $\pm 6^\circ$ to $\pm 9^\circ$ magnetic latitude and lying within almost same longitudinal strip for the analysis.

Table-1: Coordinates of ground-based magnetometer stations used to estimate EEJ

Station Locations	Station Code	Geographic Latitude	Geographic Longitude	Geomagnetic Latitude
Jicamarca, Peru	jica	11.95° S	76.87° W	0.43° N
Piura, Peru	piur	5.17° S	80.63° W	6.32° N
Puerto Maldonado, Peru	puer	12.58° S	69.18° W	2.07° S
Leticia, Columbia	leti	4.19° S	69.94° W	6.30° N
Alta Floresta, Brazil	alta	9.87° S	56.10° W	4.26° S
Cuiaba, Brazil	cuib	15.55° S	56.07° W	9.32° S
Belem, Brazil	belm	1.45° S	48.45° W	0.68° N
Petrolina, Brazil	petr	9.40° S	40.50° W	11.10° S

This analysis mainly focuses on the day-to-day and seasonal variations of the EEJ and CEJ and the correlation between them and other ionospheric parameters such as foF2 and hmF2. We try to get a clear representation of all the ionospheric parameters using the Jicamarca ionosonde located in the western meridian of South America. The F layer dynamics of the equatorial ionosphere are characterized using MED and AED events for geomagnetically quiet days in a long-term database from a pair of magnetometers (Jicamarca and Piura), both installed in the Peruvian longitude sector.

In the same tone, the equivalent vertical TEC derived from a chain of GPS receivers distributed in South American at low geomagnetic latitudes are also used to detect the strength and occurrence of the equatorial anomaly which is mediated by the vertical plasma drifts associated with the EEJ. The current study has been conducted using vertical TEC data obtained from dual frequency GPS receivers for geomagnetically quiet periods. These receivers are distributed at the magnetic equator and on either side of the magnetic equator, and they extend beyond the ionization anomaly locations in South America. The crests of TEC anomalies have a limited longitudinal extension whose distributions are determined by the plasma fountain effect that forms EIAs. To understand the dependency of the EEJ/ CEJ on electron density and its ultimate impact on ionosonde and GPS-derived TEC profiles, we examine TEC hourly variations on the western coast of South America.

4.3. Analysis and Results

This section gives an overview of the longitudinal, seasonal, and the occurrence rate variability of the EEJ and its depression. This includes its narrow spatial, long term temporal variation, based on data from a chain of magnetic and ionospheric observatories within the American low-latitude region. The significance of the variability of the depression of the EEJ current observed in the context of vertical plasma drifts, the equatorial plasma fountain effect, and variation of the height of the peak ionization in the F-layer, as well as GPS-TEC distributions, are carefully investigated.

4.3.1 Narrow Longitudinal Variability of Equatorial Electrojet (EEJ)

The horizontal component of the Earth's magnetic field variation (denoted H) for each station is normalized using the midnight average values for each day. Each on- and off-equator magnetometer data set was recalculated using the mean of the nighttime of the H component. This offset value is subtracted to give the daytime values. Then, the H component observations from these two magnetometers are subtracted to eliminate the Dst ring current or tail current and the Sq dynamo contributions to get only the electrojet contribution to the H component. The difference of H is proportional to the strength of the equatorial electrojet current. The resulting ΔH value is then only related to the ionospheric electrojet current and hence the east-west electric field. This electric field might originate from the Sq wind dynamo mechanism, could be associated with a penetration electric field from high latitudes, or both [Anderson *et al.*, 2002].

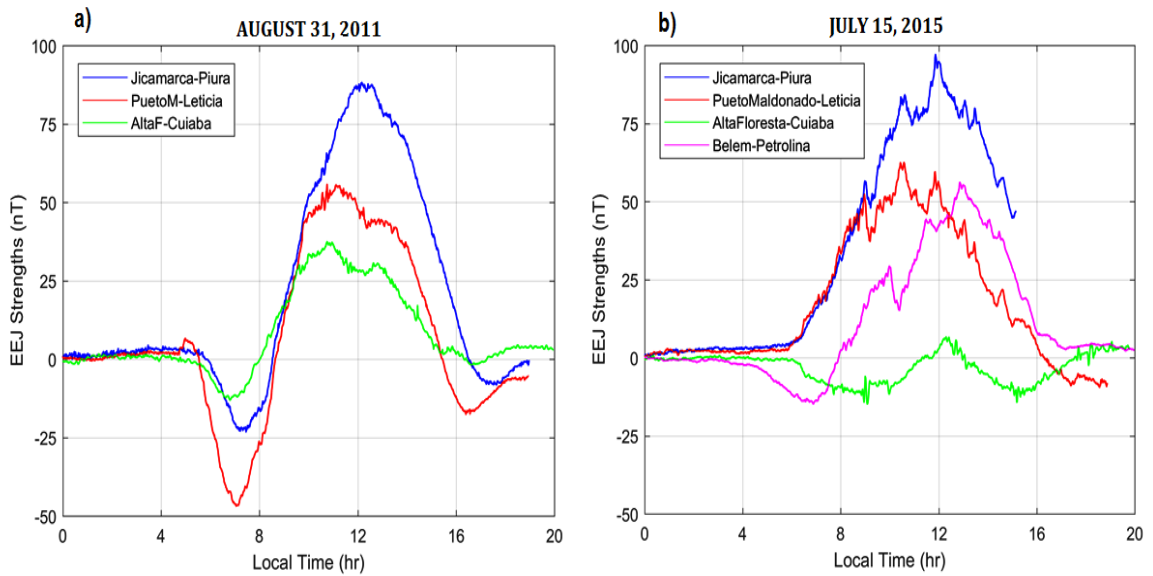


Figure 4.2: Narrow longitudinal variability of the EEJ along geomagnetic equator measured from the magnetometers located in Figure 4.1 and stations listed in table-1 of South America. The EEJ strength seems stronger in the western coast than that in the eastern coast of South America.

In Figure 4.2, the variability of the EEJ strength is presented within less than 10° longitude separation in the American sector. A clear example of the longitudinal variability of the EEJ is seen in Figure 4.2. It also shows that the maximum EEJ is attained on the western side and gradually decreases toward the east. However, the Alta Floresta magnetometer station located in Brazil was not on the magnetic equator (or EEJ zone) after 2013. Due to this unfortunate event, EEJ in 4.2(b) measured by Alta Floresta-Cuiaba magnetometers pair in July 15, 2015 is not reliable for longitudinal variability comparison. This is due to more rapid variation of the geomagnetic equator in the eastern side than that of the western side of the South American continent as presented in Figure 4.1. Magnetometers were deployed in Belem and Petrolina, Brazil only in February, 2015 so that EEJ from those longitudes is missing in Figure 4.2 (a) for August 31, 2011.

4.3.2 Day-to-Day Variability of the Counter Equatorial Electrojet (CEJ)

A case and statistical study of the geomagnetically quiet time depression of EEJ strengths is presented using a pair of magnetometers, one located at the dip equator and another off the dip equator ($\pm 6^\circ$ to $\pm 9^\circ$ away) in the American low-latitude regions. Figure 4.3 shows surface plots that show the day-to-day variability of the counter EEJ during 10UT(Universal Time) – 22UT (05LT – 17LT) observed using magnetometers located at the Jicamarca and Piura stations during (a) solar minimum 2008 and (b) solar maximum 2013. In these surface plots, all positive values of EEJ are set to zero aiming to show only the depressed or a counter portion of the EEJ.

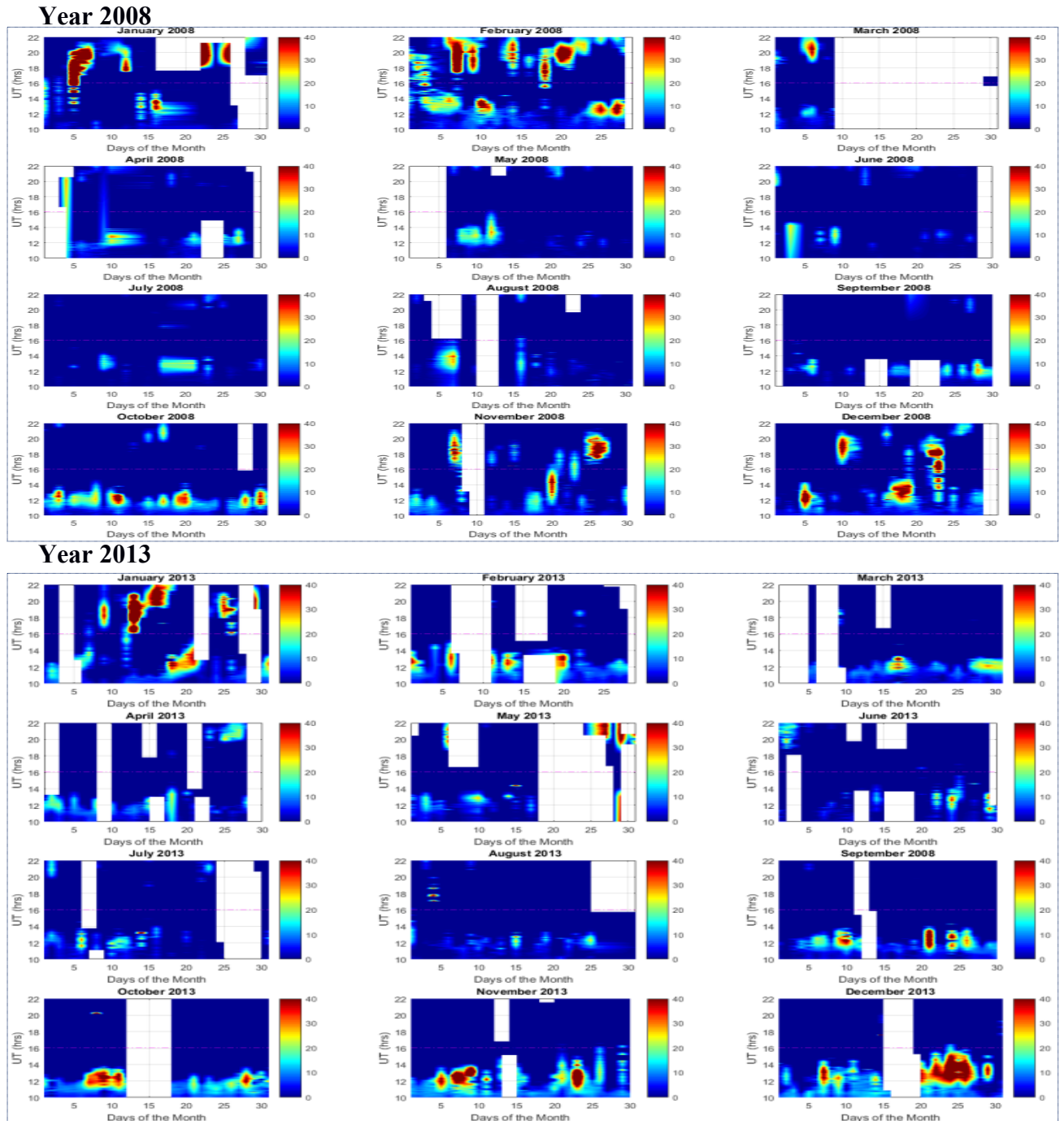


Figure 4.3: Day-to-day variability of the counter EEJ during 10–22 UT (05–17 LT) of the day observed using magnetometers located at Jicamarca and Piura stations during (a) solar minima 2008 and, (b) solar maxima 2013. Only negative values of EEJ are considered and presented in above surface plots. For each of the monthly subplots, depressions of EEJ are seen more frequently during morning hours than that of afternoon hours in both, solar minimum and maximum years.

For each of the monthly plots, EEJs are seen depressed on either side of their positive portion centered near local noon (11:00 LT) time. Remarkably, the Morning EEJ depression (MED) is observed more frequently than the afternoon EEJ depression (AED) for both (a) solar minimum, and (b) solar maximum cases.

During both solar minimum and maximum years, MED events are seen to intensify during the months of frequent scintillation occurrence period in the southern hemisphere (October, November, and December). This information might become a probing tool to understand/ forecast the occurrence and impact of the ionospheric layer dynamics and irregularities which is recognized as one of the highest priorities in the space weather program implementation plan.

4.3.3 Seasonal Variability of the Morning EEJ Depression (MED)

Figure 4.4 shows a 7-day time series mass plots of seasonal variability of the morning (05LT - 11LT) EEJ during quiet days in the years 2008, 2011, and 2013. It is to be noted that 2008 and 2013 are solar minimum and solar maximum years respectively. Seven available quiet days' are presented selecting data from a pool of one month data of ± 15 days from exact equinox and solstice days. The red curve in every subplot represents the average seasonal variability of morning section of EEJ.

A comparative study of the weekly average of the EEJ shows that the September equinox (December solstice) seasons have stronger MED events than the March equinox (June solstice) seasons. Also, the MED at the December solstice varies significantly with solar activity since it is stronger in solar maximum than during a solar minimum year.

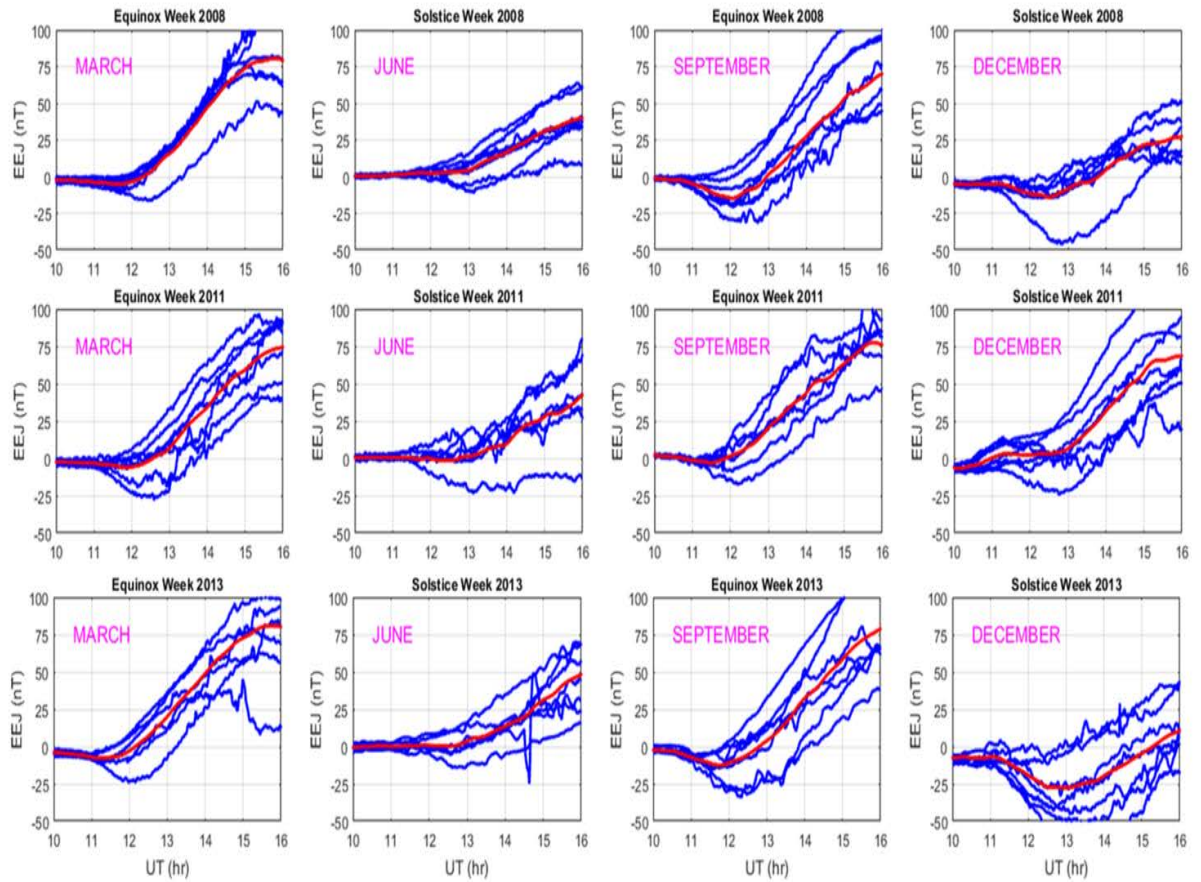
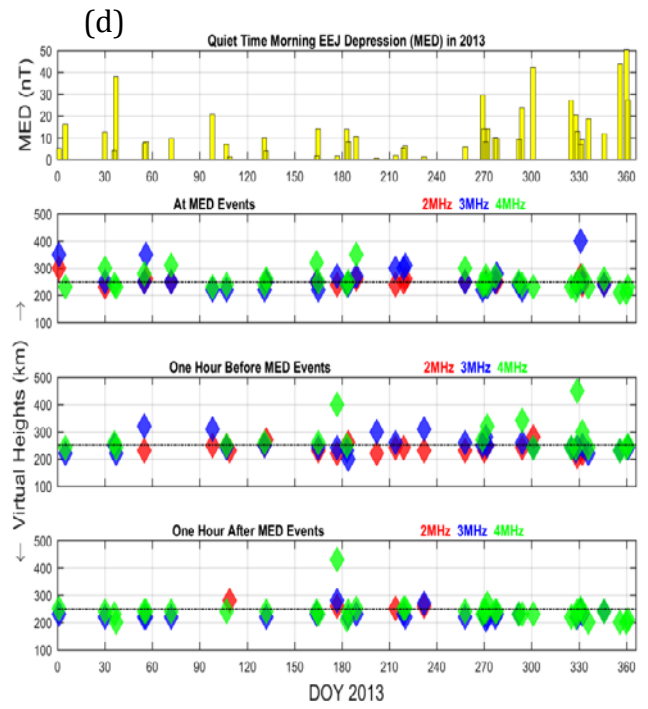
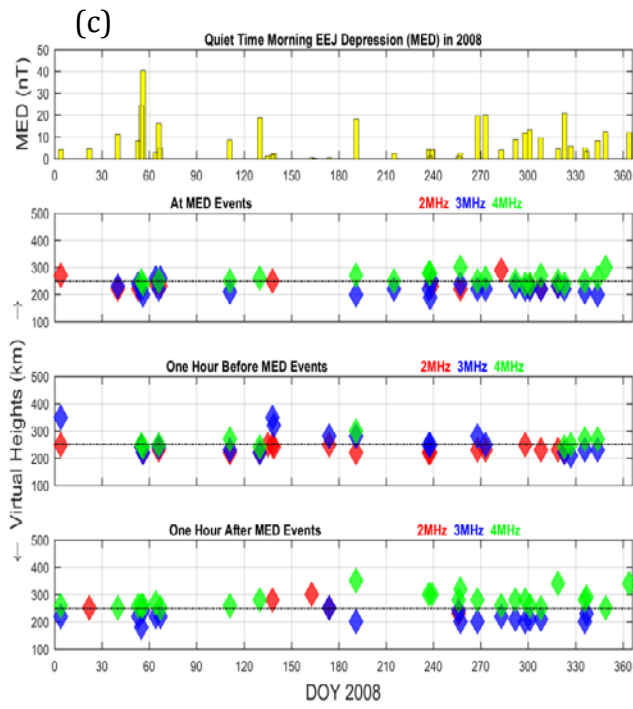
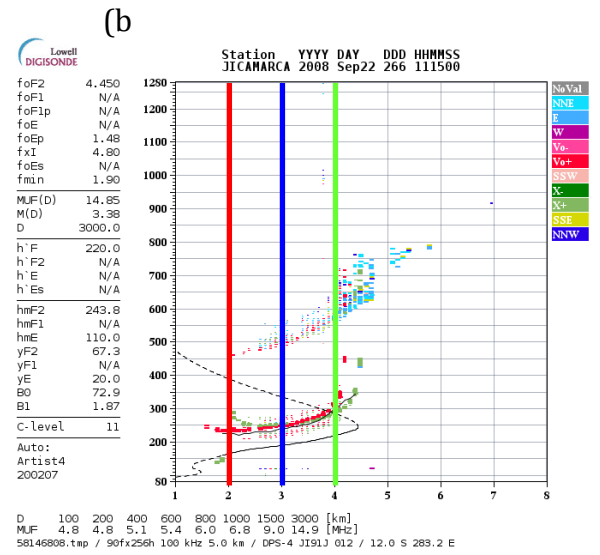
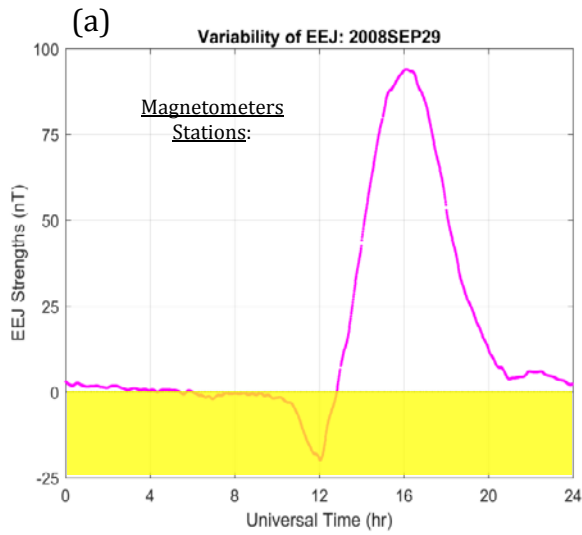


Figure 4.4: A week of time series plots of seasonal variability of the morning section 10–16 UT (05–11 LT) of EEJ during quiet days in the years 2008, 2011, and 2013. Seven quietest days’ EEJ data are chosen from one month (± 15 days from exact equinox and solstice days) window. The red curve in every subplot denotes the moving average data points of all blue EEJ curves.

4.3.4 F-Layer Height Variability in Association with MED

This sub-section highlights about how ionosonde operation frequency has been used to probe the vertical movement of the ionospheric F-layer during the MED events. Figure 4.5(a) shows a typical EEJ variability containing a short morning depression feature at 12UT (07LT). The virtual heights of the F-layer are probed using three sounding frequencies (2MHz, 3MHz, and 4MHz) as shown with the color bars in Figure 4.5(b). The yellow vertical bars in the top panel of Figure 4.5(c) show the 2008 yearlong magnitude of the MED choosing the five quietest days of each month. The remaining three panels of Figure 4.5 (c) show the virtual height variation corresponding to MED events probed by three different sounding frequencies (2MHz, 3MHz, and 4MHz). The second panel shows the F-layer height data point corresponding to the time as MED becomes maximum. Similarly, the third and fourth panels shows the height variation exactly one hour earlier and later than the occurrence of maximum MED. Figure 4.5(d) shows the same analysis corresponding to the year 2013. It can be seen that there are more virtual height data points below the reference altitude (250 km) of the F-layer corresponding to strong MED events. It seems that virtual heights associated with the 3MHz sounding frequency follows the maximum patterns of MED strengths.



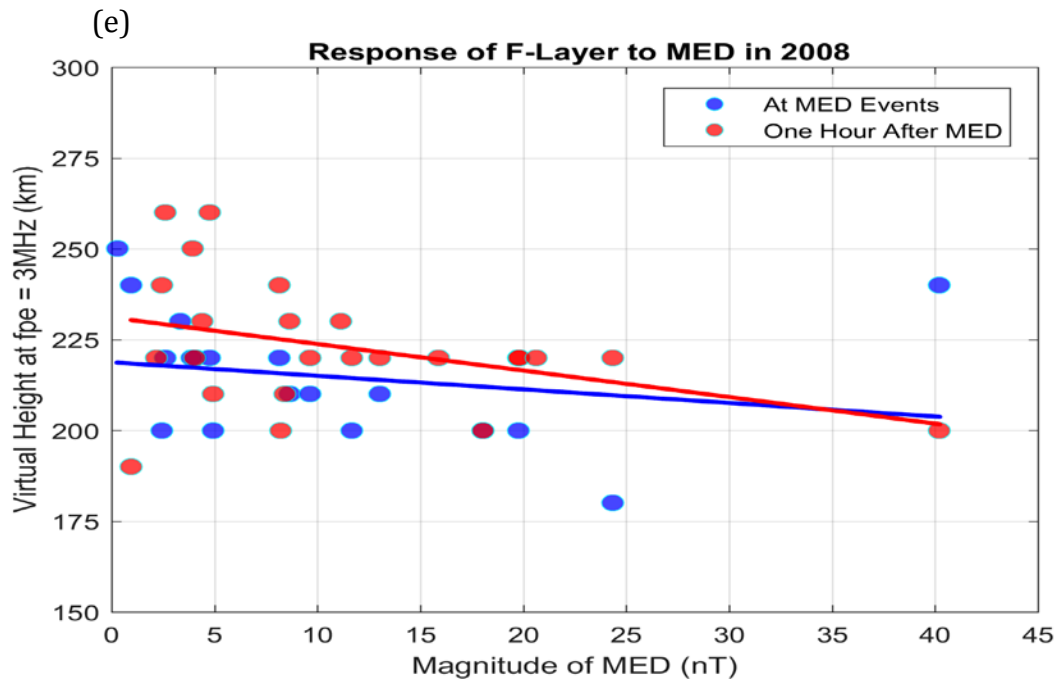


Figure 4.5:

- a. Showing a typical example of EEJ variation evaluated using a pair of magnetometers located at the magnetic equator (Jicamarca) and off- magnetic equator (Piura) in a day where the AED event is absent but not an MED event. The EEJ in the yellow shaded region is a depressed portion of EEJ during morning hours.
- b. Showing an example of the ionogram obtained from the Jicamarca Ionosonde. Virtual heights of the F-layer ionosphere corresponding to three sounding frequencies (2MHz, 3MHz, and 4MHz) are explored respectively.
- c. Showing virtual heights variation corresponding to MED events probed by three different sounding frequencies (2MHz, 3MHz, and 4MHz) of Ionosonde at the time (and also ± 1 hour) when MED becomes maximum in magnitude during the 2008 solar minimum year. There are more virtual height data points below the reference altitude (250 km) of F-layer corresponding to strong MED. It seems that virtual heights associated with 3MHz sounding frequency follow maximum patterns of MED strengths.
- d. Same as (c) for the solar maximum year 2013.
- e. Showing comparative response of virtual heights of F-layer ionosphere to the quiet days' MED events during one hour interval in 2008.

From this analysis, it was found that MED events are stronger and more frequent during solar maximum than solar minimum. As the MED becomes stronger, the virtual height of the F2-layer ionosphere becomes smaller than the reference height (250 km) of the F2 layer and drops below the value an hour earlier. This minimum stays there for an hour during the solar minimum year 2008. A similar relationship can also be seen during the solar maximum year 2013. The analysis suggests that the reference height of the F2 layer ionosphere must be revised for the solar maximum year. Also, Figure 4.5(e) illustrates the height dynamics pattern of F-layer in 2008 with respect to magnitude of the MED in one-hour interval. The slopes of the straight-line fit are -0.37 and -0.73 for MED events and one hour later respectively. The fitted line looks steeper one hour later than the occurrence time of MED. It is evidently speculated that this condition is due to a delay in response of F-layer ionosphere with the change of equatorial electric field.

4.3.5 Effects of the MED and AED on Peak Height of the F2-Layer and TEC

Plots presented in Figure 4.6 show the variability of the EEJ for three different days and associated morning and afternoon depressions in the Jicamarca longitude sector in the low latitudes. The top panel in Figure 4.6(a) shows the depression of EEJ width that occurs within a narrow (wide) time window in the morning (afternoon) for the year 2008. The second panel shows the variability of the peak height of the F2-layer (h_mF_2) ionosphere obtained from ionosonde data corresponding to the EEJ shown in the first panel. The bottom panel shows the TEC patterns derived from the ionogram associated with EEJ variation days. Figure 4.6(a) shows similar variability corresponding to the year 2013.

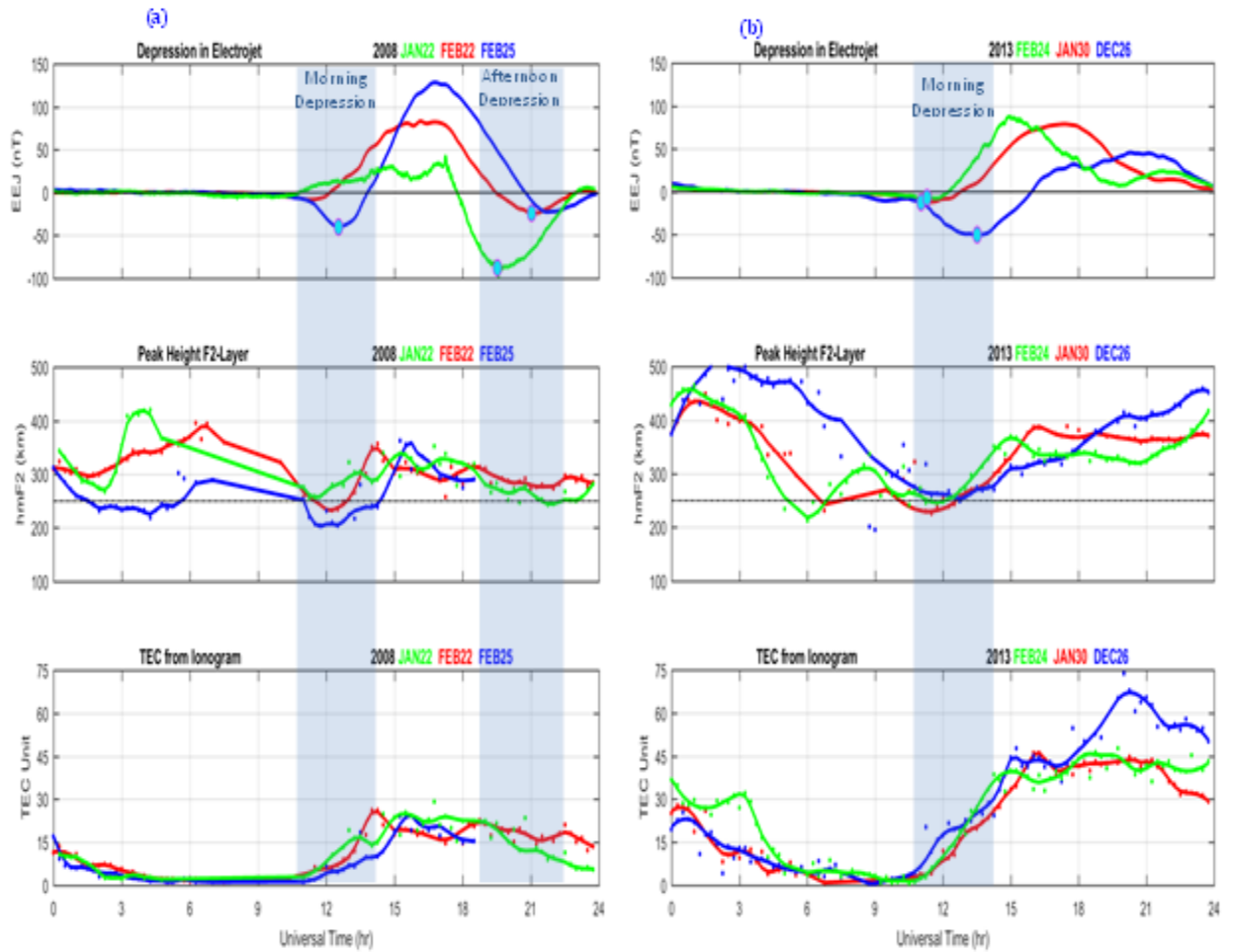


Figure 4.6:

- a) Top Panel: This plot shows the 3-day variability of the EEJ and associated morning and afternoon depressions in the low latitudes. The depression of the equatorial electrojet (EEJ) occurs within narrow (wide) time window in the morning (afternoon). Middle Panel: This plot shows the variability of the peak height of F2-layer (hmF2) ionosphere corresponding to EEJ shown in the first panel. Bottom Panel: It shows TEC patterns derived from ionogram in association with EEJ variation.
- b) Same as (a) but for the solar maximum year 2013.

A comparative study shows that even a small magnitude morning electrojet depression (MED) shows a more significant effect on the dynamics of the peak height of F2 layer than that of an afternoon depression. The peak height of F2-layer of the ionosphere during higher MED time simultaneously dips down below the reference altitude (250km) of an F2 layer in the equatorial region. For this particular analysis, the effect of MED is also seen in the TEC derived from ionograms. Since MED is a signature of a reverse electric field, consequently a negative vertical plasma drift that provides an opportunity for the plasmas to recombine with low altitude neutrals. This might be a reason for the reduction in TEC within the impact time range of the MED.

3.6 Impacts of the MED on GPS-TEC

It is well known that ionosonde is a specialized radar system able to probe only bottomside of the ionosphere and cannot detect TEC along a vertical path. Due to this reason, the TEC obtained from an ionosonde might not provide trustworthy information for the justification of impacts of the ionospheric current system in the equatorial latitudes. To overcome these issues, Figure 4.7 elucidates the hourly (total 7 hours) GPS-TEC data along the 75°W longitude sector where MED events are seen. The TEC variations are presented for three different days with different magnitude MEDs. The maximum magnitude of MED is seen with this 7 hours (11UT - 17UT) window. The electric field associated with EEJ and CEJ is a primary driver of the vertical plasma drift and the equatorial fountain that ultimately formed the equatorial ionization anomaly (EIA). The MED section of CEJ depressed plasma fountain results in a distorted EIA. It is clearly seen that hourly stratification of TEC in EIA events is more highly distorted

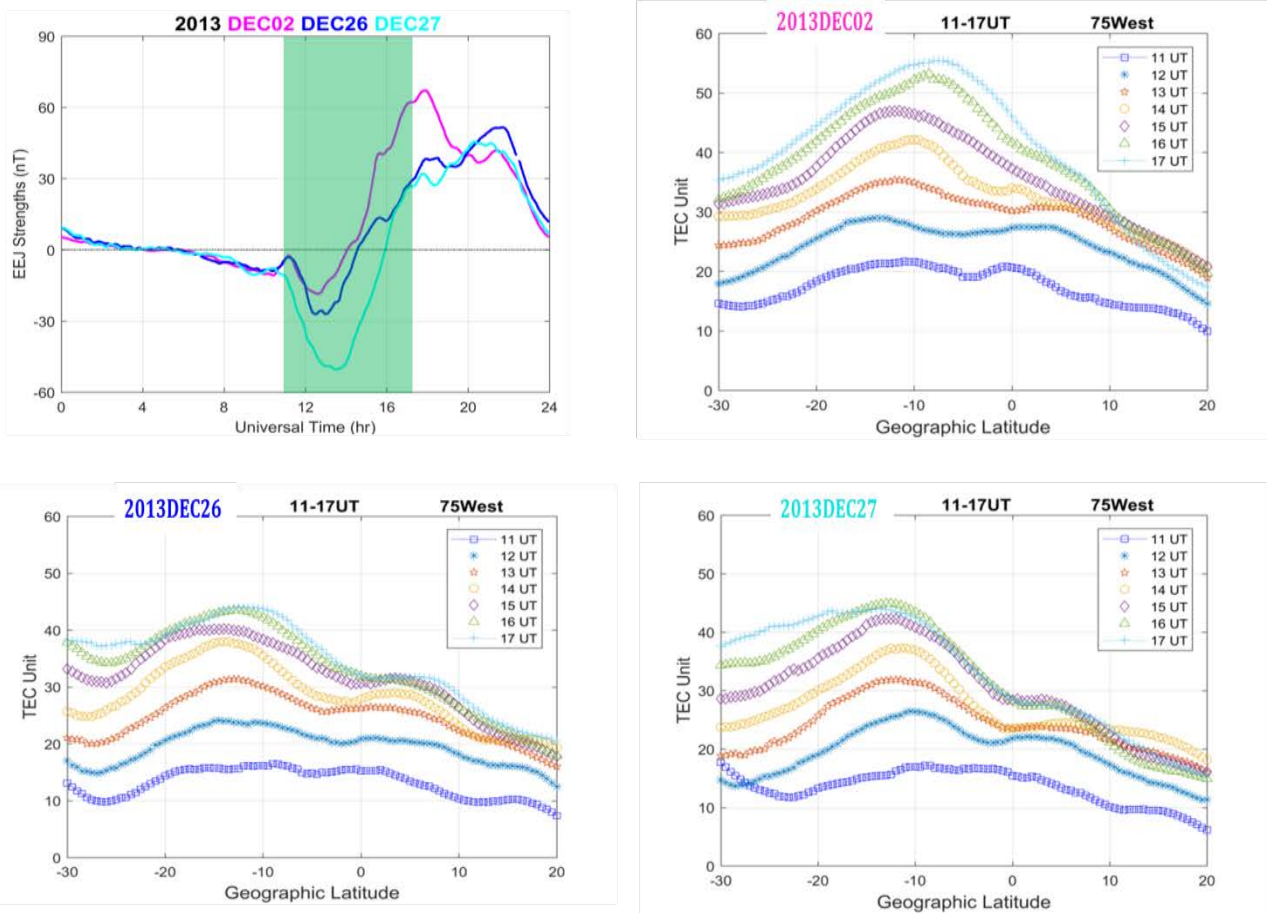


Figure 4.7: Left Top panel: These 3 curves represent three different scenario of quiet days' MED variation of magnitudes in December 2013. Rest of three panels: Showing hourly GPS-TEC variation measured using LISN network at and after impact range of maximum MED events for seven hours on the equatorial ionization anomaly (EIA) structure.

corresponding to the higher MED days (December 27, 2013) than during the lowest (December 02, 2013) and moderate (December 26, 2013) values.

Asymmetries of EIAs are seen to be more pronounced at and after EEJ depression hours than for prior hours. Symmetry in the EIA and stratification of hourly TEC curves are inhibited at and after the impact range of a depressed EEJ. Greater strength of the southern TEC crests of EIA showing evidence of summer season during December in the Southern hemisphere.

4.4. Discussion

Numerous components, e.g., equatorial electrojet (EEJ), solar quiet (Sq) current, prereversal enhancement (PRE), and evening plasma vortex, in the complex low-latitude ionospheric regime are related to the others within the ionosphere-thermosphere-electrodynamic system [Eccles *et al*, 2015]. The electrojet region provides the best avenue for current to be channeled from the dayside to meet the vertical current demands of the *F* region neutral wind dynamo after sunset [Haerendel and Eccles, 1992]. Careful analysis of magnetometer and ionosonde data drew some interesting and conclusive facts about the role of daytime electric fields variability as seen from the daytime EEJ in the *F*-layer dynamics including the TEC distributions within 75°W equatorial latitude region. The remarkable longitudinal variability of the electrojet current during quiet days in the American sector presented in Figure 4.2 is mainly governed by the unique geometry of the geomagnetic equator. The more rapid northward shifting of the geomagnetic equator (e.g. Figure 4.1) on the east coast than that of west coast of South America has created

another complexity in the ionospheric electrodynamics for the variability of EEJ. Also, the signature of the E region ionosphere electric field in the low latitude and the accompanying noontime enhancement of the H component might be connected to electron density disturbances as indicated by the TEC fluctuations in the equatorial ionosphere. This interconnectedness is examined here by choosing impacts of the morning EEJ depression events which are a small portion of the EEJ but strong drivers of the electron density variability.

The depression of the equatorial electrojet (EEJ) is marked by a westward current due to streaming movement of laterally limited ($\pm 3^\circ$) charged particles in the ionospheric E region during the day along the magnetic equator. It is a complex low-latitude phenomenon and driven by various sources of electric fields associated with global neutral wind, solar, tidal force, and the Interplanetary Magnetic Field (IMF). The controlling mechanism of the dayside ionospheric electrodynamics and the onset of the enigmatic plasma structures in the ionospheric layers are generally associated with the E and F region dynamos. The E-region dynamo current is highly variable since it is forced by upward propagating tides from the lower atmosphere due to large Hall conductivity in the E-region [Maute and Richmond, 2017]. The variability in both occurrence pattern and amplitude of the counter equatorial electrojet are presented in Figure 4.3 and seasonal variabilities of morning counter electrojet are in Figure 4.4. Occurrence and variability patterns of the MED are noticeably different in different seasons. The results presented in Figures 4.5 and 4.6 show the effect of MED for the altitudinal movement of the peak height of the F layer ionosphere. The change in electron density of the layered ionosphere

is seen clearly in Figure 4.7 as a function of TEC. Equatorial eastward electric field (EEF) is a primary factor of vertical plasma transportation. As its direction reverses (westward), the vertical plasma transportation will be suppressed, then plasma will be unable to go a higher altitude. Ultimately, the peak height of F layer ionosphere formed in lower altitudes.

Since the ionospheric dynamo is strongly organized in magnetic coordinates, the Sq current foci tends to move along the magnetic equator and appear at the same magnetic latitude at different longitudes as a result the geographic latitude of the Sq focus changes with longitude [Celik, 2013; Yamazaki and Maute, 2017]. Due to various sources of perturbations, these Sq current foci will be changed, leading to the leakage of current dynamos to another hemisphere. As leakage of the current dynamo leads to overlap, those phenomena cause a latitudinal shift of the daytime equatorial current system and ultimately form short or long term CEJ events.

4.5. SUMMARY AND CONCLUSIONS

We performed a study based on narrow spatial longitudinal observations of the EEJ and long term variation of the morning depression of the EEJ in one longitude location. Also, the effects of the MED on F layer peak ionization density and TEC are carefully analyzed. From our investigations, the following conclusions have been drawn:

1. There is strong longitudinal variability and dependency among the EEJ, ExB drift, EIA-TEC distribution in the equatorial ionosphere. In general, EEJ strength is stronger on the western coast than that on the eastern coast of South America.
2. The morning electrojet depression (MED) has a more significant effect on peak height of the F2 layer than that the afternoon depression. The peak height of the F2-layer of the ionosphere during high MED time simultaneously dips down below the reference altitude of 250 km in the equatorial region.
3. The variability of the electrojet in the dayside ionosphere controls the virtual height of the F2 layer. Not all sounding frequencies of ionosondes can probe the effect of the EEJ depression on F-layer dynamics in the equatorial ionosphere. Observation suggests that the reference height (250km) of an F2 layer in the equatorial region might be different during the solar minimum than the solar maximum period.
4. Hourly GPS-TEC distributions are clearly stratified before the EEJ depression but overlap within its impact time range and also seem to depend upon its strength. The southern crests of EIAs are stronger than northern crests since this observation is taken during the summer season in the southern hemisphere.
5. The consequence of MED, e.g., morning reversal of the equatorial eastward electric field, can be seen more clearly in ionogram-derived density as well as GPS-TEC based on above analysis.

Long-term statistics relating magnetometer, GPS, and ionogram-derived statistical characteristics can contribute significantly to a more precise as well as a more economical way to characterize the F-layer dynamics of the ionosphere.

More importantly, this study indicates that even a minor depression of the EEJ plays a significant role in the electron density variation and dynamics of the peak height of the F2-layer and TEC distributions by changing the vertical transport of the ionospheric plasma. This result suggests that a precise observation of the daytime low latitude electrojet current system can provide a precise and reliable indicator for forecasting ionospheric layer dynamics. More work on other longitude sectors will be necessary to achieve logical results, and future analyses with real data have been planned.

Chapter 5

Effects of EEJ and Wind on Equatorial Anomaly Dynamics*

Contents	Page
5.1 Introduction.....	112
5.2 Instrumentation, Datasets, and Methodology.....	117
5.3 Analysis and Results.....	119
5.3.1 Annual, Seasonal and Day-to-Day Variability of EIA.....	120
5.3.2 Day-to-Day Variability of EEJ, Drifts, and EIA Strengths.....	125
5.3.3 Comparison of Neutral Wind from LLIONS Model and SOFDI Data....	131
5.4 Interpretation and Discussions.....	141
5.5 Summary and Conclusions.....	145

*
A significant portion of this chapter has been published in:
Khadka, S. M., Valladares, C. E., Sheehan, R. & Gerrard, A. J. (2018). *Effects of electric field and neutral wind on the asymmetry of equatorial ionization anomaly*, *Radio Science*, 53, <https://doi.org/10.1029/2017RS006428>.
(I would like to thank my coauthors for their permission to include their contributions to this dissertation)

The zonal electric field and the meridional neutral wind are the principal drivers that define the geometry and characteristics of the equatorial ionization anomaly (EIA). Here, we present the response of the EIA to the variability of the zonal electric field, based on measurements of the equatorial electrojet (EEJ) currents and trans-equatorial neutral winds for the generation and control of the asymmetries of the EIA crests of TEC (Total Electron Content) in the western side of the South American continent. The EEJ strengths are determined using a pair of magnetometers. The 24-hour trans-equatorial neutral wind

profile is measured using a Second-generation, Optimized, Fabry-Perot Doppler Imager (SOFDI) located near the geomagnetic equator. EIA is evaluated using TEC data measured by Global Positioning System (GPS) receivers from the Low-Latitude Ionospheric Sensor Network (LISN) and several other networks in South America. A physics-based numerical model, LLIONS (Low-Latitude IONospheric Sector), as well as SOFDI data, are used to study the effects of daytime meridional neutral winds on the consequent evolution of an asymmetry in equatorial TEC anomalies during the afternoon and onwards for the first time. We find that the configuration parameters such as strength, shape, amplitude, and latitudinal width of the EIAs are affected by the eastward electric field associated with the EEJ under undisturbed conditions. The asymmetries of EIA crests are observed more frequently during solstices and the September equinox than in the March equinox season. Importantly, this study indicates that the meridional neutral wind plays a very significant role in the development of the EIA asymmetry by transporting the plasma up the field lines. This result suggests that a precise observation of the latitudinal TEC profile at low latitudes can be used to derive the meridional wind.

5.1 Introduction

The equatorial ionosphere is a popular area of research for the space weather community due to its unique structuring, coupling, and electrodynamics. The ionosphere exhibits both slow and rapid responses to changes in its fundamental input mechanisms, including variation induced by electric fields, plasma-neutral coupling, and modulation by solar and geomagnetic disturbances. Several observable quantities of the daytime equatorial and low latitude ionospheric phenomena offer the possibility to forecast the dynamics and

fluctuations of ionospheric plasma densities at later times. For example, the ionospheric electric fields, plasma drifts, and currents generally result from the dynamo action of E and F region neutral winds driven by solar and lunar tides in the low and mid latitudes. The ionospheric electric field is produced by the motion of plasma maintaining its fundamental properties, such as its collective behavior and the state of quasi-neutrality. Furthermore, polarization fields, conductivity variations, and atmospheric gravity and planetary waves can also significantly affect time scales from tens of minutes to about a month [Richmond, 1989; Fejer, 1991; Kelley, 2009a; Eccles et al., 2011].

The equatorial electrojet (EEJ) and equatorial ionization anomaly (EIA) are prominent daytime effects of the low latitude ionospheric phenomena which are driven by the eastward electric field (EEF) [MacDougall, 1969; Heelis, 2004]. The EEJ [Chapman, 1951] is one of the unique daytime ionospheric phenomena, defined as an intense eastward current flowing in the form of a ribbon-shaped band roughly 600 km wide in the E region ionosphere flanking the geomagnetic equator of the Earth [Egedal, 1947; Forbes, 1981; Onwumechili, 1997]. The pressure gradients from solar and auroral heating, with additional forcing by tidal energy from below, are possible drivers of the thermospheric neutral winds [Blanc and Richmond, 1980; Titheridge, 1995]. During magnetically quiet periods, the atmospheric wind dynamo mechanism within $\pm 60^\circ$ geomagnetic latitudes is the main driver of the ionospheric electric fields and currents in which ions and electrons move under the control of neutral winds and electric and magnetic fields [Richmond, 1989; Rishbeth, 1997]. The atmospheric wind at ionospheric heights sets a tidal motion current due to differential solar heating in the northern and

southern hemisphere that converges at the geomagnetic equator and forms a jet-like current in the ionosphere. In addition, the special geometry of the geomagnetic field at the equator, together with the nearly perpendicular incidence of solar radiation, causes an equatorial enhancement in the effective conductivity, which then leads to an amplification of the jet current that forms a belt-like structure flowing eastward during the day along the geomagnetic equator in the E-region ionosphere [Onwumechili, 1997; Baumjohann and Treumann, 2012], forming the EEJ. This enhanced eastward electric field acts perpendicular to the northward geomagnetic field at equatorial latitudes and lifts up plasma with vertical ExB drift to higher altitudes. When plasma is elevated to higher altitudes, it diffuses downward along the geomagnetic field lines due to gravitational and pressure gradient forces to about $\pm 17^\circ$ latitudes on both sides of the geomagnetic equator. This mechanism is known as the equatorial plasma fountain effect [Appleton, 1946; Martyn, 1947; Anderson, 1973; Schunk and Nagy, 2000]. The fountain effect removes plasma from the equator and creates a pair of electron density crests at about $\pm 17^\circ$ either sides of the geomagnetic equator, forming the EIA. The EIA was discovered by Edward V. Appleton [1946] and is also known as the Appleton anomaly. Indeed, an equatorial eastward electric field is a vital ingredient in generating EIAs and a key participant in the onset of equatorial plasma bubbles (EPBs). EIA onset is identified by an eastward electric field that subsequently expands to symmetrically $< 20^\circ$ latitudes either sides of the equator. Nevertheless, the strength of EIA crest in one hemisphere is commonly stronger than that of the opposite hemisphere forming an asymmetry structure. A long-standing research question in thermosphere-ionosphere coupling system is the process responsible for the asymmetry generation on the EIA. However, the EEJ cannot

alone give sufficient evidence of asymmetry structure of the EIAs, and the ultimate aim of the present paper is to report the results obtained from a study of the electric field as well as neutral wind dependence of the EIA structure.

The thermospheric wind also plays a significant role by controlling the vertical positions of the F-region pushing ions along the magnetic field lines and contributes to the unequal magnitude of EIA crests as well as formation of additional ionospheric layers [Rishbeth, 1972; Herrero *et al.*, 1993; Lin *et al.*, 2009; Makela *et al.*, 2013]. Neutral winds cause interhemispheric asymmetry in EIAs by modulating the plasma fountain and moving the ionospheres at the conjugate hemispheres to different altitudes [Balan *et al.*, 1995; Dang *et al.*, 2016]. The seasonal, solar activity, temporal, and longitudinal variations in EIA asymmetry also depend on the displacement of the geographic and geomagnetic equators and in the magnetic declination angle [Su, *et al.*, 1996, Tulasi Ram *et al.* 2009; Luan *et al.* 2015; Dang *et al.* 2016] which is the largest in the American sector. Change in magnitude and direction of the neutral wind field initiated by global or local pressure distribution and ambipolar diffusion associated with neutral density and scale height is one of the prime candidates to govern variability of EIA [Sastri, 1990, Kelley, 2009a]. The ions and neutral particles are dynamically coupled with each other through ion-neutral collisions via meridional neutral wind, which is responsible for asymmetric generation of the EIAs by controlling the final location of enhanced TEC in the equatorial ionosphere [Hei and Valladares, 2010; Valladares and Chau, 2012]. In contrast to the large number of studies on thermospheric neutral winds and equatorial ionization anomaly, heretofore, daytime measured meridional neutral winds and their role in

structural dynamics of EIAs has not been fully addressed. The ground-based Fabry-Perot interferometer (FPI) has shown significant effectiveness in the measurement of thermospheric neutral winds, but it is restricted to cloudless nighttime observations only [Burnside, et al., 1981; Hedin et al., 1991; Meriwether, 2006; Makela et al., 2012]. There are various limitations to obtain flawless daytime measured thermospheric neutral winds in the upper atmosphere. While there has been intense debate on the capability of various methods and models for the estimation of daytime meridional neutral winds, *Gerrard and Meriwether* [2011] developed a new design of triple-etalon interferometer, called SODFI (Second-generation, Optimized, Fabry-Perot Doppler Imager), that is able to make 24-hour measurements of thermospheric winds from OI 630-nm emission in the geomagnetic equatorial regions.

Our understanding of the role played by ionospheric electric fields and neutral winds in the formation of EIAs is still very limited despite studies done over several decades. In this study, the structural pattern of EIA strengths is observed using several networks of GPS receivers, while the trans-equatorial neutral winds are determined using SODFI. Both are operated in equatorial and low latitude regions of South America. The Jicamarca Incoherent Scatter Radar (ISR) allows for real time equatorial vertical plasma drifts. Simultaneously, the physics-based LLIONS (Low-Latitude IONospheric Sector) model is also used to estimate daytime meridional neutral winds by taking Jicamarca ISR vertical drifts as one of the model's inputs. A meridional neutral wind was inferred using the LLIONS model due to the fact that there are not enough measured wind values during the daytime. Such model-inferred meridional wind results are compared with measured

values provided by the SOFDI located in Huancayo, Peru. We found a significant correlation of the symmetry and asymmetry of EIA anomaly patterns with equatorial electrojet and meridional neutral wind respectively during quiet conditions. Thus, this observational and modeling effort suggests that the meridional neutral wind influences the generation of asymmetry of EIAs in the Earth's low latitude ionosphere. A full understanding of the link between the neutral winds and asymmetry structures of EIAs in the ionosphere requires higher resolution wind measurements. Finally, a mechanism describing the physics behind the plasma flow for the generation of asymmetry on EIAs is presented.

5.2 Instrumentation, Datasets, and Methodology

The low latitude region of the western meridian in South American continent is well instrumented with magnetometers, GPS receivers, Fabry-Perot interferometers, radars, and different types of ionosondes. We present dual-frequency GPS total electron content (TEC) datasets to study the strength, occurrence, and latitudinal distribution of EIAs around the 75°W longitude in the equatorial and low-latitude ionosphere. LISN (Low Latitude Ionospheric Sensor Network) is a distributed observatory that operates in the South American continent. It was designed to probe the disturbed and undisturbed ionospheric electrodynamics in the low-latitudes and also allows us to explore the development as well as the decay of the EIA in unprecedented detail. GPS receivers can continuously measure TEC integrated along the line-of-sight from GPS satellites to receiver. TEC is measured in units of TECU (1 TEC Unit = 10^{16} electrons/m²).

The EEJ strength is a widely-accepted proxy for the daytime EEF in the ionospheric E-region [Dunford, 1967; Deshpande, 1977; Stolle, et al., 2008a]. The EEJ is estimated using the variability of the horizontal components of Earth's magnetic field intensity (denoted H) data from a pair of ground-based magnetometers. The strengths of H component data are recorded using fluxgate magnetometers at a geomagnetic equatorial station, Jicamarca (geog.11.9°S, 283.1°E, 0.8°N dip latitude) and an off-equatorial station, Piura (geog. 5.2°S, 279.4°E, 6.8°N dip latitude) in the American low latitudes. As described in *Khadka et al. [2016]*, magnetometer readings of H from each station are normalized with its midnight average background values for each day and subtracted to get only the electrojet contribution to H. The difference of electrojet effect on H between two magnetometers located at equator and off-equator ($\pm 6^\circ$ to $\pm 9^\circ$ away) is defined as the EEJ strength.

The meridional neutral wind is measured using a specially designed interferometer system, SOFDI, and a physics-based numerical model data. SOFDI is a unique ground-based instrument and has a broad range of applications pertaining to both day and night time observations of mesosphere and thermosphere airglow emissions. We use meridional neutral wind data collected during daytime using SOFDI at the equatorial station Huancayo (geog.12.7°S, 284.8°E, and 0.6° S dip latitude), Peru. The detailed optical geometry, instrumentation, observation and extraction of neutral wind data by removing the background from dayglow emission is explained in *Gerrard and Meriwether [2011]*.

For the present study, the day to day variability of TEC for the year 2011-2013 is shown to introduce the asymmetric patterns of EIA. It is found that all instruments, magnetometers, Jicamarca ISR, GPS receivers and SOFDI operated simultaneously for a few days in August 2011; thus we discuss in detail the observations and simulations for those days. A comparison analysis between meridional neutral wind estimated from LLIONS model and that from observed SODFI data and their contributions to EIA asymmetries is also computed.

5.3 Analysis and Results

The asymmetry of the EIA is investigated using equivalent vertical TEC derived from GPS receivers spread in South America. Even though the detailed information of anomaly drivers is still in debate, our analyses logically address such questions with direct measurement and modeling technique. Most of the days, the crests of TEC anomalies have an unequal strength and are separated from the magnetic equator by less than 20° . The trough of the equatorial anomaly is located at the magnetic equator. The strength of EIA asymmetry is calculated by taking the ratio of the maximum value of the two hemispheric anomalies TEC crests values. Besides the meridional neutral winds, dragging force due to continuous ion accumulation, sudden stratospheric warming (SSW), solar fluxes, atmospheric tides, change in composition due to magnetic perturbations, photochemical process are also responsible factors for the asymmetry of the EIA peaks [*Hanson and Moffett, 1966; Abdu et al., 1990, 2008; Immel et al., 2006; Tulasi Ram et al., 2009; Goncharenko et al., 2010; Xiong et al, 2013; Jonah et al, 2015; Khadka et al., 2016, Dang et al., 2016*]. In this study, we particularly focused on

analyzing the contribution of meridional neutral wind for the asymmetry generation of EIA using observational and modeled winds in the low latitudes ionosphere.

5.3.1 Annual, Seasonal and Day-to-Day Variability of EIA

The day-to-day variability of three years (2011, 2012, and 2013) of equivalent vertical TEC derived from LISN GPS receivers within 70°W - 80°W longitude sector during 19:00 UT - 22:00 UT are presented in Figure 5.1. This Figure displays the TEC variation as a function of geomagnetic latitude and month of the year. It is observed from Figure 5.1 that the TEC displays higher values during equinoctial months and lower values during solstice months. Most of the anomaly crests are located near $\pm 17^\circ$ magnetic latitudes during all seasons. If we focus on the TEC strength in the pair of anomaly crests, asymmetry can clearly be seen in the magnitude of the strengths. The anomaly crests are well formed and extended into the northern hemisphere on and around June solstice and then into the southern hemisphere during December solstice. This characteristic follows the fact that the Southern (Northern) hemisphere is in summer season during December (June) solstice. A clear trend of increased ion density in the summer hemisphere compared with that in winter hemisphere is evident in all three year's TEC profiles.

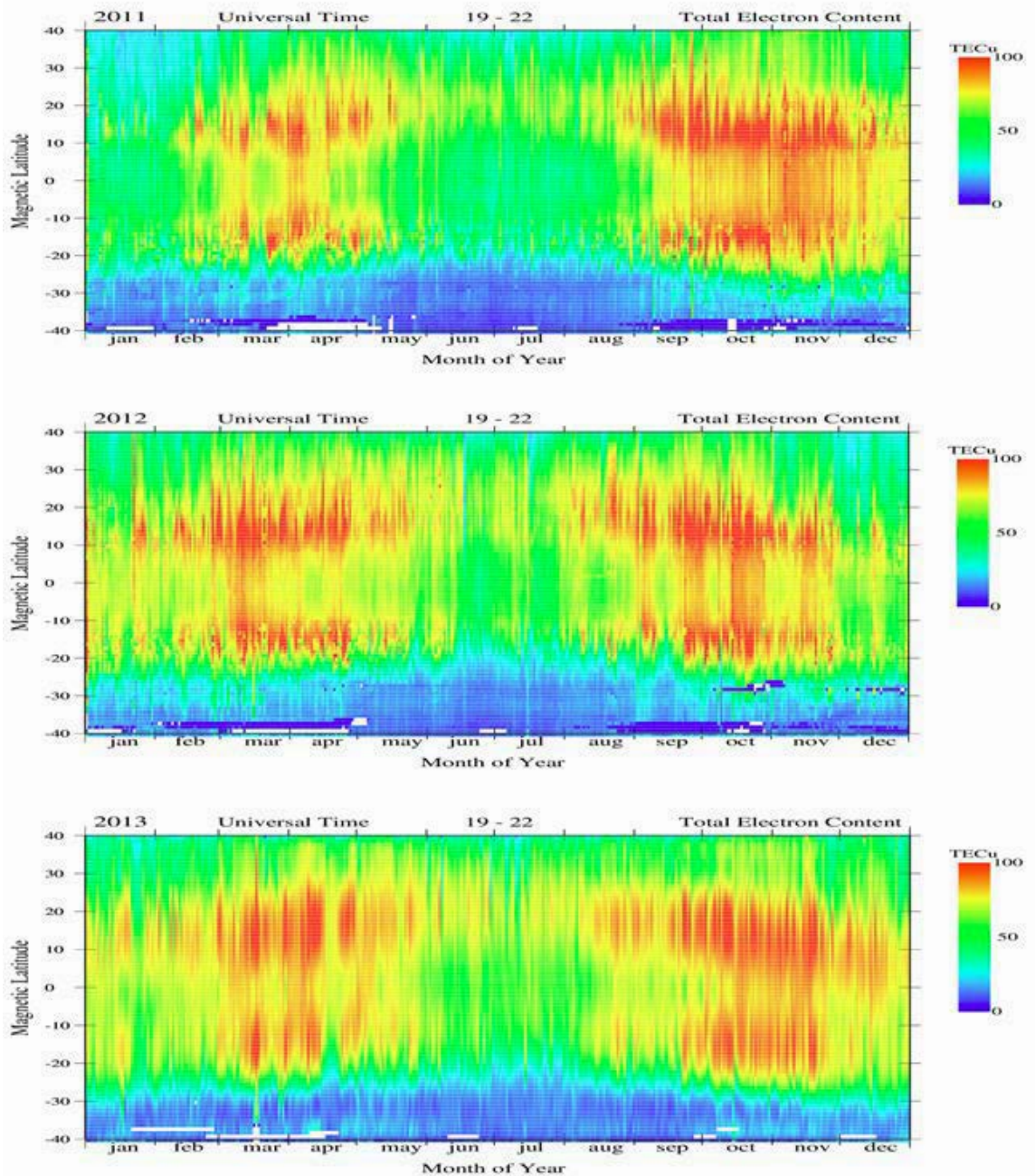


Figure 5.1 Geomagnetic latitudinal profiles of the annual and day-to-day variability of EIA crest of TEC showing an increase of the solar cycle from 2011 to 2013. The seasonal effects that alter the patterns of meridional neutral wind cause the differences of asymmetries between solstices and equinoxes.

Figure 5.1 presents clear evidence of equinoctial and solstitial asymmetry in TEC distributions. Anomaly crests are more symmetric during March equinox period than that in September equinox period. It is also seen from Figure 5.1 that the asymmetry events are more prominent during solstice seasons than in equinox seasons. Solar activity rises and falls with an 11-year cycle that affects ionospheric plasma dynamics as well as the intensity of geomagnetic activity. Figure 5.1 represents the ionospheric TEC data during the ramp up phase to solar maxima of solar cycle 24. Also, one can evidently see that the magnitude of TEC is seen increasing from 2011 towards 2013.

Figure 5.2 shows a fifteen days mass plot of seasonal characteristics of EIA during different seasons represented by ± 7 days for March and September equinox days and June and December solstice days corresponding to the years 2011 to 2013. The TEC data are chosen within $70^{\circ}\text{W} - 80^{\circ}\text{W}$ longitude of low latitude sectors during 19:00 - 22:00 UT (which is around 14:00 – 17:00 LT) period. It's been already reported that significant effects of peak (noontime) values of electric field on the EIA structural patterns can be seen within 3 hours of peak EEJ. TEC data corresponding only to geomagnetically quiet conditions is plotted to exclude effects due to prompt penetration electric fields and disturbance dynamo. The level of disturbances in the Earth's magnetic field is usually indicated using K_p index that is used to characterize the magnitude of geomagnetic storms. On 15 days duration in each season, we choose only the days having the hourly averaged $K_p \leq 4$ as provided by <http://omniweb.gsfc.nasa.gov/form/dx1.html>.

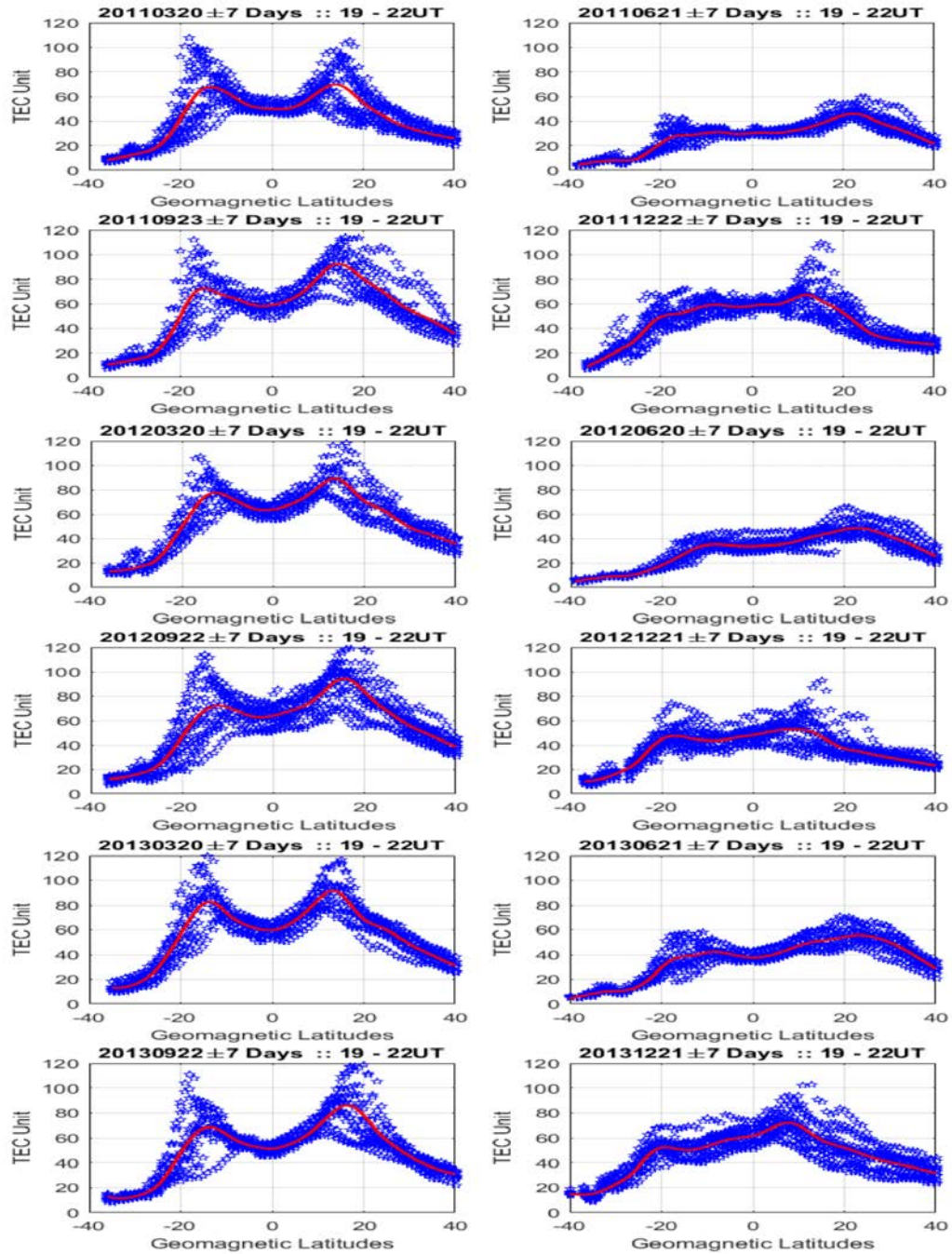


Figure 5.2 Fifteen days scatter plots of latitudinal variations of maximum TEC data in the equinox (first column) and solstice (second column). The red continuous curve represents 15-day average of available maximum TEC.

The six plots in the first column show the anomaly profiles in equinox (March and September) seasons, while plots in the second column represent those of solstice (June and December) seasons in 2011, 2012 and 2013 respectively. To determine the seasonal patterns of EIA, we construct a 15 day running average filter using a regression analysis with weighted linear least squares coefficients. The thick red curve in each plot represents the average of the corresponding scatter data distribution in that particular season. It is to be noted that out of 15 days, disturbed ($K_p > 4$) days, if existing, are excluded in analyzed seasons. The scatter plots are interrupted for a few days due to the suppression of electrojet and hence drift by storm-induced electric fields. Figure 5.2 represents an overall quiet geomagnetic condition with occasional minor magnetic perturbations. During solstice, the EIA crests are found weaker and more asymmetric than during equinoxes.

Prominent features of these plots are the dominance of the northern crest that persists during all seasons. The peak of the northern crest is generally centered near $16-18^\circ$ geomagnetic latitude although, during the June solstice, the northern crest seems located between 20 and 22° magnetic latitudes. However, during this season, the whole anomaly pattern seems shifted northward with a trough displaced from the magnetic equator by as much as $3^\circ-5^\circ$. This effect is produced during the summer in the northern hemisphere and the large offset between the geographic and magnetic equators (12° at 75° W longitude). More symmetric-anomaly events are seen in March equinox than during the September equinox. TEC values during the December solstice show higher TEC value than during the June solstice. In addition, the northern anomaly crests shift slightly towards the

equator from the north with stronger southern crests than that in June solstice. This phenomenon is reasonable since there is summer in the southern hemisphere during December solstice season. Also, asymmetries between the hemispheric geomagnetic fields give rise to an asymmetry in the solar radiation as well as the plasma and neutral composition that ultimately leads to hemispheric differences of the electron density in the F-region ionosphere [Sojka *et al.*, 1979; Laundal *et al.*, 2016]. All the average curves of Figure 5.2 indicate that the overall strength of EIA crests in the northern hemisphere is stronger than the southern hemisphere. A reason behind this is due to the large difference of geomagnetic and geographic equator since the presented data pertain to this location. It is to be noted that western part of South America possesses the largest difference ($\sim 12^\circ$) between geomagnetic and geographic equator than any other part of the world. Moreover, the role of EEJ strength for the development of anomaly crests can be seen in a simultaneous demonstration of their measured values. Following sections attempt to address and present corresponding phenomena.

5.3.2 Day-to-Day Variability of EEJ, Drifts, and EIA Strengths

The EEF associated with EEJ is a primary driving force for the vertical plasma drift. Figure 5.3 shows a variation of the H component measured using magnetometers at the equatorial station, Jicamarca (blue) and off-equatorial station Piura (green) in the American low latitudes. The red curve represents the net EEJ strength which is enhanced during local noontime.

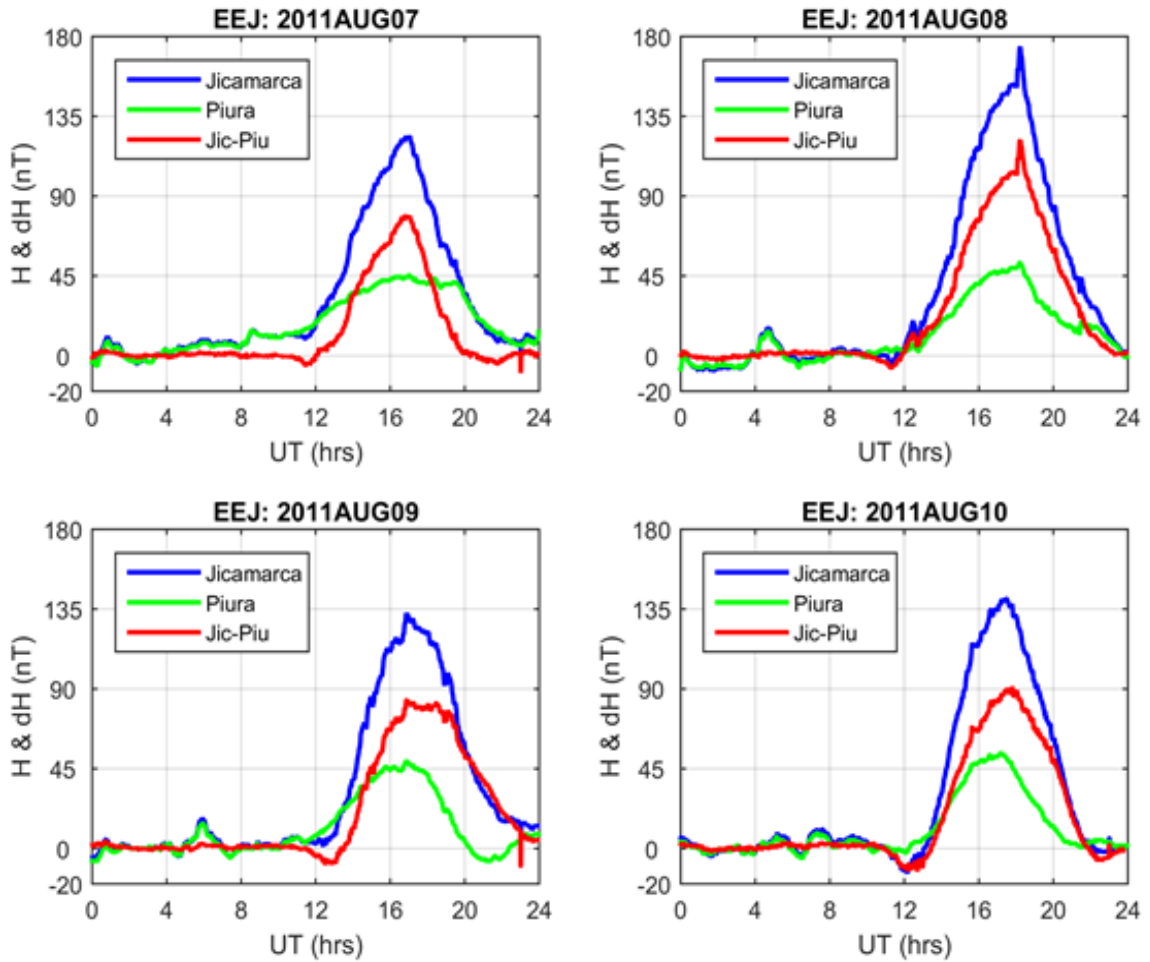


Figure 5.3 H-component magnetic field and the difference between two magnetometer stations to show the noon-time enhancement of the EEJ to be used as proxy for the EEF.

Figure 5.4 characterizes ionospheric plasma drifts measured with the Jicamarca ISR on the same days of Figure 5.3. Data are restricted to the height range 250 km to 400 km for the analysis, thus reducing uncertainties in the measurements caused by increased scatter from higher plasma densities. Not surprisingly, the variations of the ISR drift follow exactly the same patterns of EEJ, with the maximum measured values of the drifts observed at noontime along with the maximum EEJ strengths. By comparing Figure 5.3 and Figure 5.4, it is demonstrated that the stronger the EEJ strengths, the faster is the ISR plasma drifts. The diurnal configuration of vertical plasma drift mimics exactly the variation pattern of the electric field supported by EEJ measurements. This correlation between the plasma drift and the EEJ current is quite typical in the equatorial and low latitude regions since both of these are based on the same EEF.

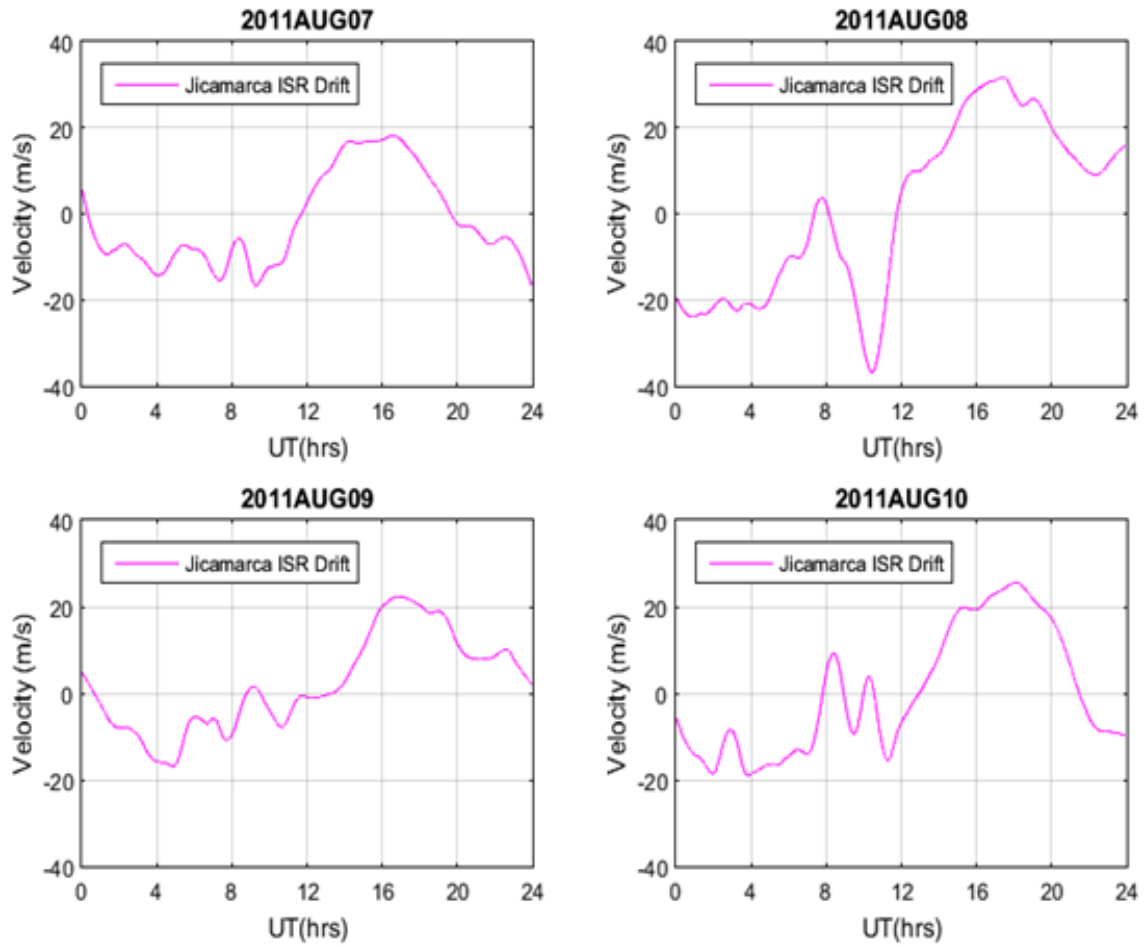


Figure 5.4 Average vertical plasma drift profiles in the ionosphere from Jicamarca incoherent scatter radar (ISR) at geomagnetic equator.

The TEC distributions of Figure 5.5 show the variability of the EIA during the days presented in Figures 5.3 and 5.4. This Figure shows the TEC variation as a function of geomagnetic latitude and universal time (UT). The anomaly crests are intense and have great latitudinal separation if there is strong EEJ leading to a higher value of plasma drifts. The weaker EEJ day has a small drift that is unable to build an effective plasma fountain for the creation of EIAs. Besides equatorial vertical drift, the day-to-day TEC variability in Figure 5.5 can also be related to changes in solar radiations even though the solar F10.7 might not show big differences on those days. The maximum strengths of anomaly crests appear a few hours after the peak value of EEJ and vertical drift. The unequal strength of anomaly crests leads to asymmetry structure of EIAs. The evidence and controlling factors behind this phenomenon seen in EIA structure will be discussed in detail in the following sections.

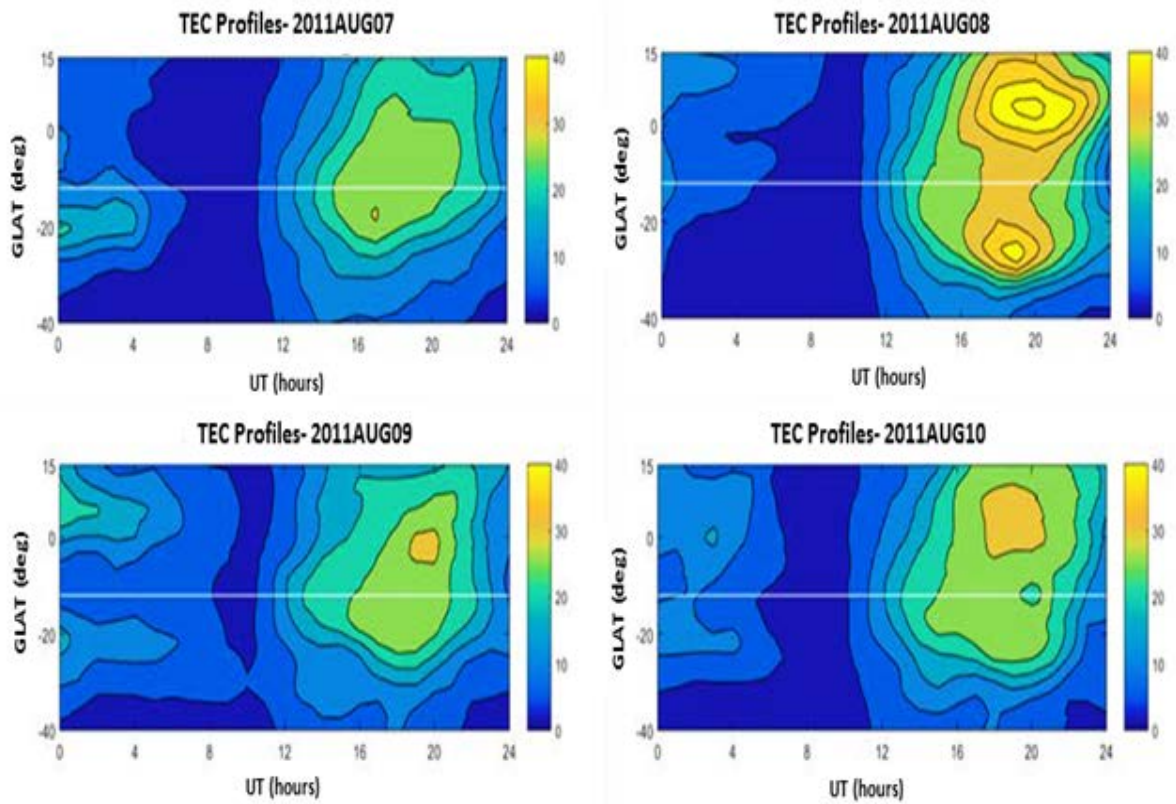


Figure 5.5 Contour plots of TEC distribution along 70°W on August 7, 8, 9, 10 for 2011. The only figure showing a double-peaked EIA is the TEC figure for 8th August 2011. The white horizontal line represents the location of the geomagnetic equatorial line.

5.3.3 Comparison of Neutral Wind From LLIONS Model & SOFDI Data

To elucidate the role of the meridional component of neutral wind on EIA asymmetry, a physics- based inverse-modeling approach was taken using the LLIONS model. Herein we utilized one week of measured neutral wind data in August 2011, as measured from SOFDI, for simultaneous comparison with LLIONS model results. We have presented four days of August 2011 neutral wind data in this discussion (Figure 5.6) for the coincident observation of ISR drift velocity and EEJ as shown in Figure 5.3 and 5.4 respectively.

The blue curve in Figure 5.6 displays the meridional neutral wind measured for a whole day at the Huancayo observatory located near the magnetic equator in South America. The green curve in Figure 5.6 gives the variation of the modeled (LLIONS) meridional neutral wind as a function of Universal time for 4 days (2011 August 07, 08, 09, and 10). The red bars represent the errors of the SOFDI measurements. A very significant day-to-day variability is shown in the SOFDI data. The neutral wind moving northward (southward) direction is called as positive (negative) wind here in the analysis. On August 07, 2011 the wind is positive between 08 and 16 UT and reaches 80 m/s at 12 UT. It is mainly negative during the day. On August 08, 2011 the wind shows values between ± 40 m/s except for a period between 00 and 05 UT when it is -40 m/s. The wind value on August 09, 2011 shows a positive peak at 10 UT, and mainly negative during the day. August 10, 2011 shows the largest temporal fluctuations with the wind varying between +80 m/s at 03 UT and -90 m/s at 22 UT. It is largely negative during the daytime hours.

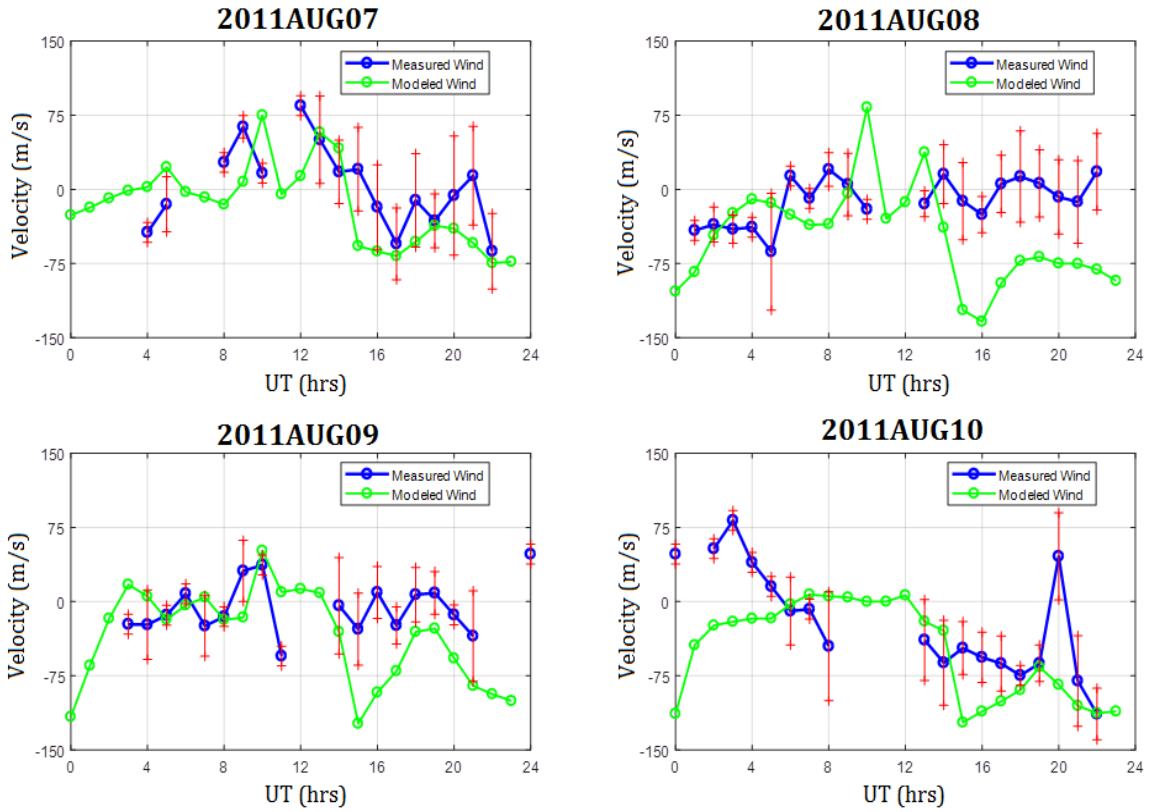


Figure 5.6. This figure shows the meridional wind velocity for each hour at Huancayo for 7, 8, 9, 10 August 2011 in the western meridian of American low-latitudes. The meridional wind velocities for 8th August 2011 are not large, and this day shows the most symmetric EIA. The blue (green) curve with circles is the measured (modeled) meridional wind velocity by SOFDI (LLIONS) and the vertical red lines represent the error bars of the measured wind.

The LLIONS model, originally inspired by the *Anderson [1973]* Low-latitude ionosphere model (LOWLAT), is based on the low-latitude portion of the Ionospheric Forecast Model [*Schunk et al., 1997*]. LLIONS calculates the two-dimensional, time-dependent density distributions of five major plasma constituents (NO^+ , O_2^+ , H^+ , O^+ , e^-) between $\pm 45^\circ$ latitude and 90-4000 km altitude. The plasma distribution is solved along magnetic field lines with many field lines used to construct a regular output 2D grid in magnetic latitude and altitude. Inputs to the model are the vertical $\text{E} \times \text{B}$ drift velocities, horizontal neutral winds, the neutral atmospheric densities and temperatures, and the Kp and F10.7 solar flux indices.

An ensemble of 143 independent runs is conducted keeping the vertical drift the same for each of the model runs, but using different meridional winds for each model run. The Horizontal Wind Model (HWM, as presented in *Hedin et al., [1991]*) provides both the zonal and the meridional wind values as a function of latitude, longitude, altitude and universal time $W(\text{lat}, \text{long}, \text{alt}, \text{UT})$. To generate 143 different functions of the wind, we multiplied $W(\text{lat}, \text{long}, \text{alt}, \text{UT})$, as given by the HWM model, by a variable factor (F1) and added another variable factor (F2). The following expression: $F1 \times W(\text{lat}, \text{lon}, \text{alt}, \text{UT}) + F2$ is used to generate the ensemble of wind functions. Where, the F1 factor is varied between 0.2 and 2.2 in steps of 0.2 (11 factors), and the F2 additional wind value is increased between -120 and +120 m/s in steps of 20 m/s (13 numbers). The result of each model run provides a two-dimensional density profile over the 75° W longitude sector. The density profiles are then used to derive TEC latitudinal distributions. Each modeled TEC profile is cross correlated with the TEC values observed in the Peruvian

sector (recall that SOFDI is located at a geographic latitude = -12°). Although this method can introduce, in some extreme cases, unrealistic wind values, retains the latitudinal and height variability of the meridional wind.

A clear example of the latitudinal variability of the meridional wind values that were obtained with the ensemble model runs is depicted in Figure 5.7. This Figure shows the latitudinal distribution of the wind system that provided the maximum cross correlation coefficient for August 09, 2011 between 00 and 06. Figure 5.7 shows the meridional wind to be negative at northern latitudes, then reversing and becoming positive in the southern hemisphere. The latitude where the wind reverses varies between 50° S observed at 00 UT and -12° S (near the magnetic equator) at 06 UT. It is worth mentioning that the meridional wind of 00 UT (Figure 5.7) produced one of the largest values (-110 m/s) at the magnetic equator (see Figure 5.6).

A close comparison between the meridional neutral wind estimated from the ensemble of LLIONS runs and SOFDI measurements shows a reasonable agreement with respect to magnitude and direction. During quiet days, electric field fluctuations in the EEJ altitudes are rare because the background electric field mostly overwhelms wind-driven perturbation electric fields [Shume *et al.*, 2014; Kelley, 2009a]. The modeled patterns of meridional neutral wind also show a trend similar to the variations of the SOFDI measurements. The best agreement was obtained on August 07, 2011 when the derived winds are between the error bars of the measured wind. On August 8 and 9, 2011 the calculated winds approximate the SOFDI measured winds between 04 and 14 UT.

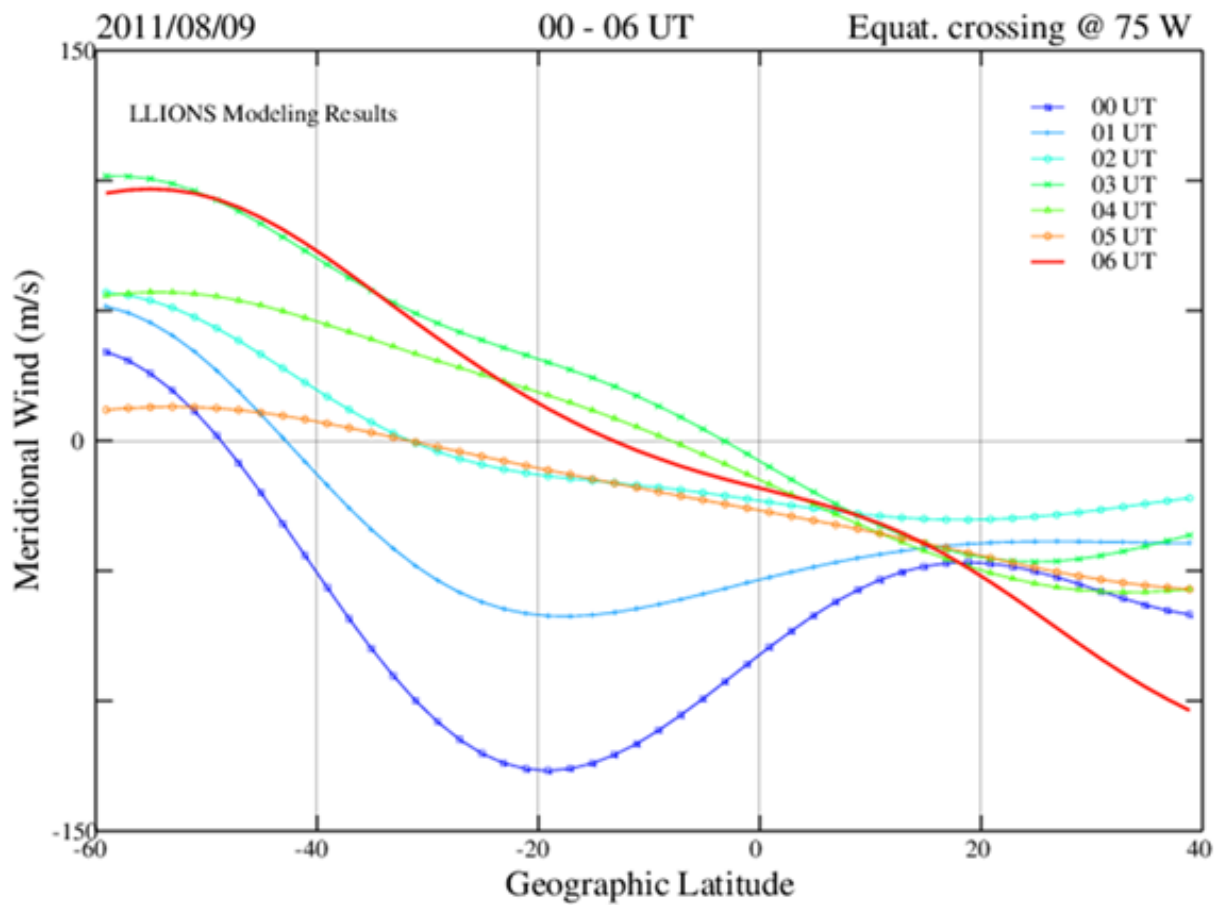


Figure 5.7 Plot showing a variation of LLIONS-modeled meridional neutral wind against geographic latitude for 7 hours.

In general, one can see that the meridional neutral wind derived by the inverse-modeling shows a good qualitative agreement rather than quantitative with the measured values presented in Figure 5.6. This result indicates that further improvements of inverse-model procedure are needed to get a quantitative agreement with the measured wind. It is suggested to consider the altitude dependence of the vertical drifts that is measured with the Jicamarca radar and can be used as input to the LLIONS model. A comparison of the TEC contours of Figures 5.5 and the meridional winds of 5.6 points out the close relationship of the meridional wind and the EIA asymmetry. On August 7, 9 and 10 the meridional wind is negative between 16 and 24 UT when the EIA shows an asymmetry with a pronounced northern crest. On August 8, 2011, the SOFDI winds show small fluctuations around zero making the anomaly more symmetric.

Figure 5.8 presents the comparison of measured TEC and modeled (LLIONS) TEC values. The latter were calculated using neutral winds estimated using the inverse modeling approach. The general trends and magnitudes of TEC from GPS and model values look comparable in the most of the cases. In Figure 5.8, it is seen that model TEC values follow exactly the same magnitude and pattern as LISN measurement at 10UT. However, there are some discrepancies between measured and model TEC at 00UT. For example, in Figure 5.8, the model and measured peak values of TEC on August 7 and 8, 2011 are highly correlated with each other regarding their magnitudes as well as in trends. While on August 9 and 10, 2011 the magnitudes of TEC values are poorly correlated, but their trends are similar. In Figure 5.8, as the meridional neutral wind is positive (northward) the southern anomaly peaks in terms of TEC seem to shift farther

from the equator towards the southern hemisphere. These cases are seen in all the subplots of Figure 5.8 at 10 UT. For the conditions of negative (southward) meridional neutral wind, the southern anomaly peaks seem to come closer towards the equator from the southern hemisphere. It is to be noted that the actual measured Jicamarca ISR vertical drift is one of the inputs in the model discussed here. However, the model does not consider the zonal ion drifts, neutral winds other than meridional, and variations of the O/N_2 ratio. These might be some of the sources of discrepancies in our results. Furthermore, the results presented here are for only four days of August of 2011. The 24-hour measured neutral wind data cannot give a detailed picture for the inference but gives the sense of interpretation of meridional neutral wind patterns for the EIA anomalies.

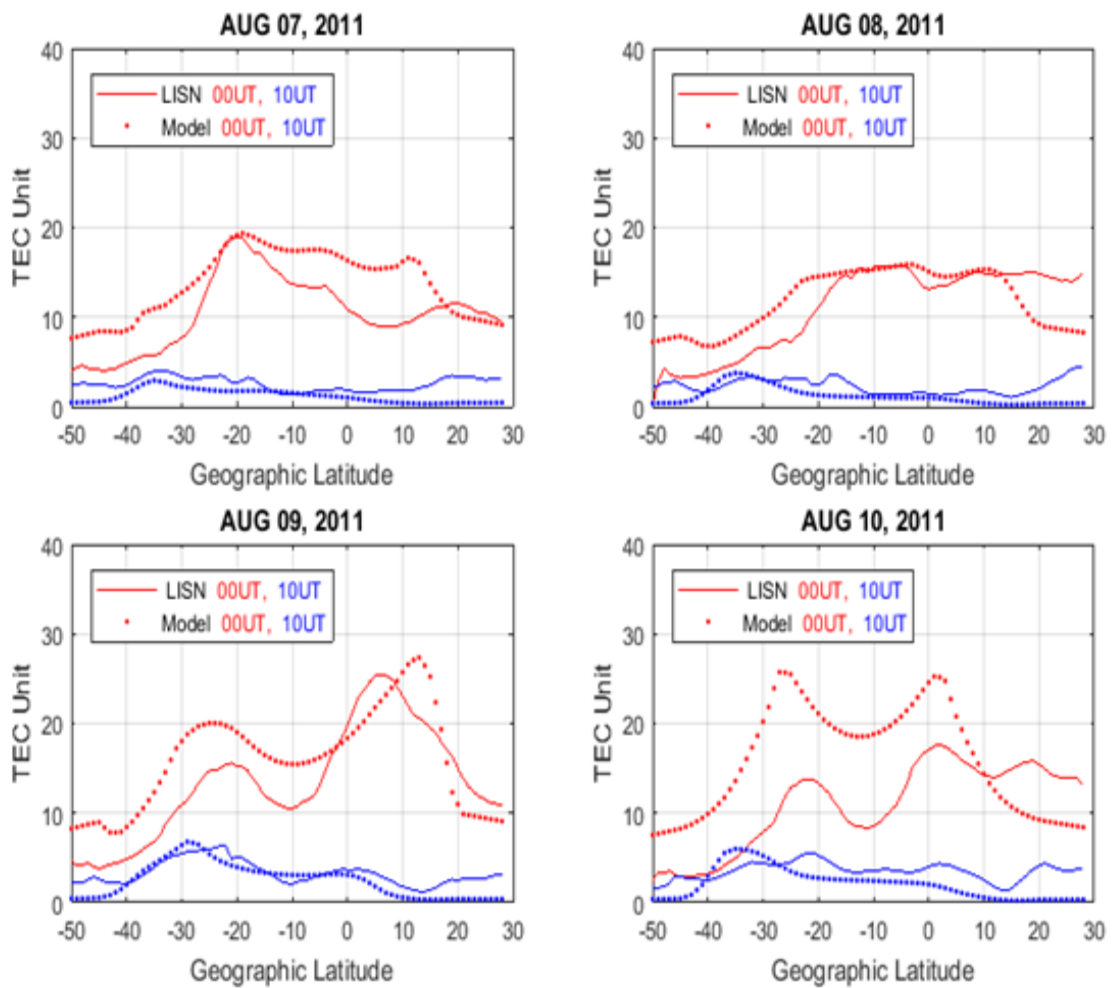


Figure 5.8: Plots showing a comparison of LISN-measured (continuous curves) and LLIONS-modeled (dotted curves) based TEC variations against geographic latitude. In each panel, TEC values are binned in every degree of latitude and plot its variation at 00 UT (red) and 10 UT (blue) for both measured and modeled cases.

Figure 5.9 shows TEC latitudinal profiles measured by several networks of GPS receivers in the Peruvian sector ($\sim 75^\circ$ W). These plots are used to relate the asymmetry of the anomaly to the sign of the meridional wind that was measured by SOFDI. The TEC anomaly curves show symmetric characteristics on August 08, 2011 between 08 and 16 UT (magnetic equator = 12° S). A highly asymmetric anomaly containing a predominant southern crest was observed on August 7, 2011, between 12 and 16 UT. An asymmetric anomaly with a dominant northern crest was measured on all 4 days at 20 UT. These symmetric and asymmetric characteristics of the anomaly are related to meridional wind. For example, on August 08, 2011 the SOFDI winds fluctuate around zero m/s and do not influence the development of any crests. On August 7 and between 12 and 16, the meridional wind has been positive for more than 4 hours making the plasma to move up the field lines in the southern hemisphere and down in the northern hemisphere. The same effect is seen in the wind value near 20 UT for each of the plots. The velocity is negative or follows a long period of negative velocities that enables the development of a northern crest.

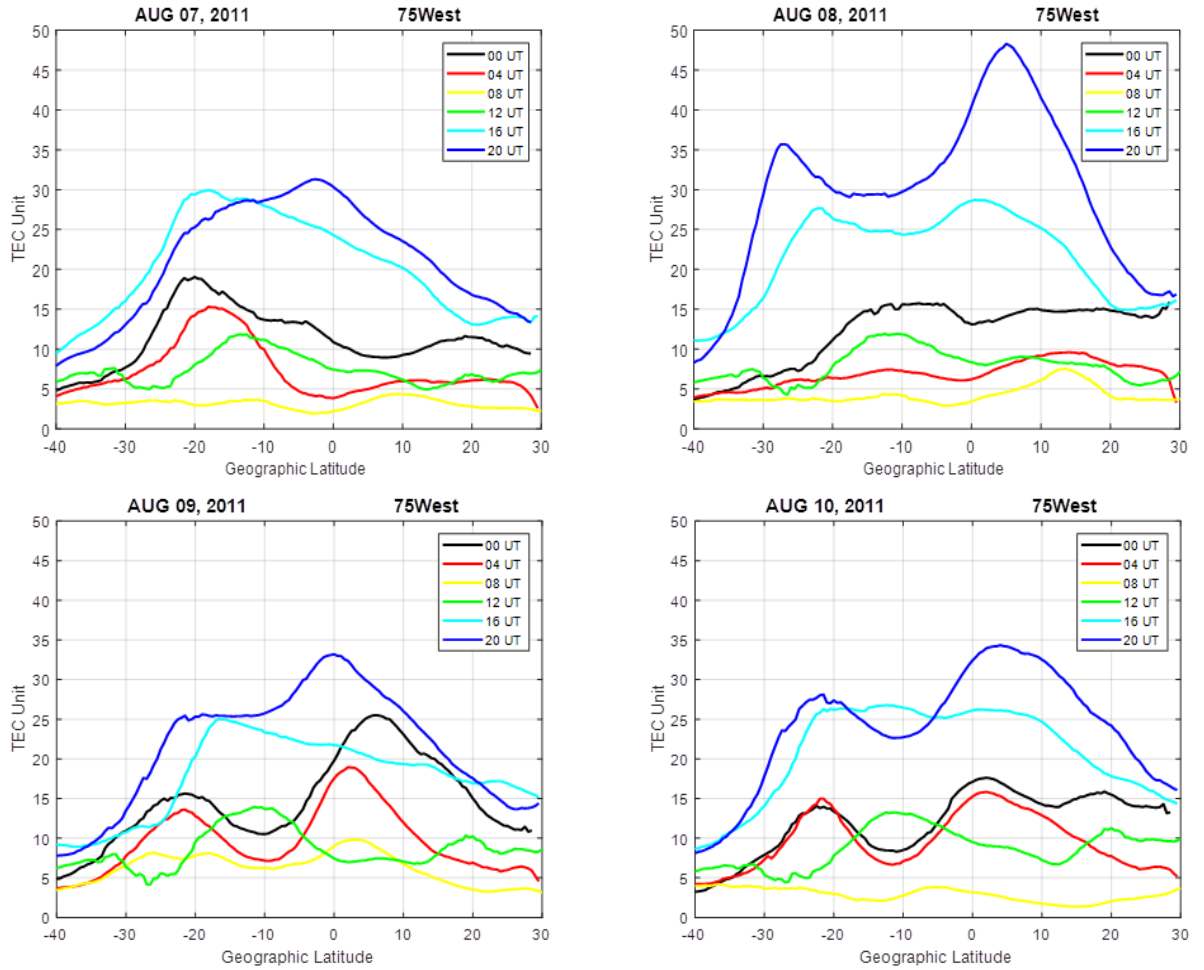


Figure 5.9 Latitudinal profiles of TEC in the four hours interval against geographic latitude for 7, 8, 9, 10 August 2011 in the western meridian of South America.

5.4 Interpretation and Discussion

Trans-equatorial neutral winds can have profound influences on numerous ionospheric processes including plasma transport, composition, and the formation of structured EIAs. We have demonstrated the contribution of the EEJ and meridional neutral wind on the prevailing asymmetry structure in equatorial ionization anomaly in the low latitude ionosphere using measured as well as model data. In general, the strength, latitudinal extension, symmetry/ asymmetry of the anomaly crests are based on regular equatorial ionospheric electrodynamical phenomena (e.g. both zonal electric field and meridional wind). It is evidently speculated that, in absence of external perturbations, the EEJ associated with zonal electric field can alone form the symmetric structure of EIAs in the low latitude ionosphere. Observations and model results show the significant role of the meridional neutral wind that blows the ionospheric plasma toward the opposite hemisphere by moving the plasma along geomagnetic field lines to generate the asymmetric structure characteristics of the equatorial anomaly [Bailey *et al.*, 1973; Schunk and Nagy, 2000; Venkatraman and Heelis, 2000].

The motion of ionized particles at ionospheric heights is affected by the Earth's magnetic field, which in turn controls the flow of the ionospheric currents as well as the bulk movement of the plasma. The EEJ and the particular geometry of the geomagnetic field lift the plasma to higher altitudes over the equator. As the vertical drift of plasma is canceled by the gravitational and pressure forces, the plasma starts moving along the flux tube of the Earth's magnetic field that transports plasma to poleward latitudes from the equator, forming the EIA. The occurrence of daytime maximum EEJ and well-developed

EIA varies in the time range difference 2.5 to 5hr over the low latitudes sectors [Abdu, et al., 1990; Venkatesh, et al., 2015]. Our analysis also lies within the already reported time frame for those parameters.

The EIA occurs during the major part of the day, and its intense ionization density irregularities distinguish the low latitude ionosphere from other regions. Its asymmetry structure can be explained in terms of neutral wind. The winds transport particle mass, momentum, and energy throughout the atmosphere. The wind also moves plasma through drag/collisions and can induce currents and electric fields. Waves also propagate within the neutral atmosphere and can perturb the normal behavior of the thermosphere. Once gravity waves and tides reach the ionospheric height, due to the neutral-ions collision of the closely coupled ions and neutrals, momentum from neutrals is transferred to ions. The ultimate fate of this phenomenon is the formation of asymmetry of ionospheric plasma concentration in EIAs. Figures 5.5, 5.6 and 5.9 have shown that when the meridional wind is near zero a symmetric anomaly is observed. Figure 5.9 indicated that a positive (south to north) wind is associated with a dominant southern crest and for negative meridional wind and northern crest prevails. These relationship supports intra-hemisphere transport of plasma in the anomaly region.

The population and distribution of excited neutral and/ or ionized species in different ionospheric regions depends not only on chemical processes (production, collision, and recombination) but also on transport processes associated with field domains and neutral winds [Schunk and Nagy, 2000]. One of the key points of this study was to characterize

the performance of the models over measured neutral wind for the understanding of EIA asymmetry. Further measurements are clearly needed with higher resolution and corresponding sensitivities to the daytime wind occurrences of interest for the detailed explanation of TEC asymmetry in EIAs. It is known that there are various factors that can cause EIA asymmetry in the low-latitude ionosphere. The role of meridional neutral winds on EIA asymmetry generation can be explained in the following ways:

a) Intra-hemisphere Transport: - The neutral winds system has ability to move the ions and electrons along the geomagnetic field lines and affects its densities because of the height dependent nature of the plasma chemical recombination in the F region ionosphere [Sastri, 1990; Hargreaves, 1992]. If the meridional neutral wind is blowing north to south (south to north), it will drive plasma to higher ionospheric heights along field lines where recombination proceeds at a slower pace. This leads to higher plasma density in the northern (southern) hemisphere. Then the population of ionospheric plasma is enhanced since a strong equatorial plasma fountain restricts the effect of wind in windward locations over that in leeward locations. Figure 5.10 (a) illustrates this case scenario where plasma density increases in the northern hemisphere.

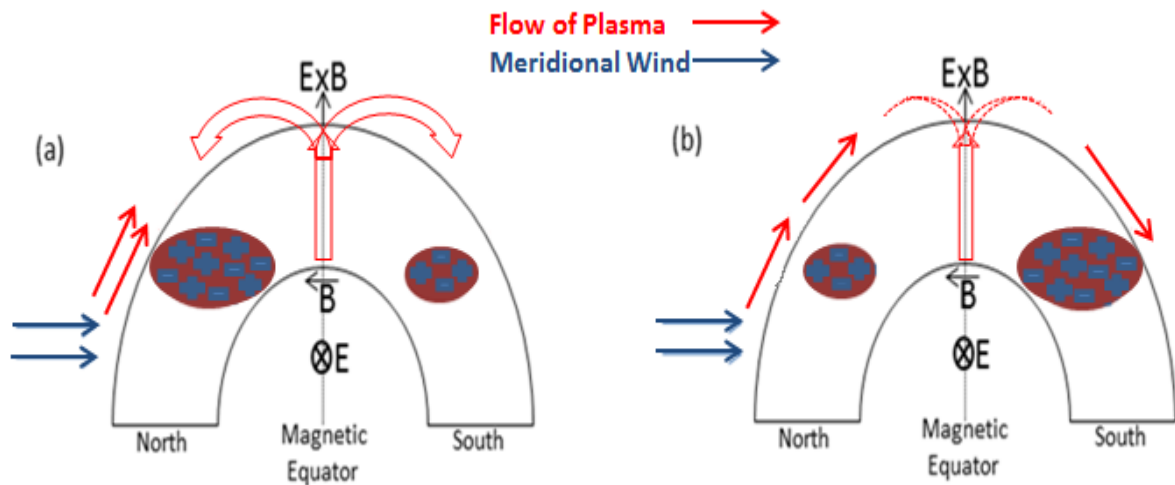


Figure 5.10 A cartoon illustration showing possible evolution and mechanism how meridional neutral wind creates asymmetry in EIA anomaly in the ionospheric F layer, looking eastward (a) Intra-hemisphere Transport and, (b) Trans-equatorial Transport. The size of shaded oval shape represents the strength of EIA crest in the two hemispheres.

b) Trans-equatorial Transport: - The interhemispheric field-aligned plasma flow organized by season and longitude, depending on the role of meridional wind, can be seen during the time of adiabatic heating and cooling at ionospheric heights [Bailey et al., 1973; Venkatraman and Heelis, 2000]. If the meridional neutral wind is blowing north to south (south to north), it will transport plasma along Earth's magnetic field lines and will dump at ionospheric height in the opposite hemisphere since the effect of a weak equatorial plasma fountain is easily overcome by wind. That leads to a higher plasma density in southern (northern) hemisphere than that in northern (southern) crests. Then the population of ionospheric plasma is less in the windward location than leeward location. Figure 5.10 (b) illustrates this case scenario where ions have the time to be transported to the opposite hemisphere and form asymmetry in EIAs.

5.5 Summary and Conclusions

This study compares 24-hour measured and modeled meridional neutral winds and investigates in detail its effects on the asymmetry of the EIA. The analysis leads to a significant advance in the study of the EIA and opens new avenues for future studies into the climatology and relationships of the EEJ, neutral winds, and EIA, during both quiet and active solar/geomagnetic conditions. The major outcomes from our study are outlined as follows.

1. The vertical $E \times B$ plasma drift associated with EEJ and geomagnetic fields, as well as the neutral wind fields, are the main drivers of EIA anomaly. The meridional component of the thermospheric wind is one of the most significant drivers of the

EIA asymmetry. The neutral particles use collision to transport ions up the field, but the plasma remains within the same hemisphere.

2. The northward (southward) propagation of intense TEC crest is clearly visible in the northern (southern) hemispheric summer seasons, while northward (southward) TEC crests during equinox periods remained intact at almost similar latitudinal locations. The latitudinal distribution of asymmetry in the intensity of northward and southward spread is caused by the different motion caused by a wind dynamo. The latitudinal extension and strength of anomaly crests are controlled by EEJ that is seen as a proxy of the EEJ development, but meridional neutral wind mainly acted to create unequal strengths of the crests to form anomaly asymmetries in the low latitudes.
3. The meridional neutral wind profiles, which also play a decisive role for the generation of asymmetry structure in the EIA, can be estimated using the LLIONS model, which utilizes vertical drift measured from Jicamarca ISR as one of the inputs. It shows reasonably good agreement within the error range of measurements by SOFDI at the geomagnetic equator for similar conditions, which strengthens the confidence of our results.
4. The anomaly crests look more symmetric in equinox than in solstice seasons. The asymmetries of the EIA observed during December solstice is greater than during June solstice, whereas September equinox is less symmetric than March equinox seasons. This variability is related to the seasonal dependence of the vertical drift [Fejer, 1991] and meridional wind.

This effect of meridional neutral wind on the EIA asymmetry is a key mechanism for the vertical and latitudinal coupling between different atmospheric layers, and also provides an important input on various forms of atmospheric mechanisms such as tides, density fluctuation, drift variability, wind dynamo, and even the extension of the EIA from low to mid latitudes. Further analysis and investigation with real time data are continuing for a better understanding of the meridional wind including zonal wind patterns on thermosphere/ neutral composition and the ionosphere over the magnetic equator, and the response of EIA under quiet and magnetosphere-induced disturbed conditions.

Chapter 6

Satellite and Ground-Based Observations of Ionospheric Plasma Irregularities

Contents	Page
6.1 Introduction.....	149
6.2 Instrumentation and Data Processing.....	153
6.3 Analysis and Results.....	156
6.3.1 Identification of EPBs and Blobs Signature from SWARM.....	156
6.3.2 Ionospheric Plasma Depletions: EPB Events	159
6.3.3 Ionospheric Plasma Enhancements: Blob Events	164
6.4 Interpretation and Discussion.....	168
6.5 Summary and Conclusions.....	171

Caveat: The contents of this chapter are based on the posters entitled: “*SWARM Observations of the Motion of Low-latitude Plasma Depletions Coordinated with Ground-based TEC Measurements*” and “*Simultaneous Observations of Equatorial Plasma Irregularities using Ground and Space-Based Instruments*”. These articles were presented at the Fall AGU meeting in San Francisco on December, 2015 and 2016 respectively.

Ionospheric plasma irregularities are one of the most important phenomena of space weather. A large variety of the numerical as well as empirical ionospheric models have been developed to understand their origin. Equatorial plasma bubbles (EPBs) as well as plasma enhancement (blobs) are main indications of ionospheric irregularities in the low latitudes that disturb the ionosphere producing deep fading of communication and

navigation signals. We have examined the behavior of total electron content (TEC), its depletions and enhancements in the low latitude ionosphere detected with GPS receivers in the American sector and correlated it with the existence of the ionospheric irregularities observed with the SWARM constellation when it flies above the Continent. Analysis of data is mainly performed in the American low latitude regions for few specific days of SWARM satellite observations during the first months of the satellites' operations. Satellite passes are used to examine density variations of the depletions between minute scale intervals. The ground-based data serve to indicate the variability of the background ionosphere prior and during the development of the EPBs. In this study, we discuss the role played by various ionospheric parameters of the equatorial ionosphere in the occurrence, growth, expansion and decay characteristics of plasma irregularities seen in the EPBs and blobs events.

6.1 Introduction

Even in the absence of intense solar activities (CMEs, Solar flares, SEPs), dynamical processes in the equatorial ionosphere, mainly governed by the special geometry of electromagnetic field, lead to plasma instabilities that cause irregularities of the plasma density almost comparable to that caused by moderate geomagnetic storms after sunset. The regions of localized plasma depletions (bubbles) and enhancements (blobs) in the low-latitude ionosphere are collectively called equatorial plasma irregularities (EPIs) which are considered to form/ redistribute along geomagnetic flux tubes after altitudinal rise. EPIs have been a vibrant issue in space weather community since these are the chief

sources of deep fading of transmission of radio signal associated with communication and navigation systems.

Irregularities in the F-layer ionosphere occur abruptly after sunset and often continue beyond midnight and usually disappear just after sunrise in the areas close to or on the magnetic equator [Kil and Heelis, 1998]. Plasma instability phenomena occurring in the equatorial F-region ionosphere is a highly dynamic state of unstable nighttime plasma irregularities evolving into various scale sizes, called equatorial spread F (ESF) that usually takes the form of EPBs [Tsunoda 1981; Abdu et al., 2001; Kelley, 2009a]. The disturbance rises to higher altitudes then later appears at sites away from the magnetic equator, indicating that the disturbance at these sites is due to an effect which develops in time along the lines of force of the earth's magnetic field [Aarons, 1993]. Disturbed plasma structures (e. g. EPBs) in the F region are triggered by strong vertical plasma density gradients in the bottomside F region under the action of the Generalized Rayleigh-Taylor instability (RTI) [Dungey, 1956; Ossakow, 1981; Haerendel et al. 1992; Sultan, 1996; Kelley, 2009a; Wu, 2015]. The gravitational force will provide a current responsible for the polarization field that drives the depleted region upward, and the background eastward electric field (EEF) produces a polarization field that ultimately establishes a rapid growth rate for the perturbations [Hanson and Bamgboye, 1984; Kil and Heelis, 1998]. In addition, EEF, the occurrence and seeding of density perturbations, may be produced by different sources such as a local variations in the vertical winds, gravity waves propagating upward from the troposphere, height of the postsunset F layer, prereversal enhancement (PRE), F region evening plasma drift vortex, geomagnetic

declination angle, and the inherent variability of low-latitude thermospheric winds [Farley *et al.*, 1970; Abdu *et al.*, 1981, 1983; Batista *et al.*, 1986; Fejer, 1991; Mendillo *et al.*, 1992; Basu *et al.*, 1996; Fejer and Scherliess, 1997; Singh *et al.*, 1997; Fejer *et al.*, 1999; Eccles *et al.*, 1999; Kudeki and Bhattacharyya, 1999; Abdu, 2001; Kudeki *et al.*, 2008]. In situ measurement techniques have the ability to detect more events confirming maximum occurrence rates and are also able to examine large scale sized EPBs [Kil and Heelis, 1998; Huang *et al.*, 2002; Gentile *et al.*, 2006; Stolle *et al.*, 2008b].

Plasma blobs occur mostly at higher magnetic latitudes (20°–30°) and form as a result of small-scale electron density instabilities essentially driven by neutral winds in the topside F region [Oya *et al.*, 1986; Watanabe and Oya, 1986]. The plasma density enhancement phenomenon in the F region ionosphere, closely related to equatorial plasma bubbles (EPBs), is termed ‘plasma blobs’ [Huang *et al.*, 2014]. Depleted plasma densities (bubbles) and enhancements (blobs) with respect to the background ionosphere occur at night in the low-latitude F region and are understood to be either causally linked or independent [Kil *et al.*, 2015]. With occasional and limited observations in the same longitudes, plasma bubble events have been understood as a cause of another plasma blob event [Le *et al.*, 2003; Pimenta *et al.*, 2004; Huang *et al.*, 2014], as both effects occurred on the same magnetic flux tube of plasma bubbles [Yokoyama *et al.*, 2007; Martinis *et al.*, 2009]. As an intermediate stage, inside the depleted region, polarization EEF drives plasma particles to move upward and causes the enhancement of plasma density over the depletions [Krall *et al.*, 2010; Retterer, 2010]. Contrary to aforementioned assumptions, Kil *et al.* [2011] proposed that bubbles and blobs are not

created by a same mechanism as observation revealed that blobs are detected in the regions where bubbles are absent. Plasma bubbles need not be a prerequisite condition for the generation of plasma enhancements since blobs frequently occur in the latitudes where bubbles cannot reach [*Choi et al., 2012; Haaser et al., 2012*]. Recent studies [*Choi et al., 2012; Miller et al., 2014*], demonstrated that medium-scale traveling ionospheric disturbances (MSTIDs) are possible driving mechanism of formation of the blobs independent of that of bubble as it modulates local F region peak altitudes.

The objective of the present investigation is to study the role played by various ionospheric parameters of the equatorial ionosphere in the different characteristics of plasma irregularities seen in the EPBs and blobs by two independent techniques – ground GPS and in situ Langmuir probe (LP) onboard SWARM measurements. SWARM is a minisatellite constellation of three satellites, two fly at a lower altitude, measuring the East-West gradient of the magnetic field, and one satellite flies at a higher altitude in a different local time sector. Low-Latitude Ionospheric Sensor Network (LISN) is a permanent array of geophysical instruments in South America to answer key questions about electrodynamics of the equatorial to mid latitude ionosphere and to develop forecasting capabilities.

Another question we want to address is the velocity of the disturbed plasma density structure (EPBs), and what are the characteristics properties and differences in such velocities probed by ground-based LISN network and space-based SWARM constellation, and how are the influenced by prevailing conditions? This study also

demonstrates results for several specific days of SWARM observations during passes throughout the South American continent. Overall, we demonstrate that the in-situ SWARM and ground GPS system can serve a useful concurrent tool for detection of the low-latitude ionospheric instability events and may essentially contribute to develop a comprehensive theory about the generation, development and decay mechanism of EPBs and blobs based on observational and modeling studies.

6.2 Instrumentation and Data Processing

Both ground- and satellite-based datasets have been heretofore extensively used to study the space plasma behavior for more than a half century. We investigated and analyzed plasma density irregularities using the space-based SWARM constellation of satellite and ground-based LISN network, simultaneously.

SWARM mission consists of the three identical Swarm satellites (A, B, and C) carrying sophisticated magnetometers and electric field instruments which were launched on 22 November 2013 into a near-polar orbit. We have examined ionospheric plasma density measurements from SWARM satellites to investigate of EPBs and blobs occurrence in the American sector at topside altitudes. Swarm A and C form the lower pair of satellites flying side-by-side in 1.4° longitude separation at inclination angle to 87.35° with polar orbits at an altitude of about 470 km, whereas Swarm B is cruising at higher orbit of about 520 km making inclination angle is equal to 87.75° as shown in Figure 6.1(a). SWARM mission provides the best ever survey of the geomagnetic field and its temporal evolution and will lead to new insights into the Earth system by improving the current understanding of the Earth's interior and its effect on Geospace, the vast region around

the Earth where electrodynamic processes are influenced by the Earth's magnetic field [Friis-Christensen et al., 2006].

The low latitude region of South American continent is well instrumented with networks of GPS receivers as shown in Figure 6.1(b). We present LISN dual-frequency GPS total electron content (TEC) datasets to study plasma densities sampled at low magnetic latitudes in the equatorial and low-latitude ionosphere. LISN (Low Latitude Ionospheric Sensor Network) [Valladares and Chau, 2012] is a distributed observatory that operates in South America. It was designed to probe both the disturbed and undisturbed ionospheric plasma density in the low-latitudes and also allows us to explore the development as well as the decay of the plasma instabilities in unprecedented detail. GPS receivers can continuously measure TEC integrated along the line-of-sight from GPS satellites to receiver. TEC is measured in units of TECU (1 TEC Unit = 10^{16} electrons/m²).

The present study fundamentally uses almost simultaneous in-situ measured data from the early phase of the SWARM when the distance between the trajectories of all three satellites of the constellation was tens of km and the temporal separation was of order one minute. This contribution selected a few typical prime local time segment associated with plasma instability events that correspond to the seeding of ionospheric irregularities [Valladares et al., 1996; Carter, et al., 2016]. Concurrently, two different ionospheric plasma processes (depletions and enhancements) have been studied using ground based GPS-TEC data from the LISN network in the low-latitude ionosphere.

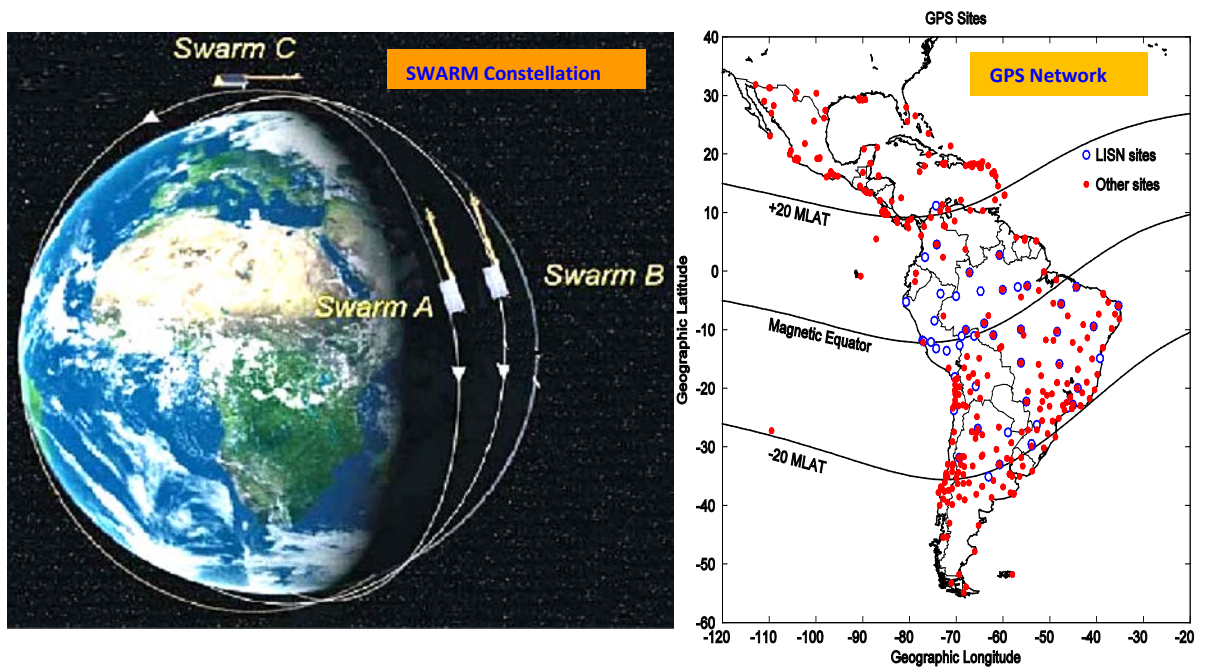


Figure 6.1

- a) SWARM constellation with equatorial projection of the SWARM orbit configuration over time (image credit: DTU Space). Satellite pair at 450 km initial altitude, flying side-by-side with 1.5° longitude separation whereas third satellite is at 550 km initial altitude,
- b) Location of GPS receivers in ‘Distributed Observatory’ of Low-Latitude Ionospheric Sensor Network (LISN) in South American continent.

6.3 Analysis and Results

In the initial stage of the SWARM mission, the trajectories of all three satellites of the constellation were no more than of a few 100's of km in terms of distance and the time-based separation was of the order of one minute. This unique geometry of satellite flight allows us to conduct multiple and almost simultaneous in-situ measurements through the same low-latitude plasma depletion to investigate their spatial coherence and the motion of structures embedded within the EPBs and blobs. We have used the number density measured with the Electric Field Instrument (EFI) on-board the three satellites of the SWARM constellation and concurrent TEC values obtained by ground-based LISN-GPS receivers to fully diagnose the bubble characteristics at multiple scale sizes. The plasma densities presented here were measured with the Langmuir Probes (LPs) on-board the three SWARM satellites. Two different ionospheric processes (bubbles and blobs) have been studied using SWARM and LISN-TEC data simultaneously. In the following first sub-section, we present how plasma bubbles and blobs events are identified using the SWARM constellation. In the second and third sub-sections, these events are probed and analyzed simultaneously using SWARM satellite and GPS receiver data sets before summarizing our results.

6.3.1 Identification of EPBs and Blobs Signature from SWARM

The current study uses plasma density measured with the SWARM satellite constellation during December 2013. The plots presented in Figure 6.2 display the observations in two different formats, logarithmic scale of plasma density [$\log(N_e/cc)$] versus time (UT) and N_e versus magnetic latitude for each of (a) plasma depletions (EPBs) and, (b) plasma

enhancements cases as SWARM satellites crossed the western edge of South American continent near 80°W longitude. The observations of density traced by each of three different satellites are color coded in Figure 6.2. The events identified in this report took place on December 10 for EPBs and 28 for blobs of the year 2013. In these events, the SWARM satellite observed EPBs from 06:12 to 06:22 UT and plasma blobs from 01:17 to 01:22 UT in the ionosphere when it flew over the American low latitude.

In Figure 6.2(a), the upper panel shows a depletion pattern of the plasma density as a signature of EPBs against Universal time for 10 minutes interval simultaneously from three satellites. It is clearly seen that there is a sharp decrease of plasma density during night time. Also, large variability inside the bubbles among satellite passes also gives important information that SWARM reveals in these observations. Lower panel in Figure 6.2(a) shows the variation of logarithmic scale of plasma density against magnetic latitude indicating bubbles within less than 10° magnetic latitudes. As we see the bubbles extend for more than 10 minutes and also span for around 20° latitudinal separations. The width of bubbles decreases from one satellite pass to the next.

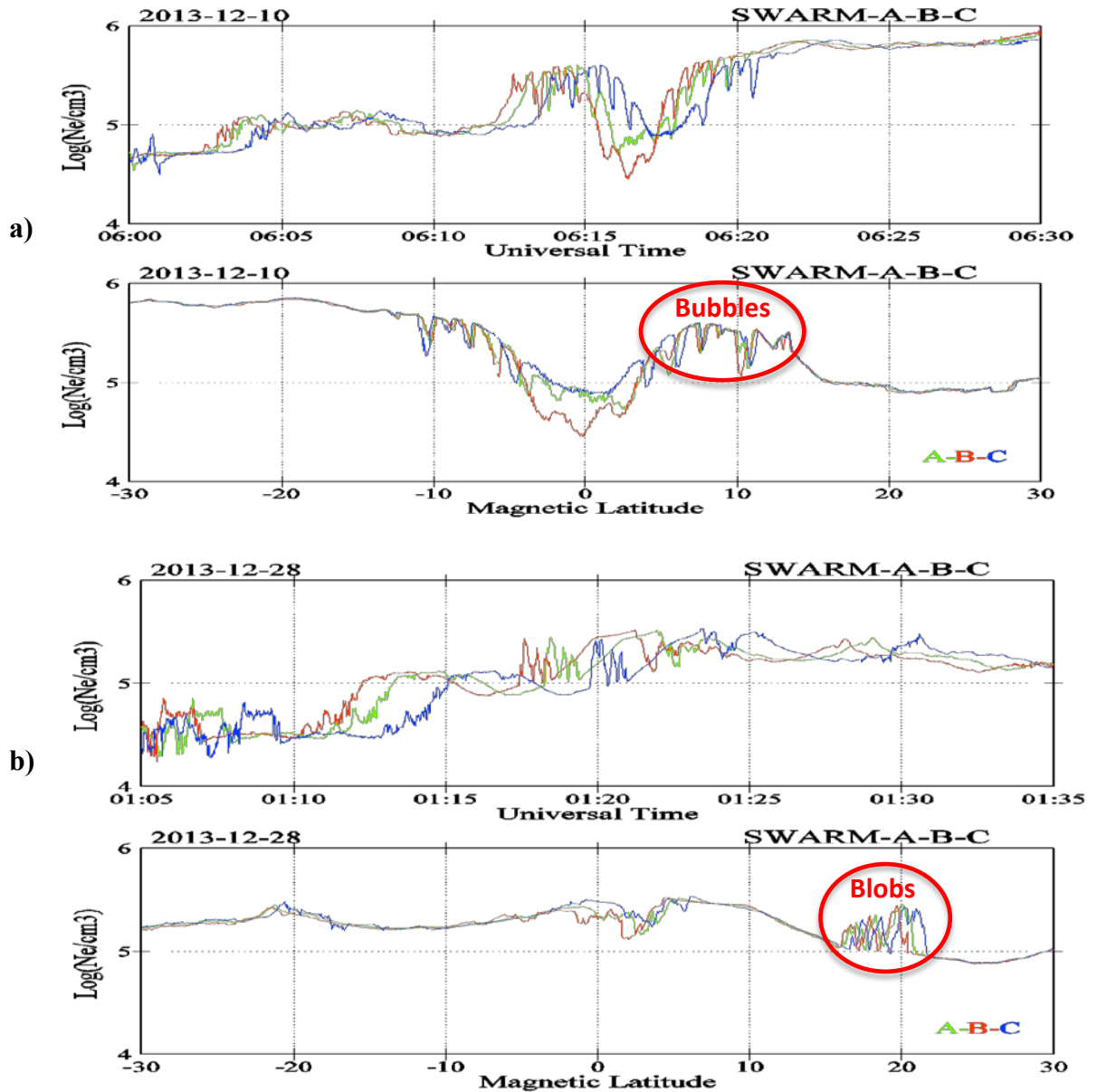


Figure 6.2

- a) Upper panel showing depletion pattern of the plasma density as a signature of EPBs against Universal time from three satellites. It is clearly seen that there is a sharp decrease of plasma density during night time. Lower panel is the variation of same against magnetic latitude indicating bubbles in the low latitude.
- b) Upper panel showing enhancement pattern of the plasma density as a signature of blobs against Universal time. It is seen that there is a sharp increase of plasma density during night time as 3 to 4 times the background density. Lower panel is the variation of same against magnetic latitude indicating blobs near 20°.

Figure 6.2 (b) shows the low latitudinal plasma density variation in a logarithmic scale [$\log (N_e/cc)$] against time measured by SWARM constellation in upper panel. It illustrates the comparison of three satellites from in-situ measurements for SWARM electron density for a 30 minutes interval. In such an interval, within around 5 minute's window, one can clearly see a trend of plasma density scenario by all of three satellites that were much higher than that in the local background region. The lower panel in Figure 6.2(b) represents the variation of low-latitude plasma density for 30° magnetic latitudes. We can see that the satellites have gone through regions of equatorial ionospheric ionization region on both sides of the geomagnetic equator and detected a plasma blob with strong ion density enhancement near 20° . The sharp increase of plasma density during night time can be estimated as 3 to 4 times than that of the background density in the lower panel of Figure 6.2(b).

In the sub-sections below, similar types of density variation scenarios will also be probed from ground GPS receivers in terms of TEC magnitudes, and corresponding phenomena relating their consequences will be presented. Certainly, the outcomes from such synchronized observations will improve our current understanding mechanism of EPBs and blobs.

6.3.2 Ionospheric Plasma Depletions: EPB Events

Figure 6.3(a) characterizes six minutes of ionospheric plasma density variation measured with the constellation of three SWARM satellites on December 16, 2013 during midnight hours. Analyzing data restricted within 4:07UT to 04:09UT, all three satellites indicate

clear plasma bubbles phenomena for 2 minutes. The non-fluctuating black curve on the top of three curves in Figure 6.3(a) demonstrates the calculated unperturbed plasma density. Not surprisingly, the magnitude of the plasma density corresponding to bubble events decreases abruptly as one compares its background density represented by the continuous curve.

Figure 6.3 (b) shows the scenario of satellite trajectories, geomagnetic field lines and the EPBs paths. The geomagnetic field lines are closely aligned with the satellite path and EPBs are aligned with the local field lines as well. There exists a longitudinal separation between the satellite paths and the field lines over South America which has a non-zero magnetic declination. Even though the satellites were flying side-by-side, the SWARM satellites will intersect the bubble at different times. The time delays are -28.5 seconds and 49.5 seconds respectively. Plasma density curves have been shifted accordingly. On comparing two plots 6.2 (a) and (b), the location of the formation of EPBs events can be confirmed by identifying trajectories of the SWARM satellite constellation. We have calculated the time delays between the individual satellite intersections of the field line that crosses the magnetic equator at 54° W longitude which is at the eastern side of the South America.

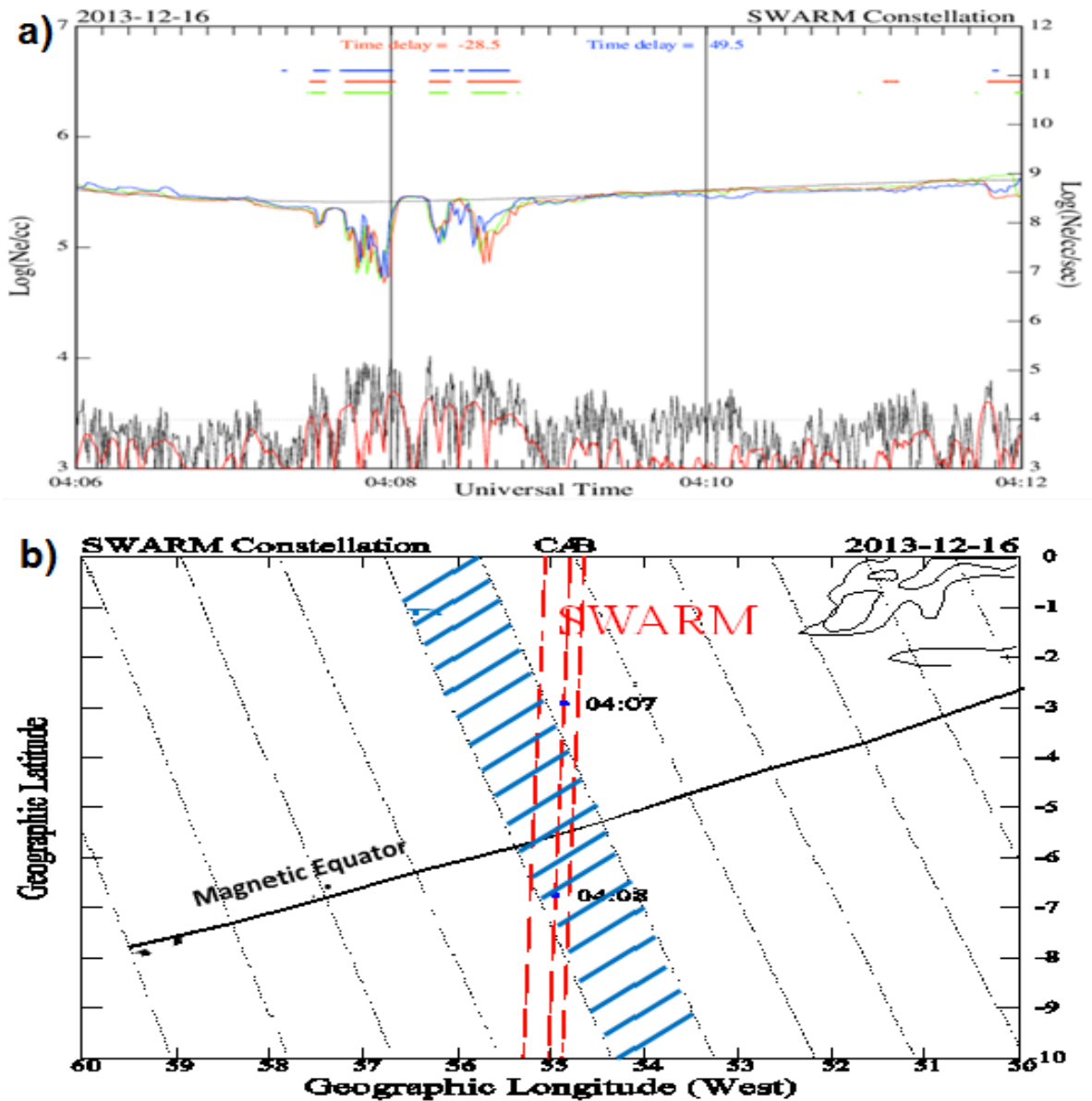


Figure 6.3

- a) This plot shows plasma density depletions during a 6 minutes interval on December 16, 2013. All three satellites are able to indicate clear plasma bubble events that occurred between 4:07UT and 4:09UT.
- b) Sketch showing the geometry of the SWARM constellation passes over the field-aligned plasma bubbles and the local magnetic field lines. It also shows the mapping of the satellite paths to the ground as plasma depletions are seen along their trajectories.

We make use of LISN GPS-TEC in corresponding time span that allows us to concentrate on the picture of the TEC variations. Our observations also provide the opportunity to investigate the impact on the TEC variation as SWARM sees EPBs events.

The mass plot GPS-TEC presented in Figure 6.4 shows how TEC is interrupted during EPBs events as seen by SWARM. The general patterns of low-latitude GPS TEC have been seen disturbed since 02UT and lasts till 06UT in the 55°W longitude sector. As shown in Figure 6.3(a), SWARM captures the EPB event at around 04UT only. The maximum distortion of TEC is seen at 03 UT. It can be said that SWARM only gives a snapshot of EPBs whereas ground GPS continuously monitor its impact for a longer period. For the examination of the generation to decay mechanism of EPBs, GPS shall be a better instrument to bring into practice.

By this simultaneous analysis, we expect to contribute to the understanding of the birth to death mechanism of different EPBs properties on a global scale and in a climatological sense, which were reported from local and time restricted observations so far.

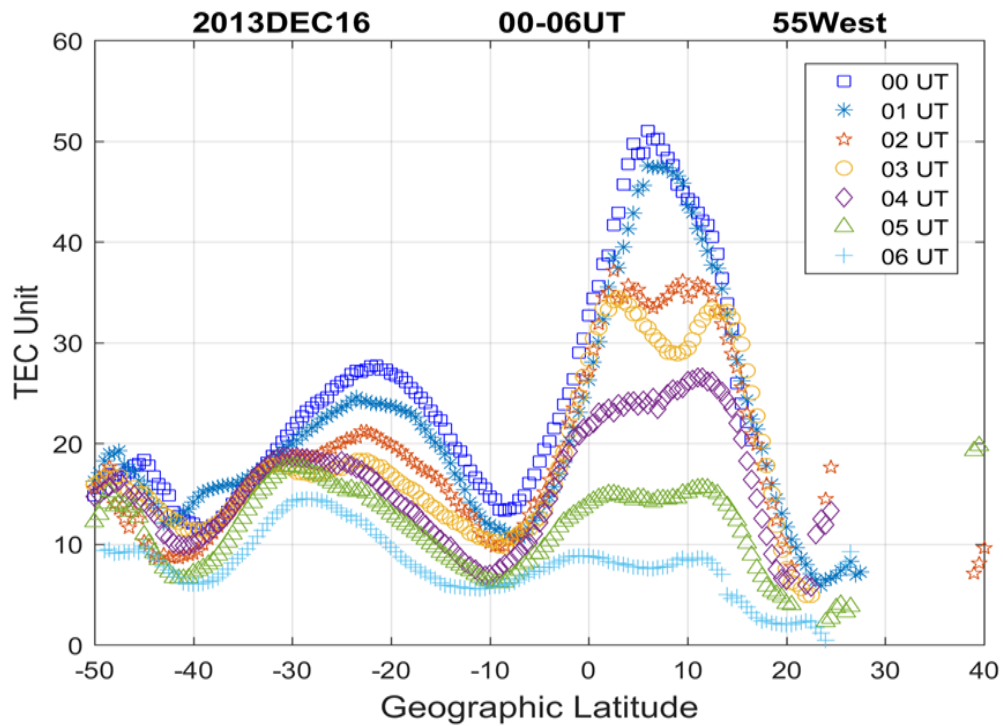


Figure-6.4:

This plot shows one-hour variations (total 7 hrs) of TEC against geographic latitude along the 55°W longitude sector. It is seen that even though SWARM observed bubbles between 4:07UT and 4:09UT, the peak of the northern anomaly crest starts to distort at 02UT because of the bubbles. In-situ measurement of bubbles is simultaneously supported by GPS-TEC measurements from the ground.

6.3.3 Ionospheric Plasma Enhancements: Blob Events

Figure 6.5 (a) demonstrates a strong plasma density enhancement during a short six minute interval of plasma density variation recorded by the SWARM constellation on December 27, 2013. The clear plasma blob events occurred during 3:16UT to 3:18UT (i.e. 2 minutes intervals) and the general pattern of the variability within the blob events seems rather similar in all three satellite observations.

The satellite track during the density variation reported in Figure 6.5(a) is shown as the thick red line over the continental map of the South America in Figure 6.5 (b). It is speculated that the enhancement of plasma (blobs) is located near the Caribbean region and the density values shifted in time by -46.5 sec (SWARM-B) and 80.5 sec (SWARM-C).

The GPS-TEC distributions of Figure 6.6(a) show the variability of the equatorial ionization anomaly (EIA) during the day and time interval presented in Figures 6.5(a). During blobs events, it is seen that the northern crest of the anomaly decreases from its peak creating a 'shoulder' rather than a sharp TEC density gradient as reported in Figure 6.4 during EPBs events.

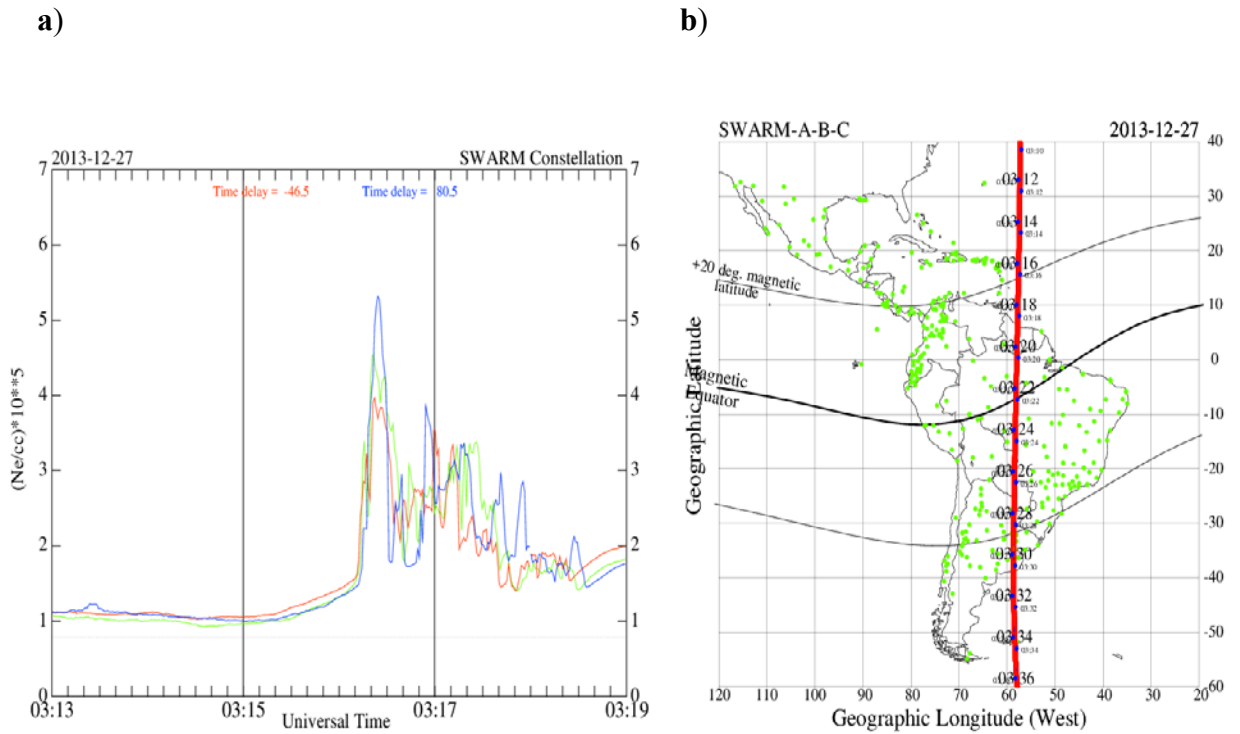


Figure-6.5

- a) Plot showing the plasma density enhancement during a 6 minutes interval on December 27, 2013. All three satellites are able to indicate a clear plasma blob event that occurred during 3:16UT and 3:18UT.
- b) South American continental map showing the geometry of the SWARM pass along thick red line and indicates that the density enhancement is near the Caribbean region.

Additionally, in order to explore the response of the plasma enhancements near the Caribbean region, TEC recorded by eight different GPS receivers location within 70°W to 55°W longitudinal regions in Figure 6.6(b). The noticeable TEC enhancements of the order larger than 5 TEC units are also detected at the same location of the SWARM blobs using these clusters of GPS receivers.

A well-accepted restriction is that, in general, these coordinated techniques cannot be extended to all cases and locations. Further, there are no sophisticated techniques able to resolve the lack of continuous and long term temporal and spatial variability of the F region topside plasma irregularities on a global scale so far. Even though limited to a few EPBs and blobs events presented in this section, the quantitative signatures of EPBs and blobs are worthwhile to develop the concept of plasma instability mechanisms in the equatorial, low and mid-latitude ionosphere. To interpret the quantitative outcomes from coordinated observation of the EPBs and blobs from space and the ground using SWARM and GPS receivers respectively, several mechanisms for bubble and blob phenomena are proposed and discussed in section 6.4 below based on our results.

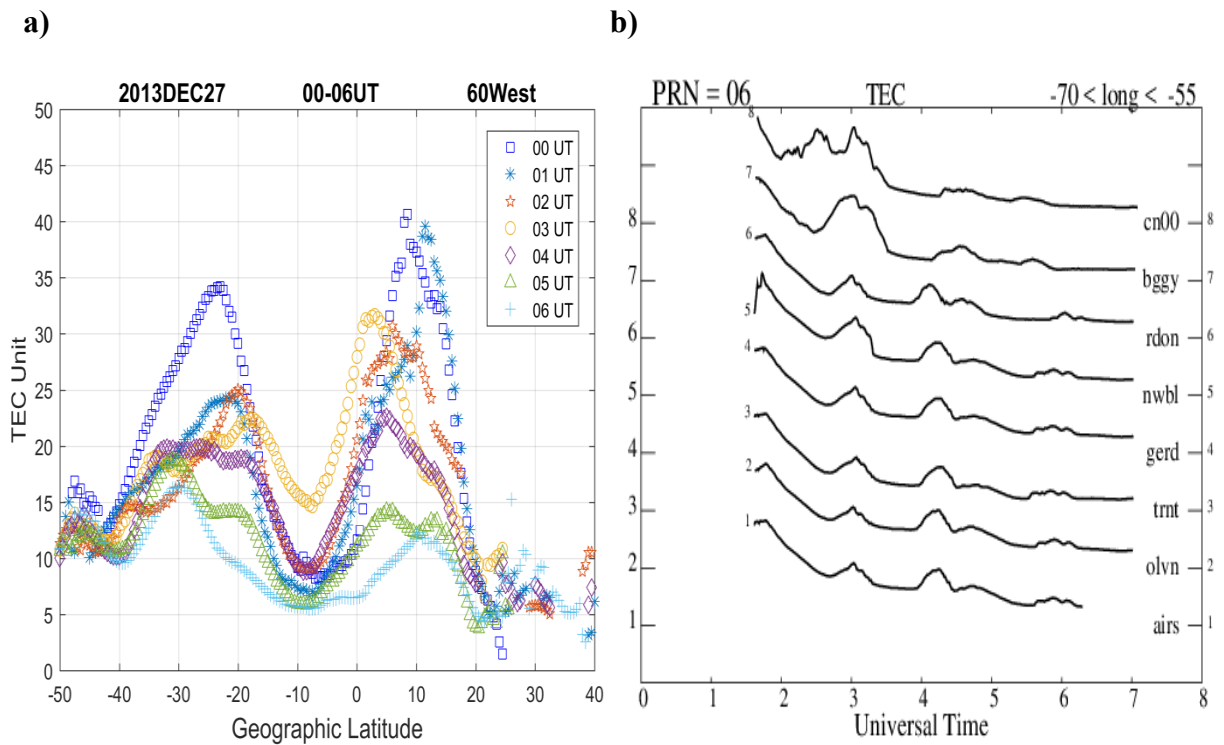


Figure 6.6

- a) Mass plots showing one-hour variations (total 7 hrs.) of TEC against geographic latitude along 60°W longitudes sector. It is seen that the northern crest of the anomaly decreases from its peak creating a ‘shoulder’ because of the plasma enhancement. The in-situ measurement of blobs is simultaneously supported by the GPS-TEC measurement from ground.
- b) Plots showing the TEC values collected by 8 GPS stations located in the Caribbean region. These receivers detected prominent TEC enhancements, larger than 5 TECu, at the same location of the SWARM blobs.

6.4 Interpretation and Discussion

With this simultaneous analysis, this report endeavors to contribute to our understanding on the initiation, growth, expansion, dynamics, and decay mechanism of different properties regarding ionospheric plasma instabilities on a global scale and in a climatological sense. Until now, in searching for explanations for the occurrence of equatorial ionospheric plasma structure, several aspects of the plasma dynamics and the properties of seed perturbations have been reported from local and time restricted observations so far.

The sharp decreases of the low latitude ionospheric plasma density also referred to as a plasma “bubble,” is thought to be formed and grown by a Rayleigh-Taylor instability (RTI) acting on the bottomside of the F layer during the nighttime [*Woodman and LaHoz, 1976; Fejer and Kelley, 1980; Hei et al., 2005*]. Regarding the plasma dynamics, it is largely understood that the postsunset enhancement in vertical plasma drift may be a strong contributor to enhancing the growth rate of the Rayleigh-Taylor instability [*Sultan, 1996; Kil and Heelis, 1998; Stolle, et al., 2008b*]. A visual inspection of EPBs events reported in figure 6.3(a) about plasma density reduction seen by 3 satellites also provides an opportunity to explore the packets of small but deep bubbles within large bubbles. One of the key points of this study is that not only snapshot of EPBs density gradient, the internal decrease in density gradients can also be distinguished for very small time intervals. As seen in section 6.3.2, SWARM basically gives snapshot of EPBs whereas ground GPS continuously monitor its impact for longer period. In spite of some unavoidable discrepancies, ground GPS shall be an appropriate tool to bring into practice

for the examination and understand the mechanism of seeding to decline phase of long-lasting EPBs.

The plasma density measurements presented in section 6.3.3 is an example of the clear and abrupt electron density enhancement by a notable factor, as much as 3–4 times the background density, beyond 20°N latitudes along the SWARM satellite tracks in the nighttime ionosphere. The sketch in Figure 6.7 illustrates the scenario describing formation mechanisms of the blob related to different stages e.g. initial, and fully developed stages of EPB evolution.

Equatorial plasma bubbles follow a non-linear evolution of the Rayleigh-Taylor instability (RTI) that uplifts the low density plasma and traverses through the high density plasma as shown in figure 6.7(a) at near magnetic equator. The region of plasma density enhancement (blob) appears just at the top of the bubble in the initial phase as a consequence of the uplift of the ionosphere. The occurrence of plasma blobs was associated with EPBs over the geomagnetic equator and linkage between their evolutions is reported from ground-based observations [*Pimenta et al., 2004*] as well as space-based observation [*Huang et al., 2014*]. As bubbles are fully grown, the blobs remain only off the magnetic equator in the EIA latitudes as a consequence of the diffusion of depleted plasma along geomagnetic field lines as shown in Figure 6.7(b). In the initial phase of blob formation as in Figure 6.7(a), F layer peak high-density plasma exists just at the top of the bubbles in the geomagnetic equator [*Le et al., 2003*]. Later, in the fully developed

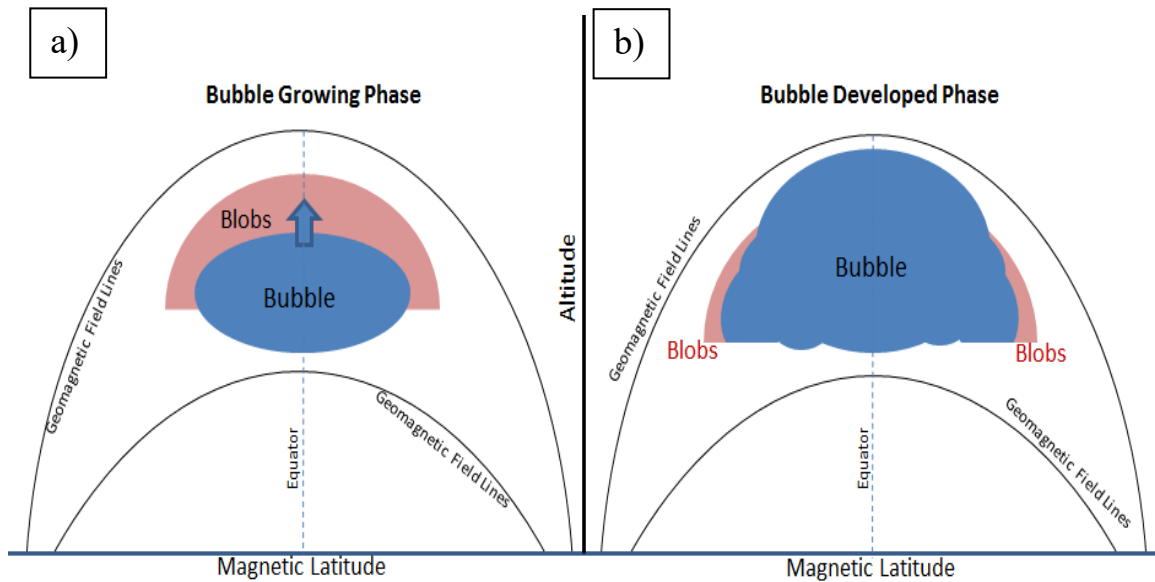


Figure 6.7

Contour illustrations of phases of EPBs and blobs.

- a) Bubble Growing Phase: Plasma bubbles follow a non-linear evolution of the Rayleigh-Taylor instability near magnetic equator, plasma density enhancement appears above the bubble as a consequence of the uplift of the ionosphere.
- b) Bubble Developed Phase: As bubbles are fully grown, the blobs remain only off the magnetic equator as a consequence of the diffusion of depleted plasma along geomagnetic field lines. But, in the most of the cases, bubbles are not the major source of blobs since bubbles are formed mainly in the equatorial region, and blobs exist more than 20° off the equator at mid-latitudes.

EPB phase as in Figure 6.7(b), the blobs are removed from geomagnetic equator and relocated around EIA latitudes [Krall *et al.*, 2010].

Rather interesting is the detection of the EPBs in the form of plasma density depletions seen at the geomagnetic equator, as expected, but the plasma enhancements (blobs) also reside near mid-latitude region in the current analysis. In most of the cases, bubbles are not the major source of blobs since bubbles are formed mainly in the equatorial region, and blobs exist more than 20° off the equator at mid-latitudes. Their climatology and periodicity suggest that blobs might be associated with nighttime MSTIDs [Klenzing *et al.*, 2011; Miller *et al.*, 2014; Kil *et al.*, 2015]. The plasma density enhancements presented here were only from selected observations from the SWARM and GPS from the LISN network. Reviewing various approaches, it is possible that different mechanisms can mutually dependent or independent for bubble/blobs formation depending on the location and time of observation. Based on additional observations and modeling studies, one can improve our understanding of ionospheric plasma behavior and advance current theoretical concepts on generation to decline mechanisms of bubble/blob phenomena.

6.5 Summary and Conclusions

The dynamic features of the equatorial and low-latitude ionosphere are full of peculiarities that often amaze space scientists from quantitative evidences using multiple probes. In the present study, we attempt to analyze different features associated with plasma depletion and enhancement phenomena at low latitudes using space and ground-

based plasma density measurement. The details of the observational results relating to our observations and analyses are enumerated below.

1. Space-based SWARM constellation and ground-based LISN network provide data of excellent quality that can be used to simultaneously study the low and mid-latitude plasma instability processes and identify cases when they are related.
2. The SWARM mission and the LISN data allow us to overcome the space-time ambiguity of past single-satellite studies and detect the dramatic changes that plasma bubbles suffer in a time frame. Also, the close location of the SWARM satellites during the early phase of the SWARM mission can allow us to measure the velocity of the plasma bubbles.
3. Ground-based GPS receivers that are part of the LISN network can fully diagnose bubbles and blobs characteristics in terms of TEC values.
4. The coordinated analysis of plasma density enhancements (blobs) has indicated that the local density at the satellite altitude can increase by a factor as high as 3. These density enhancements were accompanied by TEC enhancements of 5-10 TEC units that developed in both the northern and southern hemispheres.
5. There is evidence of the possible association of plasma blobs with EPBs based on the densities measured by the SWARM constellation of satellites. Plasma bubbles have been associated with plasma bubbles that grow at equatorial latitudes. It is believed

that bubbles as they grow in altitude they also extend to higher latitudes pushing the plasma that resides above the bubbles to higher altitudes creating an enhancement of the densities for a satellite flying at a constant altitude. This mechanism may explain some of the observations of the blobs presented here. However, an alternative explanation exists in which nighttime MSTIDs may have been excited by the Perkins instability creating sheets of enhanced and depleted densities. Further analysis of the SWARM and LISN datasets are needed to elucidate the formation mechanism of the density/TEC enhancements.

Further, it can be speculated that there is a possibility that different mechanisms can coexist or one predominates depending on time and location of the observations. Therefore, it is important to develop a comprehensive theory based on further observational, theoretical and modeling studies on the generation, dynamics and decay of bubbles/blobs occurrences in the low to mid-latitude ionosphere. A similar data product from SWARM and LISN is planned and will be presented in upcoming efforts to better understand and solve existing theoretical conflicts on bubbles/blobs phenomena.

Chapter 7

Interrelationship between Several Ionospheric Parameters*

Contents	Page
7.1 Introduction.....	175
7.2 Data Selection and Analysis.....	179
7.2.1 EEJ and Estimation of Vertical Drifts.....	180
7.2.2 Determination of Latitudinal TEC Profiles.....	183
7.2.3 Determination of Net S4.....	186
7.3 Concurrent Observations of EEJ, TEC, and S4 Index.....	188
7.4 Discussion.....	192
7.5 Summary and Conclusions.....	195

*

A significant portion of this chapter has been published in:

Khadka, S. M., C. Valladares, R. Pradipta, E. Pacheco, and P. Condor (2016), *On the mutual relationship of the equatorial electrojet, TEC and scintillation in the Peruvian sector*, *Radio Sci.*, 51, 742–751, doi:[10.1002/2016RS005966](https://doi.org/10.1002/2016RS005966).

(I would like to thank my coauthors for their permission to include their contributions to this dissertation)

This chapter presents the interrelationship between the Equatorial Electrojet (EEJ) strength, Global Positioning System (GPS)-derived total electron content (TEC) and postsunset scintillation from ground observations with the aim of finding reliable precursors of the occurrence of ionospheric irregularities. Mutual relationship studies provide a possible route to predict the occurrence of TEC fluctuation and scintillation in the ionosphere during the late afternoon and night respectively based on daytime

measurement of the equatorial ionosphere. Data from ground based observations in the low latitudes of the west American longitude sector were examined during the 2008 solar minimum. We find a strong relationship exists between the noontime equatorial electrojet and GPS-derived TEC distributions during the afternoon mediated by vertical ExB drift via the fountain effect, but there is little or no relationship with postsunset ionospheric scintillation.

7.1. Introduction

On account of its peculiar properties, low latitude ionosphere has become one of the most widely studied research areas in the past few decades. Even though forecasting the ionospheric irregularities phenomena is a challenging topic in the scientific community, many researchers have contributed significantly. The interest in the low latitude ionosphere irregularities has increased recently. This is because the behavior of equatorial ionosphere differs significantly from the behavior of the ionosphere in other regions. The special magnetic field geometry at the geomagnetic equator of the Earth leads to various geomagnetic as well as ionospheric phenomena, many of which are unique. The transport of charged particles along the geomagnetic field lines in the equatorial region is associated with a two-humped latitudinal distribution of electron density, with a minimum at the magnetic equator. Another distinguishing feature of the equatorial ionosphere is the relative abundance of ionospheric electron density irregularities [Cohen, 1967; Onwumechili, 1997; Kelley, 2009a]. The equatorial anomalies in the topside ionosphere and its correlation with E region current system near the magnetic equator of the Earth have been studied by many researchers [MacDougall, 1969; Fejer and Kelley,

1980]. Plasma structures are produced in the sporadic E layer whereas equatorial plasma bubbles (EPBs) are produced at low latitudes of the F region ionosphere. Plasma irregularities in the ionosphere are usually field-aligned and vary as a function of space and time [Balsley, 1970; Onwumechili and Agu, 1980; Onwumechili, 1997]. Predicting ionospheric irregularities is recognized as one of the highest priorities in the national space weather program implementation plan. This is because by knowing ionospheric electron density irregularities, adverse space weather effects on GPS navigation, telecommunications, and many other technologies can be prevented and will also guide the way to construct better models of irregularity development and, eventually, scintillation prediction [Kintner, et. al., 2007; Doherty, et. al, 2004]. Therefore understanding and forecasting the occurrence and impact of ionospheric irregularities is a critical societal need.

In presence of solar radiation, the electron density in the E region ionosphere starts to increase and the H component (northward) of the magnetic field shows a steady enhancement until around noon, after which it starts decreasing. Such magnetic field behavior is due to an eastward electric field during daytime that causes intense current system to exist in the low latitudes. An intense electric current flowing eastward in the ionospheric E-layer in a narrow belt at latitudes ($\pm 2^\circ$) centered at the dip equator is called the equatorial electrojet (EEJ), a term coined by Chapman [1951]. Owing to this electric field and horizontal magnetic field at the equator, $E \times B$ drifts are produced and the electrons (plasma) are lifted to higher altitudes. The plasma lifts to a certain height and then diffuses down along magnetic field lines to the F region at higher latitudes ($15^\circ -$

20°). The plasma, diffused down around 15° - 20° latitudes from either sides of magnetic equator creating two plasma crests, is called Equatorial Ionization Anomaly (EIA). The daytime vertical plasma drift in the equatorial F-region of the ionosphere is the key transport mechanism for determining the electron density profiles as a function of altitude, latitude, and local time [Deshpande, et al., 1977; Chen et al, 2008; Banola, et al., 2001]. The equatorial daytime vertical drift is a very important element for ionospheric theoretical models. The strength of the daytime equatorial electrojet can be measured using a pair of magnetometers, one situated on the magnetic equator and the other displaced by 6° to 9° latitude away. The difference between noontime enhancement of the H component observed by two magnetometers placed on and off-equator by ~6° to 9° is related to the equatorial electrojet strengths and also quantitatively with vertical ExB drift in the F region ionosphere [Rastogi, et al., 1962; Rastogi and Klobuchar, 1990; Anderson, et al., 2002, 2004]. In the absence of EEJ, the magnetometers do not provide reliable vertical drifts.

The equatorial ionosphere starts to structure after sunset causing plasma instabilities called equatorial plasma bubbles (EPB). Consequently, one can expect the occurrence of TEC depletions and scintillation in the low latitudes after sunset because of the changes in noontime EEJ strengths and vertical drifts. The TEC distribution is an indicator of ionospheric variability and defined as the total number of electrons integrated along the path from receiver (GPS) to satellite. It is measured in units of TECU (1 TEC Unit = 10^{16} electrons/m²). The EPB that occurs at the bottom side of the F-region ionosphere thereby adversely affect the amplitude and phase of the radio waves in various frequency bands.

An unusual fluctuation in the phase/ amplitude of a radio-frequency signal, when it passes through an ionospheric region of random irregularities in electron density that acts as a variable refractive index in the medium, is called ionospheric scintillation. These scintillation phenomena mainly occur in the geomagnetic equatorial region even though observed at all latitudes with less intensity. The signal distortion caused by scintillation can degrade the performance of navigation system and generate errors in received messages. High priority has been given to the study of ionospheric scintillation because of its significant impact on satellite radio communication. Quantitatively, scintillation intensity is measured as scintillation index (S_4) and defined as normalized variance of the signal power [Basu et al., 2002, Valladares, et al., 2004; Wernik, et al., 2004]. The physical processes concerning the generation, dynamics and decay of scintillations are known to vary widely. Observational results provide consistent evidence that day time EEJ and ExB drifts are well correlated. Association between post sunset EIA, EPB/scintillation and ExB drift is also reported in many research articles. Near sunset prereversal ExB drifts is the most likely key mechanism responsible for the global large-scale variations in longitudinal distribution of evening EIA enhancement and plasma bubble occurrence rates [Li, et al., 2008]. Equatorial plasma bubbles are the prominent candidate for the cause of scintillation in radio wave propagation, but there are almost no studies on correlating daytime EEJ hence vertical ExB drift and night time scintillation. The present study focuses on particular characteristic of scintillation and irregularities. Incorporating such evidences, our study aims to develop a technique to predict the interconnection of disturbances of afternoon GPS-derived TEC and scintillation after sunset on the basis of noontime electrojet strengths.

7.2. Data Selection and Analysis

The data from a permanent array of geophysical instruments deployed in the low latitude region of South America has had great impact in the study of equatorial ionospheric phenomena. It has already been revealed that the equatorial vertical ExB drift velocity is an important parameter for the prediction and analysis of the structures and dynamics of the ionosphere [*Scherliess and Fejer, 1999; Kelley, 2009a; Stoneback, et al, 2011; Stoneback and Helis, 2014*]. Because of its quite different characteristics, the magnetic equator is a unique region in the ionosphere. The low latitude region along the western meridian of South America is very useful for a long term study of equatorial ionospheric electrodynamic. This is because the magnetic equator in the Peruvian sector has not changed significantly for more than a decade. The geomagnetic equator passes through Jicamarca (Peru) located at 12° latitude south of the geographic equator.

Data analysis is mostly executed for low solar activity conditions from the stations located in the Peruvian sector. The daily average of the solar radio flux F10.7 index was less than 85 during most of this period of extremely low solar activity period and offers an opportunity to study the quiet time relationship at lower solar activity levels than that previously observed. For the current analysis, we have used data from the recent solar minimum years 2008. Measurements from ground based chains of GPS (Global Positioning System) receivers and magnetometers at low latitudes in the Peruvian sector of South America were examined.

7.2.1 EEJ & Estimation of Vertical Drifts

For the current analysis, magnetometer data from Jicamarca (geog. 11.9°S, 283.1°E, 0.8°N dip latitude) and Piura (geog. 5.2°S, 279.4°E, 6.8°N dip latitude) in the Peruvian sector where universal time is local time + 5 hours, are used to get the EEJ strengths. The horizontal components of earth's magnetic field (denoted H) from each station are normalized with its midnight average background values for each day. Then the H component observations from these two magnetometers are subtracted to eliminate the Dst ring current and Sq dynamo contributions to get only the electrojet contribution to H [Rastogi and Klobuchar., 1990; Anderson, et al., 2002]. The magnetometer inferred vertical drift is accurate if there is ionospheric current in the E layer of the ionosphere. Here, an artificial neural network technique has been considered in order to establish the nonlinear relationship between ExB drift velocities and the most relevant six inputs to the network. Artificial multilayer feed-forward neural networks have powerful function-approximation capabilities for pattern recognition, control and signal processing [Haykin, 2005]. The six inputs for the neural network we have used are the year, DOY (day of the year), F10.7, ap index, LT (local time) and dH (difference of H measured at Jicamarca and Piura), which are regarded as controlling parameters for the vertical drifts.

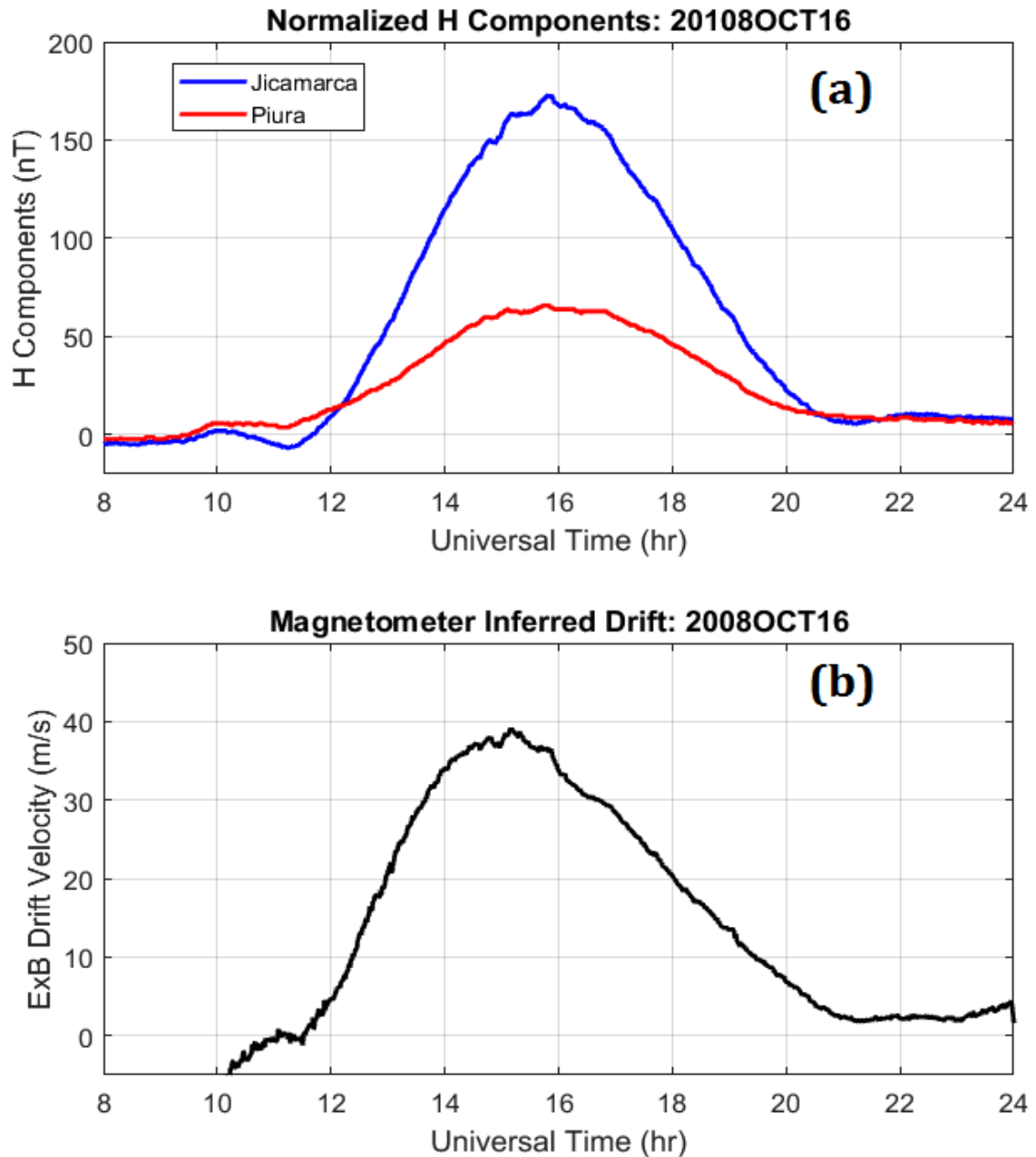


Figure 7.1

- (a) Normalized horizontal component, H of the Earth from two magnetometer stations; one at EEJ zone (blue curve) in Jicamarca and other off the EEJ zone (red curve) in Piura, whose difference refers EEJ,
- (b) Magnetometer inferred vertical ExB drift using artificial neural network technique.

The final output from the neural network training analysis is compared with the desired output which is measured Jicamarca Incoherent Scatter Radar (ISR) drift in the existing case. The weights in the multilayer neural network are obtained from many epochs of the six inputs in order to calculate the relationship with ExB drift velocities.

Figure-7.1 (a) shows the variation of the normalized H components of the Earth against universal time (UT) observed from equatorial magnetometer station, Jicamarca (blue curve) and off-equator station, Piura (red curve). It is clear that there is an enhancement of H at local noon time. The difference of two curves (blue and red) gives the net EEJ contribution to H at the geomagnetic equator. Figure 7.1 (b) is a sample plot of the ExB vertical drift velocity using the neural network technique with six inputs as described above. The plot in Figure 7.1 (b) shows that the ExB vertical drift gradually increases and becomes maximum around local noontime then starts to decrease gradually following the variation pattern of EEJ. Equatorial electrojet (EEJ) and hence vertical drift strength is one of the key factors that determine the evolution of EIA anomaly formed by TEC distributions. It is a driving force for vertical plasma drift that lifts equatorial plasma to higher altitudes which then diffuses down the Earth's magnetic field lines to form EIA crests around $\pm 15^\circ$ geomagnetic latitude, consequently removing plasma from around the magnetic equator. Having established the quantitative relationship between daytime Electrojet strengths and inferred ExB vertical drifts in the ionospheric F region in the west coast of South America using the *Anderson, et al. [2004]* technique, our next intention is to investigate the dependence of the TEC and nighttime scintillation.

7.2.2 Determination of Latitudinal TEC Profiles

The equivalent vertical TEC derived from GPS receivers spread along the Peruvian sector (as seen in Figure-7.1 of *Seemala and Valladares, 2011*) of South America (76°W) at about 12° geographic latitude is used to detect the strength and occurrence of the equatorial anomaly which is caused by vertical plasma drifts in association with EEJ. The current study has been done using vertical TEC data obtained from dual frequency GPS receivers during the low solar activity period of the years 2008 distributed at the magnetic equator and either side of it up to and beyond the ionization anomaly locations in South America. The TEC enhancements that are measured with the LISN (Low Latitude Ionospheric Sensor Network) and other networks of GPS receivers operating in South American occurred quite often during low solar activity periods [*Valladares and Chau, 2012*]. Crests of TEC anomalies have a limited longitudinal extension whose distributions are determined by the fountain effect that forms EIAs.

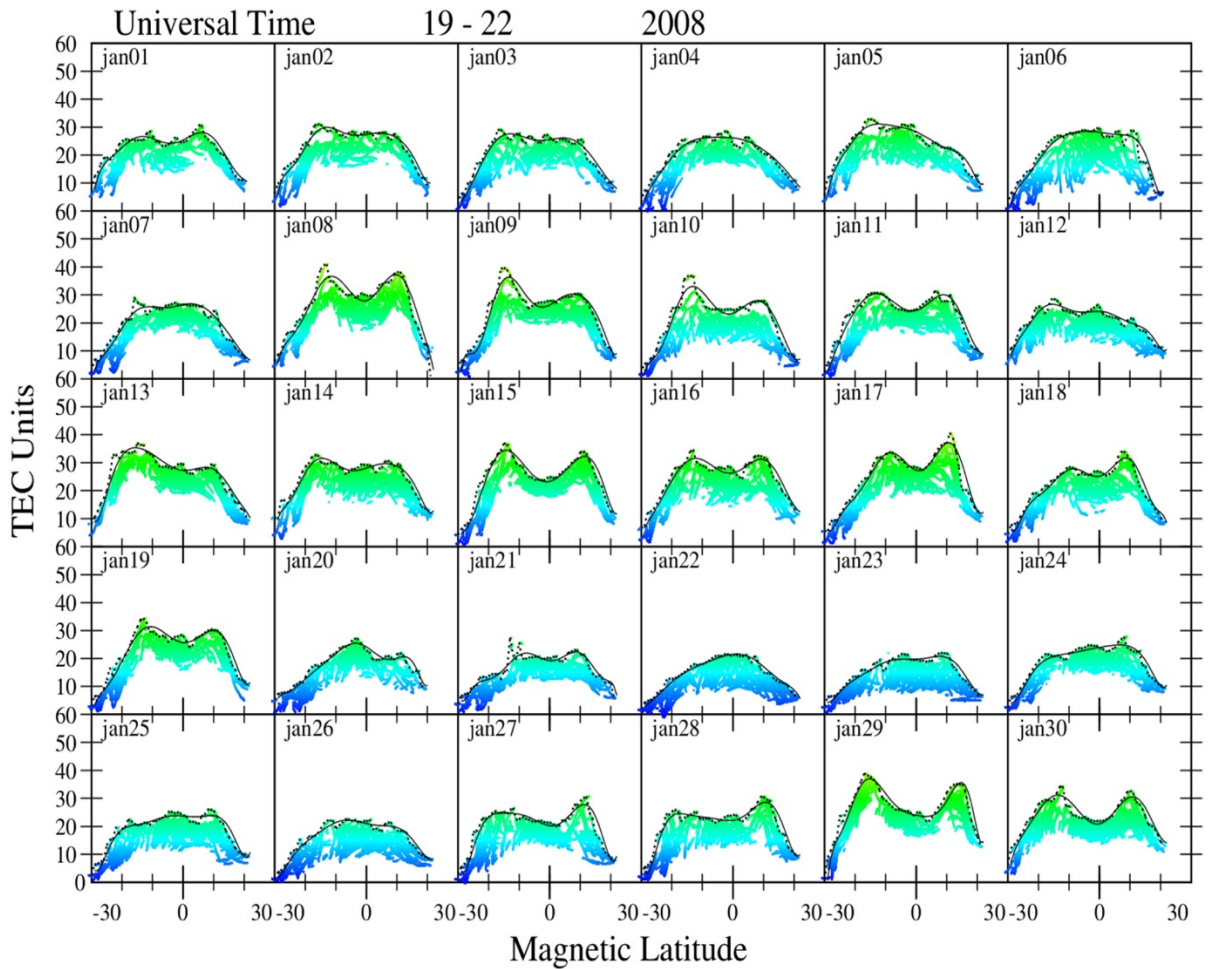


Figure 7.2. Vertical TEC data during 19 – 22 UT obtained from GPS networks and their profiles within $\pm 30^\circ$ magnetic latitude in January 2008. Dotted and continuous black curve represent maximum values of TEC data and fitted data points respectively.

Figure 7.2 shows how TEC observed from different GPS stations are extracted for the present analysis. First, TEC data for particular hours are sorted and then plotted against $\pm 30^\circ$ magnetic latitude. On the scatter plot of TEC, a polynomial fit is done about their maximum values. Such extracted polynomial fitted data are then further utilized to get surface plots to see their day to day variability and the shape of the anomalies. Figure 7.2 shows 30 days' of January 2008 data against magnetic latitude during 19 - 22UT to indicate the strengths and spatial separations of anomaly peaks in EIAs. The continuous black curves on each of these plots are the polynomial fit on particular magnetic latitude whereas dotted black points represent maximum data points in each of magnetic latitude. The strength of TEC anomaly is calculated by taking the maximum value of the TEC. Exceptions are seen in the most of the days during and near solstice period. As reported by *Chau, et al. [2009]*, there was a strong Sudden Stratospheric Warming (SSW) event from January 17-26, 2008 which strongly affects the daytime, vertical ExB drift velocities and is largely responsible for the lack of EIA in the afternoon from January 20 – 26. Our analysis has also replicated the physical evidence as signatures of SSW's impact on EIAs to eliminate its anomaly peaks for those days as seen in Figure 7.2. The separation of the anomaly peaks is calculated in the unit of latitude by taking the difference of latitudinal location of the crests. That many anomaly peaks look asymmetric might be due to other effects than EEJ, such as meridional neutral winds, composition changes due to magnetic perturbations, etc.

7.2.3 Determination of Net Ionospheric Scintillation S4 Index

The strongest level of ionospheric scintillation is observed in the equatorial regions (*Rastogi, 1983, Basu et. al, 2002, Jiao, et.al, 2013*). It should be noted here that the term scintillation S4 index used in this paper refers to the amplitude fluctuations received by GPS. Multipath interference and background scintillation can also produce fluctuations in signal intensity.

We develop a model threshold that removed such contamination in the raw S4 data and gives net S4 index associated with scintillations. The threshold model has been used to filter scintillation from the raw data. The S4 index is detrended based on the threshold line. We construct a statistical distribution of the general S4 index as a function of the line-of-sight elevation. The mean value of S4 index is calculated for each 5° of elevation angle. A threshold value is calculated using the mean value plus two times the standard deviation for each elevation interval. The net values of scintillation (S4 index) are obtained after removing the effect of the low elevations and background values. Subtracting threshold values from S4 data gives net S4 index values.

The example plots shown in Figure 7.3 illustrate the above procedure. Figure 7.3 (a) shows altitudinal variations of S4 index as observed by GPS receiver located at Antofagasta (near the southern crest of the EIAs). The pink line over S4 data is a model threshold curve which is a border curve between background (below pink curve) and net S4 index (above pink curve) data. When the model threshold curve is subtracted and plotted against universal time, the result of Figure 7.3 (a) looks like that in the 7.3 (b). Figure 7.3 (b) is the 12 hours variation of net S4 index after sunset.

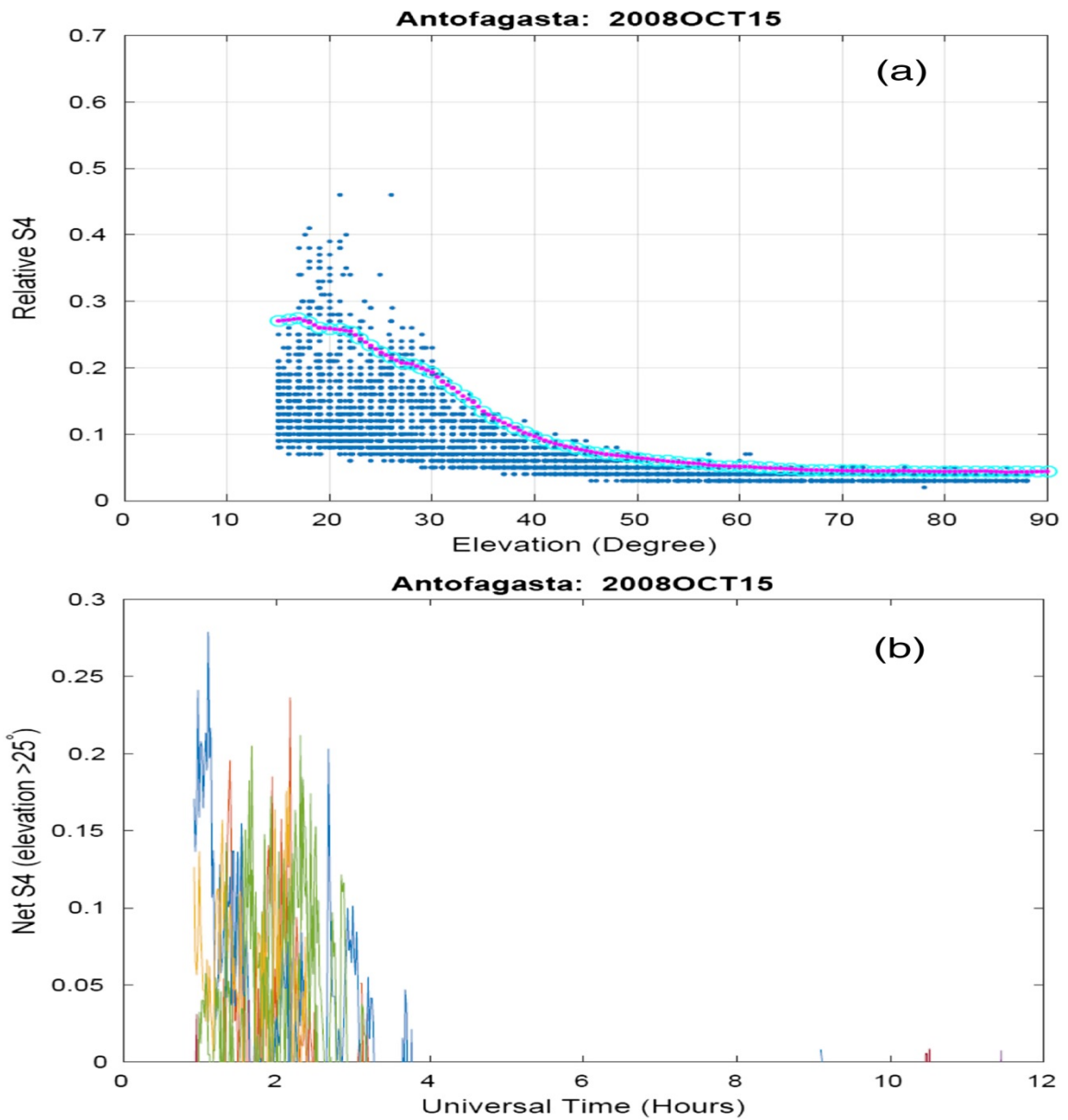


Figure 7.3 (a) Relative S4 index observed at Antofagasta GPS station and threshold line (pink) against elevation, (b) Net S4 index against universal time after subtracting the background and low elevation contribution.

This study mainly emphasizes the occurrence of ionospheric disturbances phenomena observed via TEC, S₄ index and associated EEJ accompanied by daytime equatorial vertical ExB drift from Magnetometer data. This paper addresses the linkage of such phenomena with EEJ strength, TEC and scintillation S₄ index.

7.3. Concurrent Observations of EEJ, TEC and S₄ Index

The data plots presented here are chosen from the pool of analysis that has been done for the year 2008. The results of the day-to-day analysis of EEJ, TEC and S₄ data of 2008 are demonstrated in the comparative surface plots in Figures 7.4, 7.5 and 7.6. For each of the monthly plots, EEJs are clearly seen enhanced and centered about local noon (17UT) time. The characteristics of the surface plot in figure 7.4 show that local noontime EEJ is more intense during/around equinox months than that in solstice months. Latitudinal TEC variations during 19-20UT on equinox and solstice days in figure 7.5 show a similar variation pattern as that seen in electrojet variations. The location, strengths and the span of the anomaly crests show a large degree of variability. From visual inspection of figure 7.4, it can be said that the EEJ on March and September equinox (around ± 30) days become strong and a similar pattern is followed by TEC profiles in figure 7.5. The corresponding distributions of EEJ and TEC are faint in June and December solstice days. These observations show that local late afternoon TEC variations are very dependent on the corresponding EEJ variations near local noontime. This relationship study can support the idea of forecasting TEC fluctuations a few hours earlier than their occurrence by knowing EEJ at low latitudes.

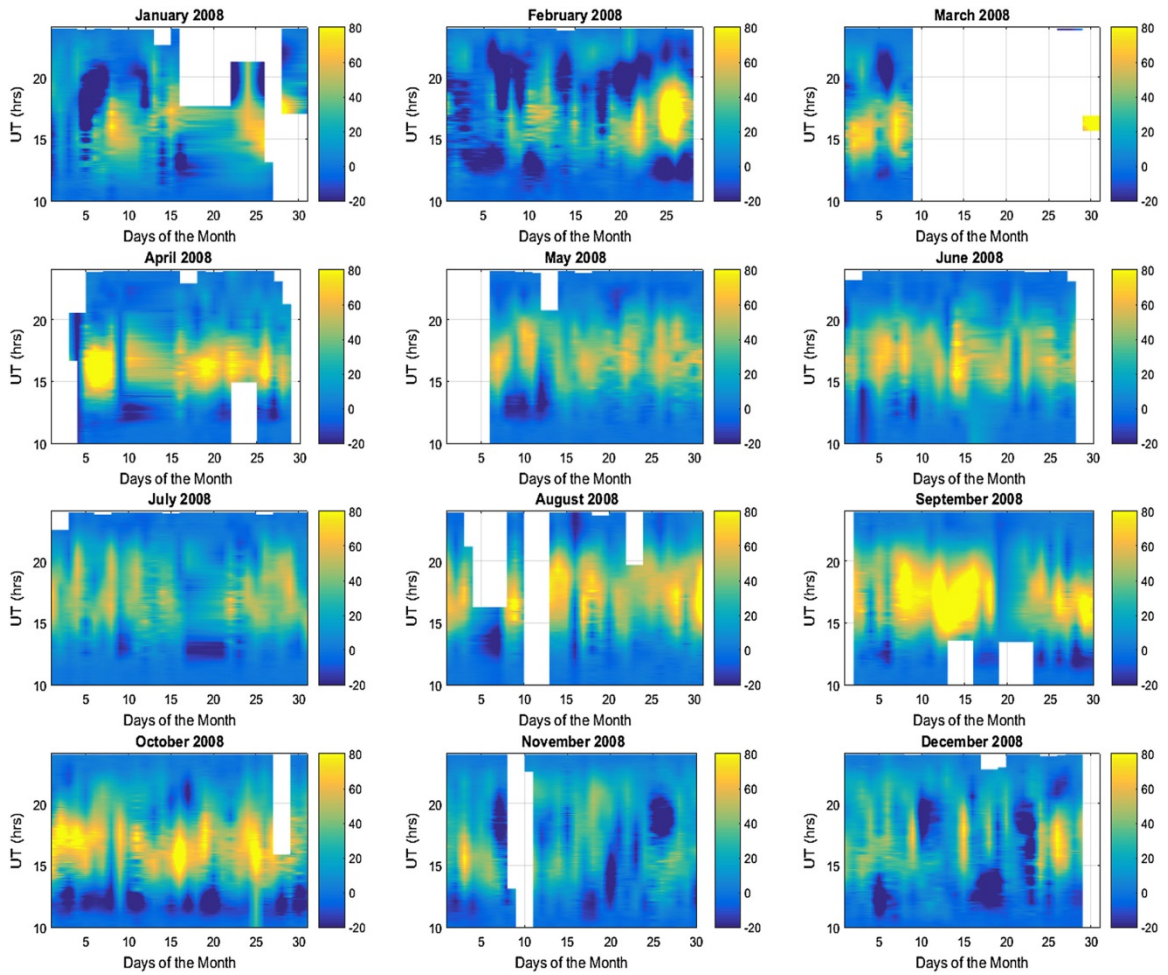


Figure 7.4. Surface plots showing the day-to-day variability of EEJ during 10 - 24 UT of the day observed using magnetometers located at Jicamarca and Piura stations during solar minimum 2008.

Anomaly Strength: 19 - 22 UT

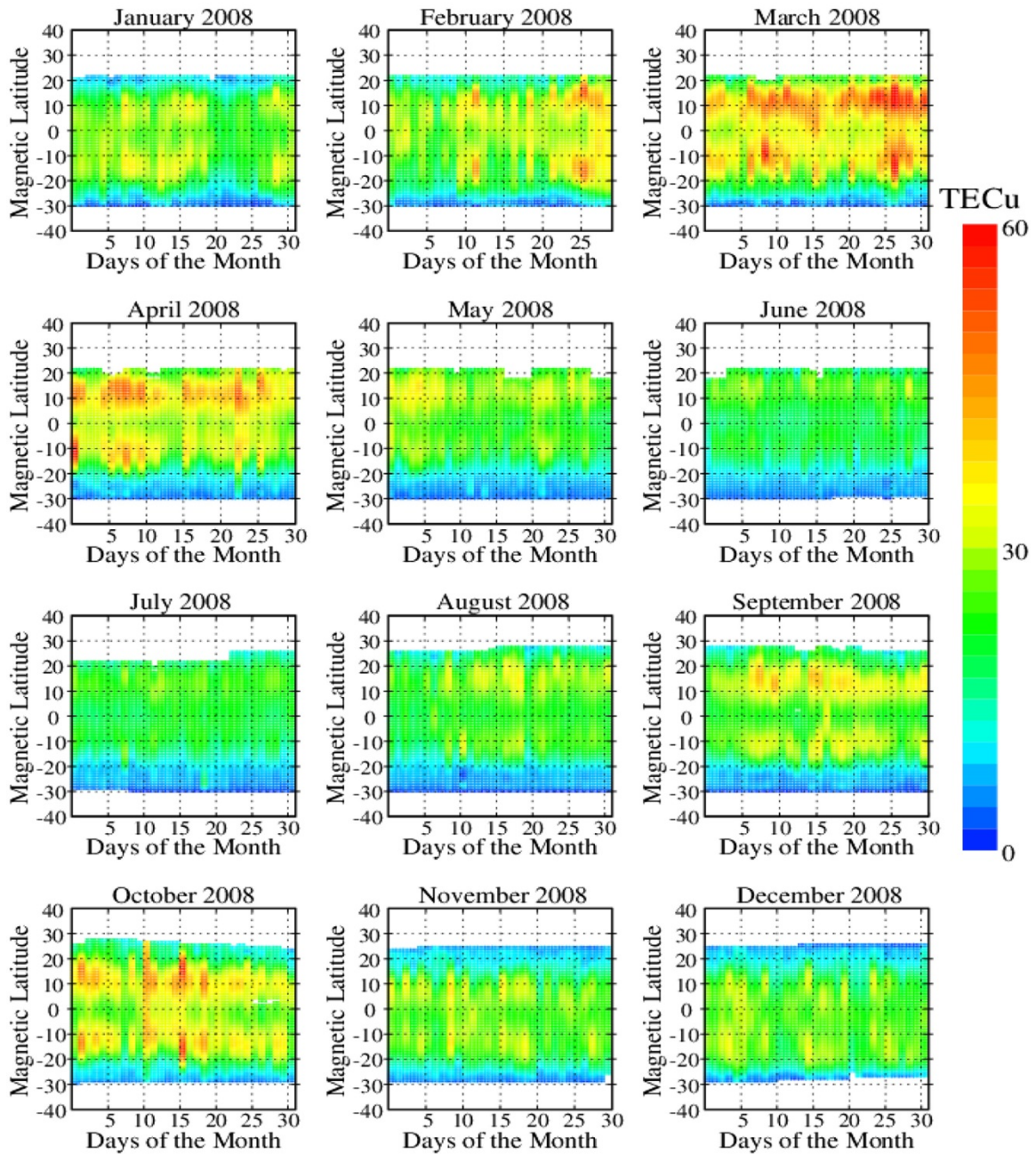


Figure 7.5 Latitudinal distributions of day-to-day variability TEC profiles within $\pm 30^\circ$ from magnetic equator in the Peruvian sector.

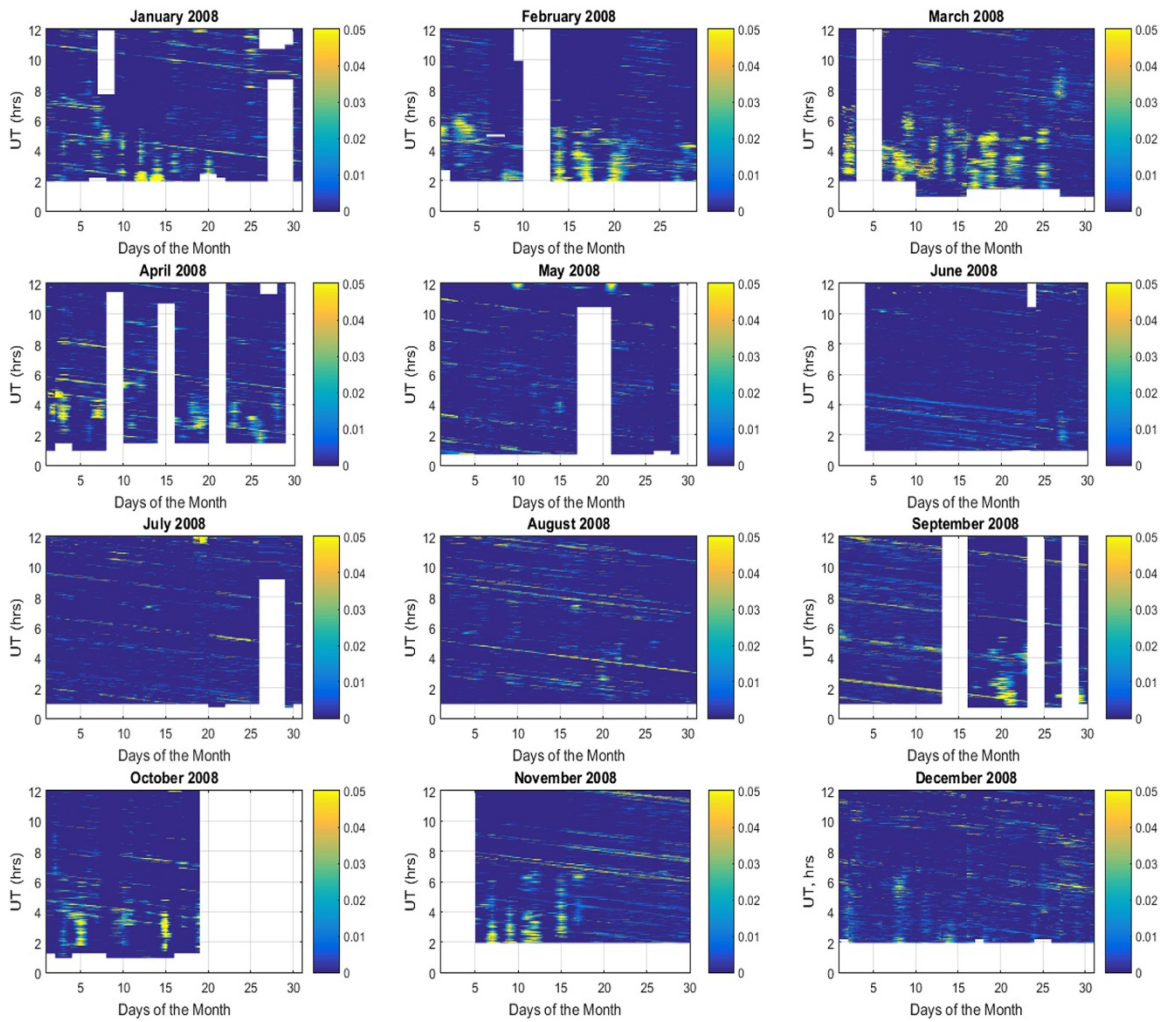


Figure 7.6. Day-to-day variability of scintillation S4 index during 00 - 12 UT obtained from GPS receivers spread on magnetic equator to either sides of anomaly region during solar minimum 2008.

On the other hand, the net S4 variation observed from GPS stations in the Peruvian longitude sector does not show any concrete relationship with daytime EEJ variation during equinox and solstice days. In figure 7.6, day-to-day variation of net S4 during 00 – 12UT has greater values not only during equinox but also beyond. As seen in figure 7.6, net S4 is higher in January as well as in November. The next section presents the case study events for the correlation analysis between EEJ and the net S4 index. This study corroborates that there is not a strong relationship between peak value of EEJ and S4 index in solar minimum periods.

7.4. Discussion

We have conducted a careful analysis of magnetometer, GPS and scintillation data to draw some conclusions on the role of daytime electric fields on the TEC distributions and S4 scintillation index. The strong Electrojet current in the E region ionosphere associated equatorial vertical ExB plasma drift in the F region ionosphere, and the accompanying noontime enhancement of H component, might be connected to electron density irregularities and corresponding plasma bubbles that show an indication of the TEC disturbances after sunset in the F region ionosphere.

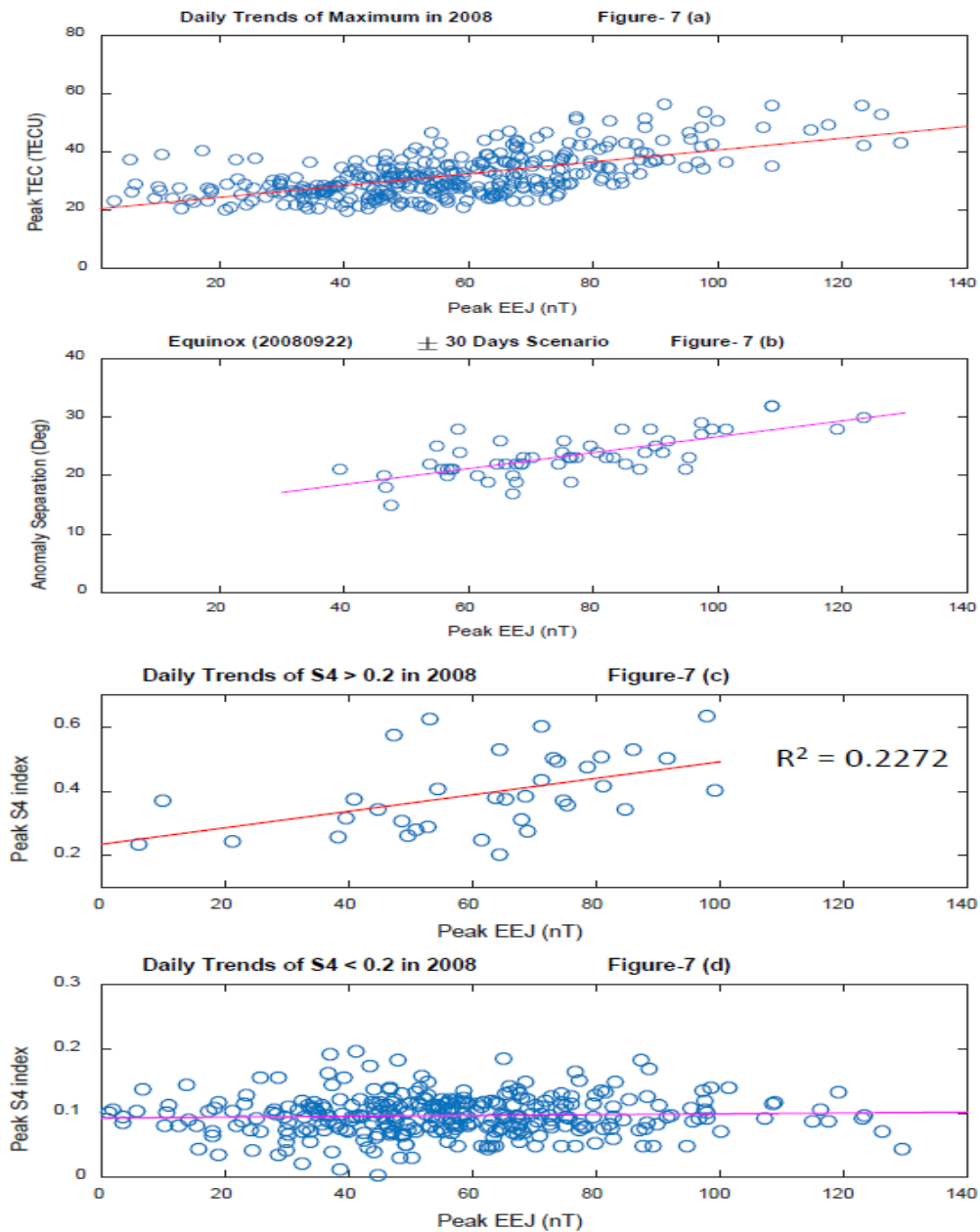


Figure 7.7. Correlation analysis of the daily trends of the peak value of equatorial electrojet data in the year 2008 with (a) maximum TEC during 19 - 22 UT, (b) the separation of the anomaly crests on equinox (September - 22) \pm 30 days, (c) S4 index greater than 0.2, and (d) S4 less than 0.2 observed during 00-12UT.

The study of the daytime equatorial electrojet can provide a precise and reliable signature for forecasting ionospheric dynamics. The data presented in figure 7.7 supports the statement that the studies of noontime EEJ have some sort of pre-information on the forthcoming ionospheric plasma behavior. As demonstrated in figure 7.4, EEJ reflects an intense band of eastward electric field at local noontime along the magnetic equator. The daytime eastward current in E region ionosphere regulates the strength of EEJ as well as vertical drift. Strong EEJ makes greater vertical drift. EEJ looks stronger during March and September equinoxes seasons than that in June and December solstice seasons as shown in figure 7.4. There are well-formed late afternoon anomaly crests if there is a strong corresponding noontime EEJ. The transport of the low latitude ionospheric plasma controls the TEC distribution which is originated by the vertical ExB drift and electrojet; both of these are driven by eastward electric field. TEC distributions most of the days are not placed symmetrically with respect to the magnetic equator and do not have the same latitudinal span of anomaly crests as seen in figure 7.5. We have chosen clear anomaly crest periods in September equinox and analyzed for ± 30 days from the equinox day to see the dependence of anomaly separation on EEJ strengths. The strengths and separation of anomaly crests shown in figure 7.5 are in good agreement with the EEJ strengths.

The correlation plot in figure 7.7 (a) gives a clear picture of the linear dependence of peak values of late afternoon (19-22UT) TEC and 7.7 (b) that of the separation of the anomaly crests on the noontime EEJ strength. By comparing the TEC in Figures 7.5 and 7.7 (a), (b), it can be said that higher EEJ and hence vertical drift causes higher electron density in the equatorial ionization anomaly regions and also causes the EIA crests to

move farther from the magnetic equator region. The simultaneous study of the dependence of EIA strengths and the separation of anomaly crests upon the noontime electrojet is one of the main aspects of this analysis.

Another analysis is done to obtain information of nighttime scintillation index S₄ based on corresponding daytime electrojet strength. For the dependence analysis, looking at the S₄ data distributions against EEJ variation, the correlation is studied in two regimes as in figures 7.7 (c) and (d). S₄ Data demonstrated in figures 7.7 (c) and (d) are taken from Cuzco GPS station located near the magnetic equator region during 00-12UT in 2008. There is a signature of linear dependence of S₄ index (>0.2) on peak value of EEJ as shown in figure 7.7 (c) but the linear curve looks parallel to the x axis for S₄ index (<0.2) in figure 7.7 (d). Slight dependence of nighttime S₄ index with value greater than 0.2 is seen with daytime peak value of EEJ but no correlation is seen with it if S₄ index value goes below 0.2. There are many factors that inhibit nighttime scintillation. One clue is that, the scintillation should be interpreted on the basis of the starting time of magnetic disturbance. This study also reveals that the noontime EEJ is not a good predictor for the nighttime ionospheric scintillation in the low latitude during low solar activity periods.

7.5. Summary and Conclusions

A comparative study of electrojet current strength, TEC, and S₄ scintillation index from magnetometers, and GPS receivers at low latitude stations has been conducted to investigate potential predictive signatures for the occurrence of disturbances in the equatorial ionosphere. We found that days with higher value of the equatorial electrojet

and hence higher daytime vertical ExB drift are associated with higher TEC values and a greater separation of the equatorial anomaly crests. But there is no apparent correlation with the S₄ scintillation index observed later during the nighttime. Minor correlation of peak value of electrojet with net S₄ greater than 0.2 likely exists but there is no correlation at all below 0.2 for the solar minimum year 2008. This research study suggests that there is a clear association between magnetometer observed daytime EEJ and the strength and distribution of GPS-derived TEC during late afternoon in magnetic low latitudes. However, there is little correlation between peak EEJ and the corresponding S₄ scintillation index observed after sunset.

A large dataset on EEJ strength, ExB drift velocity, and TEC using magnetometers, ionosondes, GPS receivers, and radar measurements are needed to establish the precise relationships between them under various background conditions. As in the polar region, the equatorial region is also highly susceptible to ionospheric scintillations during strong solar activity periods. Extending the analysis to solar maximum conditions with a larger database of nighttime S₄ index (above 0.2) will certainly be worthwhile project in accessing correlations with peak values of daytime EEJ. Collection of long-term statistics relating magnetometer-derived drifts and radar-measured drifts can contribute significantly to a more economical way to characterize the occurrence of ionospheric irregularities. The development of such model and statistical relations can help in real-time ionospheric monitoring and improvement in GPS navigation capabilities.

Chapter 8

SUMMARY AND FUTURE RESEARCH

Contents	Page
8.1. Overview of Dissertation Results.....	197
8.1.1 Variability of EEJ and its Consequences.....	198
8.1.2 Asymmetry of EIAs.....	199
8.1.3 Evolution to Decay of EPB/ Blobs	199
8.1.4 Mutual Relationship between Ionospheric Parameters	200
8.2. Space Weather and Impacts on Space-Based Technologies.....	200
8.3. Directions for Future Research.....	204

8.1 Overview of Dissertation Results

The guiding principle behind this dissertation is to seek ways that can be used to predict and mitigate space weather effects on spaced-based technological devices useful to mankind with a general understanding of the structure and electrodynamics of the equatorial and low-latitude ionosphere based on ground and space-based observations. We started, as described in Chapter 1, with the motivation of the investigation by designing a set of research questions. It also introduces how low-latitude phenomena confined within a very thin shell of ionospheric layer, and their variability affect our

practical life being a source of disruptions for critical infrastructure. In chapter 2, a brief description of the structure, features, and physics of the geospace environment in the low-latitude regions are presented. Particularly, the general features, caprices and vagaries of the most prevalent ionospheric phenomena in the low-latitude phenomena e.g., EEJ, EIA, and EPBs/Blobs, are discussed. The physics and mechanism behind each of these phenomena are also presented to look for possible interconnectedness between them. The ionosphere is a suitable laboratory for studying various plasma processes that exist in near-Earth space environment. Further, Chapter 3 provides an overview of geographical area of interest for the study, data sources, methodology for data analysis, and description of instruments chosen from ground and space for current investigation. Besides probing ionospheric event using single instrument, benefit of the coordinated analysis of an ionospheric plasma density observation has also been discussed. With the help of these theories, instruments, and approaches, novel conclusions of this dissertation are summarized as follows.

8.1.1 Variability of EEJ and its Consequences

With the analysis developed in Chapter 4, it is clear that EEJ shows a strong variability with longitude, season, day-to-day variability and solar activity. Probably for the first time, variability of EEJ in a very narrow spatial separation in South American low-latitude is presented. Overall, the EEJ current is higher in the western American meridian and keep decreasing towards the eastern meridian sector of South America. The vertical dynamics of F-layer ionosphere and TEC distribution in EIA show a substantial association with the variability of the EEJ and its counter portion in the morning period.

8.1.2 Asymmetry of EIAs

We explored the basic characteristics, and then took a look at the asymmetric structure in the EIA via the SOFDI measurements and the LLIONS physics-based model in Chapter 5. For the first time, 24-hours measured meridional neutral wind is presented in order to demonstrate its role on the development of asymmetric structure of the EIA in the low-latitude ionosphere. EEJ as a proxy of EEF is a primary source of the EIA, whereas and the trans-equatorial neutral wind controls its asymmetric structure by influencing the equatorial plasma fountain mechanism.

8.1.3 Evolution to Decay of EPBs/ Blobs

The unique geometry of the path of the SWARM satellite constellation allows us to conduct multiple and almost simultaneous in-situ measurement through the same set of EPBs/ Blobs over low latitude regions, to investigate their coherence and the motion of structures embedded within the EPBs. This benefit of the SWARM satellite is used for the coordinated quantitative analysis of a plasma density from ground LISN observation as well, and is presented in Chapter 6. The simultaneous analysis provides evidence of the initial association of EPBs with plasma blobs at equator and later the blobs are separated at EIA latitudes via fountain effect. Different ionospheric processes are also discussed and further analysis has been suggested to provide universal theory for generation, dynamics, and decay of EPBs and plasma blobs.

8.1.4 Mutual Relationship between Ionospheric Parameters

Understanding and forecasting the occurrence and impact of ionospheric irregularities in the space- and ground-based instruments is a critical societal need. To fulfil this necessity, this study looks for a mutual relationship between the midday, afternoon and nighttime ionospheric phenomena to advance our space weather forecasting capability as presented in Chapter 7. Almost all behaviors of the afternoon EIA are influenced by noontime EEJ but only a weak influence of the peak EEJ is seen in the ionospheric amplitude scintillation (S4) after sunset, above a certain threshold. It is reveal that the daytime EEJ can provide a precise and reliable signature for forecasting the nighttime ionospheric dynamics, and have some sort of pre-information on the forthcoming ionospheric plasma behavior.

8.2 Space Weather and Impacts on Space-Based Technologies

Exclusively, there is weather in space; mainly driven by solar activities that influence modern technologies analogous to what the tropospheric weather does to life of living beings on the Earth surface. The dynamic Sun and its subsequent effects in the interplanetary space are the main sources of space weather activity on Earth. With the establishment of The U. S. National Space Weather Program in 1994, as mentioned in *Robinson and Behnke, [2001]*, space weather is officially defined as the conditions on the Sun and in the solar wind, magnetosphere, ionosphere, and thermosphere that can influence the performance and reliability of space-borne and ground-based technological systems and can endanger human life or health. Adverse conditions in the space environment can cause disruption of satellite operations, communications, navigation,

and electric power distribution grids, leading to a variety of socioeconomic losses. However, space weather is affecting us, our space-borne and ground-based technologies; it has presented challenges as well as opportunities for the scientific community to show the practical benefits of solar-terrestrial research. Figure 8.1 highlights some of the adverse effects of space weather that arise from solar transients on systems, and the mechanisms behind the effects. These include damages/ failures in the spacecraft electronics caused by high energy protons, electron induced spacecraft surface and internal charging leading to discharge currents, solar panel degradation due to particle bombardment, human tissue damages due to particle radiation, atmospheric drag experienced by low orbit spacecraft, interruptions in the HF communication and navigation systems caused by irregularities in the ionosphere (e.g., EPBs), cosmic ray induced neutron radiation at airline heights, geomagnetically induced currents (GIC) in long conductor systems on the ground caused by rapidly varying ionospheric currents, and the possible modulation of the neutral atmospheric weather by space weather [Pulkkinen, 2003; MacAlester and Murtagh, 2014].

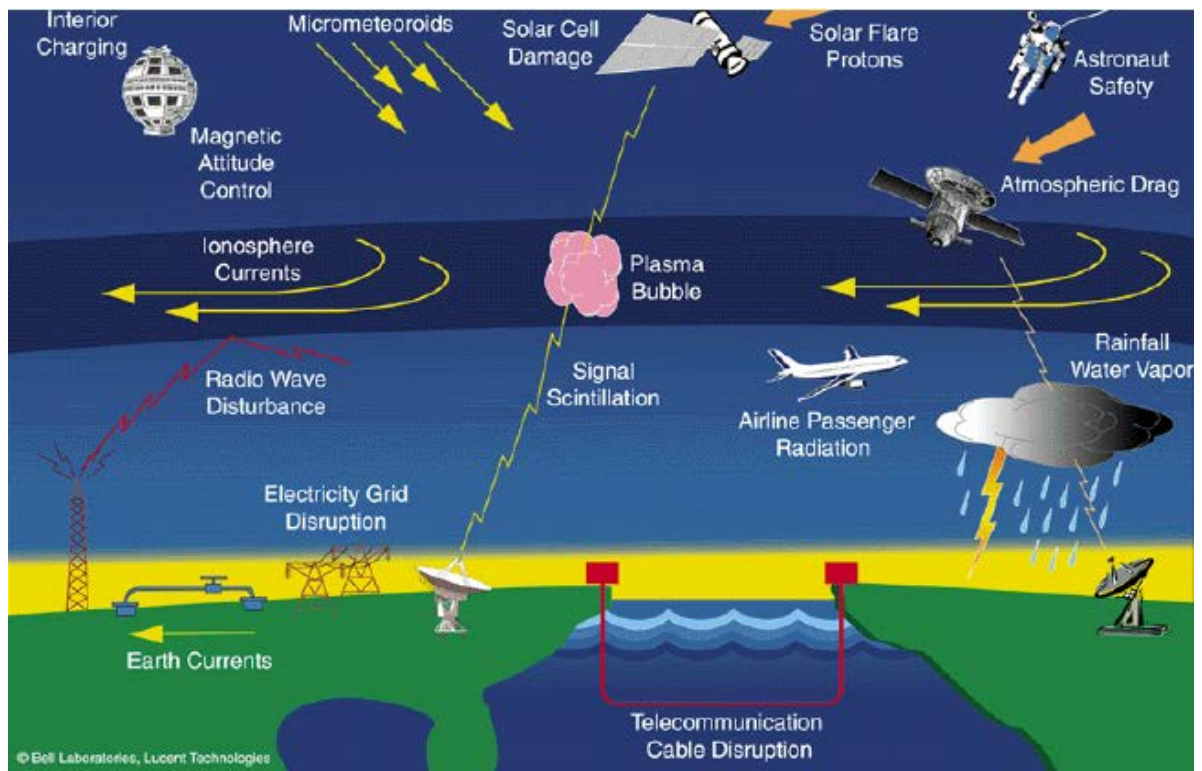


Figure 8.1: Highlights of space weather effects arise from solar transients [Image: Subramanian, 2009].

The driving mechanism of space weather is linked by the chain of causal connections and physical processes starting from the Sun. Solar events such as Coronal Mass Ejections (CMEs), solar flares and associated recombination events are some of the driving factors in space weather that can cause potentially devastating effects on the terrestrial power grid, associated infrastructure, and assets [Gaunt, 2015; Johnson et al., 2016]. CMEs and CIRs (Corotating Interaction Regions) expelled from solar corona have been established as the primary source of major geomagnetic storms and large SEP (Solar Energetic particle) events [Gosling et al., 1976; Gonzalez et al., 1994; Gopalswamy, 2008]. Interplanetary (IP) shocks and the underlying CMEs modify the magnetosphere and ionosphere current systems, which then can cause magnetic field variability on the ground. These variations cause geomagnetically induced currents (GICs) in terrestrial conductors such as electric power grids, buried pipelines, telegraph lines, submarine cables and railroads etc. [Boteler et al., 1998; Eroshenko et al., 2010; Knipp, 2015].

Interplanetary (IP) shocks are mainly responsible for the sudden compression of the magnetosphere, causing storm sudden commencements (SCs) and sudden impulses (SIs) which are detected by ground-based magnetometers [Veenadhari et al, 2012]. The SC events are often the precursors to strong geomagnetic storms and can indicate the onset of a more intense solar wind driving and buffeting the magnetosphere [Belakhovsky et al. 2017]. The stronger dB/dt magnetic spikes at the arrival of interplanetary shocks could cause significant GICs and electric fields that might have damaging effects on modern ground-based technological infrastructures. The strength of these currents can be detected by the time derivative of the ground-based magnetometer observations (dB/dt) [Coles

and Boteler, 1993; Forbes and St. Cyr, 2008] and is also significantly quantifiable in the equatorial and auroral electrojets [Kappernman and Albertson, 1990; Carter et al., 2015]. This dissertation also pursues a correlation between the noontime EEJ, the GPS-derived TEC distributions in EIA during the afternoon, and postsunset ionospheric scintillation. A strong correlation between EEJ and EIA was found, but; only a minor correlation exists between the peak EEJ and postsunset ionospheric scintillation index (S4) above a certain threshold. Our finding not only establishes a mutual relationship between the midday, afternoon and nighttime ionospheric phenomena but also opens an avenue for a possible route to improve current space weather forecasting capability at the equatorial and low latitudes. The understanding of physical processes involved in this correlation could lead to the possible improvement in predicting and forecasting the quiet as well as storm-time plasma redistribution and the creation of irregularities. Both the *U.S. Department of Homeland Security [2011]* and *U.S. Federal Energy Regulatory Commission [2016]* have the highest concern for preparedness against adverse space weather events, and address the impacts of geomagnetic disturbances. New developments in observational sensors now allow for virtualizing and detailing the magnetosphere and ionosphere variations in response to solar conditions with great fidelity in space and time which therefore provide great potential for new discoveries.

8.3 Directions for Future Research

The work presented in this dissertation provokes many questions and challenges that need to be addressed in future studies. A few possibilities that seem most useful are outlined in this section.

- *Global longitudinal variability of EEJ.*

Day-to-day longitudinal variability of EEJ and its counter feature is always an essential baseline to understand ionospheric electrodynamics since it is a proxy of ionospheric electric field and is used as inputs in many models in space physics community. Currently, a dense network of magnetometers have been installed in the low-latitude region around the globe by various research organizations with the purpose of studying and forecasting ionospheric phenomena, with special emphasis in the dynamics and energy transport processes. New insights need to be continued similar to what has been mentioned in Chapter 4, for the study of the occurrence, cause and accompanying phenomena of the narrow longitudinal variability of electrojet and counter electrojet globally from ground magnetometers and also coordinated with radar, optical, radio and satellite observations.

- *EEJ as a signature of GIC.*

Influence level of electrojet profile on GICs as dB/dt , ground magnetic signatures, at magnetic equator and high latitudes will be used to examine its impact level during geomagnetic storms. Extreme space weather events have a low occurrence rate but a potentially high impact in high as well as low latitudes region that presents a major challenge for our understanding of GIC activity [Carter et al., 2015; Pulkkinen et al., 2017; Ngwira and Pulkkinen, 2018]. Signatures of GICs at EEJ ultimately become another asset for space weather prediction. The extension of the relationship study as discussed in Chapter 7, will significantly advance our understanding and modeling capabilities describing solar and magnetosphere-ionospheric dynamics, ground

conductivity, and accurate forecasting to avoid catastrophic failures of systems and to enhance the performance of infrastructures having long metal conductor systems, e.g. in electric power lines, underground pipelines, telegraph lines, submarine cables, and railroads etc.

- *Role of EEJ and its depression on F-region dynamics and onsets of PRE and ESF.*

The ultimate cause of the PRE is associated with the F region zonal neutral wind dynamo near the sunset terminator [Haerendel and Eccles, 1992]. The increase in the F-layer height and the onsets of equatorial spread-F (ESF) during the evening hours were well connected with the ground-measured EEJ strength before sunset, namely, both the height increase and ESF onsets were suppressed with afternoon EEJ depression (AED) [Uemoto et al., 2010; Eccles et al., 2015]. It would be very important analysis to extend the study of the contribution of the morning EEJ depression (MED) discussed in Chapter 4, as a regulating current path during pre-sunset E-region dynamo current and how these electric fields are related to evening PRE, the F-region dynamics, and the ESF onsets after sunset.

- *Thermospheric neutral wind on EIA asymmetry.*

The thermospheric neutral wind is an unavoidable factor causing the formation of the EIA asymmetry formation. To draw more quantitative conclusions about the role of neutral wind as an ionospheric driver of EIA asymmetry, which was discussed in Chapter 5, a rigorous long-term neutral wind data from real time measurement systems is going to be required. Further analysis and investigation with real time data will certainly be a very important study to distinguish the relative contribution between the meridional, zonal and

vertical component of the thermospheric neutral wind for the transportation of plasma along the entire flux-tube geometry. This study would eventually be helpful to validate the neutral wind in the upper atmosphere derived from existing physics-based as well as empirical models under quiet and magnetosphere-induced disturbed conditions.

- *Coordinated ground and space-based measurements of ionospheric plasma structures for the understanding of generation to decay mechanism.*

There are numerous studies on generation, dynamics, and decay mechanism of plasma depletions (bubbles) and enhancements (blobs) in the low-latitude ionosphere. *Kil et al., [2015]* proposed that bubbles and blobs are created by different mechanism whereas *Huang et al. [2014]* claimed that these are created by the same mechanism. But, recent studies by *Choi et al., [2012]* and *Miller et al., [2014]* demonstrated that medium-scale traveling ionospheric disturbances (MSTIDs) are possible driving mechanism for the formation of the blobs independent of that of bubbles. Using coordinated ground and space-based multi-probe measurement from different locations as presented in Chapter 6, we will be able to address role of aforementioned sources, their relationship, and provide universal theory behind generation, dynamics, and decay of plasma bubbles and blobs in the low-latitude ionosphere.

Chapter 9

References

- Aarons, J. (1993), The longitudinal morphology of equatorial F layer irregularities relevant to their occurrence, *Space Sci. Rev.*, 63, 209.
- Abdu, M. A. (2001), Outstanding problems in the equatorial ionosphere-thermosphere electrodynamics relevant to spread F , *J. Atmos. Terr. Phys.*, 63, 869-884.
- Abdu, M. A., G. O. Walker, B. M. Reddy, J. H. A. Sobral, B. G. Fejer, T. Kikuchi, N. B. Trivedi, and E. P. Szuszczewicz (1990), Electric field versus neutral wind control of the equatorial anomaly under quiet and disturbed condition: A global perspective from SUNDIAL 86, *Ann. Geophys.*, 8, 419–430.
- Abdu, M. A., J. A. Bittencourt, and I. S. Batista (1981), Magnetic declination control of the equatorial F region dynamo electric field development and spread F, *J. Geophys. Res.*, 86(A13), 11443–11446, doi:10.1029/JA086iA13p11443.
- Abdu, M. A., R. T. Medeiros, J. A. Bittencourt, and I. S. Batista (1983), Vertical ionization drift velocities and range type spread F in the evening equatorial ionosphere, *J. Geophys. Res.* 88, 399-402.
- Abdu, M.A., C. G. M. Brum, I.S. Batista, J. H. A. Sobral, E.R. de Paula, J. R. Souza (2008), Solar flux effects on equatorial ionization anomaly and total electron content over Brazil: observational results versus IRI representations, *Advances in Space Research*, Vol. 42(4), pp. 617–625, doi:10.1016/j.asr.2007.09.043.

- Akasofu, S.-I., and Y. Kamide, (1985), Meridian chains of magnetometers as a powerful “remote-sensing” tool in determining electromagnetic quantities in the ionosphere on a global scale, *Eos Trans. AGU.*, 66, 465.
- Akbari, H. (2015), Beam-plasma interactions and Langmuir turbulence in the auroral ionosphere, PhD thesis, Boston University.
- Akbari, H., Bhatt, A., La Hoz, C., and Semeter, J. L. (2017), Incoherent Scatter Plasma Lines: Observations and Applications, *Space Sci. Rev.*, <https://doi.org/10.1007/s11214-017-0355-7>.
- Alken, P., S. Maus, P. Vigneron, O. Sirol, and G. Hulot (2013), Swarm SCARF equatorial electric field inversion chain, *Earth Planets Space*, **65**, this issue, 1309–1317.
- Anandarao BG (1976), Effects of gravity wave winds and wind shears on equatorial Electrojet. *Geophys Res Lett* 3:545–547.
- Anderson D. N. (1973), A theoretical study of the ionospheric F region equatorial anomaly, I, Theory, *Planet. Space Sci.*, Vol. 21(3), 409–419. doi:10.1016/0032-0633(73)90040-8.
- Anderson, D., A. Anghel, J. Chau, and O. Veliz (2004), Daytime vertical ExB drift velocities inferred from ground-based magnetometer observations at low latitudes, *Space Weather*, Vol. 2, and S11001, doi:10.1029/2004SW000095.
- Anderson, D., A. Anghel, K. Yumoto, M. Ishitsuka, and E. Kudeki (2002), Estimating daytime vertical ExB drift velocities in the equatorial F-region using ground-based magnetometer observations, *Geophys. Res. Lett.*, Vol. 29 (12), doi:10.1029/2001GL014562.

- Anderson, D., A. Anghel, K. Yumoto, M. Ishitsuka, and E. Kudeki (2002), Estimating daytime vertical ExB drift velocities in the equatorial F-region using ground-based magnetometer observations, *Geophys. Res. Lett.*, Vol. 29 (12), doi: 10.1029/2001GL014562.
- Appleton, E. V. (1946), Two anomalies in the ionosphere, *Nature*, Vol. 157 (3995), 691, doi: 10.1038/157691a0.
- Appleton, E. V., M. A. F. Barnett (1925), On some direct evidence for downward atmospheric reflection of electric rays, *Proc. R. Soc. London, Ser. A*, 109, 621–641.
- Babcock, H. D. (1923), A study of the green auroral line by the interference method, *Astrophys. J.*, 57, 209-221.
- Bailey, G. J., N. Balan, and Y. Z. Su (1997), The Sheffield University plasmasphere ionosphere model—A review, *J. Atmos. Sol. Terr. Phys.*, 59, 1541–1552, doi:10.1016/S1364-6826(96)00155-1.
- Bailey, G. J., R. J. Moffett, W. B. Hanson, and S. Sanatani (1973), Effects of interhemisphere transport on plasma temperatures at low latitudes, *J. Geophys. Res.*, 78(25), 5597–5610, doi:10.1029/JA078i025p05597.
- Balan, N., G. J. Bailey (1995), Modeling studies of the equatorial plasma fountain and equatorial anomaly, *Adv. Space Res.*.
- Balan, N., J.J. Bailey, R.J. Moffett, Y.Z. Su, J.E. Titheridge (1995), Modeling studies of the conjugate-hemisphere differences in ionospheric ionization at equatorial anomaly latitudes, *J. Atmos. Terr. Phys.* 57(3), 279-292.
- Balfour Steward (1882), Terrestrial magnetism, *Encyclopedia Britannica*, 9th ed., 16, 181

- Balsley, B B. (1970), Equatorial Electrojet: Seasonal Variation of the Reversal Times, *J. Geophys. Res., Space Physics*, Vol. 75 (22), 4369–4371, doi: 10.1029/JA075i022p04369.
- Balsley, B B. (1970), Longitudinal variation of electron drift velocity in the equatorial electrojet, *J. Geophys. Res., Space Physics*, Vol. 75 (22), 4291–4297, doi:10.1029/JA075i022p04291.
- Balsley, B. B. (1973), Electric fields in the equatorial ionosphere: A review of techniques and measurements, *J. Atmos. Terr. Phys.*, 35, 1035–1044.
- Banola, S., B. M. Pathan, and D. R. K. Rao (2001), Strength of the equatorial electrojet and geomagnetic activity control on VHF scintillations at the Indian longitudinal zone, *Indian J. of Radio Space Phys.*, Vol. 30, 163-171.
- Bartels J, Johnston HF (1940) Geomagnetic tides in horizontal intensity at Huancayo. *Terr. Mag. Atmos. Elec.* 45:269–308.
- Basu, S., *et al.* (1996), Scintillations, plasma drifts, and neutral winds in the equatorial ionosphere after sunset, *J. Geophys. Res.*, 101(A12), 26795–26809, doi:10.1029/96JA00760.
- Basu, S., K. M. Groves, Su. Basu, and P. J. Sultan (2002), Specification and forecasting of scintillations in communication and navigation links: Current status and future plans, *J. Atmos. Sol. Terr. Phys.*, 64 (16), 1745-1754, doi: 10.1016/S1364-6826(02)00124-4.
- Batista, I. S., M. A. Abdu, and J. A. Bittencourt (1986), Equatorial F region vertical plasma drifts: Seasonal and longitudinal asymmetries in the American sector, *J. Geophys. Res.*, 91(A11), 12055–12064, doi:10.1029/JA091iA11p12055.

- Bauer, S. J., A. F. Nagy (1975), Ionospheric direct measurement techniques, *Proc. IEEE*, 63, 230.
- Bauer, S. J., and R. E. Hartle (1973), On the extent of the Martian ionosphere, *J. Geophys. Res.*, 78(16), 3169–3171, doi:10.1029/JA078i016p03169.
- Baumjohann, W. and R. A. Treumann (2012), Basic Space Plasma Physics, Revised Edition, Imperial College Press, London.
- Belakhovsky, V. B., V. Pilipenko, Y.A. Sakharov, D.L. Lorentsen, S.N. Samsonov, (2017), Geomagnetic and ionospheric response to the interplanetary shock on Jan. 24, 2012, *Earth, Planets Space*, 69 (105), 1-25, doi:10.1186/s40623-017-0696-1
- Bhardwaj, S.K. & Subba Rao, P.B.V.(2017) The afternoon counter-electrojet current system along the 75°E meridian during the IEEY, *Earth Planets Space*, 69: 91. <https://doi-org.proxy.bc.edu/10.1186/s40623-017-0675-6>.
- Bhatt, A. N. (2010), Exploring the electron component in incoherent scatter from the ionosphere. Ph.D. Thesis, Cornell University.
- Bhuyan P.K. and Borah RR (2007) TEC derived from GPS network in India and comparison with IRI. *Advances in Space Research*, Vol. 39(5), 830-840, doi:10.1016/j.asr.2006.12.042
- Blanc, M. and A. D. Richmond (1980), The ionospheric disturbance dynamo, *J. Geophys. Res.*, Vol. 85 (A4), 1669–1686, doi: 10.1029/JA085iA04p01669.
- Boteler, D., R. Pirjola, and H. Nevanlinna (1998), The effects of geomagnetic disturbances on electrical systems at the Earth's surface, *Adv. Space Res.*, 22(1), 17–27, doi:10.1016/S0273-1177(97)01096-X.

- Burnside, R. G., F. A. Herrero, J. W. Meriwether, and J. C. G. Walker (1981), Optical observations of thermospheric dynamics at Arecibo, *J. Geophys. Res.*, 86(A7), 5532–5540, doi:10.1029/JA086iA07p05532.
- Carter, B. A., E. Yizengaw, R. Pradipta, A. J. Halford, R. Norman, and K. Zhang (2015), Interplanetary shocks and the resulting geomagnetically induced currents at the equator, *Geophys. Res. Lett.*, 42, 6554–6559, doi:10.1002/2015GL065060.
- Carter, B. A., E. Yizengaw, R. Pradipta, J. M. Retterer, K. Groves, C. Valladares, R. Caton, C. Bridgwood, R. Norman, and K. Zhang (2016), Global equatorial plasma bubble occurrence during the 2015 St. Patrick's Day storm, *J. Geophys. Res. Space Physics*, 121, 894–905, doi:10.1002/2015JA022194.
- Çelik, C. (2013), The solar daily geomagnetic variation and its dependence on sunspot number. *J. Atmos. Sol.-Terr. Phys.* 104, 75–86.
- Chakrabarti, N., and G. S. Lakhina (2003), Collisional Rayleigh-Taylor instability and shear-flow in equatorial spread *F* plasma, *Ann. Geophys.*, 21, 1153.
- Chandrasekhar NP, Archana RK, Nagarajan N, Arora K (2017), Variability of Equatorial counter electrojet signatures in the Indian region. *J Geophys Res.* doi: 10.1002/2016JA022904.
- Chapagain, Narayan P. (2011), Dynamics of Equatorial Spread F Using Ground-Based Optical and Radar Measurements, Ph.D. Thesis, Utah State University, Logan, Utah,
- Chapman, S. (1951), The equatorial electrojet as detected from the abnormal electric current distribution above Huancayo, Peru and elsewhere, *Arch. Meteorol., Geophys. Bioklimatol.*, Ser. A, Vol.4(1), 368–390, doi: 10.1007/BF02246814.

- Chau, J. L., B. G. Fejer, and L. P. Goncharenko (2009), Quiet variability of equatorial ExB drifts during a sudden stratospheric warming event, *Geophys. Res. Lett.*, 36, L05101, doi: 10.1029/2008GL036785.
- Chen, C. H., J. Y. Liu, K. Yumoto, C. H. Lin, and T. W. Fang (2008), Equatorial ionization anomaly of the total electron content and equatorial electrojet of ground-based geomagnetic field strengths, *J. Atmos. Sol. Terr. Phys.*, Vol.70 (17), 2172-2183, doi:10.1016/j.jastp.2008.09.021
- Choi, H.-S., H. Kil, Y.-S. Kwak, R. A. Heelis, W. R. Coley, Y.-D. Park, and K.-S. Cho (2012), Comparison of the bubble and blob distributions during the solar minimum, *J. Geophys. Res.*, 117, A04314, doi:10.1029/2011JA017292.
- Cohen, R. (1967), The equatorial ionosphere, *Physics of Geomagnetic Phenomena*. S. Matushita and W. Campbell, eds. Academic Press, New York.
- Coles, R. L. and Boteler, D. H. (1993), Geomagnetic induced currents: assessment of geomagnetic hazard, *GSC (Geological Survey of Canada), Open File 2635*, 93 pages <https://doi.org/10.4095/184063>.
- Coster, A. J., J. C. Foster, and P. J. Erickson (2003), Monitoring the ionosphere with GPS, *GPS World*, 14(5), 42–49.
- Dang, T., X. Luan, J. Lei, X. Dou, and W. Wan (2016), A numerical study of the interhemispheric asymmetry of the equatorial ionization anomaly in solstice at solar minimum, *J. Geophys. Res. Space Physics*, 121, doi: 10.1002/2016JA023012.
- Davies, K. (1989), Ionospheric Radio, *IEE Electromagnetic Wave Series* 31, <http://www.digisonde.com/instrument-description.html>.

- Deshpande, M. R., et al. (1977), Effect of electrojet on the total electron content of the ionosphere over the Indian subcontinent, *Nature* 267, 599-600, doi: 10.1038/267599a0.
- Deshpande, M. R., et al. (1977), Effect of electrojet on the total electron content of the ionosphere over the Indian subcontinent, *Nature* 267, 599-600, doi: 10.1038/267599a0.
- Doherty, P., A. J. Coster, and W. Murtagh (2004), Space weather effects of October–November 2003. *GPS Solutions*, Vol. 8 (4), 267-271, doi: 10.1007/s10291-0040109-3.
- Dougherty, J. P., and D. T. Farley (1960), A theory of incoherent scattering of radio waves by plasma, *Proc. Roy. Soc. London, A*, 259, 79-99.
- Dougherty, J. P., and D. T. Farley Jr. (1963), A theory of incoherent scattering of radio waves by a plasma: 3. Scattering in a partly ionized gas, *J. Geophys. Res.*, 68(19), 5473–5486, doi:10.1029/JZ068i019p05473.
- Dunford, E. (1967), The relationship between the ionospheric equatorial anomaly and the E-region current system, *J. Atmos. Terr. Phys.*, 29, 1489–1498.
- Dungey, J. W. (1956), Convective diffusion in the equatorial F-region, *J. Atmos. Terr. Phys.* 9, 304.
- Eccles, J. V., J. P. St. Maurice, and R. W. Schunk (2015), Mechanisms underlying the prereversal enhancement of the vertical plasma drift in the low-latitude ionosphere, *J. Geophys. Res. Space Physics*, 120, 4950–4970, doi:10.1002/2014JA020664.

- Eccles, J. V., N. Maynard, and G. Wilson (1999), Study of the evening plasma drift vortex in the low-latitude ionosphere using San Marco electric field measurements, *J. Geophys. Res.*, 104(A12), 28133-28143.
- Eccles, V., D. D. Rice, J. J. Sojka, C. E. Valladares, T. Bullett, and J. L. Chau (2011), Lunar atmospheric tidal effects in the plasma drifts observed by the Low-Latitude Ionospheric Sensor Network, *J. Geophys. Res.*, 116, A07309, doi:10.1029/2010JA016282.
- Egedal, J. (1947), The magnetic diurnal variation of the horizontal force near magnetic equator, *J. Geophys. Research*, Vol. 52(4), 449-451, doi: 10.1029/TE052i004p00449.
- Eroshenko E. A., Belov A. V., Boteler, D., Gaidash S. P., Lobkov S. L., et al. (2010), Effects of Strong Geomagnetic Storms on Northern Railways in Russia, *Adv. Space Res.*, 46, 1102- 1110, <http://dx.doi.org/10.1016/j.asr.2010.05.017>
- Evans, J. (1969). Theory and practice of ionosphere study by Thomson scatter radar. *Proceedings of the IEEE*, 57(4), 496–530. <https://doi.org/10.1109/PROC.1969.7005>
- Fabry, Charles and Alfred Pérot (1897), Sur les franges des lames minces argentées et leur application a`la mesure de petites épaisseurs d`air, *Ann.Chim. Phys.*12, 459–501.
- Farley, D. T., B. B. Basley, R. F. Woodman, and J. P. McClure (1970), Equatorial spread F: Implications of VHF radar observations, *J. Geophys. Res.*, 75, 7199-7216.

- Farley, D. T., E. Bonelli, B. G. Fejer, and M. F. Larsen (1986), The prereversal enhancement of the zonal electric field in the equatorial ionosphere, *J. Geophys. Res.*, *91*, 13723.
- Fejer, B. G. (1981), The equatorial ionospheric electric fields: A review, *J. Atmos. Terr. Phys.*, *43*(516), 377–386, doi:10.1016/0021-9169(81)90101-X.
- Fejer, B. G. (1991), Low latitude electrodynamic plasma drifts: A review, *J. Atmos. Terr. Phys.*, Vol. 53, 677, doi:10.1016/0021-9169(91)90121-M.
- Fejer, B. G. and M. C. Kelley (1980), Ionospheric Irregularities, *Review of Geophysics*, Vol. 18 (2), 401-454, doi: 10.1029/RG018i002p00401.
- Fejer, B. G., (2015) The Equatorial Ionosphere: A Tutorial, Lecture presented in CEDAR Workshop, Seattle.
- Fejer, B. G., and M. C. Kelley (1980), Ionospheric irregularities, *Rev. Geophys.*, *18*, 401–454.
- Fejer, B. G., Gonzales, C. A., Farley, D. T., Kelley, M. C., & Woodman, R. F. (1979). Equatorial electric fields during magnetically disturbed conditions 1. The effect of the interplanetary magnetic field. *Journal of Geophysical Research*, *84*(13), 5797–5802.
- Fejer, B. G., M. E. Olson, J. L. Chau, C. Stolle, H. Lühr, L. P. Goncharenko, K. Yumoto, and T. Nagatsuma (2010), Lunar-dependent equatorial ionospheric electrodynamic effects during sudden stratospheric warmings, *J. Geophys. Res.*, *115*, A00G03, doi:10.1029/2010JA015273.
- Fejer, B.G., Scherliess, L. (1997), Empirical models of storm time equatorial zonal electric fields, *Journal of Geophysical Research* *102* (24), 047.

- Fejer, B.G., Scherliess, L., de Paula, E.R. (1999), Effects of the vertical plasma drift velocity on the generation and evolution of equatorial spread F, *Journal of Geophysical Research* 104, 19859–19869.
- Forbes, J. M. (1981), The Equatorial electrojet, *Rev. of Geophysics and space science*, Vol. 19 (3), 469-504, doi: 10.1029/RG019i003p00469.
- Forbes, J. M., R.S. Lindzen (1976), Atmospheric solar tides and their electrodynamic effects, II the equatorial electrojet, *J. Atmos. Terr. Phys.* 38, 911–920.
- Forbes, K. F., and O. C. St. Cyr (2008), Solar activity and economic fundamentals: Evidence from 12 geographically disparate power grids, *Space Weather*, 6, S10003, doi:10.1029/2007SW000350
- Francis, S. H., (1975), Global propagation of atmospheric gravity waves: A review, *J. Atmos. Terr. Phys.*, 37, 1011.
- Friis-Christensen, E., Lühr, H. & Hulot, G. (2006), Swarm: a constellation to study the Earth's magnetic field, *Earth, Planets, Space*, 58, 351–358.
- Fuller-Rowell, T. J., et al. (2008), Impact of terrestrial weather on the upper atmosphere, *Geophys. Res. Lett.*, 35, L09808, doi:10.1029/2007GL032911.
- Gaunt, C. T. (2015), Why Space Weather Is Relevant to Electrical Power Systems, *Space Weather*, 14, 2–9, doi:10.1002/2015SW001306.
- Gentile, L. C., W. J. Burke, and F. J. Rich (2006), A global climatology for equatorial plasma bubbles in the topside ionosphere, *Ann. Geophys.*, 24, 163–172.
- Gerrard A. J. (2011b), Multi-Instrument Study to Investigate the Formation and Growth of Equatorial Irregularities, Proposal Report submitted to the Air Force Office of Scientific Research.

- Gerrard, A. J. (2011a), Application of the Fabry-Pérot Interferometer to Thermospheric/Ionospheric Measurements (Available at https://web.njit.edu/~cao/Fabry_Perot_overview_Gerrard.pdf).
- Gerrard, A. J., and J. W. Meriwether (2011), Initial daytime and nighttime SOFDI observations of thermospheric winds from Fabry-Perot Doppler shift measurements of the 630-nm OI line-shape profile, *Ann. Geophys.*, 29, 1529–1536, doi: 10.5194/angeo-29-1529-2011.
- Goncharenko, L. P., A.J. Coster, J.L. Chau, C.E. Valladares (2010), Impact of sudden stratospheric warmings on equatorial ionization anomaly, *J. Geophys. Res.* 115, 1–11, doi: 10.1029/2010JA015400
- Gonzalez, W. D., J. A. Joselyn, Y. Kamide, H. W. Kroehl, G. Rostoker, B. T. Tsurutani, and V. M. Vasyliunas (1994), What is a geomagnetic storm?, *J. Geophys. Res.*, 99, 5771–5792, doi:10.1029/93JA02867.
- Gopalswamy, N. (2008), Solar connections of geoeffective magnetic structures, *J. Atmos. Sol. Terr. Phys.*, 70, 2078-2100, 10.1016/j.jastp.2008.06.010.
- Gordon W.E. (1958), Incoherent scattering of radio waves by free electrons with applications to space exploration by radar, *Proc. I.R.E.*, 46, 1824-1829.
- Gosling, J. T., J. R. Asbridge, S. J. Bame, and W. C. Feldman (1976), Solar wind speed variations: 1962–1974, *J. Geophys. Res.*, 81(28), 5061–5070, doi:10.1029/JA081i028p05061.
- Gouin, P. and P. N. Mayaud, (1967), A propos de l'existence possible d'un "Counter Electrojet" aux latitudes magnetiques equatoriales, *Ann. Geophys.*, 23,41–47.

- Gouin,P. (1962), Reversal of the magnetic daily variation at Addis Ababa,, *Nature* London, 193, 1145-1146.
- Haaser, R. A., G. D. Earle, R. A. Heelis, J. Klenzing, R. Stoneback, W. R. Coley, and A. G. Burrell (2012), Characteristics of low-latitude ionospheric depletions and enhancements during solar minimum, *J. Geophys. Res.*, 117, A10305, doi:10.1029/2012JA017814.
- Haerendel, G., and J. V. Eccles (1992), The role of the equatorial electrojet in the evening ionosphere, *J. Geophys. Res.*, 97(A2), 1181–1192, doi:10.1029/91JA02227.
- Haerendel, G., J. V. Eccles, and S. Cakir (1992), Theory for modeling the equatorial evening ionosphere and the origin of the shear in the horizontal plasma flow, *J. Geophys. Res.*, 97, 1209.
- Hagan, M. E., A. Maute, R. G. Roble, A. D. Richmond, T. J. Immel, and S. L. England (2007), Connections between deep tropical clouds and the Earth's ionosphere, *Geophys. Res. Lett.*, 34, L20109, doi:10.1029/2007GL030142.
- Hagan, M. E., R. G. Roble, and J. Hackney (2001), Migrating thermospheric tides, *J. Geophys. Res.*, 106(A7), 12739–12752, doi:10.1029/2000JA000344.
- Hanson, W. B., and R. J. Moffett (1966), Ionization transport effects in the equatorial *F* region, *J. Geophys. Res.*, 71(23), 5559–5572, doi:10.1029/JZ071i023p05559.
- Hargreaves, J. K. (1992), *The Solar-Terrestrial Environment*, Cambridge University Press, Cambridge.
- Haykin, S. (2005), *Neural Networks: A Comprehensive Foundation*, 2nd edition, Pearson Education, Delhi, India.

- Hedin, A. E., et al. (1991), Revised global model of thermosphere winds using satellite and ground-based observations, *J. Geophys. Res.*, 96(A5), 7657–7688, doi:10.1029/91JA00251.
- Heelis, R. A. (2004), Electrodynamics in the low and middle latitude ionosphere: a tutorial, *Journal of Atmospheric and Solar-Terrestrial Physics*, Vol. 66(10), 825–838, doi:10.1016/j.jastp.2004.01.034.
- Hei, M. A. and C. E. Valladares (2010), The November 2004 superstorm: Comparison of low latitude TEC observations with LLIONS model results, *Journal of Atmospheric and Solar-Terrestrial Physics*, Vol. 72(4), 334–343, doi:10.1016/j.jastp.2009.03.025.
- Hei, M. A., R. A. Heelis, and J. P. McClure (2005), Seasonal and longitudinal variation of large-scale topside equatorial plasma depletions, *J. Geophys. Res.*, 110, A12315, doi:10.1029/2005JA011153.
- Hernandez, G. (1986), *Fabry-Perot Interferometers*, Cambridge Studies in Modern Optics, Cambridge: University Press, 1986.
- Herrero, F. A., N. W. Spencer, and H. G. Mayr (1993), Thermosphere and F-region plasma dynamics in the equatorial region, *Adv. Space Res.*, 13, 201–220.
- Huang, C.-S., G. Le, O. de La Beaujardiere, P. A. Roddy, D. E. Hunton, R. F. Pfaff, and M. R. Hairston (2014), Relationship between plasma bubbles and density enhancements: Observations and interpretation, *J. Geophys. Res. Space Physics*, 119, 1325–1336, doi:10.1002/2013JA019579.

- Huang, Y.-N., K. Cheng, and S.-W. Chen (1989), On the equatorial anomaly of the ionospheric total electron content near the northern anomaly crest region, *J. Geophys. Res.*, 94(A10), 13515–13525, doi:10.1029/JA094iA10p13515.
- Hunsucker, H. D. (1991), *Radio Techniques for Probing the Terrestrial Ionosphere*, Springer Berlin Heidelberg.
- Hysell, D. L., J. Drexler, E.B. Shume, J. L. Chau, D. E. Scipion, M. Vlasov, R. Cuevas, and C. Heinselman (2007), Combined radar observations of equatorial electrojet irregularities at Jicamarca, *Ann. Geophys.*, Vol. 25 (2), 457–473, 2007, doi:10.5194/angeo-25-457-2007.
- Immel, T. J., E. Sagawa, S. L. England, S. B. Henderson, M. E. Hagan, S. B. Mende, H. U. Frey, C. M. Swenson, and L. J. Paxton (2006), Control of equatorial ionospheric morphology by atmospheric tides, *Geophys. Res. Lett.*, 33, L15108, doi:10.1029/2006GL026161.
- James J. Spilker Jr., Penina Axelrad ; Bradford W. Parkinson ; Per Enge (1996), *Global Positioning System: Theory and Applications, Volume I*, American Institute of Aeronautics and Astronautics Washington DC
- Jee, G., R.W. Schunk, L. Scherliess (2005), On the sensitivity of total electron content (TEC) to upper atmospheric/ ionospheric parameters, *J. Atmos. Sol. Terr. Phys.*, Vol.67, 1040–1052.
- Jiao, Y., Y. T. Morton, S. Taylor, and W. Pelgrum (2013), Characterization of high-latitude ionospheric scintillation of GPS signals, *Radio Science*, Vol. 48 (6), 698-708, doi: 10.1002/2013RS005259.

- Johnson, M., G. Gorospe, J. Landry, A. Schuster (2016), Review of mitigation technologies for terrestrial power grids against space weather effects, *Int'l Journal of Electrical Power & Energy System*, 82, 382-391. doi.org/10.1016/j.ijepes.2016.02.049.
- Jonah, O. F., E.R. de Paula, M.T.A.H. Muella, S.L.G. Dutra, E.A. Kherani, P.M.S. Negreti, Y. Otsuka (2015), TEC variation during high and low solar activities over South American sector, *Journal of Atmospheric and Solar-Terrestrial Physics*, Vol. 135, 22–35, doi:10.1016/j.jastp.2015.10.005.
- Kane, R. P. (1975), Day-to-day variability of ionospheric electron content at mid-latitudes, *J. Geophys. Res.*, Vol. 80(22), 3091–3099, doi:10.1029/JA080i022p03091.
- Kao, S. P., Y. C. Chen, and F. S. Ning (2014), A MARS-based method for estimating regional 2-D ionospheric VTEC and receiver differential code bias, *Adv. Space Res.*, 53 (2), 190–200, doi: 10.1016/j.asr.2013.11.001.
- Kappernman, J., and V. D. Albertson (1990), Bracing for the geomagnetic storms, *IEEE Spectr.*, 27 (3), 27–33, doi:10.1109/6.48847.
- Kelley, M . C. (1989), *The Earth's Ionosphere Plasma Physics and Electrodynamics*, Geophys Set., vol. 43, Academic, San Diego, Calif.,
- Kelley, M. C. (2009a), *The Earth's Ionosphere: Plasma Physics and Electrodynamics*, 2nd edition, Academic Press, San Diego, Calif.
- Kelley, M. C., (2009b) *Ionospheric Measurement Techniques: A Tutorial*, Lecture presented in CEDAR Workshop, Santa Fe.

- Khadka, S. M., C. Valladares, R. Pradipta, E. Pacheco, and P. Condor (2016), On the mutual relationship of the equatorial electrojet, TEC and scintillation in the Peruvian Sector. *Radio Sci.*, Vol. 51(6), 742-751, doi: 10.1002/2016RS005966.
- Khadka, S. M., Valladares, C. E., Sheehan, R., and Gerrard, A. J. (2018). Effects of electric field and neutral wind on the asymmetry of equatorial ionization anomaly. *Radio Science*, 53. <https://doi.org/10.1029/2017RS006428>.
- Kil H, Heelis RA (1998), Global distribution of density irregularities in the equatorial ionosphere. *J Geophys Res* 103(A1):407–417. doi:<https://doi.org/10.1029/97JA02698>.
- Kil, H., H.-S. Choi, R. A. Heelis, L. J. Paxton, W. R. Coley, and E. S. Miller (2011), Onset conditions of bubbles and blobs: A case study on 2 March 2009, *Geophys. Res. Lett.*, 38, L06101, doi:10.1029/2011GL046885.
- Kil, H., Y.-S. Kwak, W. K. Lee, E. S. Miller, S.-J. Oh, and H.-S. Choi (2015), The causal relationship between plasma bubbles and blobs in the low-latitude F region during a solar minimum. *J. Geophys. Res. Space Physics*, 120, 3961–3969. doi: 10.1002/2014JA020847.
- Kim VP, Hegai VV, (2016), On the variability of the ionospheric F2-layer during the quietest days in December 2009, *J. Astron. Space Sci.* 33, 273-278. <https://doi.org/10.5140/JASS.2016.33.4.273>
- Kintner, P. M., B. M. Ledvina, and E. R. de Paula (2007), GPS and Ionospheric scintillations, *Space Weather*, Vol. 5, S09003, doi:10.1029/2006SW000260.
- Klenzing, J. H., D. E. Rowland, R. F. Pfaff, G. Le, H. Freudenreich, R. A. Haaser, A. G. Burrell, R. A. Stoneback, W. R. Coley, and R. A. Heelis (2011), Observations of

- low-latitude plasma density enhancements and their associated plasma drifts, *J. Geophys. Res.*, 116, A09324.
- Klobuchar, John A. (1991), Ionospheric effects on GPS, GPS World magazine, Volume 2, Nx.4.
- Knight, M. F. (2000), Ionospheric Scintillation effects on Global Positioning System Receivers, PhD Thesis, The University of Adelaide.
- Knipp, D. J. (2015), Synthesis of Geomagnetically Induced Currents: Commentary and Research, *Space Weather*, 13, 727–729, doi:10.1002/2015SW001317.
- Knipp, D.J. (2011), Understanding Space Weather and the Physics Behind It, McGraw-Hill, New York, pp. 1–727.
- Krall, J., J. D. Huba, G. Joyce, and T. Yokoyama (2010), Density enhancements associated with equatorial spread F, *Ann. Geophys.*, 28, 327, doi:10.5194/angeo-28-327-2010.
- Kudeki, E., A. Akgiray, M. Milla, J. L. Chau, D. L. Hysell (2008), Equatorial spread F initiation: Post-sunset vortex, thermospheric winds, gravity waves, *J. Atmos. Sol.-Terr. Phys.*, 69, 2416–2427.
- Kudeki, E., and S. Bhattacharyya (1999), Postsunset vortex in equatorial F region plasma drifts and implications for bottomside spread F, *J. Geophys. Res.*, 104, 28,163-28,170.
- Langley, Richard B. (2000), GPS, the ionosphere, and the solar maximum, GPS World magazine, Volume11, N.x7.

- Laundal, K. M., I. Cnossen, S. E. Milan, S. E. Haaland, J. Coxon, N. M. Pedatella, M. Förster, and J. P. Reistad (2016), North–south asymmetries in Earth's magnetic field, *Space Sci. Rev.*, 1–33, doi:10.1007/s11214-016-0273-0.
- Le, G., C.-S. Huang, R. F. Pfaff, S.-Y. Su, H.-C. Yeh, R. A. Heelis, F. J. Rich, and M. Hairston (2003), Plasma density enhancements associated with equatorial spread F: ROCSAT-1 and DMSP observations, *J. Geophys. Res.*, 108(A8), 1318, doi:10.1029/2002JA009592.
- Li, G., B. Ning, L. Liu, B. Zhao X. Yei, J. S.-Y. Su, and S. Venkatraman (2008), Correlative study of plasma bubbles, evening equatorial ionization anomaly, and equatorial prereversal ExB drifts at solar minimum, *Radio Science*, Vol. 43, RS4005, doi:10.1029/2007RS003760.
- Lin, C. H., A. D. Richmond, G. J. Bailey, J. Y. Liu, G. Lu, and R. A. Heelis (2009), Neutral wind effect in producing a storm time ionospheric additional layer in the equatorial ionization anomaly region, *J. Geophys. Res.*, 114, A09306, doi:10.1029/2009JA014050.
- Lotko, W. (2017), Magnetosphere-Ionosphere Coupling, Lecture presented in CISM summer school, Boulder.
- Love, J. J., (2008), Magnetic monitoring of Earth and space, *Physics Today*, 61, 31-37.
- Luan, X., P. Wang, X. Dou, and Y. C.-M. Liu (2015), Interhemispheric asymmetry of the equatorial ionization anomaly in solstices observed by COSMIC during 2007 – 2012, *J. Geophys. Res. Space Physics*, 120, 3059 – 3073, doi: 10.1002/2014JA020820.

- MacAlester, M. H., and W. Murtagh (2014), Extreme Space Weather Impact: An Emergency Management Perspective, *Space Weather*, 12, 530–537, doi:10.1002/2014SW001095.
- MacDougall, J. W. (1969), The equatorial ionospheric anomaly and equatorial electrojet, *Radio Science*, Vol. 4 (9), doi: 10.1029/RS004i009p00805.
- Makela, J. J., D. J. Fisher, J. W. Meriwether, R. A. Buriti, and A. F. Medeiros (2013), Near-continual ground-based nighttime observations of thermospheric neutral winds and temperatures over equatorial Brazil from 2009 to 2012, *J. Atmos. Sol. Terr. Phys.*, 103, 94–102, doi:10.1016/j.jastp.2012.11.019.
- Makela, J. J., J. W. Meriwether, A. J. Ridley, M. Ciocca, and M. W. Castellez (2012), Large-scale measurements of thermospheric dynamics with a multisite Fabry-Perot interferometer network: Overview of plans and results from midlatitude measurements, *Int. J. Geophys.*, 2012, 1–10, doi:10.1155/2012/872140
- Manheimer, Wallace, Linda E. Sugiyama, Thomas H. Stix, (1996), Plasma Science and the Environment, Springer Science & Business Media, 328 pages
- Marriot RT, Richmond AD, Venkateswaram SV (1979) The quiet time equatorial electrojet and counter electrojet, *J Geomag Geoelectr* 31:311–340.
- Martinis, C., J. Baumgardner, M. Mendillo, S.-Y. Su, and N. Aponte (2009), Brightening of 630.0 nm equatorial spread-*F* airglow depletions, *J. Geophys. Res.*, 114, A06318, doi:10.1029/2008JA013931.
- Martyn, D. F. (1947), Atmospheric tides in the ionosphere.1. Solar tides in the F2 region, *Proceedings of the Royal Society of London A*, Vol. 189 (1017), 241-260, doi: 10.1098/rspa.1947.0037

- Maute, A., & Richmond, A. D. (2017). F-region dynamo simulations at low and mid-latitude. *Space Science Reviews*, 206, 471–493. <https://doi.org/10.1007/s11214-016-0262-3>
- McDaniel, R. (1998), A review of Equatorial Spread-F, (<https://www.hsu.edu/academicforum/1998-1999/1998-9AFA%20Review%20of%20Equatorial%20Spread%20F.pdf>)
- Mendillo, M., J. Baumgardner, X. Pi, P. J. Sultan, and R. Tsunoda (1992), Onset conditions for equatorial spread *F*, *J. Geophys. Res.*, 97(A9), 13865–13876, *doi:10.1029/92JA00647*.
- Meriwether, J. W. (2004), The design and construction of the Second-Generation Optimized Fabry-Perot Doppler Imager, Proposal Report submitted to the Air Force Office of Scientific Research.
- Meriwether, J. W. (2006), Studies of thermospheric dynamics with a Fabry-Perot interferometer network: a review, *Journal of Atmospheric and Solar-Terrestrial Physics*, vol. 68, no. 13, pp. 1576–1589, *doi: 10.1016/j.jastp.2005.11.014*.
- Miles, D. (2017), Advances in Fluxgate Magnetometry for Space Physics, PhD Thesis, University of Alberta, Canada
- Miles, D. M. (2013), Towards a Radiation Hardened Fluxgate Magnetometer for Space Physics Applications, Master's Thesis, University of Alberta, Edmonton, Alberta, Canada.
- Miller, E. S., H. Kil, J. J. Makela, R. A. Heelis, E. R. Talaat, and A. Gross (2014), Topside signature of medium-scale traveling ionospheric disturbances, *Ann. Geophys.*, 32, 959–965, *doi:10.5194/angeo-32-959-2014*.

- Muralikrishna, P., V.H. Kulkarni (2008), Modeling the meteoric dust effect on the equatorial electrojet. *Adv. Space Res.* 42, 164–170, doi:10.1016/asr.2007.11.019.
- National Academies of Sciences, Engineering, and Medicine (2015), A Strategy for Active Remote Sensing Amid Increased Demand for Radio Spectrum. Washington, DC: The National Academies Press.
- Ngwira, C. M., and Pulkkinen, A. A. (2018), An overview of Science challenges pertaining to our understanding of extreme geomagnetically induced currents, Chapter 8, Extreme Events in Geospace Origins, Predictability, and Consequences, *edited by Natalia Buzulukova*, Elsevier, Amsterdam.
- Ogawa, T., K. Igarashi, K. Aikyo, and H. Maeno (1987), NNSS Satellite observations of medium-scale traveling ionospheric disturbances at southern high-latitudes, *J. Geomagn. Geoelectr.*, 39, 709–721.
- Olivarez, N. (2013), Mitigating the Effects of Ionospheric Scintillation on GPS Carrier Recovery, MS Thesis, Worcester Polytechnic Institute, USA.
- Onwumechili, C. A. (1997): The Equatorial Electrojet, Gordon and Breach Science Publishers, Netherlands.
- Onwumechili, C. A. (1997): The Equatorial Electrojet, Gordon and Breach Science Publishers, Netherlands.
- Onwumechili, C. A. and C. E. Agu (1981), Longitudinal variation of equatorial electrojet parameters derived from POGO satellite observation, *Planetary and Space Science*, Vol. 29 (6), 627-634, doi: 10.1016/0032-0633(81)90111-2.

- Onwumechili, C. A. and C. E. Agu (1981), Longitudinal variation of equatorial electrojet parameters derived from POGO satellite observation, *Planet. Space Sci.*, Vol. 29 (6), 627-634, doi: 10.1016/0032-0633(81)90111-2.
- Onwumechilli, A., and S.-I. Akasofu (1972), On the abnormal depression of Sq(H) under the equatorial electrojet in the afternoon, *J. Geomagn. Geoelectr.*, 24, 161–173.
- Ossakow, S. L. (1981), Spread F theories – a review, *J. Atmos. Terr. Phys.*, 43, 437.
- Ott, E. (1978), Theory of Rayleigh-Taylor bubbles in the equatorial ionosphere, *J. Geophys. Res.*, 83, 2066–2070.
- Oya, H., T. Takahashi, and S. Watanabe (1986), Observation of low latitude ionosphere by the impedance probe on board the Hinotori satellite, *J. Geomagn. Geoelectr.*, 38, 111–123.
- Pandey, K., Sekar, R., Anandarao, B. G., Gupta, S. P., & Chakrabarty, D. (2018). On the occurrence of afternoon counter electrojet over Indian longitudes during June solstice in solar minimum, *Journal of Geophysical Research: Space Physics*, 123. <https://doi.org/10.1002/2017JA024725>
- Parkinson W. D., (1983), Introduction to Geomagnetism, Scottish Academic Press, Edinburgh, 1983
- Patil, A. R., D. R. K. Rao, and R. G. Rastogi (1990), Equatorial electrojet strengths in the Indian and American sectors Part II. During high solar activity, *J. Geomagn. Geoelec.*, Vol. 42 (7), 813–823, doi.org/10.5636/jgg.42.813
- Pfaff, R. F. (2012), The near-Earth plasma environment, *Space Sci. Rev.* 168(1), 23–112. *Phys.*, 9, 304-310.

- Pimenta, A. A., Y. Sahai, J. A. Bittencourt, M. A. Abdu, H. Takahashi, and M. J. Taylor (2004), Plasma blobs observed by ground-based optical and radio techniques in the Brazilian tropical sector, *Geophys. Res. Lett.*, 31, L12810, doi:10.1029/2004GL020233.
- Priyadarshi, S. (2015a), A review of ionospheric scintillation models, *Surv. Geophys.*, 36, 295–324, doi:10.1007/s10712-015-9319-1.
- Pulkkinen, A. (2003), Geomagnetic induction during highly disturbed Space Weather conditions: Study of ground effects, Ph.D. thesis, Univ. of Helsinki, Helsinki.
- Pulkkinen, A., et al. (2017), Geomagnetically induced currents: Science, engineering, and applications readiness, *Space Weather*, 15, 828–856, doi:10.1002/2016SW001501.
- Rabiu, A. B., Folarin, O. O., Uozumi, T., Abdul Hamid, N. S., and Yoshikawa, A., (2017), Longitudinal variation of equatorial electrojet and the occurrence of its counter electrojet, *Ann. Geophys.*, 35, 535 - 545, doi:10.5194/angeo – 35 – 535 - 2017.
- Raghavarao R., and Anandarao B. G. (1980), Vertical winds as a plausible cause for equatorial counter electrojet. *Geophys Res Lett* 7:357–360.
- Rama Rao, P. V. S. (2006), Characteristics of the Indian equatorial ionosphere, Lecture notes in Workshop at ICTP, Italy.
- Rangarajan G. K. and Rastogi R. G. (1981), Solar flare effect in equatorial magnetic field during morning counter electrojet. *Ind. J Radio Space Phys* 10:190–192.
- Rastogi R. G. (1974), Westward Equatorial Electrojet during daytime hours. *J Geophys Res* 79:1503–1512.

- Rastogi R. G., Deshpande M. R., Sastri N. S. (1975), Solar flare effect in equatorial counter Electrojet current. *Nature* 258:218–219. doi: 10.1038/258218a0
- Rastogi, R. G. (1962), Longitudinal variation in the equatorial electrojet, *Journal of Atmospheric and Terrestrial Physics*, Vol. 24 (12), 1031-1040, doi: 10.1016/0021-9169(62)90158-7.
- Rastogi, R. G. (1983), Equatorial electrojet and radio scintillations, *Journal of Atmospheric and Terrestrial Physics*, Vol. 45(10), 719-728, doi: 10.1016/S0021-9169(83)80030-0.
- Rastogi, R. G. and J. A. Klobuchar (1990): Ionospheric electron content within the equatorial F2 layer anomaly belt, *J. of Geophys. Res.*, Vol. 95(A11), 19045–19052, doi: 10.1029/JA095iA11p19045.
- Rastogi, R. G. (1962), Longitudinal variation in the equatorial electrojet, *Journal of Atmospheric and Terrestrial Physics*, Vol. 24(12), 1031-1040, doi: 10.1016/0021-9169(62)90158-7.
- Rastogi, R. G., and J. A. Klobuchar (1990), Ionospheric Electron Content Within the Equatorial F2 Layer Anomaly Belt, *J. Geophys. Res.*, 95, 19,045 –19,052.
- Rayleigh, Lord (1883), Investigation of the character of the equilibrium of an incompressible heavy fluid of variable density, *Proceedings of the London Mathematical Society*, 14: 170–177. doi:10.1112/plms/s1-14.1.170
- Retterer, J. M. (2010), Forecasting low-latitude radio scintillation with 3-D ionospheric plume models: 1. Plume model, *J. Geophys. Res.*, 115, A03306, doi:10.1029/2008JA013839

- Richmond A. D. (1973), Equatorial electrojet. I. Development of model including winds and instabilities, *J. Atmos Solar Terr Phys* 35:1083–1103
- Richmond, A. D. (1989), Modeling the Ionospheric Wind Dynamo: A Review, *Pure and Applied Geophysics PAGEOPH*, Vol.131 (3), 413-435, doi: 10.1007/BF00876837.
- Ripka, P. (2003), Advances in fluxgate sensors, *Sens. Actuators Phys.*, 106(1), 8–14.
- Ripka, P. (2001), Magnetic Sensors and Magnetometers, *Artech House Inc.*, Norwood, MA, USA.
- Rishbeth, H, (1997), The ionospheric E-layer and F-layer dynamos—a tutorial review *Journal of Atmospheric and Space Physics*, Vol. 59 (15), 1873-1880, doi: 10.1016/S1364-6826(97)00005-9.
- Rishbeth, H. (1972), Thermospheric winds and the F-region: A review, *J. Atmos. Terr. Phys.*, 34, 1–47, doi: 10.1016/0021-9169(72)90003-7.
- Rishbeth, H. (1998), How the thermospheric circulation affects the ionospheric F₂-layer. *Journal of Atmospheric and Solar: Terrestrial Physics*, 60, 1385–1402.
- Rishbeth, H. (2006), F region links with the lower atmosphere, *J. Atmos. Sol. Terr. Phys.*, 68, 469–478, doi:10.1016/j.jastp.2005.03.017.
- Robinson, R. M, and R. A. Behnke (2001), The U.S. National Space Weather Program: A Retrospective, *Space Weather*, AGU Geophysical Monograph, 125, 1.
- Sagawa, E., T. J. Immel, H. U. Frey, and S. B. Mende (2005), Longitudinal structure of the equatorial anomaly in the nighttime ionosphere observed by IMAGE/FUV, *J. Geophys. Res.*, 110, A11302, doi:10.1029/2004JA010848.

- Sastri, J. H. (1990), Equatorial anomaly in F region: A review, *Indian J. Radio Space Phys.*, 19, 225–240.
- Sastri, J. H., Kamide, Y., & Yumoto, K. (2003). Signatures for magnetospheric substorms in the geomagnetic field of dayside equatorial region: Origin of the ionospheric component, *Journal of Geophysical Research*, 108(A10), 1375. <https://doi-org.proxy.bc.edu/10.1029/2003JA009962>
- Scherliess, L., and B. G. Fejer (1999), Radar and satellite global equatorial F region vertical drift model, *J. Geophys. Res.*, Vol. 104 (A4), 6829-6842, doi: 10.1029/1999JA900025.
- Scherliess, L., and B. G. Fejer (1999), Radar and satellite global equatorial F region vertical drift model, *J. Geophys. Res.*, Vol. 104 (A4), 6829-6842, doi: 10.1029/1999JA900025.
- Scherliess, L., D. C. Thompson, and R. W. Schunk (2008), Longitudinal variability of low-latitude total electron content: Tidal influences, *J. Geophys. Res.*, Vol. 113(A1), A01311, doi:10.1029/2007JA012480.
- Schunk R. W. & Nagy A. F. (2000), *Ionosphere: Physics, plasma and chemistry*, Cambridge University Press, New York.
- Schunk, R. W., J. J. Sojka, and J. V. Eccles (1997), Expanded capabilities for the ionospheric forecast model, Rep. AFRL-VS-HA-TR-98-0001, Space Vehicles Dir., Air Force Res. Lab., Hanscom AFB, Mass.
- Schuster, A. (1908), The diurnal variation of terrestrial magnetism, *Philos. Trans. R. Soc. Lond. Ser. A* 208, 163–204

- Seemala, G. K., and C. E. Valladares (2011), Statistics of total electron content depletions observed over the South American continent for the year 2008, *Radio Sci.*, Vol.46(5), RS5019, doi:10.1029/2011RS004722.
- Seemala, G. K., and C. E. Valladares (2011), Statistics of total electron content depletions observed over the South American continent for the year 2008, *Radio Sci.*, 46, RS5019, doi:10.1029/2011RS004722.
- Senior C, Blanc M (1984) On the control of magnetospheric convection by the spatial distribution of ionospheric conductivities, *J. Geophys Res* 89(A1):261–284. <https://doi-org.proxy.bc.edu/10.1029/JA089iA01p00261>.
- Shiokawa, K., T. Kadota, M. K. Ejiri, Y. Otsuka, Y. Katoh, M. Satoh, and T. Ogawa, Three-channel imaging Fabry-Perot interferometer for midlatitude airglow measurement, *Appl. Opt.*, 40, 4286–4296, 2001.
- Shume, E. B., F. S. Rodrigues, A. J. Mannucci, and E. R. de Paula (2014), Modulation of equatorial electrojet irregularities by atmospheric gravity waves, *J. Geophys. Res. Space Physics*, 119, 366–374, doi:10.1002/2013JA019300.
- Singh, S., Johnson, F. S., Power, R. A. (1997), Gravity wave seeding of equatorial plasma bubbles, *Journal of Geophysical Research*, 102, 7399.
- Sojka, J., W. Raitt, and R. Schunk (1979), Effect of displaced geomagnetic and geographic poles on high-latitude plasma convection and ionospheric depletions, *J. Geophys. Res.*, 84 (A10), 5943–5951, doi:10.1029/JA084iA10p05943..
- Solomon, S. C., (2017), Ionospheric structures, Lecture presented in CISM summer school, Boulder.

- Spiro, R. W., Wolf, R. A., & Fejer, B. G. (1988), Penetrating of high-latitude-electric-field effects to low latitudes during SUNDIAL 1984, *Annales Geophysicae*, 6, 39–49.
- Sreeja, V., S. Ravindran, T. K. Pant, C. V. Devasia, and L. J. Paxton (2009), Equatorial and low-latitude ionosphere-thermosphere system response to the space weather event of August 2005, *J. Geophys. Res.*, 114, A12307, doi:10.1029/2009JA014491.
- Sridharan, R. (1998), Equatorial and low latitude thermosphere-ionosphere interaction, *PINSA*, 64, A No 3, pp. 315-340.
- Sridharan, R., N. K. Modi, D. Pallam Raju, R. Narayanan, T. K. Pant, A. Taori, and D. Chakrabarty (1998), A multi-wavelength daytime photometer—A new tool for the investigation of atmospheric processes, *Meas. Sci. Tech.*, 9, 585–591.
- Sridharan, R., R. Sekar, S. Gurubaran (1993), Two-dimensional high-resolution imaging of the equatorial plasma fountain, *J. Atmos. Terr. Phys.*, 55, 1661.
- Sridharan, S., S. Sathis hkumar, and S. Gurubaran (2009), Variabilities of mesospheric tides and equatorial electrojet strength during major stratospheric warming events, *Ann. Geophys.*, 27, 4125–4130.
- Stening, R. J. (1977), Electron density profile changes associated with the equatorial electrojet, *J. Atmos. Terr. Phys.*, 39, 157–164, do i:10.1016/ 0021-9169(77)90109-X.
- Steward, Balfour, (1882), Terrestrial magnetism, *Encyclopedia Britannica*, 9th ed., 16, 181.

- Stolle, C., C. Manoj, H. Lühr, S. Maus, and P. Alken (2008a), Estimating the daytime Equatorial Ionization Anomaly strength from electric field proxies, *J. Geophys. Res.*, 113, A09310, doi: 10.1029/2007JA012781.
- Stolle, C., H. Lühr, and B. G. Fejer (2008b), Relation between the occurrence rate of ESF and the vertical plasma drift velocity at sunset derived from global observations, *Annales Geophys.*, 26, 3979-3988, 2008.
- Stolle, C., R. Floberghagen, H. Lühr, S. Maus, D. Knudsen, P. Alken, E. Doornbos, B. Hamilton, A. Thomson, and P. Visser (2013), Space weather opportunities from the Swarm mission including near real time applications, *Earth Planets Space*, 65(111), 1375–1383, doi:10.5047/eps.2013.10.002.
- Stoneback, R. A. and Heelis, R. A. (2014), Identifying equatorial ionospheric irregularities using in situ ion drifts, *Ann. Geophys.*, 32, 421-429, doi: 10.5194/angeo-32-421-2014.
- Stoneback, R. A., R. A. Heelis, A. G. Burrell, W. R. Coley, B. G. Fejer, and E. Pacheco (2011), Observations of quiet time vertical ion drift in the equatorial ionosphere during the solar minimum period of 2009, *J. of Geophys. Res.*, Vol. 116, A12327, doi: 10.1029/2011JA016712.
- Stoneback, R. A., R. A. Heelis, A. G. Burrell, W. R. Coley, B. G. Fejer, and E. Pacheco (2011), Observations of quiet time vertical ion drift in the equatorial ionosphere during the solar minimum period of 2009, *J. of Geophys. Res.*, Vol. 116, A12327, doi: 10.1029/2011JA016712.

- Su, Y. Z., G. J. Bailey, K. I., Oyama, and N. Balan (1997), A modelling study of the longitudinal variations in the north-south asymmetries of the ionospheric equatorial anomaly, *J. Atmos. Terr. Phys.*, 59(11), 1299-1310.
- Subramanian, P. (2009), Forbush decreases and Space weather, Lectures, *Indian Institute of Astrophysics*, p.1-10.
- Sultan, P. J. (1996), Linear theory and modeling of the Rayleigh-Taylor instability leading to the occurrence of equatorial spread F, *J. Geophys. Res.*, 101, 26,875–26,891.
- Taylor, Sir Geoffrey Ingram (1950). The instability of liquid surfaces when accelerated in a direction perpendicular to their planes, *Proceedings of the Royal Society of London. Series A, Mathematical and Physical Sciences*. 201 (1065): 192–196, doi:10.1098/rspa.1950.0052
- Titheridge, J.E. (1995), Winds in the ionosphere-review, *J. Atmos. Terr. Phys.* Vol. 57(14), 1681-1714, doi:10.1016/0021-9169(95)00091-F.
- Tsunoda, R. T., White B. R. (1981), On the generation and growth of equatorial backscatter plumes 1. Wave structure in the bottomside F layer. *J. Geophys Res* 86(A5):3610–3616. doi:https://doi.org/10.1029/JA086iA05p03610
- Tulasi Ram, S., S. Y. Su, and C. H. Liu (2009), FORMOSAT-3/COSMIC observations of seasonal and longitudinal variations of equatorial ionization anomaly and its interhemispheric asymmetry during the solar minimum period, *J. Geophys. Res.*, Vol. 114, A06311, doi: 10.1029/2008JA013880

- Uemoto, J., T. Maruyama, S. Saito, M. Ishii, and R. Yoshimura (2010), Relationships between PRE-sunset electrojet strength, pre-reversal enhancement and equatorial spread-F onset, *Ann. Geophys.*, 28, 449–454, doi:10.5194/angeo-28-449-2010.
- US Department of Homeland Security (2011), The Strategic National Risk Assessment in Support of Presidential Policy Directive 8: A Comprehensive Risk-Based Approach Toward a Secure and Resilient Nation, *Department of Homeland Security*, Washington, D. C.
- US Federal Energy Regulatory Commission (2016), Reliability standard for Transmission System Planned performance for geomagnetic disturbance Events, *order No. 830*, 22 September, Washington, D. C.
- Valladares, C. E., and J. L. Chau (2012), The low-Latitude Ionospheric Sensor Network: Initial results, *Radio Science*, Vol. 47, RS0L17, doi: 10.1029/2011RS004978.
- Valladares, C. E., and J. L. Chau (2012), The low-Latitude Ionospheric Sensor Network: Initial results, *Radio Science*, Vol. 47, RS0L17, doi: 10.1029/2011RS004978.
- Valladares, C. E., J. Villalobos, R. Sheehan, and M. P. Hagan (2004), Latitudinal extension of low-latitude scintillations measured with a network of GPS, *Annales Geophysicae*, Vol. 22, 3355-3175, doi: 10.5194/angeo-22-3155-2004.
- Valladares, C. E., R. Sheehan, S. Basu, H. Kuenzler, and J. Espinoza, (1996), The multi-instrumented studies of equatorial thermosphere aeronomy scintillation system: Climatology of zonal drifts, *J. Geophys. Res.*, 101, 26,839.
- Valladares, C. E., S. Basu, K. Groves, M. P. Hagan, D. Hysell, A. J. Mazella, and R. E. Sheehan (2001), Measurement of the latitudinal distributions of total electron

content during equatorial spread F events, *J. Geophys. Res.*, 106, 29,133–29,152, doi:10.1029/2000JA000426.

Veenadhari, B., R. Selvakumaran, R. Singh, A. K. Maurya, N. Gopalswamy, S. Kumar, and T. Kikuchi (2012), Coronal mass ejection–driven shocks and the associated sudden commencements/sudden impulses, *J. Geophys. Res.*, 117, A04210, doi:10.1029/2011JA017216.

Venkatesh, K. (2013), Studies on equatorial and low-latitude ionospheric phenomena and their effect on satellite based communication and navigation systems, PhD thesis, Andhra University, India.

Venkatesh, K., P. R. Fagundes, D. S. V. V. D. Prasad, C. M. Denardini, A. J. de Abreu, R. de Jesus, and M. Gende (2015), Day-to-day variability of equatorial electrojet and its role on the day-to-day characteristics of the equatorial ionization anomaly over the Indian and Brazilian sectors, *J. Geophys. Res. Space Physics*, Vol. 120 (10), 9117–9131, doi: 10.1002/2015JA021307.

Venkatraman, S., and R. Heelis (2000), Interhemispheric plasma flows in the equatorial topside ionosphere, *J. Geophys. Res.*, 105, 18,457–18,464, doi: 10.1029/2000JA000012.

Vestine, E.H. (1954), Winds in the upper atmosphere deduced from the dynamo theory of geomagnetic disturbance, *J. Geophys. Res.* 59(1), 93–128.

Vineeth C, Pant T. K., Devasia C. V., Sridharan R (2007), Highly localized cooling in daytime mesopause temperature over the dip equator during counter electrojet events: first results, *Geophys Res Lett*, 34:L14101. doi: 10.1029/2007GL030298.

- Vineeth C., Pant T. K., Sridharan R (2009), Equatorial counter electrojets and polar stratospheric sudden warmings – a classical example of high latitude–low latitude coupling? *Ann Geophys* 27:3147–3153.
- Vineeth, C., N. Mridula, P. Muralikrishna, K. K. Kumar, T.K. Pant (2016), First observational evidence for the connection between the meteoric activity and occurrence of equatorial counter electrojet, *J. Atmos. Sol.-Terr. Phys.* 147, 71–75.
- Walker, G. O., J. H. K. Ma, E. Golton, The equatorial ionospheric anomaly in electron content from solar minimum to solar maximum for south East Asia, *Ann. Geophys.*, 12, 195, 1994.
- Watanabe, S., and H. Oya (1986), Occurrence characteristics of low latitude ionosphere irregularities observed by the impedance probe on board the Hinotori satellite, *J. Geomagn. Geoelectr.* 38, 125–149.
- Wautelet, G. (2013), Characterization of ionospheric irregularities and their influence on high-accuracy positioning with GPS over mid-latitudes, PhD Thesis, University de Liege, Belgium
- Wernik, A. W., L. Alfonsi, and M. Materassi (2004), Ionospheric irregularities, scintillation and its effect on systems, *Acta Geophysica Polonica*, Vol. 52 (2), 237-249.
- Woodmen, R. F. (1970), Vertical plasma drift velocities and east-west electric fields at the magnetic equator, *J. Geophys. Res.*, Vol. 75 (31), 6249–6259, doi: 10.1029/JA075i031p06249.

- Woodman, R. F., and C. La Hoz (1976), Radar observations of *F* region equatorial irregularities, *J. Geophys. Res.*, 81(31), 5447–5466, doi:10.1029/JA081i031p05447.
- Wu, Q. (2015), Longitudinal and seasonal variation of the equatorial flux tube integrated Rayleigh-Taylor instability growth rate, *J. Geophys. Res. Space Physics*, 120, 7952–7957, doi:10.1002/2015JA021553.
- Xiong, C., H. Lühr, and S. Y. Ma (2013), The magnitude and inter-hemispheric asymmetry of equatorial ionization anomaly-based on CHAMP and GRACE observations, *J. Atmos. Terr. Phys.*, 105, 160–169, doi:10.1016/j.jastp.2013.09.010.
- Yamazaki, Y. & Maute, A. (2017), Sq and EEJ—A Review on the Daily Variation of the Geomagnetic Field Caused by Ionospheric Dynamo Currents, *Space Sci Rev*, 206: 299. <https://doi-org.proxy.bc.edu/10.1007/s11214-016-0282-z>.
- Yamazaki, Y., Stolle, C., Matzka, J., Siddiqui, T. A., Lühr, H., & Alken, P. (2017). Longitudinal variation of the lunar tide in the equatorial electrojet, *Journal of Geophysical Research: Space Physics*, 122, 12,445–12,463. <https://doi-org.proxy.bc.edu/10.1002/2017JA024601>
- Yeh, K. C., and C. H. Liu (1974), Acoustic-gravity waves in the upper atmosphere, *Rev. Geophys.*, 12(2), 193–216, doi:10.1029/RG012i002p00193.
- Yizengaw, E., M. B. Moldwin, E. Zesta, C. M. Biouele, B. Dantie, A. Mebrahtu, B. Rabiou, C. E. Valladares, and R. Stonrback (2014), The longitudinal variability of equatorial electrojet and vertical drift velocity in the African and American sectors, *Annales Geophysicae*, Vol. 32, 231-238, doi:10.5194/angeo-32-231-2014.

Yokoyama, T., S.-Y. Su, and S. Fukao (2007), Plasma blobs and irregularities concurrently observed by ROCSAT-1 and Equatorial Atmosphere Radar, *J. Geophys. Res.*, 112, A05311, doi:10.1029/2006JA012044.

Zalesak, S. T. and Ossakow, S. L. (1982), On the prospect for artificially inducing equatorial spread F, *Memo. Rep. 4899, Nav. Res. Lab.*, Washington, D.C.

Appendix I

Abbreviations

AED: Afternoon EEJ Depression

AGW: Atmospheric Gravity Wave

C/NOFS: Communications/Navigation Outage Forecasting System

CEDAR: Coupling, Energetics and Dynamics of Atmospheric Regions

CEJ: Counter Electrojet

CIRs: Corotating Interaction Regions

CISM: Center for Integrated Space Weather Modeling

CMEs: Coronal Mass Ejections

DoD: Department of Defense

EEF: Eastward Electric Field

EEJ: Equatorial Electrojet

EFI: Electric Field Instrument

EIA: Equatorial Ionization Anomaly

EPB: Equatorial Plasma Bubble

EPIs: Equatorial Plasma Irregularities

ESA: European Space Agency

ESF: Equatorial Spread-F

EUV: Extreme Ultraviolet

FPI: Fabry Perot Interferometer

FUV: Far Ultraviolet

GIC: Geomagnetically Induced Currents

GNSS: Global Navigation Satellite System

GPS: Global Positioning System

HF: High Frequency

IP: Interplanetary

JRO: Jicamarca Radio Observatory

LISN: Low-Latitude Ionospheric Sensor Network

LLIONS: Low-Latitude IONospheric Sector

LP: Langmuir Probe

LSTID: Large-Scale Traveling Ionospheric Disturbance

LT: Local Time

MED: Morning EEJ Depression

MHz: Mega Hertz

MSTID: Medium-Scale Traveling Ionospheric Disturbance

NASA: National Aeronautics and Space Administration

NJIT: New Jersey Institute of Technology

NNSS: Navy Navigation Satellite System

PRE: Pre-Reversal Enhancement

PRN: Pseudo Random Noise

PW: Planetary Wave

RTI: Rayleigh-Taylor instability

SCs: Sudden Commencements

SEPs: Solar Energetic Particles

SIs: Sudden Impulses

SLC: School Leaving Certificate

SOFDI: Second-Generation, Optimized, Fabry-Perot Doppler Imager

SQ: Solar Quiet

SSW: Sudden Stratospheric Warming

TEC: Total Electron Content

TID: Traveling Ionospheric Disturbance

TU: Tribhuvan University

UT: Universal Time

Appendix II

Publications and Manuscripts

Space Plasma/Weather Physics | Advisor: Dr. Cesar E. Valladares

1. **Khadka, Sovit M.**, Cesar E. Valladares, Rezy Pradipta, Edgardo Pacheco, and Percy Condor (2016), *On the mutual relationship of the equatorial electrojet, TEC and scintillation in the Peruvian sector*, **Radio Science**, Vol. 51 (6), 742-751, doi:10.1002/2016RS005966.
2. **Khadka, Sovit M.**, Valladares, C. E., Sheehan, R. & Gerrard, A. J. (2018), *Effects of electric field and neutral wind on the asymmetry of equatorial ionization anomaly*, **Radio Science**, Vol. 53, <https://doi.org/10.1029/2017RS006428>.
3. Valladares, Cesar E., **Sovit M. Khadka**, P. Coisson, and S. Buchert (2018), *Observations of the Motion of Plasma Depletions using SWARM Constellation and LISN TEC Measurements* (Under Preparation).
4. **Khadka, Sovit M.**, Cesar E. Valladares, and Patricia H. Doherty (2018), *Day-to-day variability of the counter electrojet and F-layer dynamics during geomagnetically quiet days* (Under Preparation).
5. **Khadka, Sovit M.**, Cesar E. Valladares, and Endawoke Yizengaw (2018), *Narrow longitudinal and seasonal variability of equatorial electrojet and their consequences in American low latitudes* (Under Preparation).

Material/ Condensed Matter Physics | Advisor: Prof. Stephen D. Wilson

1. Chetan Dhital, **Sovit Khadka (Equal Contribution)**, Z Yamani, Clarina de la Cruz, TC Hogan, SM Disseler, Mani Pokharel, KC Lukas, Wei Tian, C. P. Opeil, Ziqiang Wang, Stephen D Wilson (2012), *Spin ordering and electronic texture in the bilayer iridate Sr3Ir2O7*, **Physical Review B** 86, 100401.
2. Chetan Dhital, Tom Hogan, Z Yamani, Clarina de la Cruz, Xiang Chen, **Sovit Khadka**, Z. Ren, Stephen D Wilson (2012), *Neutron scattering study of correlated phase behavior in Sr2IrO4*, **Physical Review B** 87, 144405.
3. Yoshinori Okada, Daniel Walkup, Hsin Lin, Chetan Dhital, Tay-Rong Chang, **Sovit Khadka**, Wenwen Zhou, H-T Jeng, M. Paranjape, A. Bansil, Z. Wang, Stephen D. Wilson, Vidya Madhavan (2013), *Imaging the evolution of metallic states in a correlated iridate*, **Nature Materials** 12,707–713.
4. Chang Liu, Su-Yang Xu, Nasser Alidoust, Tay-Rong Chang, Hsin Lin, Chetan Dhital, **Sovit Khadka**, Madhab Neupane, Ilya Belopolski, Gabriel Landolt, Horng-Tay Jeng, Robert S. Markiewicz, J. Hugo Dil, Arun Bansil, Stephen D. Wilson, M. Zahid Hasan (2014), *Spin-correlated electronic state on the surface of a spin-orbit Mott system*, **Physical Review B** 90, 045127.

Appendix III

VITA

I, Sovit Khadka, was born in Urlabari Municipality - 09 (formerly Rajghat VDC - 07), Morang, Nepal. After passing SLC (School Leaving Certificate) from Araniko Secondary School in my hometown, I joined Mahendra Morang Adarsh Multiple Campus (Tribhuvan University, TU), Biratnagar, Nepal where I earned my Intermediate and Bachelor's degrees in Physical Sciences and finally Master's degree in Physics from Central Department of Physics, TU, Kathmandu, Nepal. Then, I taught Physics to undergraduate students in TU affiliated colleges. I have also received M.S. in Physics from Western Illinois University, Macomb, IL in 2010. Lastly, I joined Boston College and completed Ph.D. degree in Space Plasma/Weather Physics in April 2018.